ENTE PER LE NUOVE TECNOLOGIE,
L'ENERGIA E L'AMBIENTE

Dipartimento Ambiente

IT9700638

STUDIES ON THE HOMOGENEITY OF PHOTON FIELDS FOR CONTEMPORARY CALIBRATION OF PERSONAL DOSEMETERS ON SLAB PHANTOMS

G.F. GUALDRINI, B. MORELLI

ENEA - Centro Ricerche "Ezio Clementel", Bologna

RT/AMB/96/22

Testo pervenuto nel dicembre 1996

SUMMARY

The most recent ICRU recommendations suggest to calibrate photon personal dosemeters on a slab phantom instead of a spherical phantom as previously proposed.
This kind of phantoms, due to their geometric characteristics, can in principle allow a contemporary calibration of several dosemeters at a time. In this framework, particular attention has to be devoted to the evaluation of the limits of the so-called "homogeneity area" to be employed. According to the ISO Standard 4037 an homogeneity of the calibration field within 5% (±2.5%) is permissible.
A rather detailed analysis on this subject has been therefore carried out using the Monte Carlo code MCNP to evaluate the backscattering profiles on PMMA and water filled PMMA phantoms both for normal and oblique incident radiation. At the same time, some air kerma free in air profiles for seven ISO Narrow and Wide Series beams measured at PTB (Braunchweig Germany) were used to model a more realistic irradiation situation. The calculated data were partially compared with experimental results from other European Laboratories.

The present work has been supported in the framework of the CEC Contract F13P-CT92-0064 "The Measurent of the Spectral and Angular Distribution of External Radiations in Workplace and Implications for Personal Dosimetry."

keywords: Photon personal dosemeters, calibration slab phantoms, field homogeneity, phantom rotation, Monte Carlo method.

RIASSUNTO

Le più recenti raccomandazioni ICRU suggeriscono di calibrare i dosimetri personali per fotoni su un fantoccio piano invece che su un fantoccio sferico, come proposto in precedenza.
Questi tipi di fantoccio, per le loro caratteristiche geometriche, possono in linea di principio consentire la calibrazione contemporanea di diversi dosimetri. In questo contesto, di particolare interesse pratico è la valutazione dei limiti della cosiddetta area di omogeneità utilizzabile. Seguendo le indicazioni dell'ISO Standard 4037 risulta accettabile una omogeneità del campo usato per la calibrazione all'interno del 5% (±2.5%) .
Una analisi piuttosto dettagliata è stata quindi svolta mediante il codice Monte Carlo MCNP per valutare i profili di retrodiffusione su fantocci di PMMA e di acqua contenuta in PMMA per incidenza normale ed obliqua della radiazione. Allo stssso tempo alcune mappature di kerma in aria libera prodotte presso il PTB (Braunchweig Germania) per sette fasci delle Serie ISO Wide e Narrow sono stati impiegati per modellare situazioni di irraggiamento più realistiche. I dati calcolati sono stati parzialmente confrontati con risultati sperimentali di altri Laboratori europei .

Il presente lavoro é stato finanziato nell'ambito del Contratto CEC F13P-CT92-0064 "The Measurent of the Spectral and Angular Distribution of External Radiations in Workplace and Implications for Personal Dosimetry."

parole chiave: dosimetri personali per fotoni, fantocci piani per calibrazione, omogeneità del campo, rotazione del fantoccio, metodo Monte Carlo.

1. INTRODUCTION

The most recent ICRU recommendations /1/ /2/ suggest to calibrate photon personal dosemeters under simplified conventional conditions on a phantom sufficiently representative of the average human trunk and with defined reference radiation beams. At the beginning ICRU-39 /3/ proposed the ICRU sphere as a suitable calibration phantom for individual monitoring. In this case to completely irradiate the sphere a field diameter of 30 cm is necessary.
A series of criticisms, especially practical but also theoretical, were formulated against the choice of the ICRU sphere as a suitable calibration phantom. One of the theoretical aspects was related to the so-called "ears effect" that generated dose maxima towards 90° position from the radiation incident direction: this effect, that was experienced at higher energies due to the forward peaked incoherent scattering coupled with the spherical shape of the phantom, was completely non-physical for the human trunk that is indeed more similar to an elliptic cylinder.
A further practical criticism was based on the impossibility of contemporary calibration of several dosemeters at a time; in fact the spherical shape allowed only one dosemeter to be calibrated during an irradiation. Moreover, from the manufacturing point of view the ICRU sphere is not easy to be provided whilst slab phantoms are very easy to be built and allow contemporary calibration of a number of personal dosemeters.
This was one of the main reasons why ICRU in a second time suggested a 30X30X15 PMMA phantom and more recently ISO /4/ suggested a 30X30X15 water phantom with PMMA walls (a 2.5 mm thick front wall and the other five walls of 1 cm thickness).

2. PHOTON FIELD HOMOGENEITY REQUIREMENTS FOR CALIBRATION ON SLAB PHANTOMS.

The new recommended calibration slab phantoms imply that the field diameter to be supplied in order to guarantee an homogeneous phantom irradiation has to be increased to about 42-45 cm whilst for the ICRU sphere a 30 cm wide field was sufficient. Such large homogeneous fields can be achieved in principle employing larger distances from the source. For practical reasons however this is often not possible. The backscattering from the rear walls of the irradiation

room has to be negligible and the air kerma rate of the primary radiation should be high enough to perform testing and calibration of dosemeters also with very heavily filtered X-rays.

In Italy about 40 qualified Dosimetric Services are performing their activity. It is foreseen that their number could be increased in the forthcoming year to about 80.
This implies that the Secondary Standard Dosimetry Laboratory at ENEA in Bologna should in principle perform several different type tests of these dosimetric systems.
It is therefore necessary to shorten the irradiation time as much as possible so that an High Kerma Rate X-ray Series should be used. Notwithstanding the fact that ISO recommends the Narrow Spectrum Series for calibration purposes, the Wide Spectrum Series is foreseen to be adopted in the future to fulfil the mentioned short irradiation time limits.
In order to characterise the X-ray fields in terms of their penumbra film slabs were used. A micro-densitometer was employed to read the film slab blackening and the homogeneity of the field area was verified within ± 2.5% as stated by ISO 4037 /5/. The high energy dependence of the film slab response was limited using adequate filtering in order to cut the lower energy spectrum component to which the film is very sensitive. A useful field of 15 cm width at 1 meter from the source was in this way determined.

To enter in more detail in the study of the field homogeneity conditions on a slab phantom, two aspects are to be taken into account. The first problem is that X-rays are emitted rather anisotropically from the tube especially when trying to obtain rather broad beams. Secondly the backscattered radiation from the phantom decreases from the central axis to the edges of the slab phantom.

The already mentioned tests developed at the ENEA Secondary Standard Dosimetry Laboratory using film slabs were carried out for a limited number of ISO reference beams /6/.

On the other hand some very accurate measurements carried out by Shimizu and Minami /7/ and Will /8/ demonstrated that the non-homogeneity of the calibration field due to both the source X-ray beam anisotropy and the calibration phantom backscattered component decrement from the central axis towards the phantom edges should be carefully taken into account to establish a self consistent calibration procedure.

Moreover recently at PTB/9/ it was produced a complete mapping of air kerma measurements (free in air) for the ISO Narrow Series and for the ISO Wide Series, that can allow a comprehensive analysis of the field homogeneity in realistic calibration conditions.

The present numerical studies were therefore devoted to determine the homogeneity field limits in presence of tissue equivalent slab phantoms of various kinds. Some evaluations on the effect of phantom rotation on the backscatter factor as a function of the measurement point were also carried out.

3. NUMERICAL STUDIES

The study was performed using the MCNP Monte Carlo code /10/. The code, that is able to treat neutron, photon and electron transport problems, is endowed with point-wise cross section libraries. The photon interaction data are derived from the Hubbell /11/. Moreover very powerful geometry modelling capabilities, besides a large variety of variance reduction techniques are available. Furthermore the code allows to describe very complex source energy and space distributions (this capability was used in the present study).

The analysis was developed through various progressive steps.

Originally monochromatic beams were studied in order to validate the procedure versus literature data. Afterwards the Narrow and Wide Spectrum Series were investigated.

The various studies can be summarised in the following main chapters:

a) Study of air kerma backscatter factors on the central axis of various tissue equivalent slabs for monoenergetic normally incident photon beams;

b) Study of the field homogeneity in terms of air kerma backscatter factor at various positions on the phantom surface for normally incident ISO series beams;

c) Study of the effect of phantom rotation on the backscatter factor profile;

d) Backscatter factor mapping using realistic air kerma in free air profiles.

3.1 Air Kerma backscatter factors on the central axis of a slab phantom

Some comparisons with literature data have been carried out with satisfactory agreement. The values were taken from Bartlett D. T., Dimbylow P. J. and Francis T. M./12/. In the mentioned paper the air kerma backscatter factors have been calculated for 15, 25, 50, 75, 100, 150 and 662 keV, whilst the ENEA set of data was obtained at 20, 30, 40, 50, 60, 70, 80, 100, 300 and 1000 keV.

Figures 1 and 2 show the comparison between the two sets of results for the ICRU theoretical slab as well as for the PMMA slab. A satisfactory agreement has to be pointed out in the whole investigated energy domain.

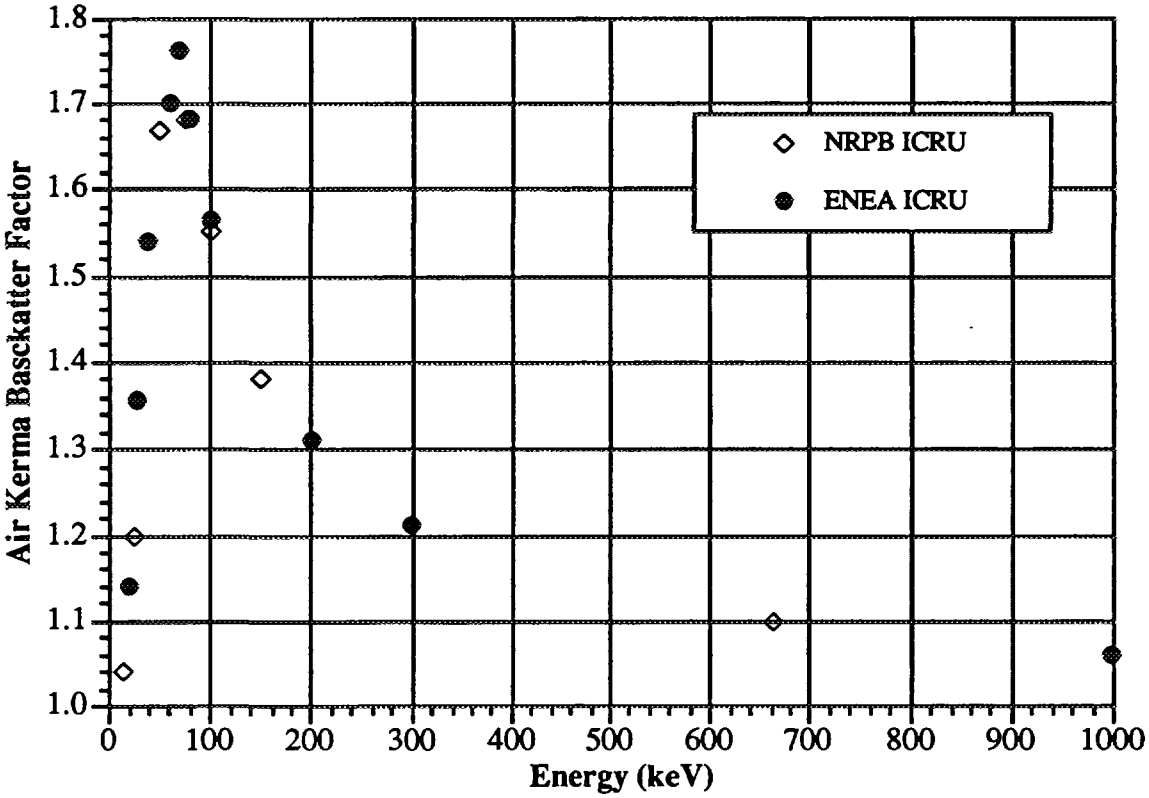

Fig. 1: Air kerma backscatter factors for 4-element ICRU tissue material 30x30x15 slab phantom: comparison between NRPB and ENEA results

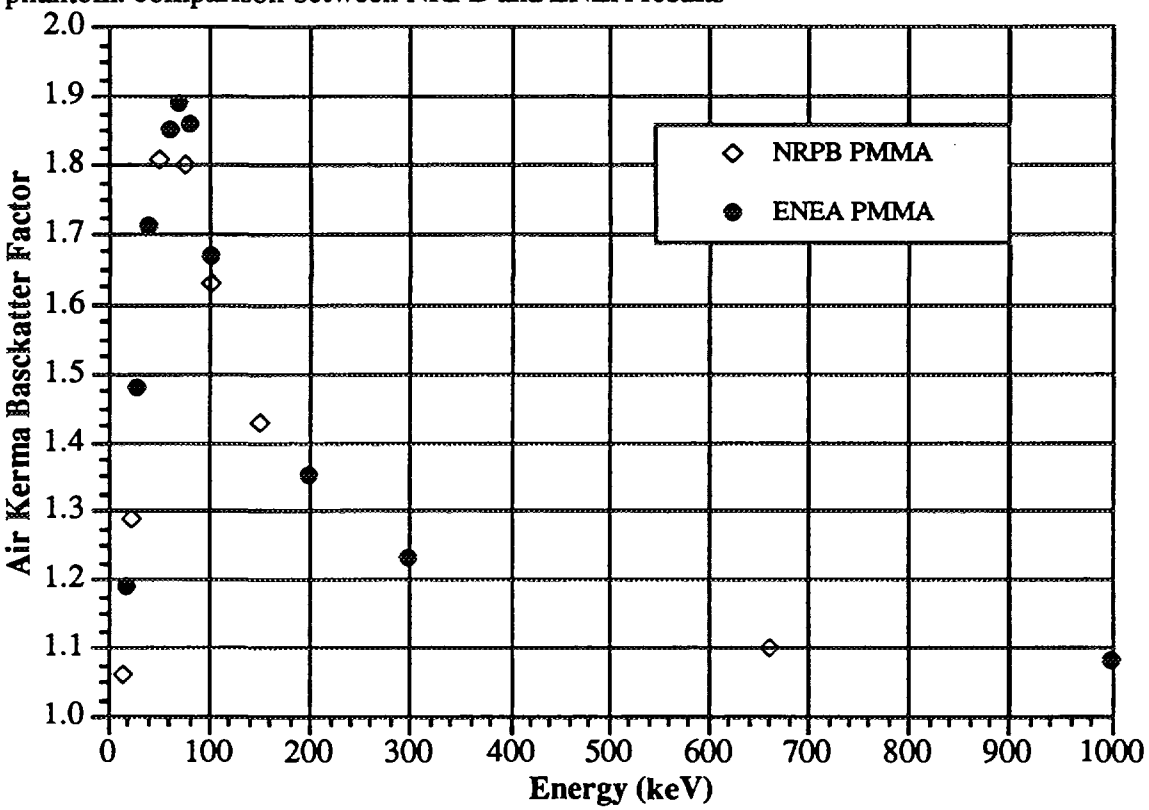

Fig. 2: Air kerma backscatter factors for PMMA material 30x30x15 slab phantom: comparison between NRPB and ENEA results

The two figures demonstrate the higher backscattering characteristics of the PMMA material as compared with the ICRU theoretical one.
This effect, that is mainly due to the significant difference between the densities of the two materials (PMMA =1.19 g/cm^3 , ICRU-4 element =1 g/cm^3), implies that a particle phantom based on PMMA material cannot be taken as a completely satisfactory substitute for the ICRU theoretical one.
The ISO recommended phantom, based on a water filled 30x30x15 PMMA slab (1 cm thick walls except for the wall facing the source, that is 0.2 cm thick) appears to be a better substitute for the theoretical standard. This conclusion was confirmed in a previous ENEA study /13/.

3.2 Study of the field homogeneity in terms of air kerma for normally incident ISO series beams.

The first simplified study was developed for PMMA and water in PMMA slab phantoms irradiated with the two complete normally incident Narrow and Wide Spectrum Series.
A thin vacuum 5 mm layer on the front face was subdivided into concentric square cells surrounding the central axis of the phantom (figure 3). The cell pitch was 0.5 cm.

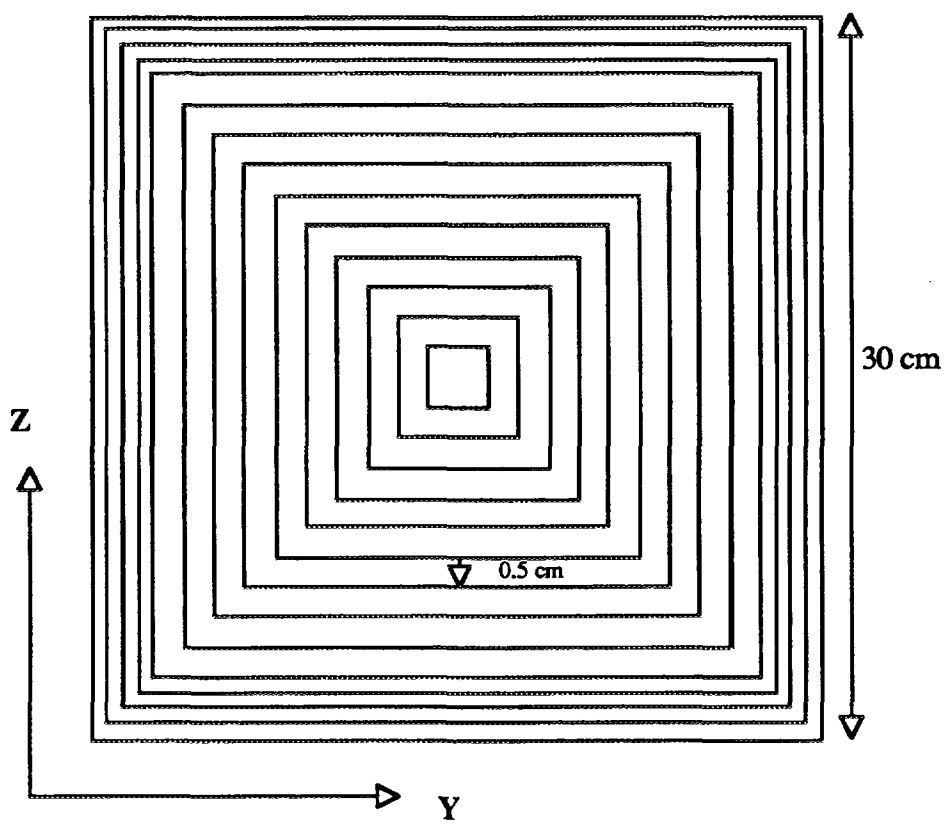

Fig. 3: Description of the MCNP geometry in the case of irradiation by a normal homogeneous expanded and aligned field.

A tracklength estimator was therefore employed for estimating the spectral photon fluence in each cell. Fluence to absorbed dose conversion factors have been applied as a response function during the particle tracking and scoring to obtain the spatial distribution of the collision air kerma on the phantom front face, according to the formula:

$$ka_J = \int_0^{\infty} (d\phi/dE)_J \; E\,[\mu_{en}/\rho]_{air}\, dE$$

where:

ka_J is the air kerma in the J-th cell starting from the central cell towards the phantom edge; $(d\Phi/dE)_J$ is the spectral photon fluence in the J-th cell evaluated using the tracklength estimator; E is the particle energy and $[\mu_{en}/\rho]_{air}$ is the air mass energy absorption coefficient.
The collision air kerma backscatter coefficient is defined as:

$$B_{ka} = (ka_J)_{phantom} / (ka)_{free\ air}$$

According to this formula a number of collision air kerma backscatter coefficient profiles have been obtained in simplified conditions, i. e. homogeneous parallel beam characterised by the same spectrum at every emission direction.
Figure 4 shows the backscatter factor as a function of the distance from the PMMA slab central axis for the 110 kV beam (average energy = 78 keV) of the Wide Spectrum Series.

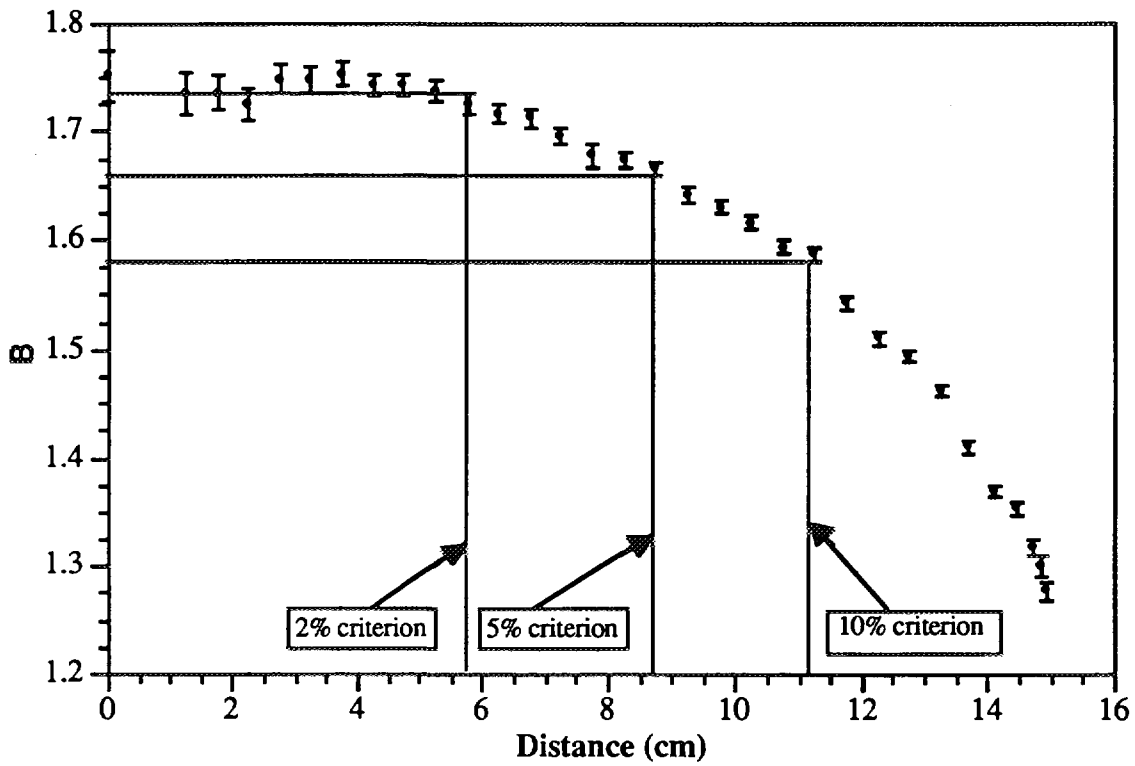

Fig. 4: Application of three criteria to evaluate the homogeneity area for an homogeneous parallel beam on a PMMA phantom (Wide Spectrum Series 110 kV beam).

Three criteria for selecting the useful irradiation area were adopted: 2%, 5% (that is the ISO one) as well as 10% Citroen. Appendix A supplies the complete set of graphs for both Wide Spectrum Series and the Narrow Spectrum Series for PMMA phantom and water in PMMA phantom.

3.3 Phantom rotation

According to the ICRU-47 document the dosemeter should be characterised by an angular response with the same behaviour of the Personal Dose Equivalent Hp(d,α), where α is the angle of rotation. The type test of a personal dosemeter should be therefore performed as a function not only of the energy, but also of the radiation incident angle.
The ICRU and ISO proposals to adopt slab phantoms for calibration leading to the already explained possibility of contemporary calibration of several dosemeters at a time, implies the need of quantifying the different irradiation conditions' effects on each calibrated dosemeter, depending on its location on the phantom front face during a non-normal irradiation (figure 5). At a first glance it is easy to understand that the various dosemeters are subject to different air kerma rates, according to the inverse square law, depending on their position on the phantom surface. This implies the necessity to correct the effect of the different incident air kerma rates to obtain irradiation situations independent from the source to target distance, that is equivalent to produce a set of readings for the various dosemeters as they were irradiated by a plane radiation wave impinging on the calibration phantom with a given incident angle.

This correction can be obtained in two different ways:

1) Applying an appropriate correction factor for each dosemeter on the basis of the inverse square law taking the front face centre as the reference point (that corresponds also to the centre of rotation).
2) Splitting the irradiation in two equal time steps with the phantom placed in two symmetric positions (figure 6). To apply this kind of procedure it is necessary that we can assume that the air kerma free in air variations are linear along the irradiated phantom front face. It is easy to demonstrate that, for the kind of source to phantom distances employed in the calibration practice (that are determined by the need to guarantee an adequate width beam), this kind of condition is always fulfilled. The divergence from linearity is in fact about 0.1% for 3 meters source to phantom distance and about 1% for 1 meter source to phantom distance.

The two procedures guarantee in practice that every dosemeter placed on the phantom face is calibrated in "identical" incident kerma rate conditions.
In the first case the calibration beam is transformed in a plane parallel beam impinging on the phantom: the dose imparted to the dosemeter (and therefore the backscatter factor) is in this case only due to the backscatter characteristics of the investigated phantom and to its orientation within the radiation field. On the other hand the second procedure tends to avoid the application of a correction factor to every dosemeter reading: as it will be shown later, this procedures causes also useful effects compensating also the backscattered radiation component on the irradiated dosemeters.

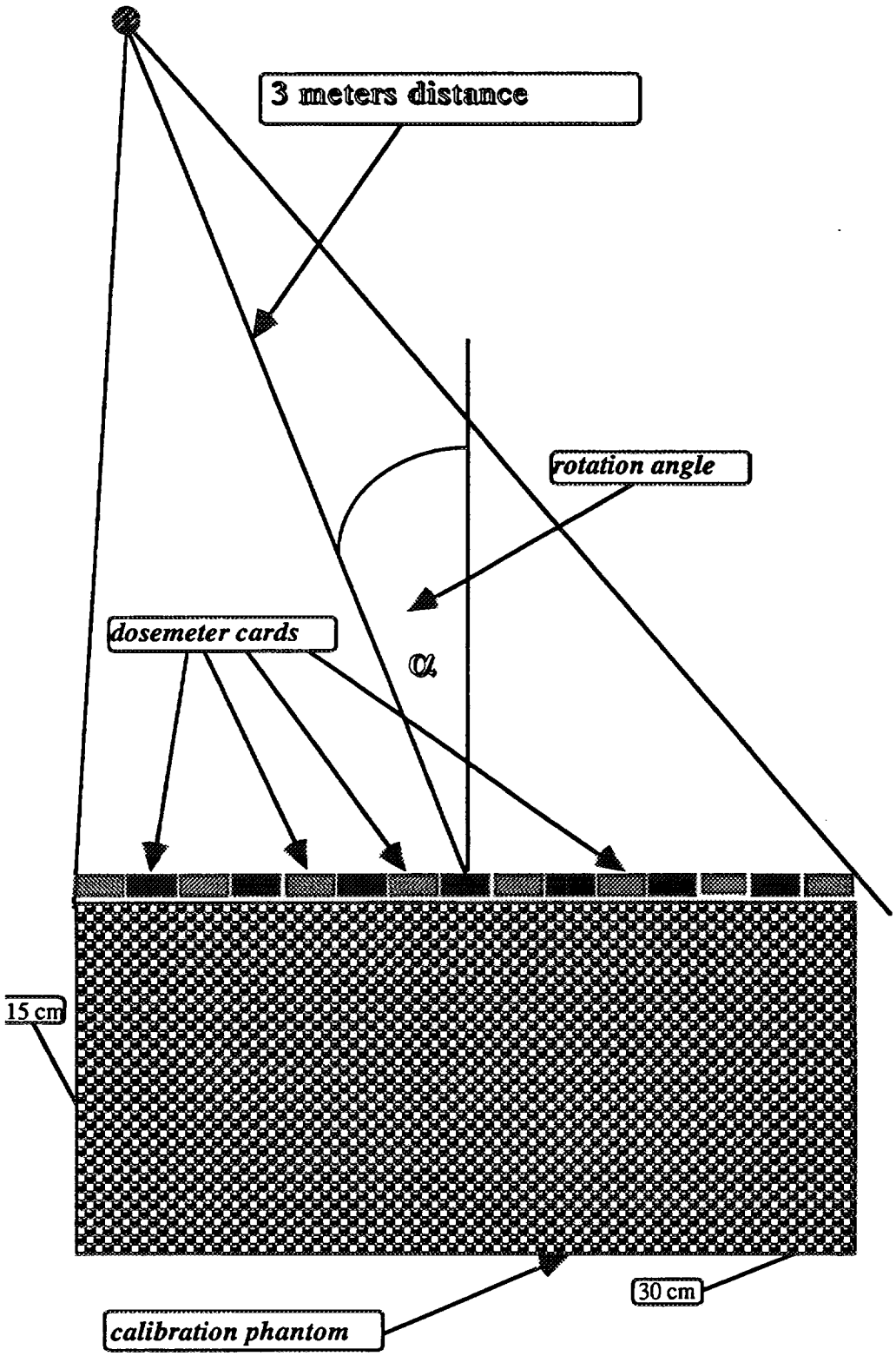

Fig. 5 : Phantom irradiation geometry

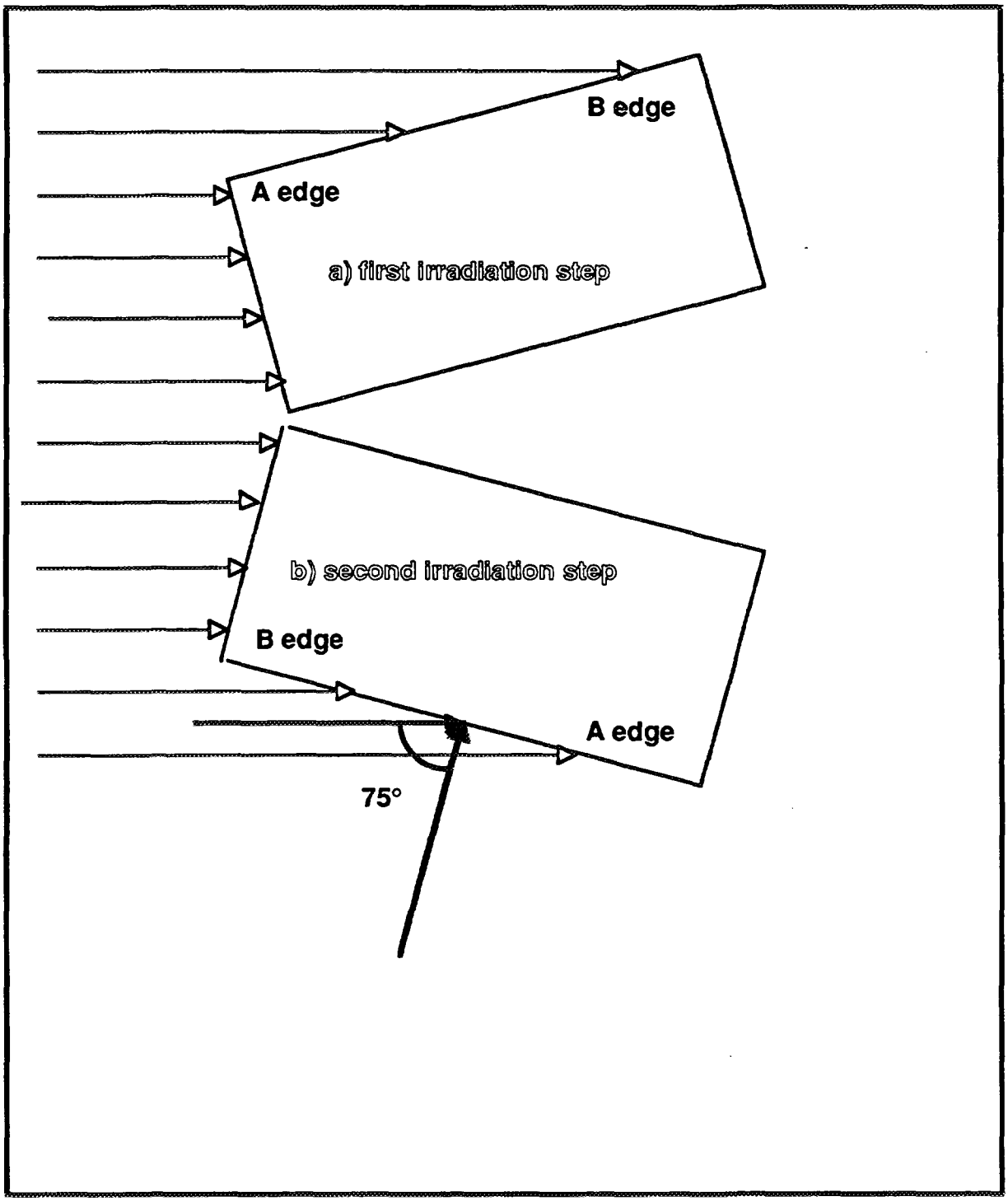

Fig. 6: Irradiation of several dosemeters through two equal time intervals to guarantee homogeneous irradiation conditions.

To quantify the backscattered component behaviour along the irradiated face of the employed phantom, a Monte Carlo study was therefore carried out with the following procedure.
A parallel photon beam was treated in the same way as for the normal incidence.
The surface was subdivided into equally wide rectangles (0.5 x 14 cm each) as shown in figure 7. The 14 cm width was taken from the results obtained for normally incident beams and guarantees an homogeneity area as a function of Y.

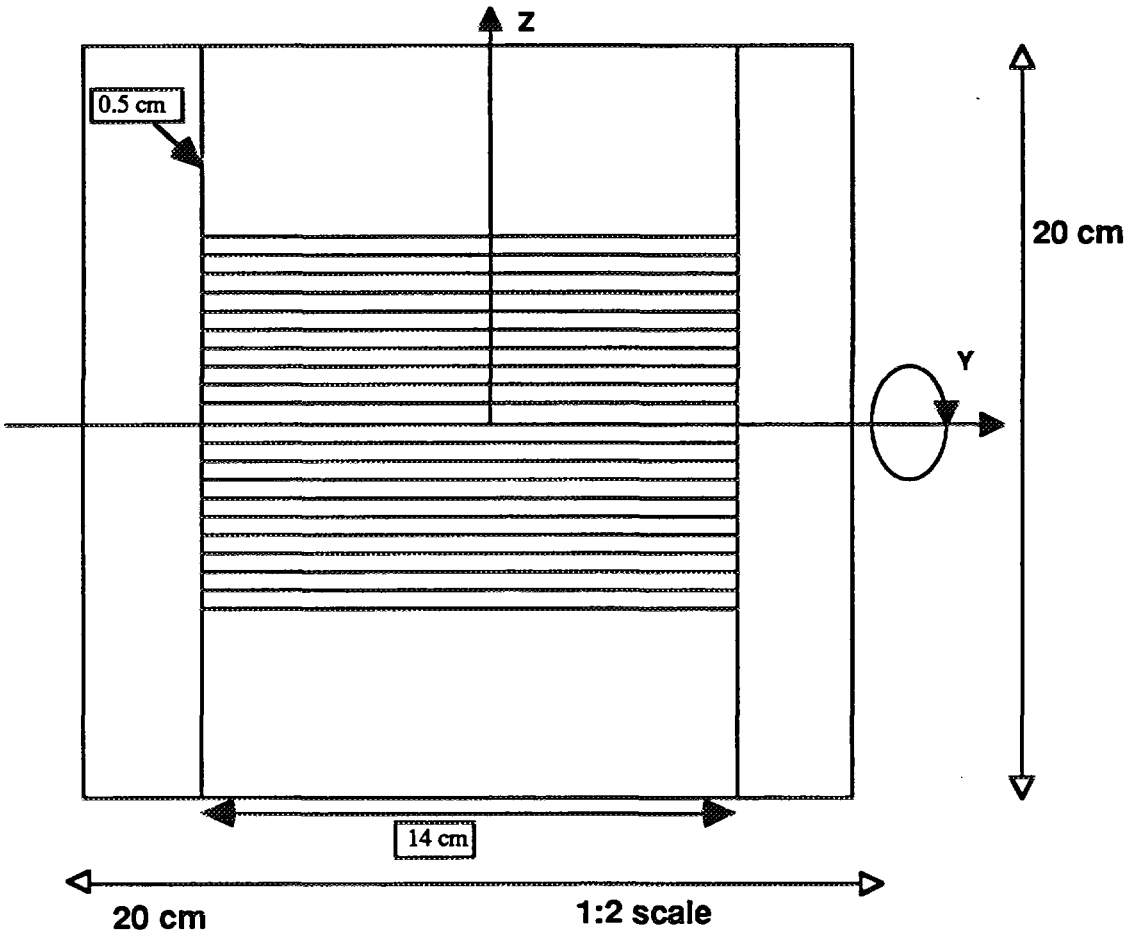

Fig. 7: Geometry for the phantom rotation around the Y axis as adopted in MCNP.

Figure 8 shows an example of the behaviour of the air kerma backscatter factor as a function of the incident angle and of the dosemeter's distance from the calibration phantom's centreline. The 110 kV Wide Spectrum Series beam was selected because its mean energy (78 keV) corresponds to the highest backscattering values (see previously reported graphs in figures 1 and 2).
The effect of phantom rotation on the kerma imparted to the dosemeters for a parallel beam can be significantly detected only at angles greater than 60 degrees and at 75 degrees angle the effect is quite evident, due to the contribution to the scattered component of the phantom edge closest to the source. At 75 degrees incident angle, the air kerma per unit fluence values for the points closest to the front edge are about 15% higher than for the most far away points. The same graphs show the progressive shift of the backscatter factor maximum towards the same phantom edge (the arrows show this behaviour). In appendix B the complete set of data at 45°, 60° and 75° for a PMMA phantom is supplied.

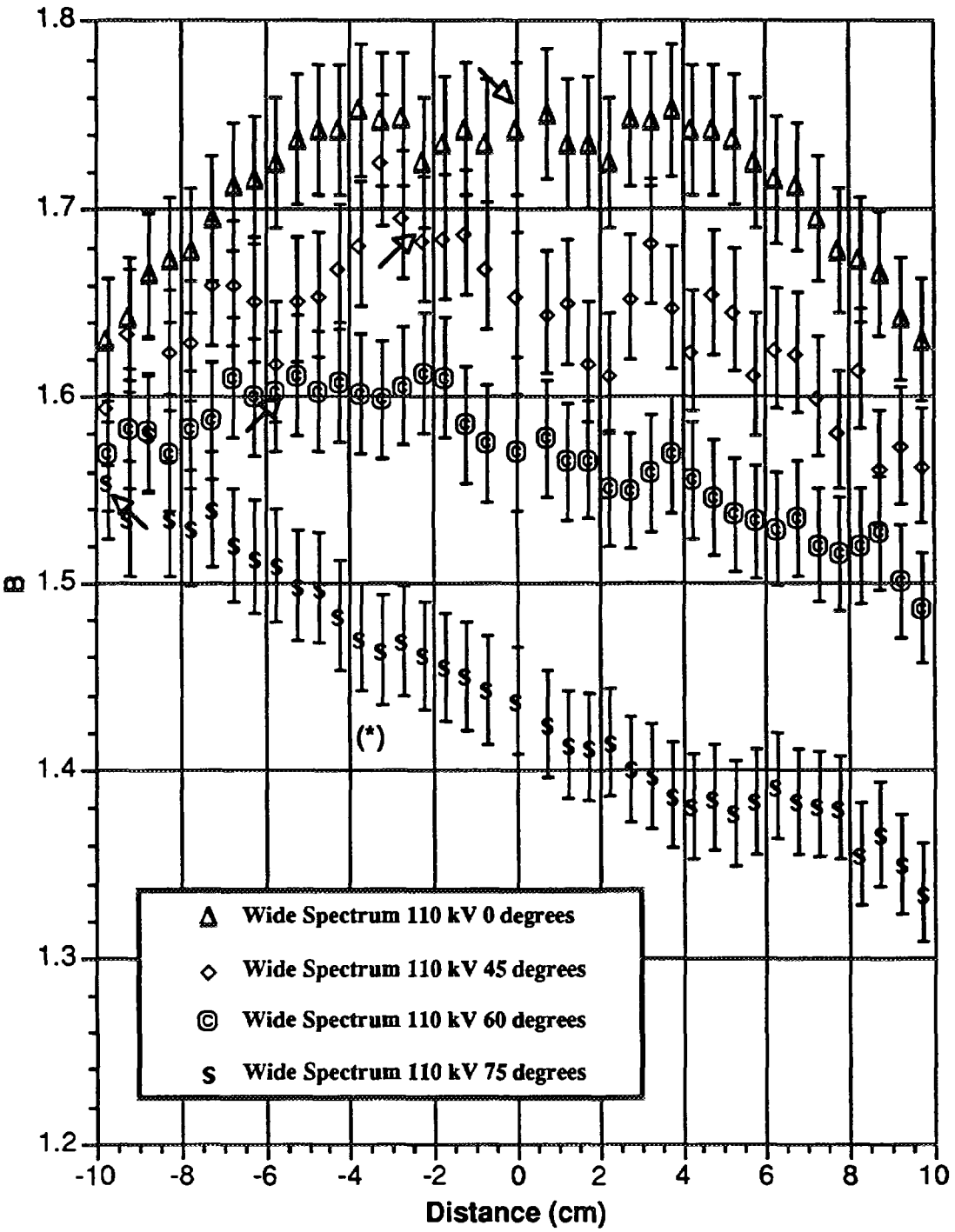

Fig. 8: Air kerma backscatter factor behaviour as a function of the dosemeter distance from the calibration phantom front face centerline for four given incident angles.

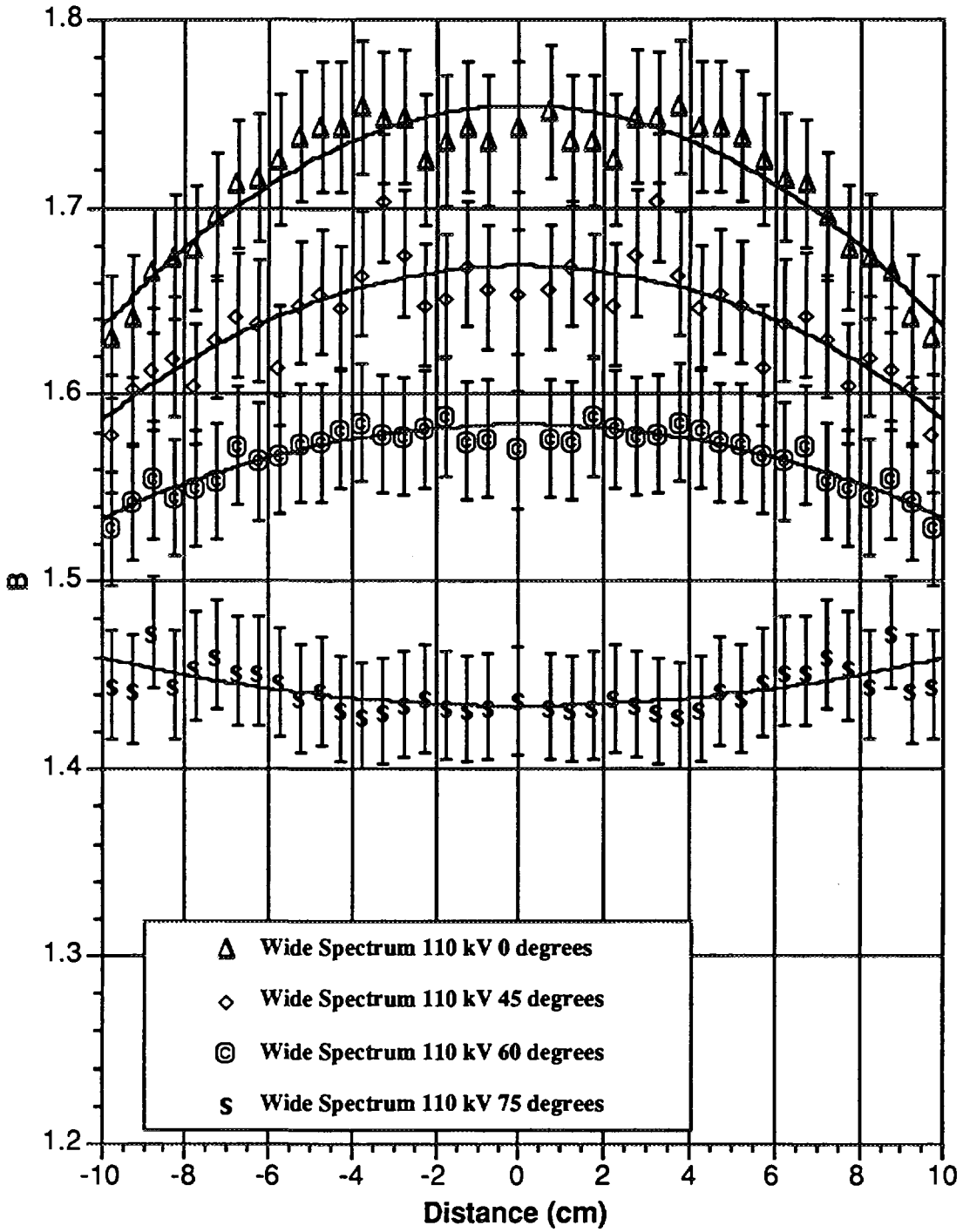

Fig. 9: Air kerma backscatter factor to which the dosemeters are subject when using a two equal step irradiation procedure. The data are presented as a function of the distance from the phantom front face centerline for given beam incident angles.

A useful compensating effect can be obtained, as already mentioned, splitting the calibration procedure into two equal time steps (procedure 2). In this situation (see Figure 9) the dosemeters are subject to a total field (incident + backscattered) symmetric around the face centreline, similar to that corresponding to the normal incidence. It can be immediately

observed on the graph that the percentage variation of the backscatter factor for the various incident angles becomes the lower the higher is the beam incident angle. This allows to conclude that the homogeneity limits on the front face area as stated for the normally incident beam are still valid also for non-normal incidence if a two-step-procedure is used for oblique-incidence-beams.

3.4 Backscatter factor mapping using realistic air kerma in free air profiles.

Recently PTB produced a complete spatial mapping of air kerma measurements (free in air) for the ISO Narrow Series as well as Wide Series X-ray reference beams, that allowed a rather comprehensive analysis of the field homogeneity in realistic calibration conditions. The measurements were performed at 1 meter from the source with a grid of 0.5 cm pitch and 33x33 measurement points. The size of the field corresponds to the largest divergence used at PTB Laboratory (a diameter of 15 cm. at 1 m. distance from the focus) that is in agreement with the largest field divergence adopted at ENEA. Figure 10 shows the irradiation geometry whilst in Appendix C the three dimensional profiles of the air kerma free in air values for the Wide and Narrow Spectrum Series are supplied. The same Appendix supplies also a set of two-dimensional plots of the air kerma profiles on the two perpendicular centrelines of the field(Y-Z). The irradiation on the phantom is performed at PTB at 3 meters from the source: a preliminary check on the supplied experimental values showed largest variations of about 5% from the maximum in the area of interest for the phantom irradiation.

Some studies were performed to evaluate the effect of the source asymmetry on phantom backscatter profiles.

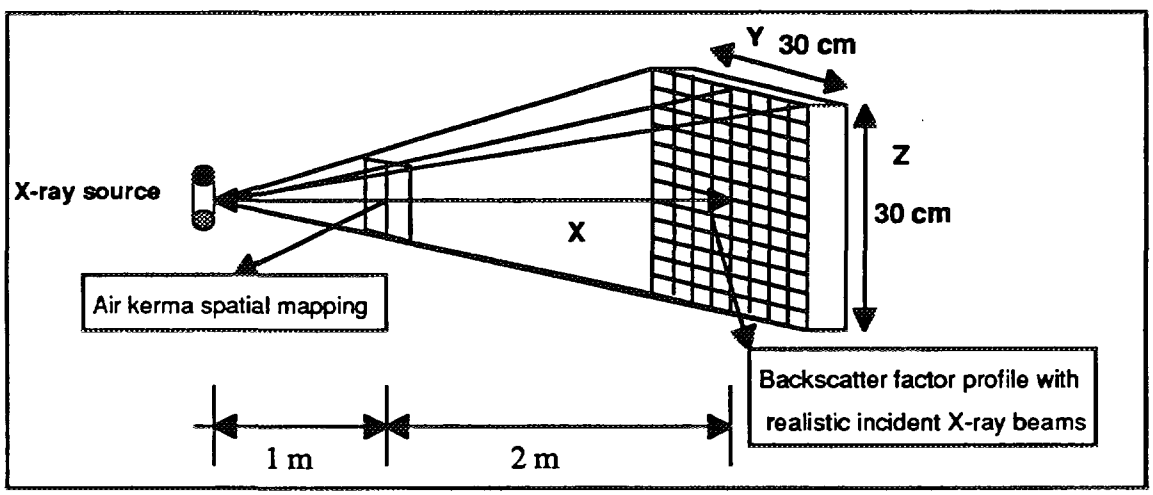

Fig. 10: Calibration phantom irradiation geometry.

The spectrum was as a first approximation assumed as constant at every measurement point so that the source photon fluence profile could be represented by the air kerma profile. A special source model was prepared for MCNP to supply the probability density function depending on the two Y-Z spatial variables. The source was thereafter expanded and aligned to match with the irradiation area at 3 m from the source. The real source was therefore defined on a grid of 21x21 values (i. e. a central subset of the 33x33 original matrix) with a 1.5 cm pitch. The slab

surface was subdivided in little squares like a chequeboard (see fig. 11) with dimensions close to those of a dosimeter card (2.5x2.5 cm) for a total of 144 geometry cells. The air kerma values for every position were thereafter sampled tracking about 1.500.000 particles per run.

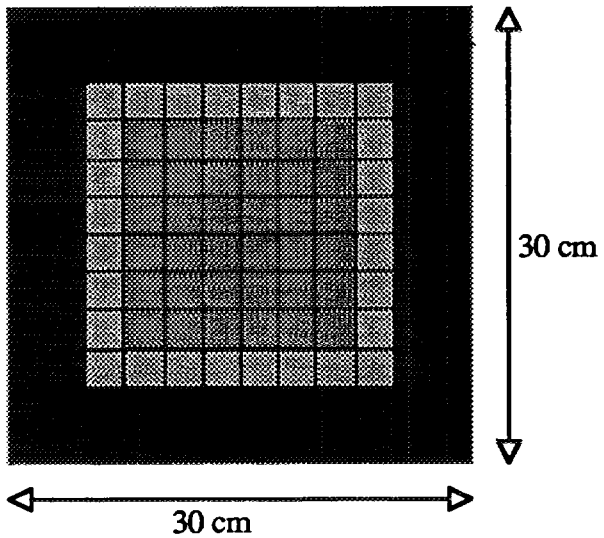

Fig. 11: MCNP geometry qualitative example of the scoring cells on the front face of the calibration phantom irradiated with a realistic X-ray beam.

As already mentioned the beam area that is used for the calibration is quite small as compared with the area where the air kerma free in air profile has been measured. This implies that, as expected, the statistical fluctuations of the results could at some extent hide the effect of the small source field asymmetry. This was the reason why an high number of particles were followed in the studies based on the realistic photon source shape as measured at PTB: this allowed to obtain standard deviations of the order of 1% for each scoring cell.

Figures 12-18 show the results based on the realistic source as compared with those previously presented for parallel homogeneous beams. Apart from the intrinsic stochastic fluctuations associated with the Monte Carlo results especially in small sampling volumes[3], a rather satisfactory agreement has to be pointed out between the two approaches. The agreement is usually within 1-2% with some exceptions with largest deviations of about 3% (Narrow Spectrum Series 150 kV) and 4-5% (Narrow Spectrum Series 80 kV, Narrow Spectrum Series 300 kV and Wide Spectrum Series 300 kV). Being the comparison performed on the Y centreline, it is difficult to draw some general conclusion only on the basis of these graphs. Their meaning is only to confirm that, taking into account the substantially different source spatial distribution as well as the different scoring areas , the two approaches supply results in reasonable agreement.

[3] For homogeneous parallel photon beam the scoring geometry was represented by nested square shells (see figure 3) so that the central values are affected by somewhat higher uncertainties (1.5 - 2%) associated with fluctuations and undersampling. The photon population in this area could be improved by a radial biasing of the source sampling. It has on the other hand to be pointed out that this very central area is practically characterised by a backscatter coefficient plateau, so that satisfactory conclusions can be nevertheless reached on the basis of this set of results.

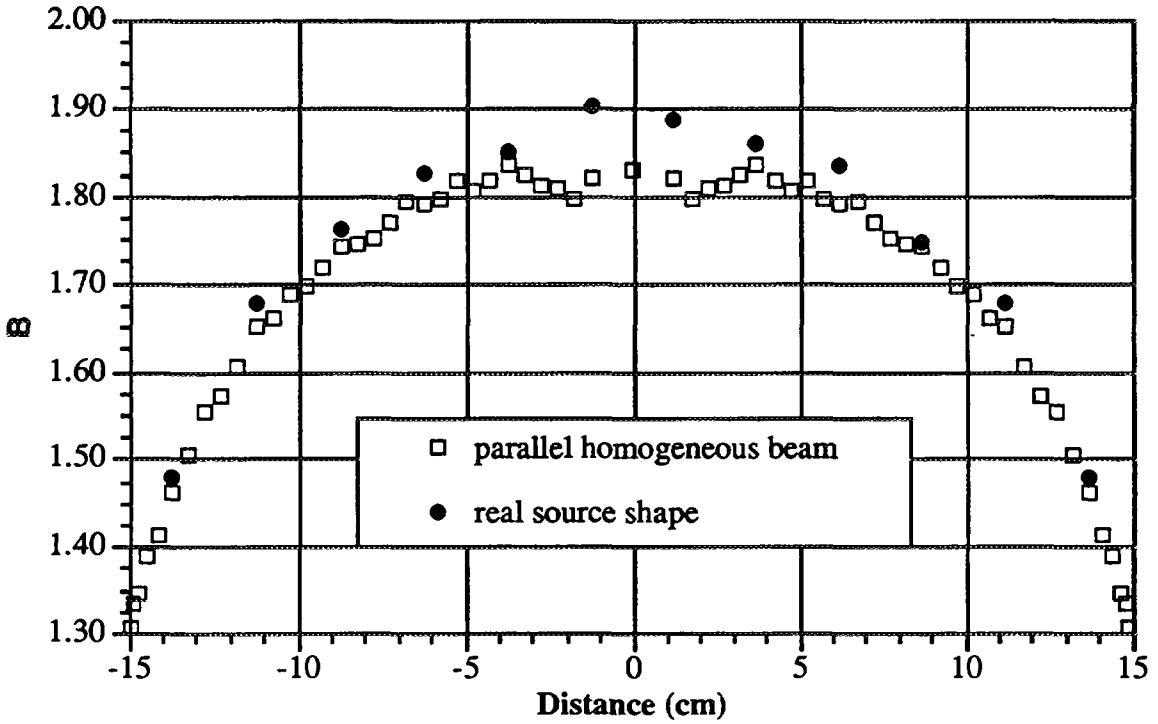

Fig. 12: Narrow Spectrum Series 80 kV. Air kerma backscatter profile on the horizontal slab centreline (<Z>=0 , -15<Y<+15)

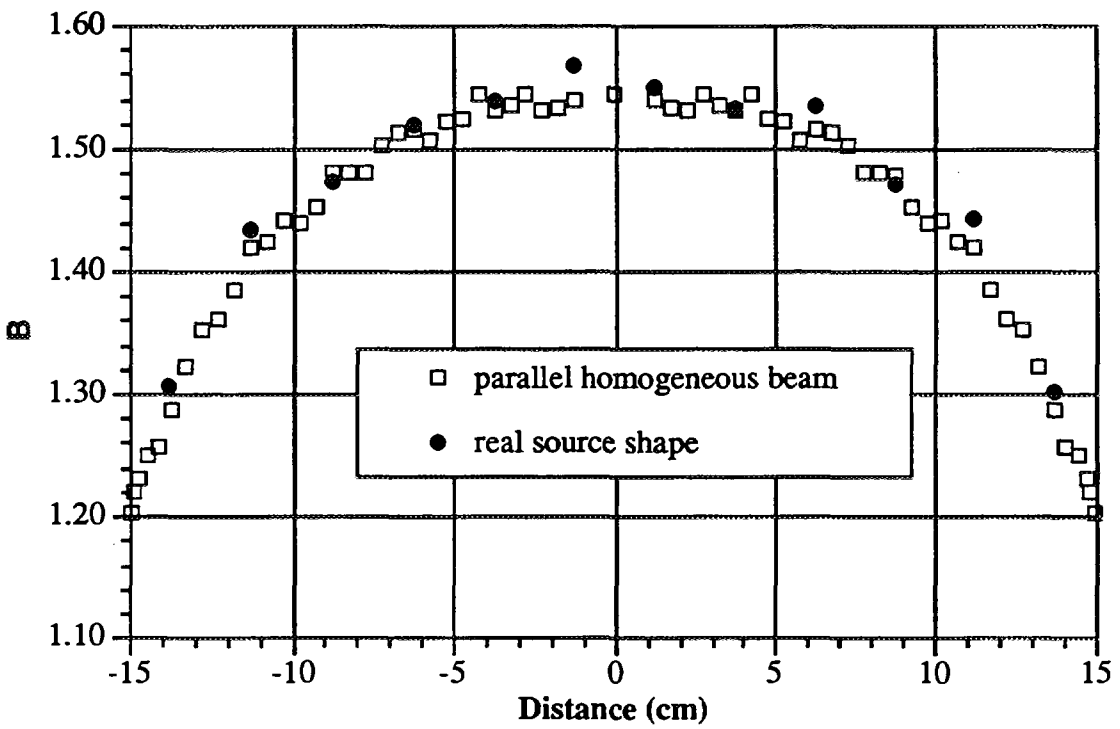

Fig. 13: Narrow Spectrum Series 150 kV. Air kerma backscatter profile on the horizontal slab centreline (<Z>=0 , -15<Y<+15)

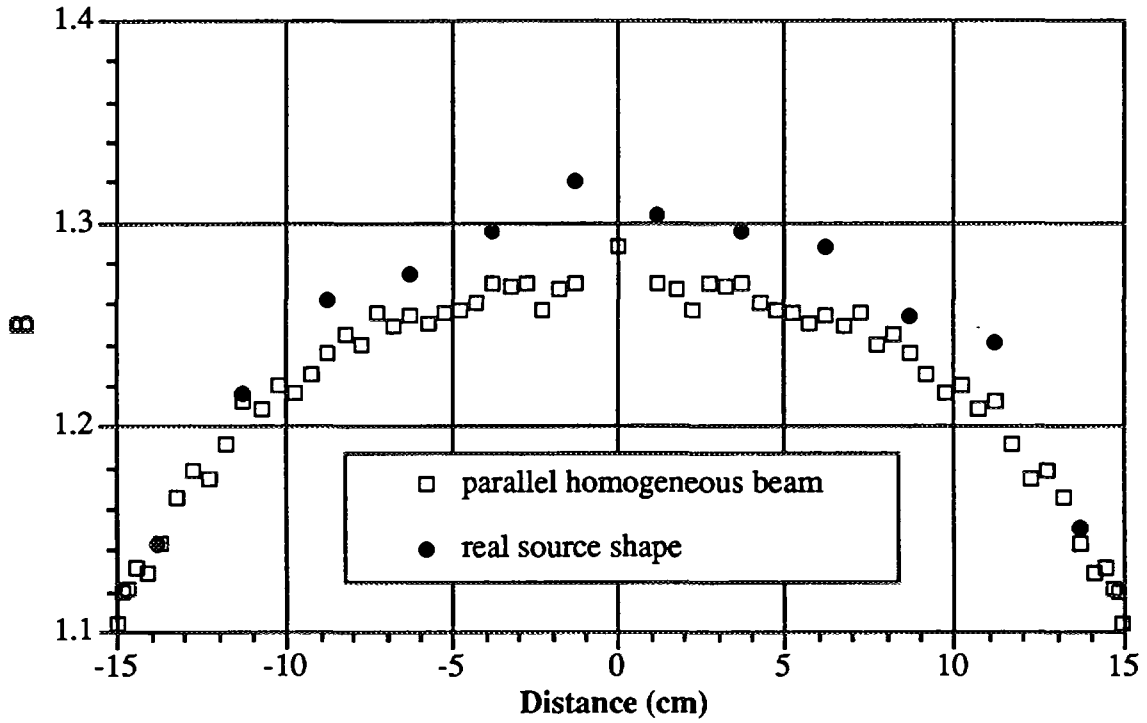

Fig. 14: Narrow Spectrum Series 300 kV. Air kerma backscatter profile on the horizontal slab centreline (<Z>=0 , -15<Y<+15)

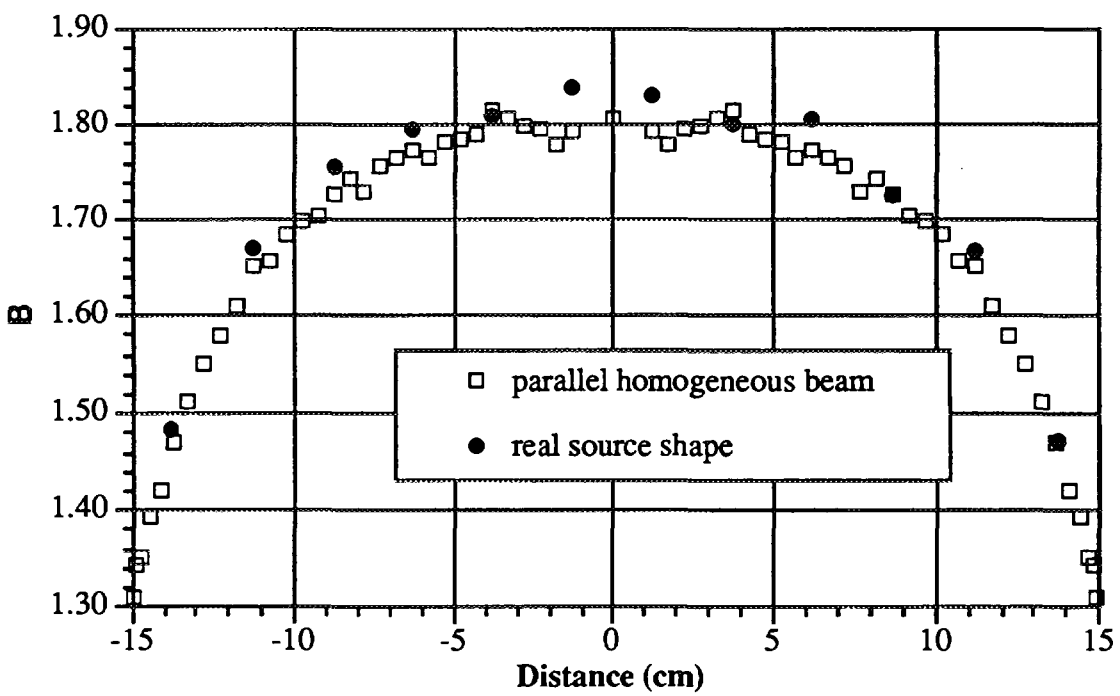

Fig. 15: Wide Spectrum Series 80 kV. Air kerma backscatter profile on the horizontal slab centreline (<Z>=0 , -15<Y<+15)

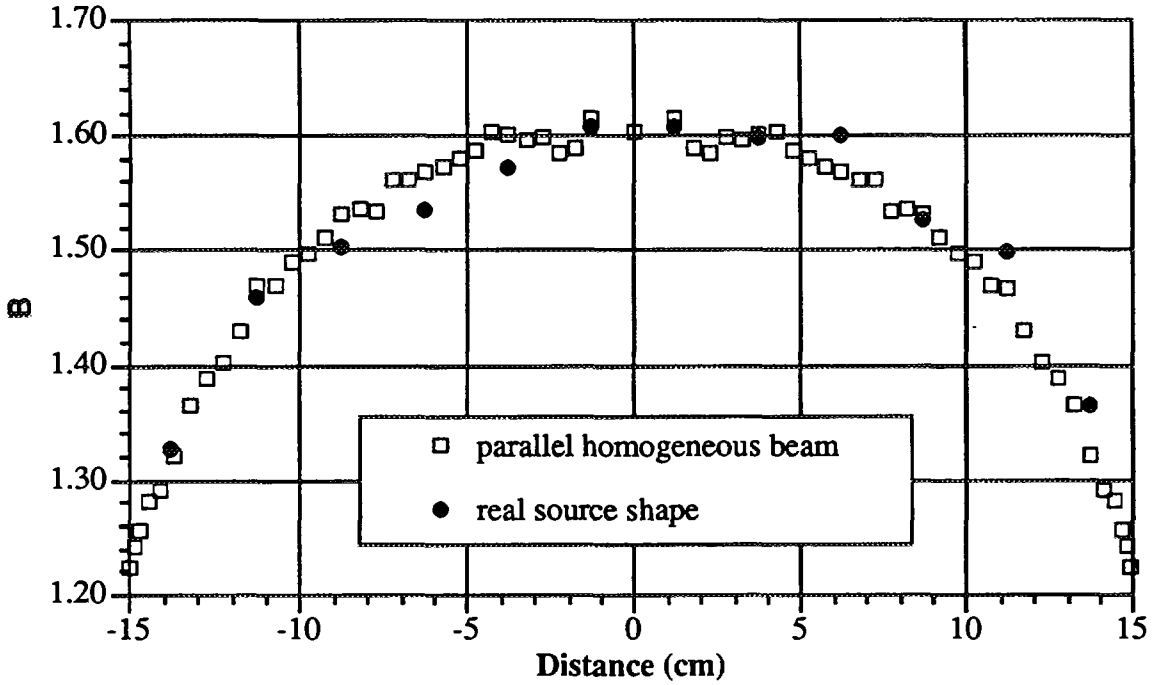

Fig. 16: Wide Spectrum Series 150 kV. Air kerma backscatter profile on the horizontal slab centreline (<Z>=0 , -15<Y<+15)

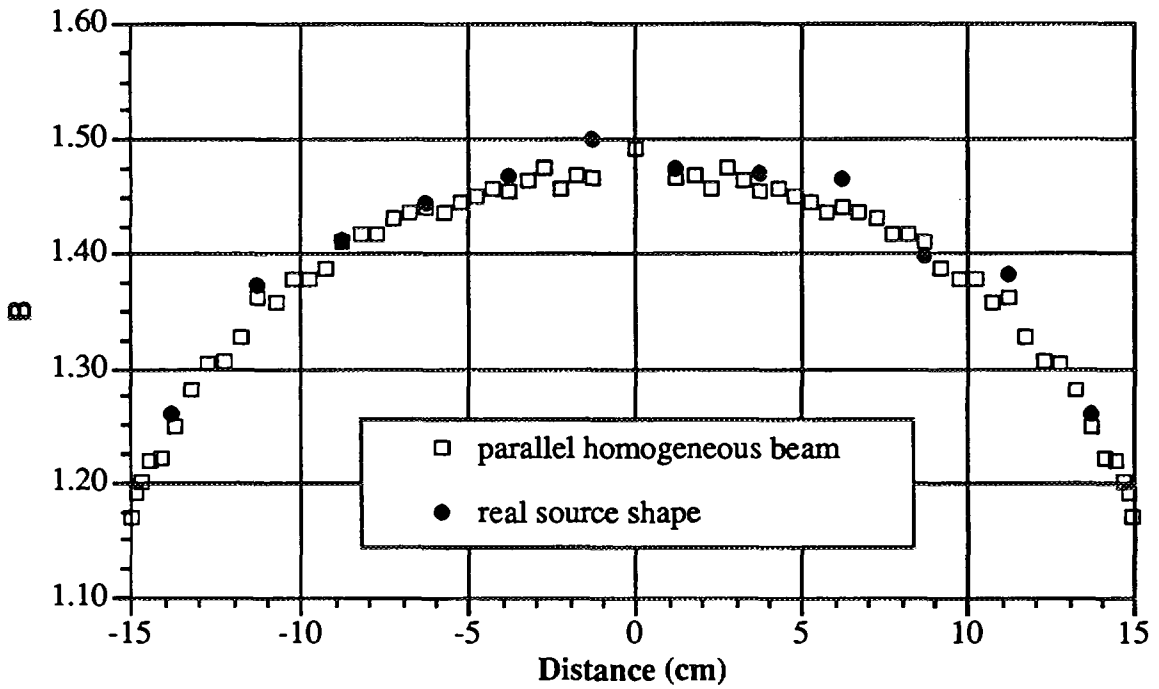

Fig. 17: Wide Spectrum Series 200 kV. Air kerma backscatter profile on the horizontal slab centreline (<Z>=0 , -15<Y<+15)

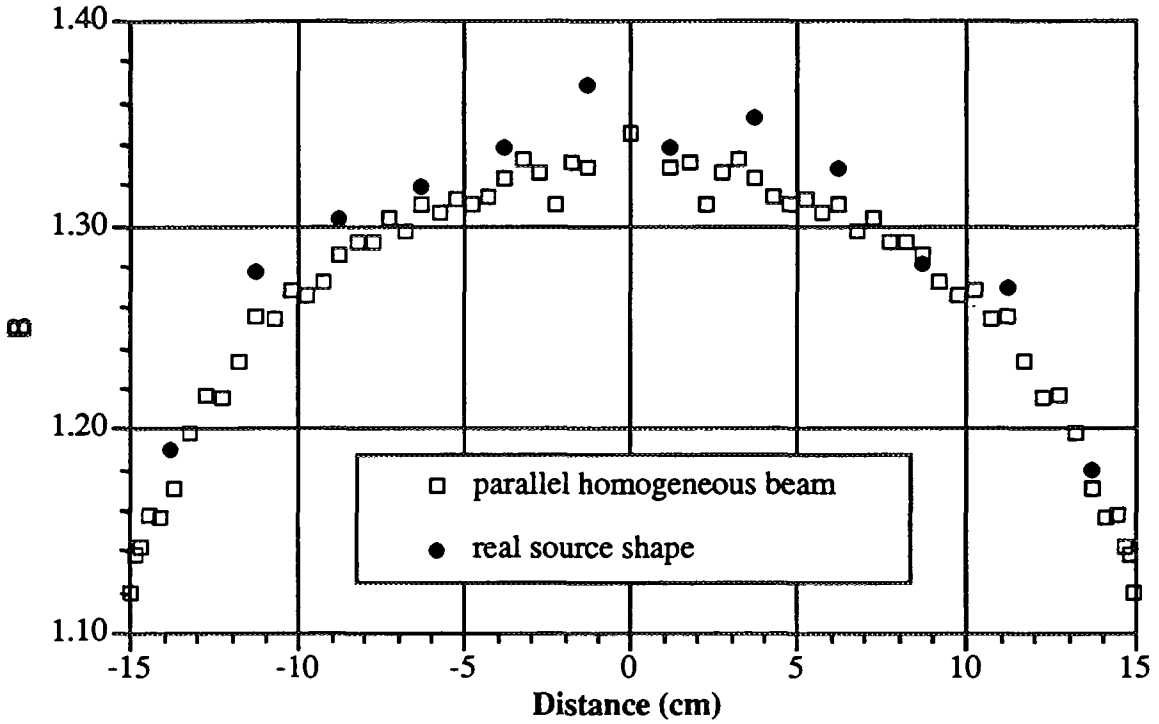

Fig. 18: Wide Spectrum Series 300 kV. Air kerma backscatter profile on the horizontal slab centreline (<Z>=0 , -15<Y<+15)

A rather interesting information is concerned with the backscatter profile asymmetry determined by the realistic source distribution on the phantom surface.
Figures 20 - 33 supply the backscatter profiles on the two centrelines as well as on the diagonals of a PMMA slab phantom for the seven investigated beams. In figure 19 the plotting criterion of the diagonal data is shown.

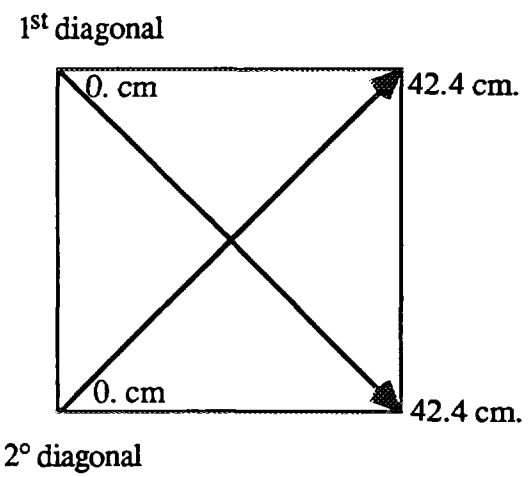

Fig.19: Scheme illustrating the criterion for plotting diagonal backscatter factor values.

The results are obviously affected by statistical uncertainties and sampling fluctuations but systematic trends can be pointed out, that can be ascribed to the source profile asymmetries (a quite significant asymmetry was experienced in the air kerma backscatter factor for the real spatial distribution of the 150 kV Wide Spectrum Series beam.)
Appendix C supplies further plots for comparison.

The discrepancies between the two approaches (homogeneous normally incident beam and real beam) are usually within 2% with some cases reaching values > 4%.
Taking into account the two sensibly different spatial distributions of the source in the two cases, the agreement can be considered satisfactory.
To give some preliminary quantitative indication on the homogeneity areas on the slab phantom, we can say that for PMMA material variations of B within ± 1% (2% from the maximum central value) occur inside a 6x6 - 10x10 cm square, ± 2.5% variations (5% from the maximum central value) occur inside a 12x12 - 16x16 cm square, whilst variations within ± 5% (10% from the maximum central value) occur inside a 20x20 - 24x24 cm square.
To supply a more comprehensive information on the backscatter factor mapping Appendix D shows a series of profiles for fixed <Z> values.

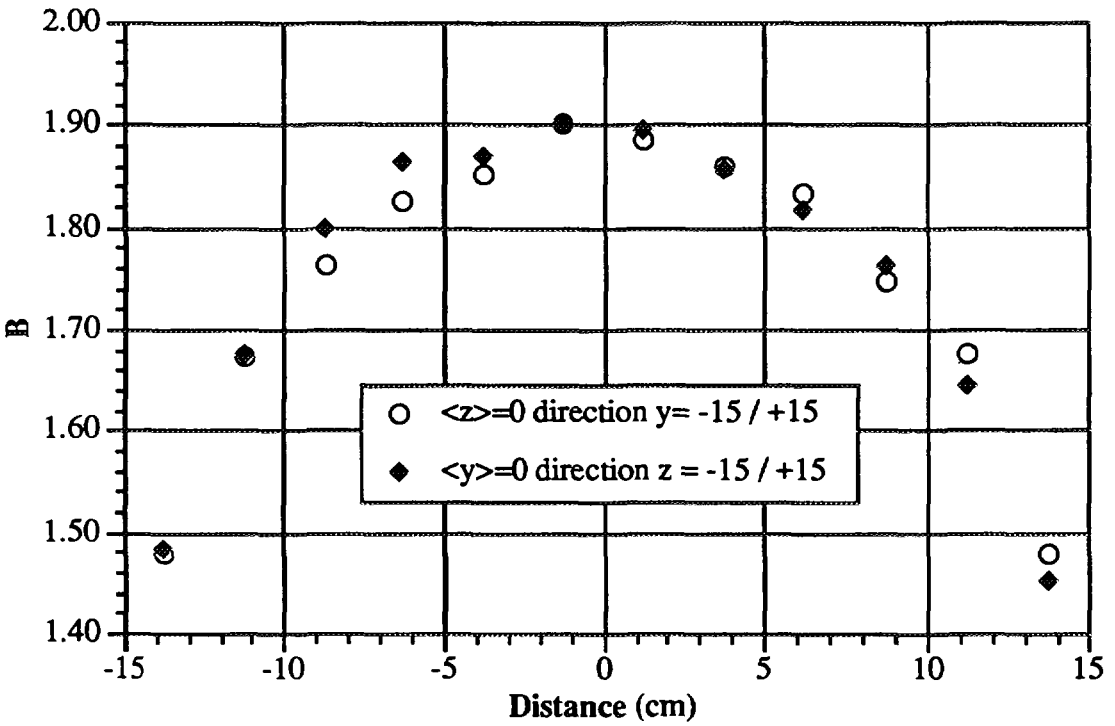

Fig. 20: Narrow Spectrum Series 80 kV. Air kerma backscatter profiles on the two slab centrelines (real source shape).

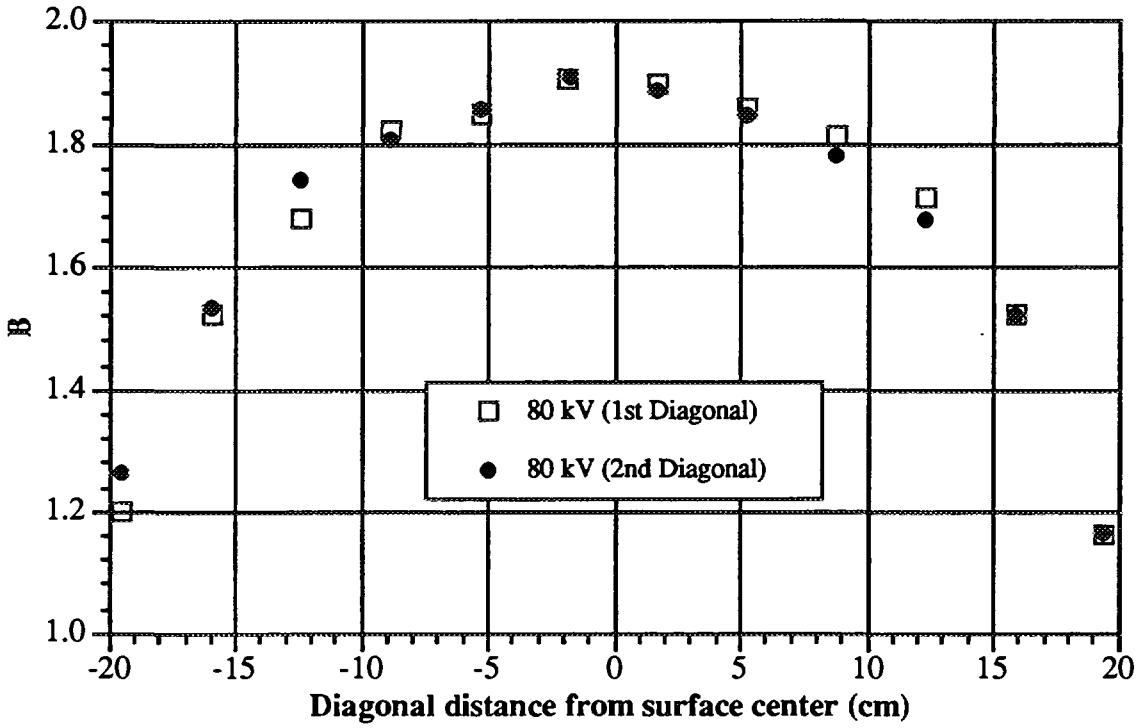

Fig. 21: Narrow Spectrum Series 80 kV. Air kerma backscatter profiles on the two slab diagonals (real source shape).

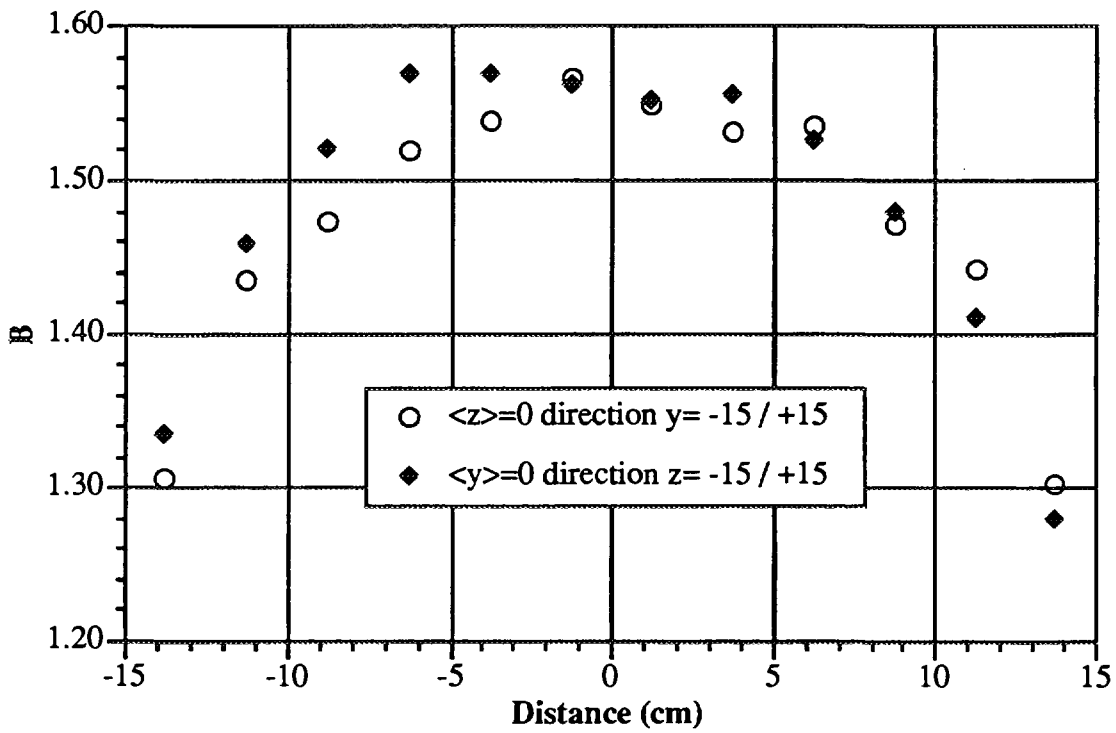

Fig. 22: Narrow Spectrum Series 150 kV. Air kerma backscatter profiles on the two slab centrelines (real source shape).

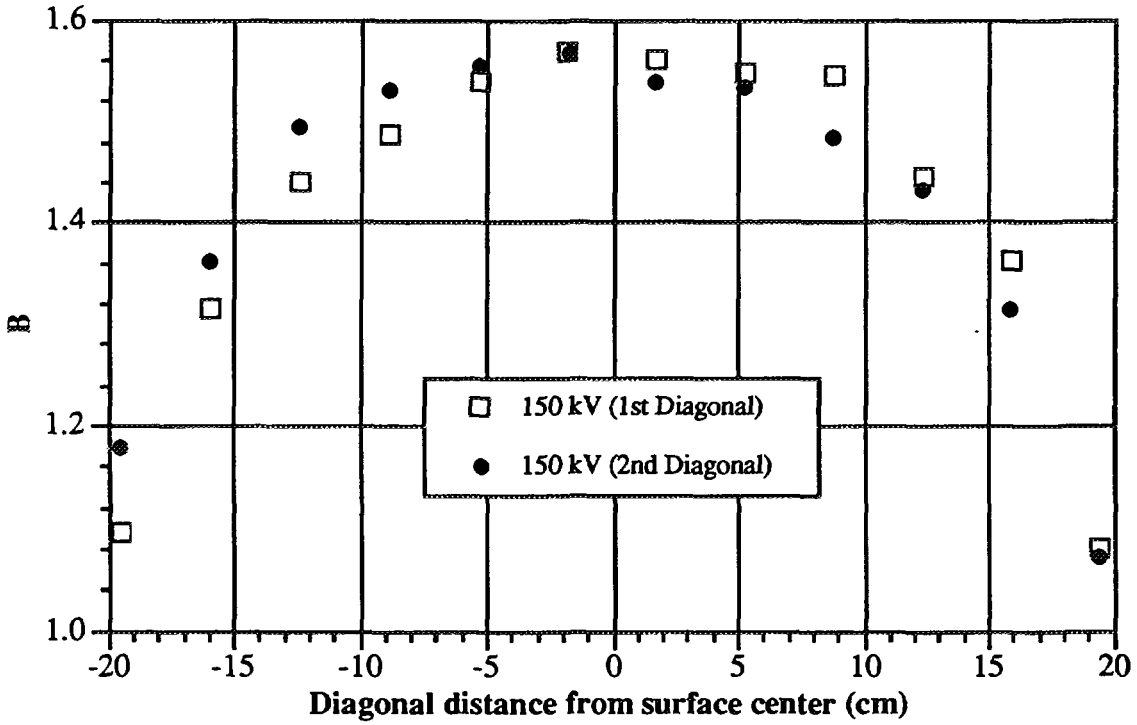

Fig. 23: Narrow Spectrum Series 150 kV. Air kerma backscatter profiles on the two slab diagonals (real source shape).

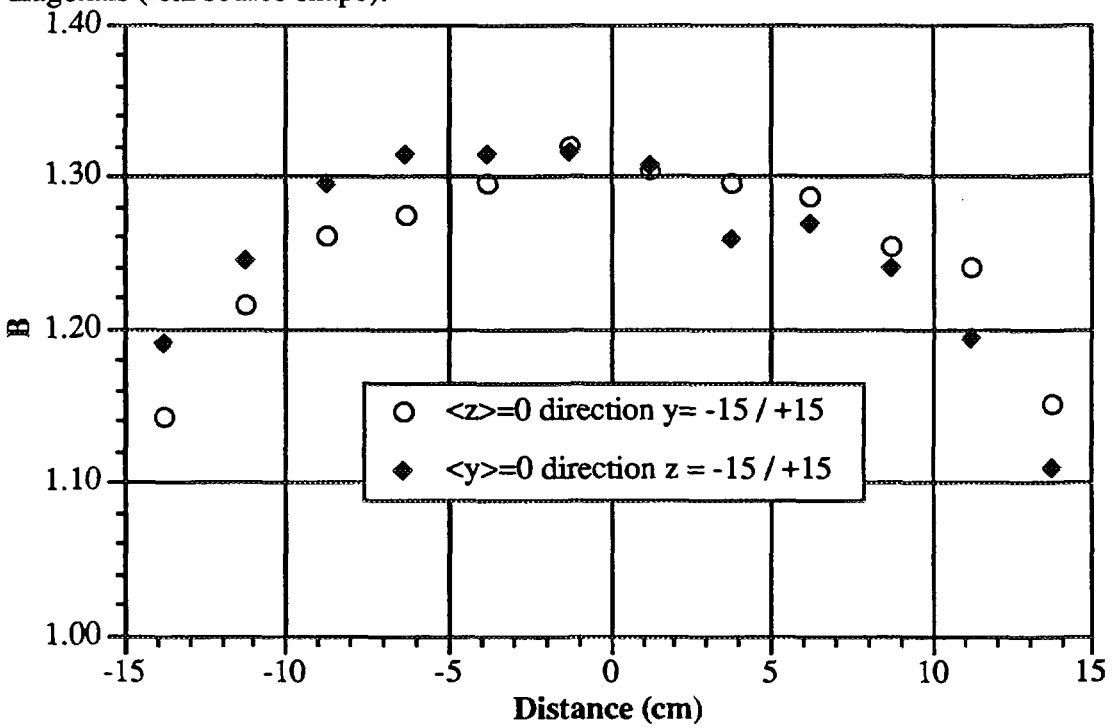

Fig. 24: Narrow Spectrum Series 300 kV. Air kerma backscatter profiles on the two slab centrelines (real source shape).

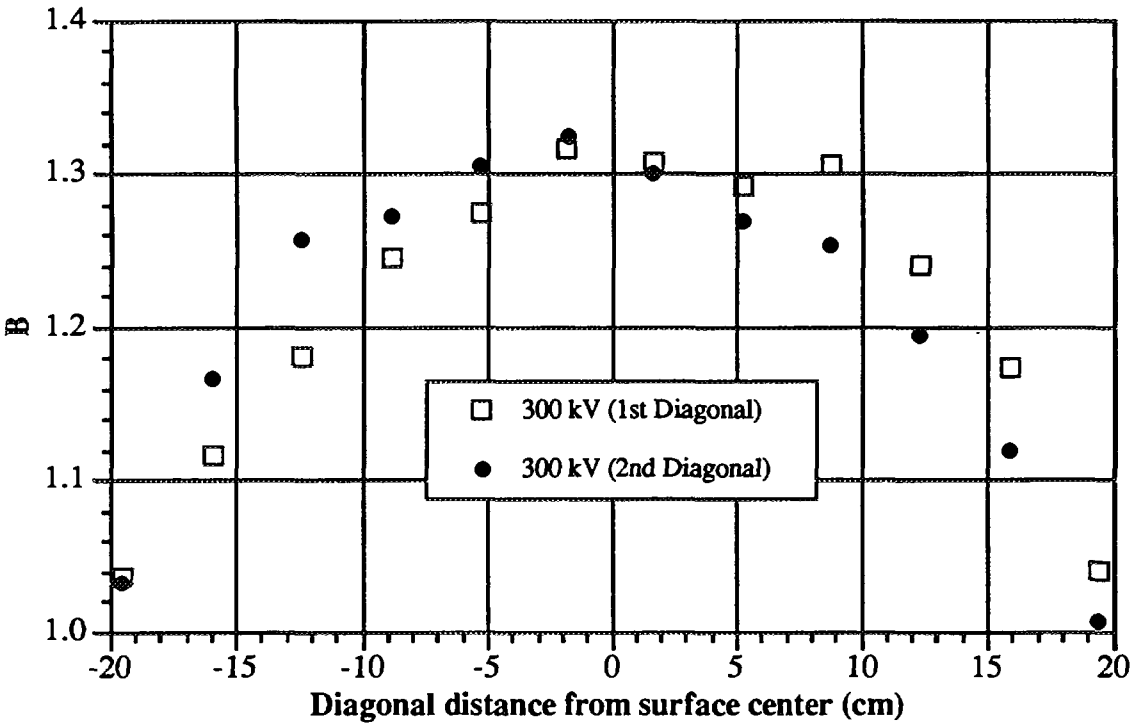

Fig. 25: Narrow Spectrum Series 300 kV. Air kerma backscatter profiles on the two slab diagonals (real source shape).

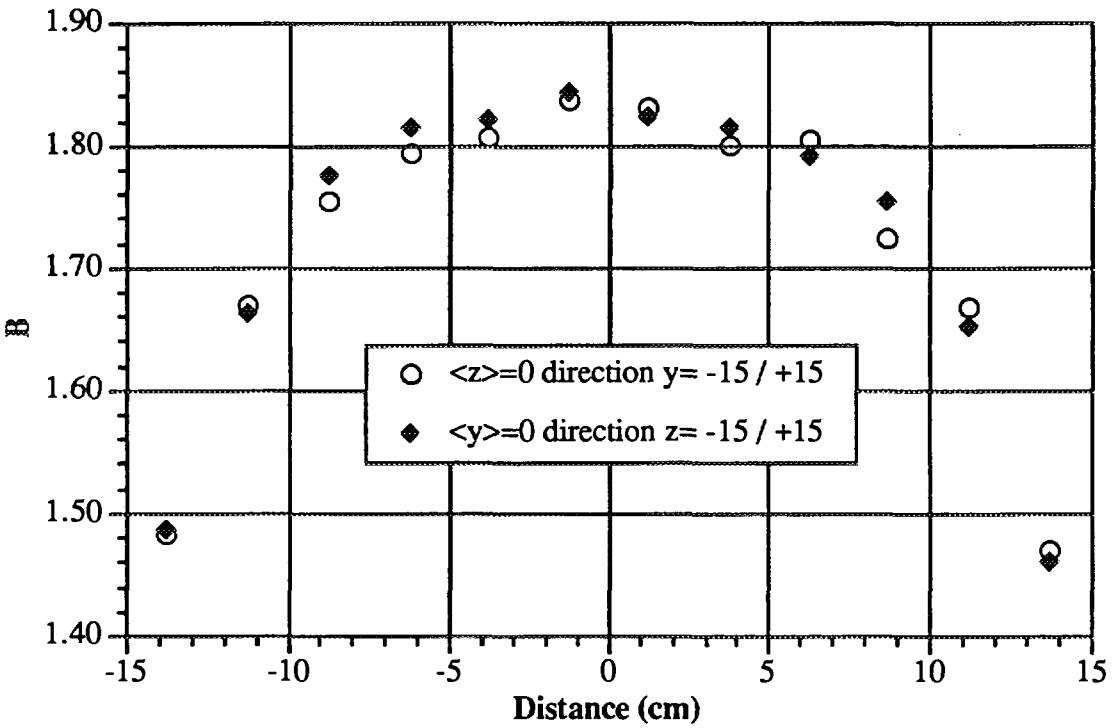

Fig. 26: Wide Spectrum Series 80 kV. Air kerma backscatter profile on slab centrelines on the two slab centrelines (real source shape).

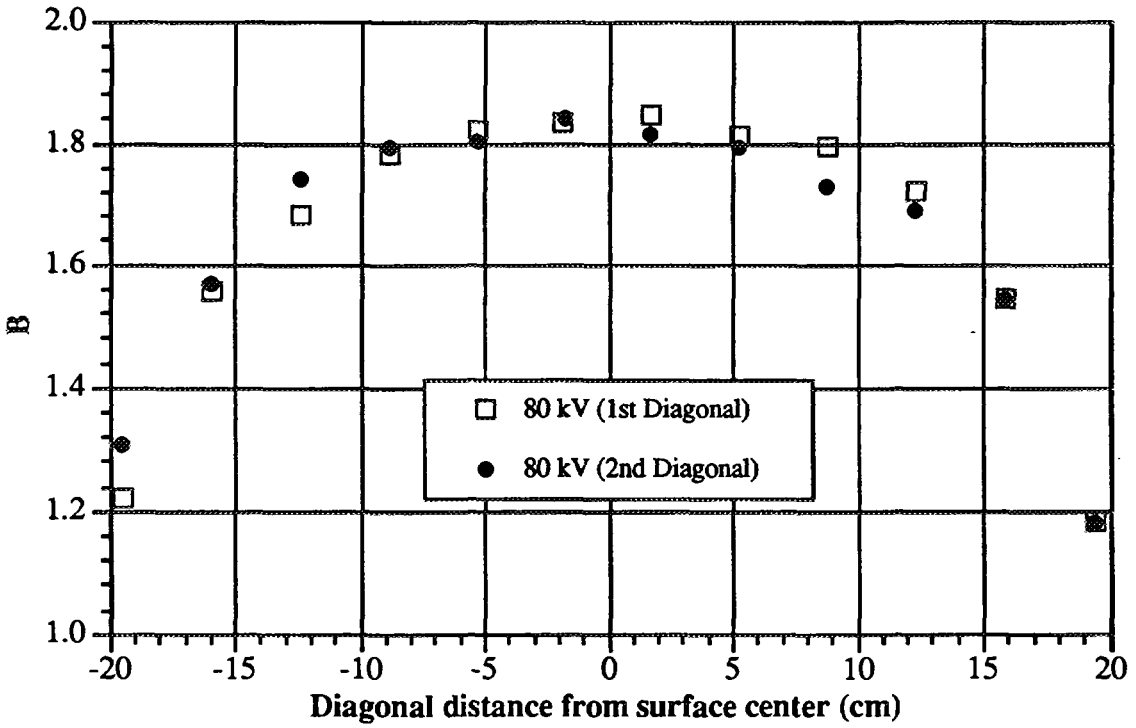

Fig. 27: Wide Spectrum Series 80 kV. Air kerma backscatter profile on slab centrelines on the two slab diagonals (real source shape).

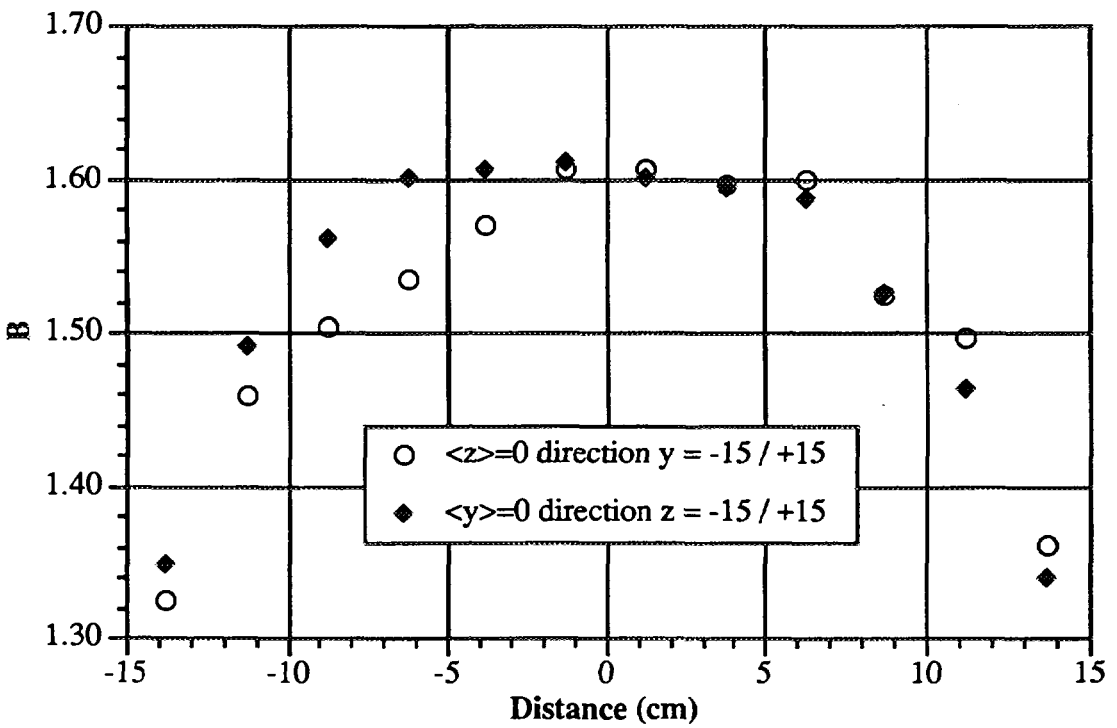

Fig. 28: Wide Spectrum Series 150 kV. Air kerma backscatter profile on slab centrelines on the two slab centrelines (real source shape).

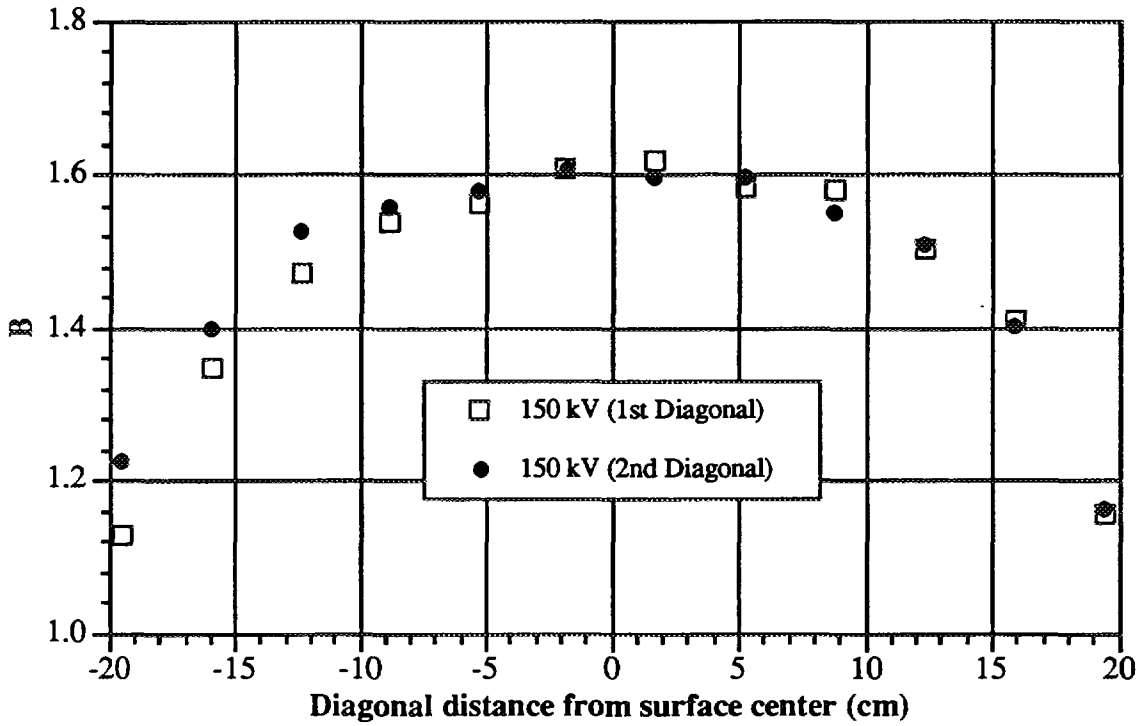

Fig. 29: Wide Spectrum Series 150 kV. Air kerma backscatter profile on slab centrelines on the two slab diagonals (real source shape).

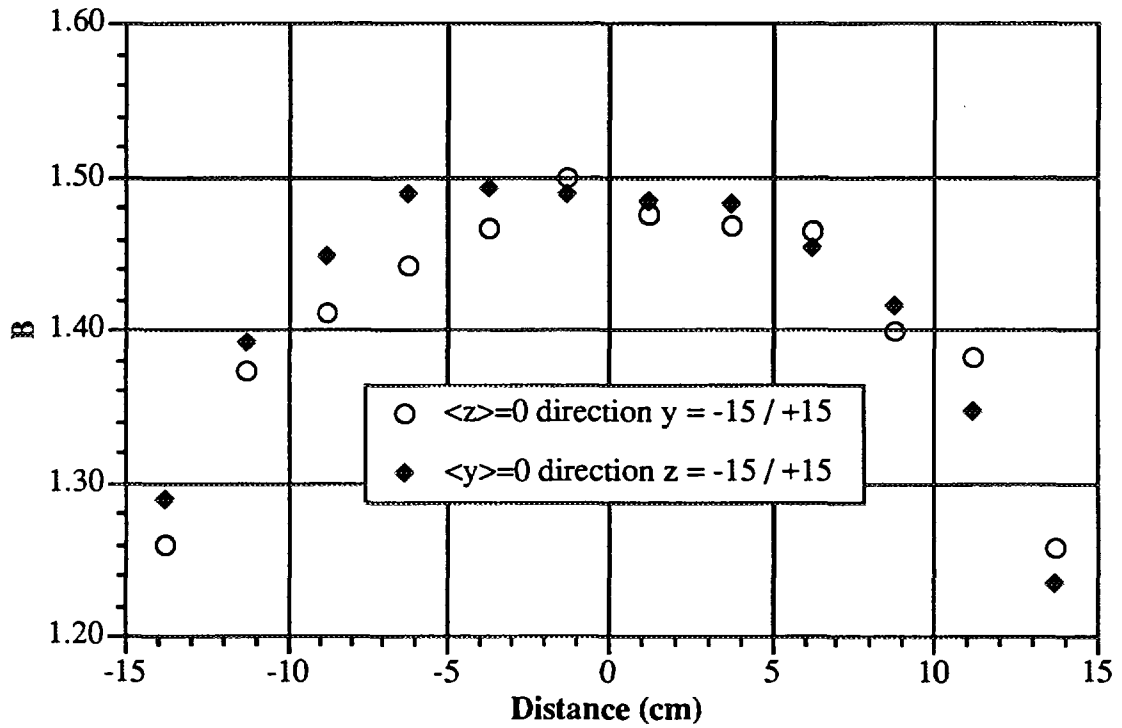

Fig. 30: Wide Spectrum Series 200 kV. Air kerma backscatter profile on slab centrelines on the two slab centrelines (real source shape).

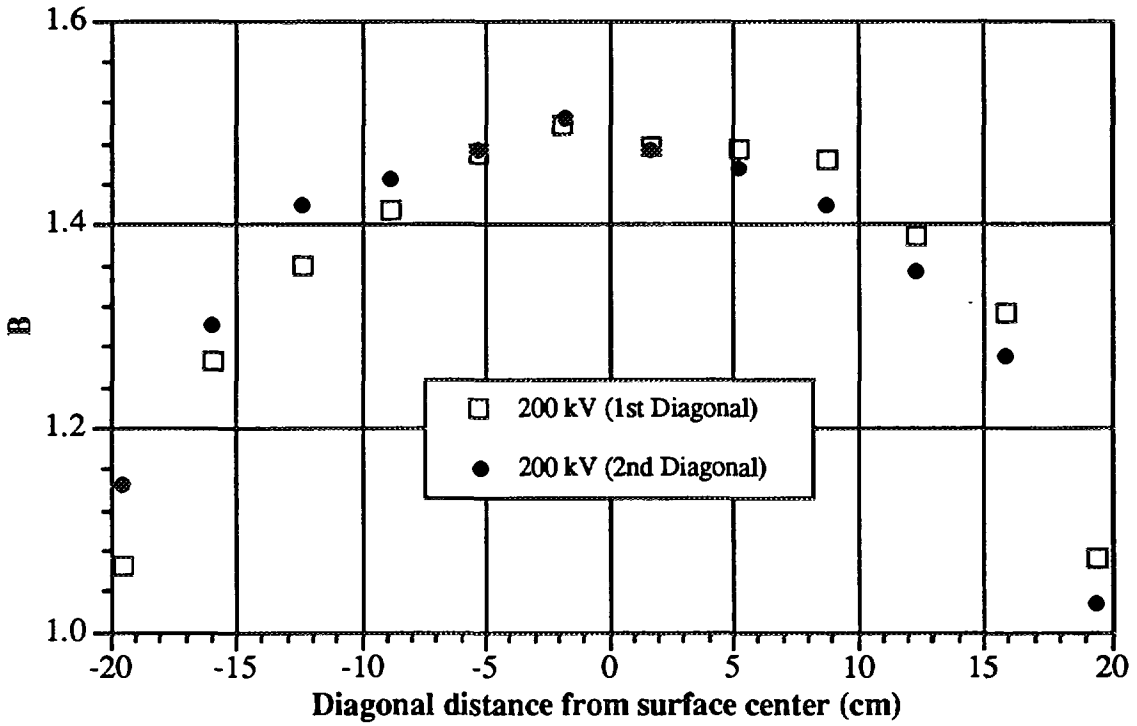

Fig. 31: Wide Spectrum Series 200 kV. Air kerma backscatter profile on slab centrelines on the two slab diagonals (real source shape).

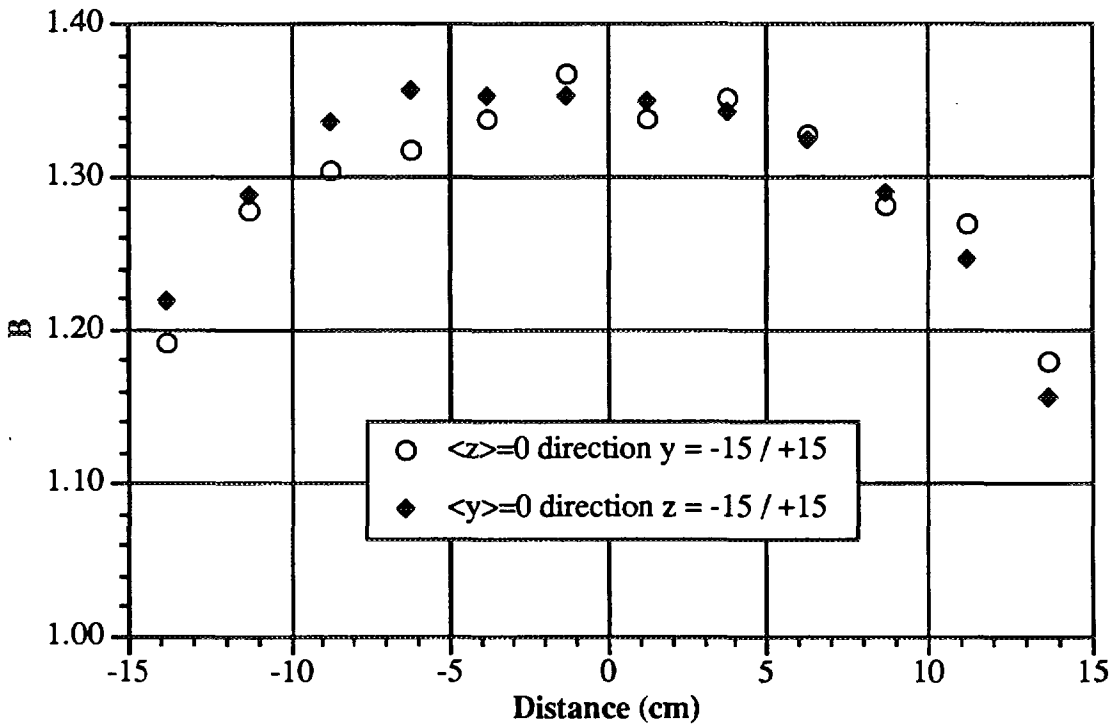

Fig. 32: Wide Spectrum Series 300 kV. Air kerma backscatter profile on slab centrelines on the two slab centrelines (real source shape).

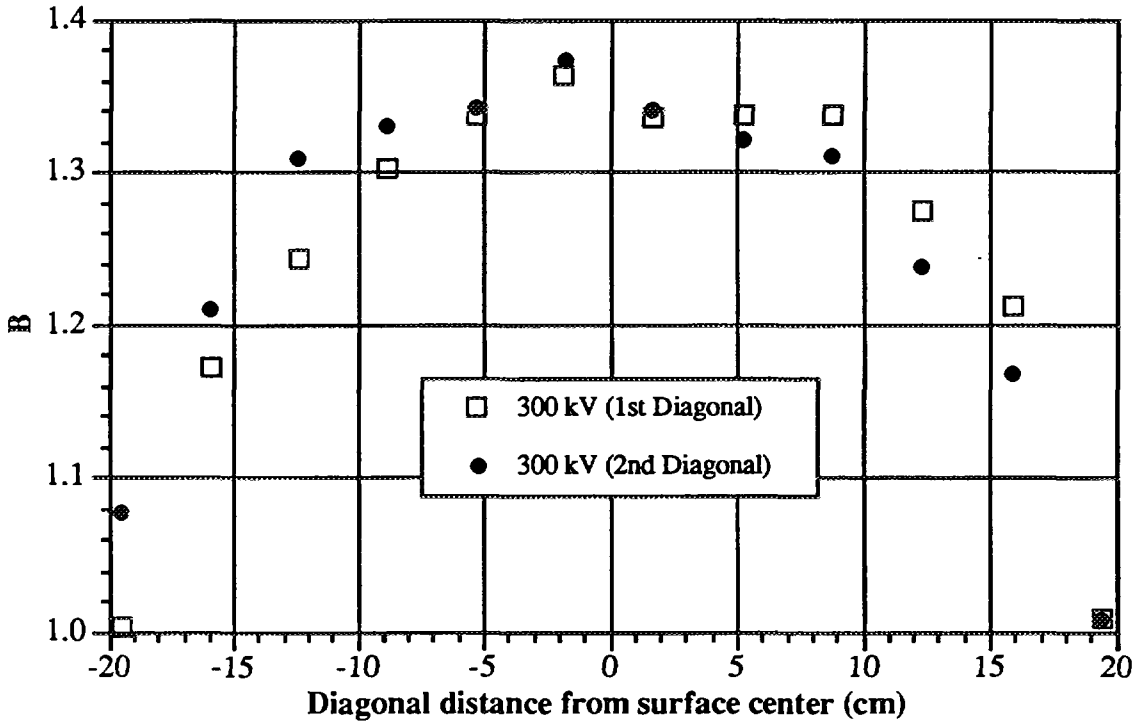

Fig. 33: Wide Spectrum Series 300 kV. Air kerma backscatter profile on slab centrelines on the two slab diagonals (real source shape).

Furthermore figures 34 - 40 supply arrays with the indication of the percentage deviation of backscatter factor for each card as compared with the central value on the surface (X symbols correspond to deviations of less than -1% from the maximum whilst & symbols correspond to deviation > 10%).

Narrow Spectrum Series
(80 kV)

&	&	&	&	&	&	&	&	&	&
&	&	&	9	7	7	9	&	&	&
&	8	4	5	4	4	5	7	10	&
&	6	5	3	1	3	3	4	7	&
&	7	3	2	X	1	1	3	8	&
&	7	4	2	X	X	2	4	8	&
&	7	3	2	1	2	2	3	7	&
&	7	5	3	1	1	4	5	8	&
&	9	9	6	6	6	6	&	&	&
&	&	&	&	&	&	&	&	&	&

&= >10%

Fig. 34

Narrow Spectrum Series
(150 kV)

&	&	&	&	10	10	&	&	&	&
&	9	8	6	6	6	6	8	9	&
&	6	6	6	3	3	4	6	8	10
9	5	3	3	X	1	1	1	6	8
8	7	3	3	X	2	2	3	8	8
10	6	3	1	X	X	3	1	6	9
7	6	2	X	X	1	2	3	6	9
10	5	3	X	X	X	1	1	6	&
&	5	3	4	3	3	2	5	8	10
&	&	10	7	8	7	10	7	10	&

&= >10%

Fig. 35

Narrow Spectrum Series
(300 kV)

&	&	&	&	&	&	&	&	&	&
&	&	&	8	7	7	8	8	&	&
9	6	6	6	4	4	5	5	8	8
8	4	3	3	2	3	4	3	6	9
8	4	3	3	X	2	X	3	6	7
9	4	3	X	X	X	3	3	4	7
6	4	3	X	X	2	2	3	4	8
8	4	3	X	X	X	X	1	4	8
&	5	3	3	3	2	1	4	7	7
&	8	7	4	7	6	7	6	8	&

&= >10%

Fig. 36

Wide Spectrum Series
(80 kV)

&	&	&	&	&	&	&	&	&	&
&	10	8	4	4	5	5	7	9	&
&	5	3	4	2	3	2	7	7	&
&	3	3	X	X	2	3	3	7	10
10	4	3	2	X	1	2	2	7	10
&	5	3	1	X	X	2	1	6	&
7	5	3	2	1	1	2	2	4	10
10	5	3	1	1	2	2	3	5	&
&	6	5	3	3	3	3	7	7	&
&	&	&	7	&	&	&	&	&	&

&= >10%

Fig. 37

Wide Spectrum Series
(150 kV)

&	&	&	&	&	&	&	&	&	&
&	&	10	9	7	7	6	7	9	&
&	9	6	7	3	3	3	5	5	10
&	5	5	4	1	3	2	2	3	8
&	8	6	3	1	2	3	2	7	9
&	7	6	3	1	X	1	1	6	8
&	8	4	3	X	X	2	X	5	8
&	7	4	1	3	X	1	3	5	10
&	7	5	5	5	3	2	5	8	&
&	&	&	8	9	8	&	&	&	&

&= >10%

Fig. 38

Wide Spectrum Series
(200 kV)

&	&	&	&	10	10	10	10	&	&
&	10	8	6	5	7	9	8	10	&
&	5	5	4	3	3	4	5	8	9
8	5	2	2	X	2	2	2	5	8
8	7	4	4	X	2	2	3	7	8
9	5	4	2	X	2	2	2	7	8
8	5	2	2	X	2	2	2	5	9
8	5	4	2	2	X	2	2	5	10
&	5	4	5	4	4	3	5	8	10
&	&	9	6	7	8	9	7	10	&

&= >10%

Fig. 39

Wide Spectrum Series (300 kV)

&	&	10	&	9	10	10	10	&	&
9	7	7	6	5	6	6	6	7	&
10	5	5	4	3	3	5	4	7	9
7	4	4	3	X	3	3	3	6	9
7	5	4	3	X	2	X	3	7	8
7	5	4	2	X	3	3	3	6	7
5	4	2	2	X	2	2	2	5	7
6	5	4	X	X	2	2	2	5	9
9	5	3	4	3	3	3	5	7	7
&	8	7	5	6	6	7	6	8	&

&= >10%

Fig. 40

The previous figures at first glance can provide an idea of the percentage deviation of the backscatter factor for each card location from the central value and can help the operator when deciding what area to employ for his calibration procedure to fulfil the ISO 5% requirement.
A quite significant asymmetry in the distribution has to be pointed out.
On the other hand, from the practical point of view, TLD cards have to be placed on square symmetric areas. Table 3.I supplies the values of the percentage deviation interval from the central value for the seven investigated beams in three different size calibration areas.

Tab. 3.I: Range of deviations from the maximum backscatter factor value as a function of calibration area.

Series		Calibration Area		
Beam	Voltage	10x10 cm^2	15x15 cm^2	20x20 cm^2
A80	80 kV	2% - 3%	5%	7% - >10%
A150	150 kV	1% - 3%	3% - 6%	2% - 9%
A300	300 kV	1% - 4%	1% - 6%	1% - >10%
B80	80 kV	1% - 3%	1% - 7%	3% - 10%
B150	150 kV	1% - 4%	1% - 6/7%	2% - >10%
B200	200 kV	1% - 2%	2% - 5%	3% - 10%
B300	300 kV	1% - 3%	2% - 5%	3% - 7%

Some comparisons were performed with experimental data from Mc Clure and Steele /14/

They performed measurements using the ISO 100 kV Narrow Spectrum Series. Nine LiF TLDs were placed on the horizontal centreline of a crude water commercial phantom.
The comparison was possible only with the MCNP results in the simplified condition of parallel homogeneous beam (see appendix A). Table 3.II supplies the values of the measured and calculated variations as a function of the distance from the central beam.

Tab. 3.II: Comparison between MCNP and experimental results on the calibration phantom centreline for ISO 100 kV Narrow Series X-ray beam.

Distance from the beam centre	5 cm	7.5 cm	10. cm
MCNP PMMA	1%	3-4%	7%
MCNP WATER in PMMA	<1%	2%	6-7%
Mc. Clure WATER in PMMA	1%	2-3%	4-6%

Taking into account the intrinsic uncertainty of the single TLD measurements as well as the fluctuations associated with the Monte Carlo approach, the comparison has to be considered satisfactory.

Another confirmation of the Monte Carlo results is based on the already mentioned data obtained by Will. The paper does not report results in tabular form and the general conclusion was: "Thus it can be concluded that the dose rate across the axis changes by not more than 2% up to a distance from the central beam of about 5 cm and by less than 5% up to 8 cm. The latter distance is about half of the width of the phantom...". Again a qualitative agreement with the calculated limits has to be pointed out, notwithstanding the fact that a more detailed comparison should be interesting.

4. CONCLUSIONS

A rather comprehensive study on the homogeneity areas for contemporary calibration of photon personal dosemeters has been carried out using the Monte Carlo code MCNP. The study was performed for both normal and oblique incidence and was concerned with homogeneous theoretical parallel beams as well as realistic beams. Some simplifications on the spectra had to be introduced to treat the realistic source situation.
Experimental data obtained on the phantom centrelines substantially confirmed the numerical evaluations.
As far as the irradiation with oblique incidence is concerned, it was shown that the homogeneity limits on the phantom's front face are the same as for the normal incidence, if two irradiation equal time steps are adopted in the calibration procedure.
A more comprehensive 2-dimensional experimental study of the homogeneity area should be of interest to be compared with the numerical study especially around the corners of the investigated area. In this case a good choice could be to adopt micro ionisation chambers to scan the area of interest.
Furthermore also the availability of experimental data for oblique incidence should be interesting to investigate the irradiation criteria for this situation.
Due to the fact that the beam behaviour can be in practice described by its mean energy /13/, the homogeneity limits stated for the investigated ISO X-ray beams can be used for other beams

with the same (or close) mean energy.

Acknowledgement: The authors are indebted with Dr. B. Grosswendt of PTB Braunschweig for supplying measured data used in the MCNP calculations.

References

/1/ ICRU Report 47 "Measurement of Dose Equivalents from External Photon and Electron Radiations". Bethesda Maryland (1992).
/2/ ICRU Report 51 "Quantities and Units in Radiation Protection Dosimetry". Bethesda Maryland (1993).
/3/ ICRU Report 39 "Determination of Dose Equivalents Resulting from External Radiation sources.", Bethesda - Maryland (1985).
/4/ Bohm J. "Minutes of the ISO/TC85/SC2/WG2 Meeting in London on 25-27 October 1993", PTB Braunschweig, November 1993.
/5/ ISO X and Gamma Reference Radiations for Calibrating Dosemeters and Dose Ratemeters and for Determining their Response as a Function of Energy. ISO 4037 (Geneva: ISO) (1979).
/6/ Laitano F., Toni M.P. et al. " Energy Distributions and B.I.P.M. References Filtered X-Radiation", ENEA Report, December 1990.
/7/ Shimizu S. and Minami K. "Relation between degree of X-ray monochromaticity and dose distribution non-uniformity of irradiation field" IAEA-SM-330/11.
/8/ Will W. "Homogeneity of photon fields for calibrating individual dosemeters on a slab phantom" Rad. Prot. Dosim. Vol. 48 N°3 (1993).
/9/ Grosswendt B: private communication
/10/ "MCNP: A General Monte Carlo Code for Neutron and Photon Transport". LA-7396-M rev. Sept 2 (1986).
/11/ J. H. Hubbell, et al. "Atomic Form Factors, Incoherent Scattering Functions, and Photon Scattering Cross Sections." J. Phys. Chem. Ref. Data 4,471 (1975)
/12/ Bartlett D.T., Dimbylow P.J. and Francis T.M. "Calculated Backscatter from Phantoms for Photon Dosemeter Calibration." Rad. Prot. Dosim. Vol. 32 N°2 (1990)
/13/ Gualdrini G. F. and Morelli B. " Air Kerma to Personal Dose Equivalent Conversion Factors for the ICRU and ISO Recommended Slab Phantoms for Photons from 20 keV to 1 MeV." RT/ENEA/AMB in press
/14/ M. Clure D. M. and Steele J. D. "The Use of Phantoms in the Calibration and Type Testing of Photon Personal Dosemeters." IRPA Regional Congress on Radiological Protection Portsmouth 94 Proceedings Pages 77-88 Nuclear Technology Publishing.

APPENDIX A

Backscatter Factor as a function of distance from PMMA and Water in PMMA slab central axis for Narrow and Wide Spectrum Series

Narrow Spectrum Series (S1 40 kV) - PMMA slab phantom

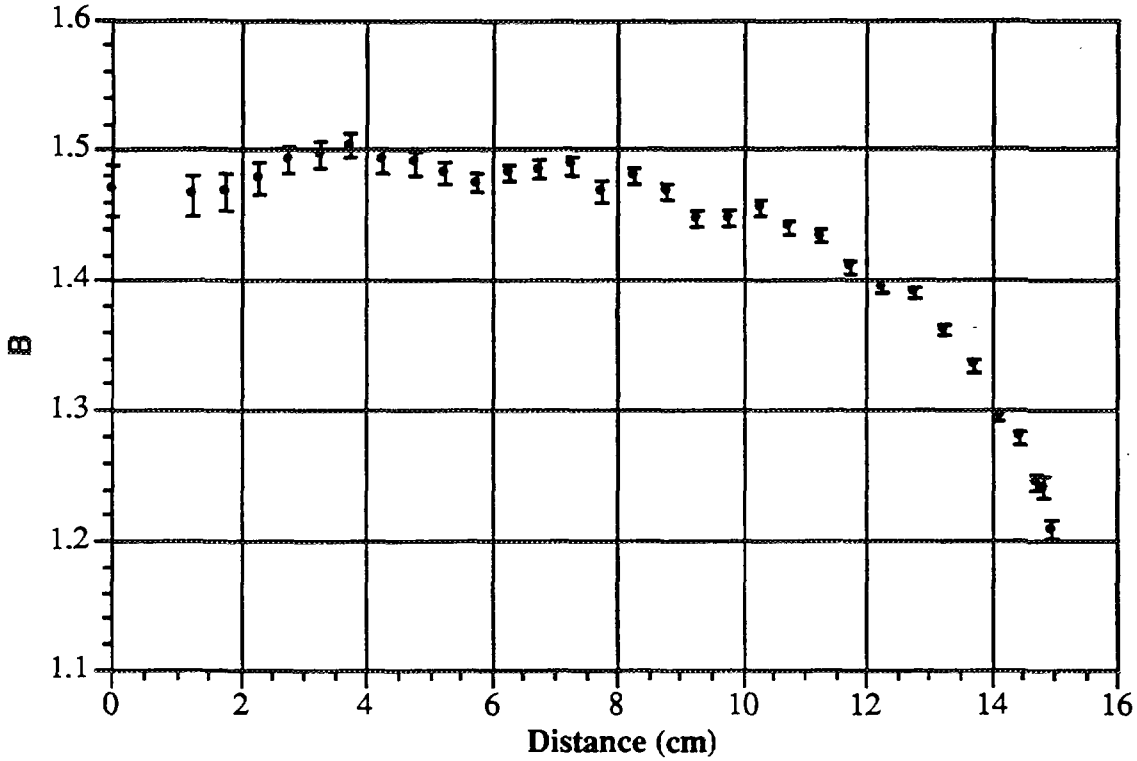

Narrow Spectrum Series (S1 40 kV) - Water in PMMA slab phantom

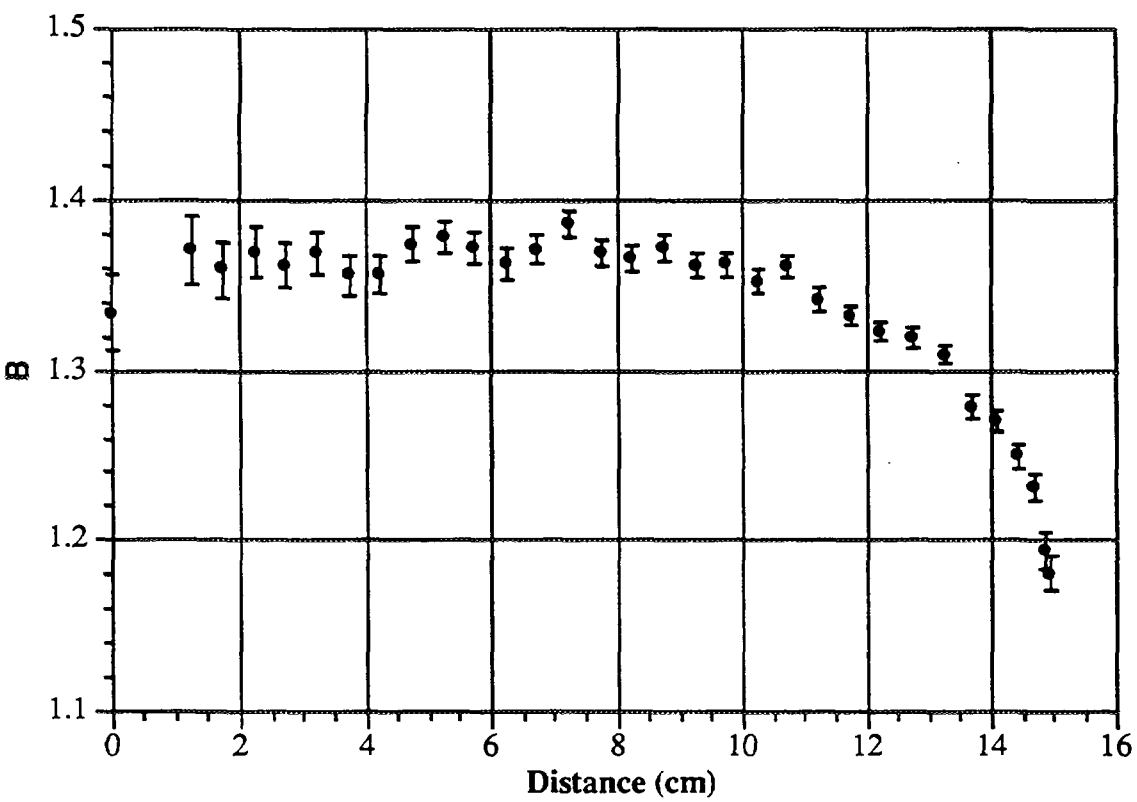

Narrow Spectrum Series (S2 60 kV) - PMMA slab phantom

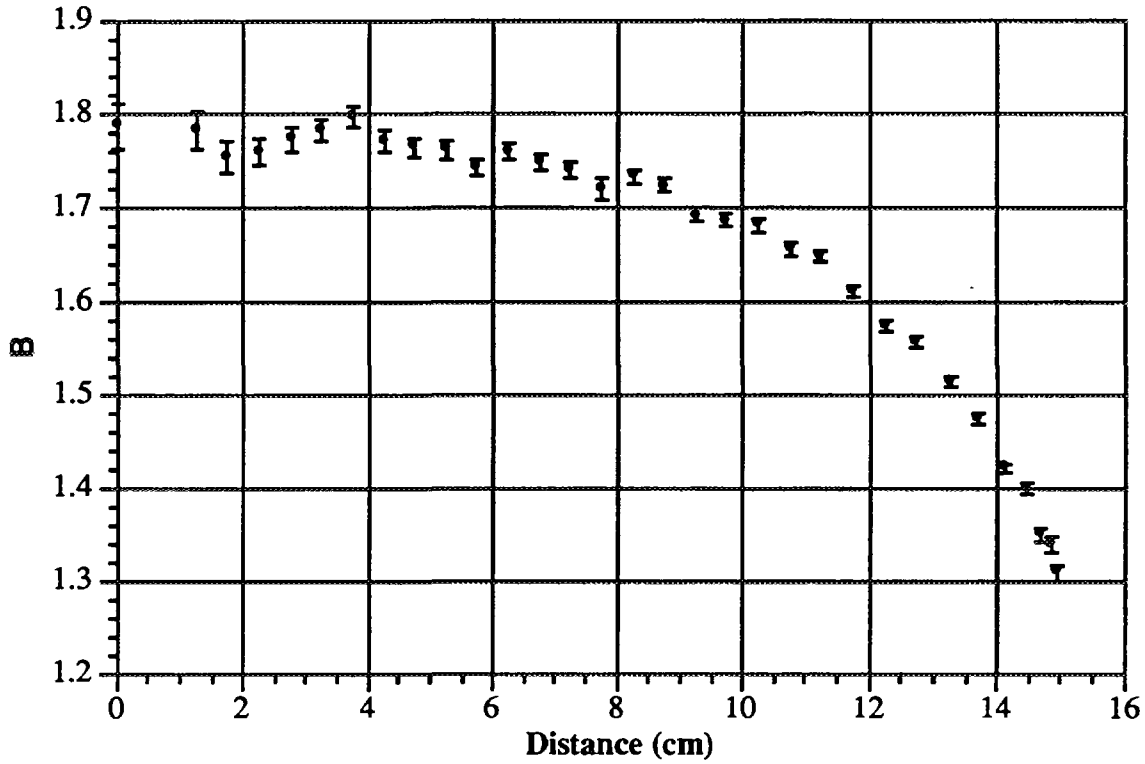

Narrow Spectrum Series (S2 60 kV) - Water in PMMA slab phantom

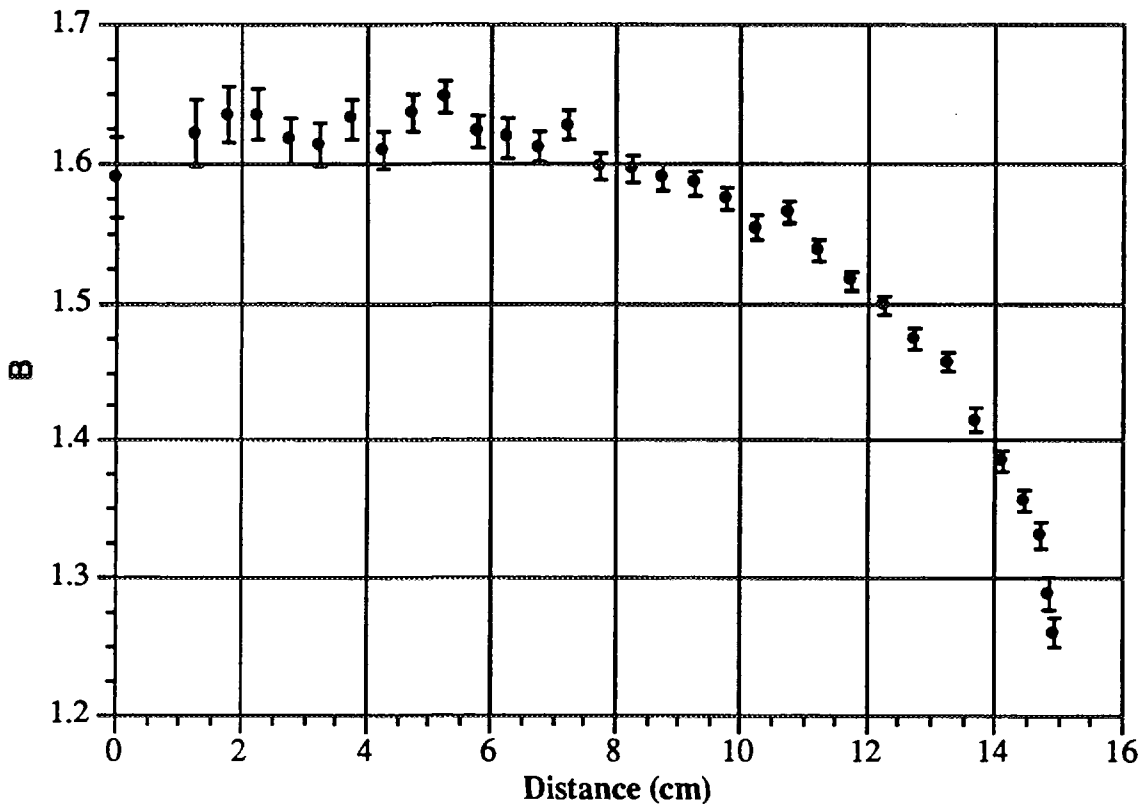

Narrow Spectrum Series (S3 80 kV) - PMMA slab phantom

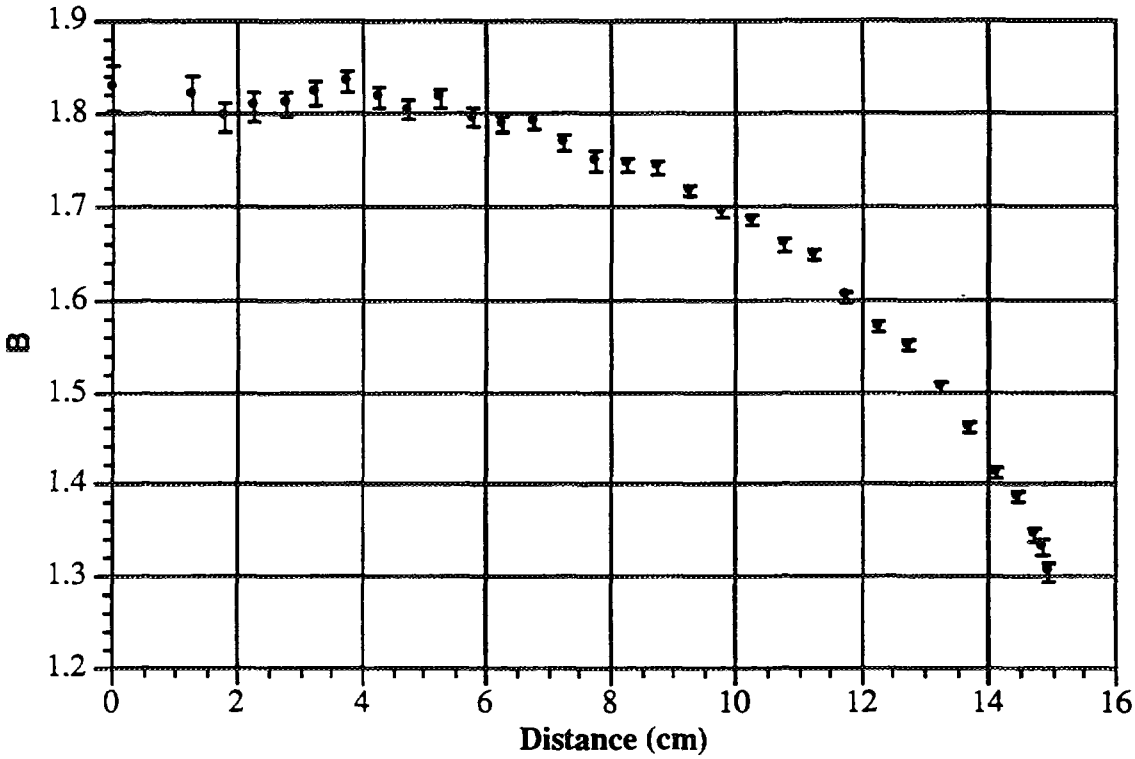

Narrow Spectrum Series (S3 80 kV) - Water in PMMA slab phantom

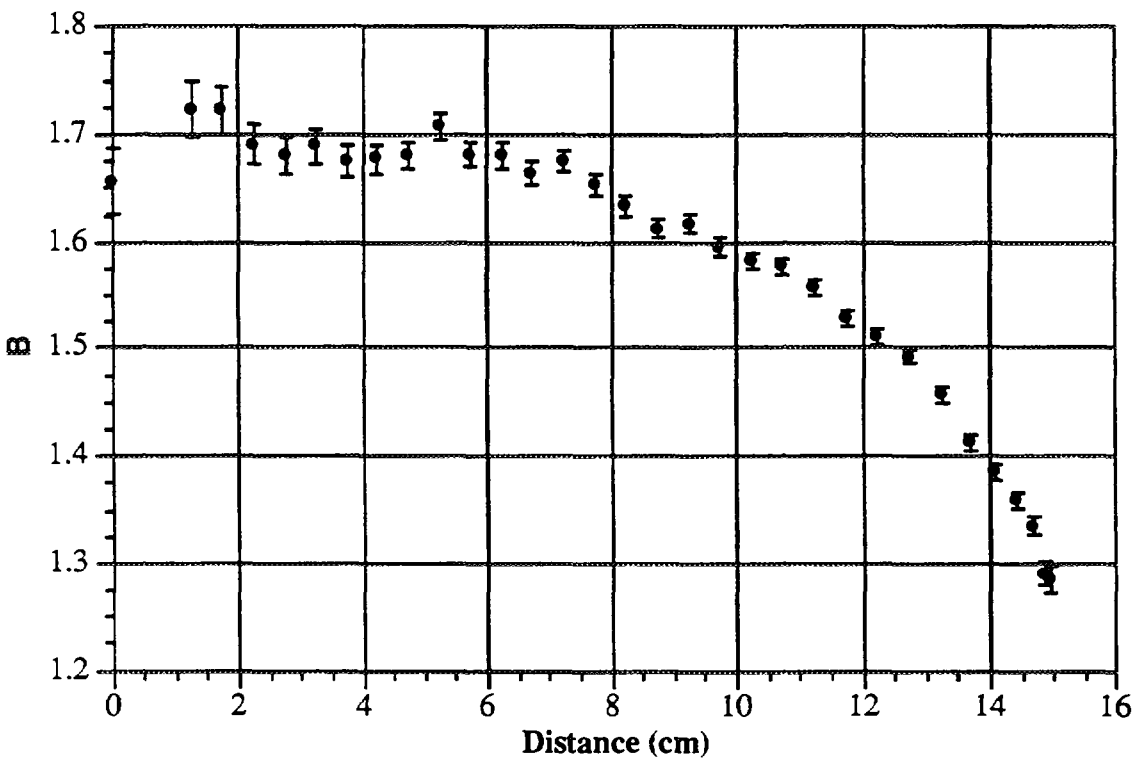

Narrow Spectrum Series (S4 100 kV) - PMMA slab phantom

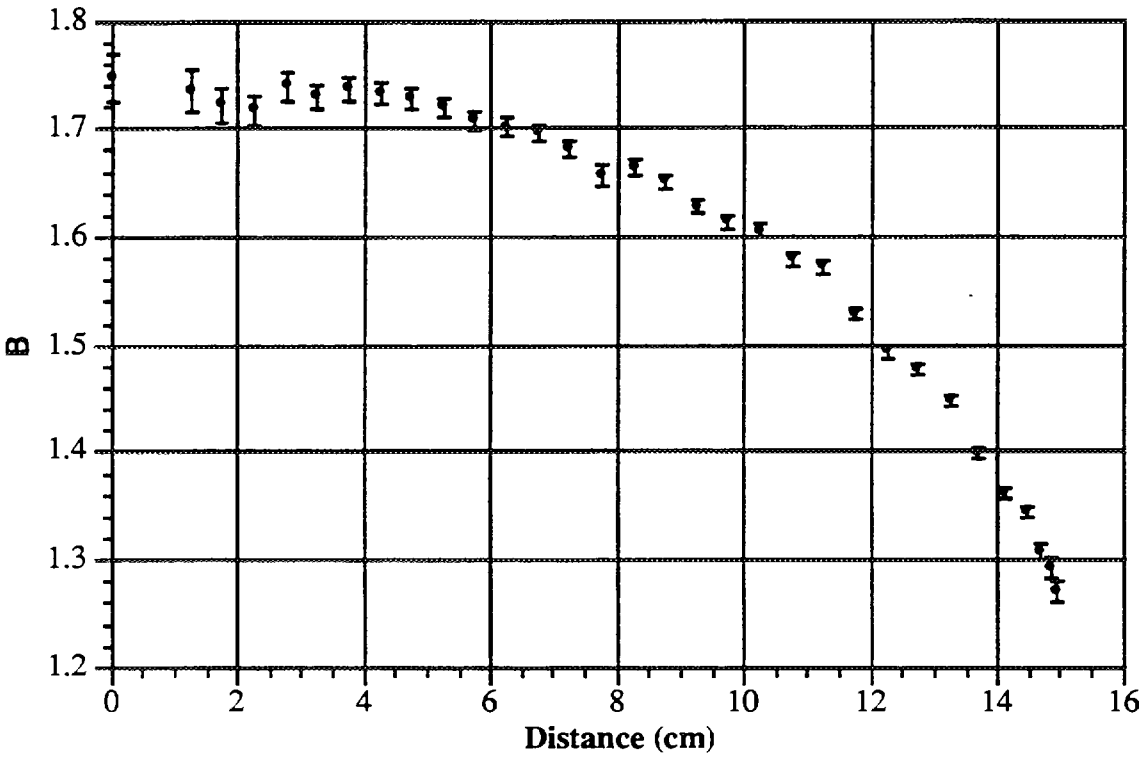

Narrow Spectrum Series (S4 100 kV) - Water in PMMA slab phantom

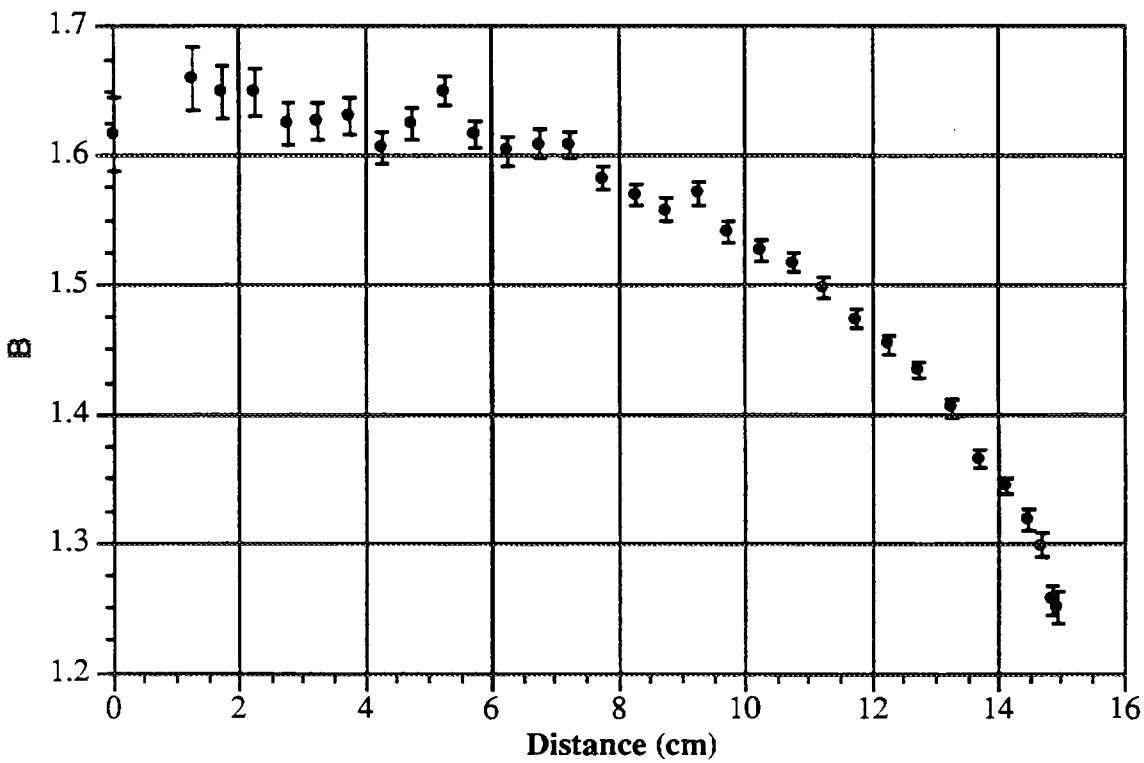

Narrow Spectrum Series (S5 120 kV) - PMMA slab phantom

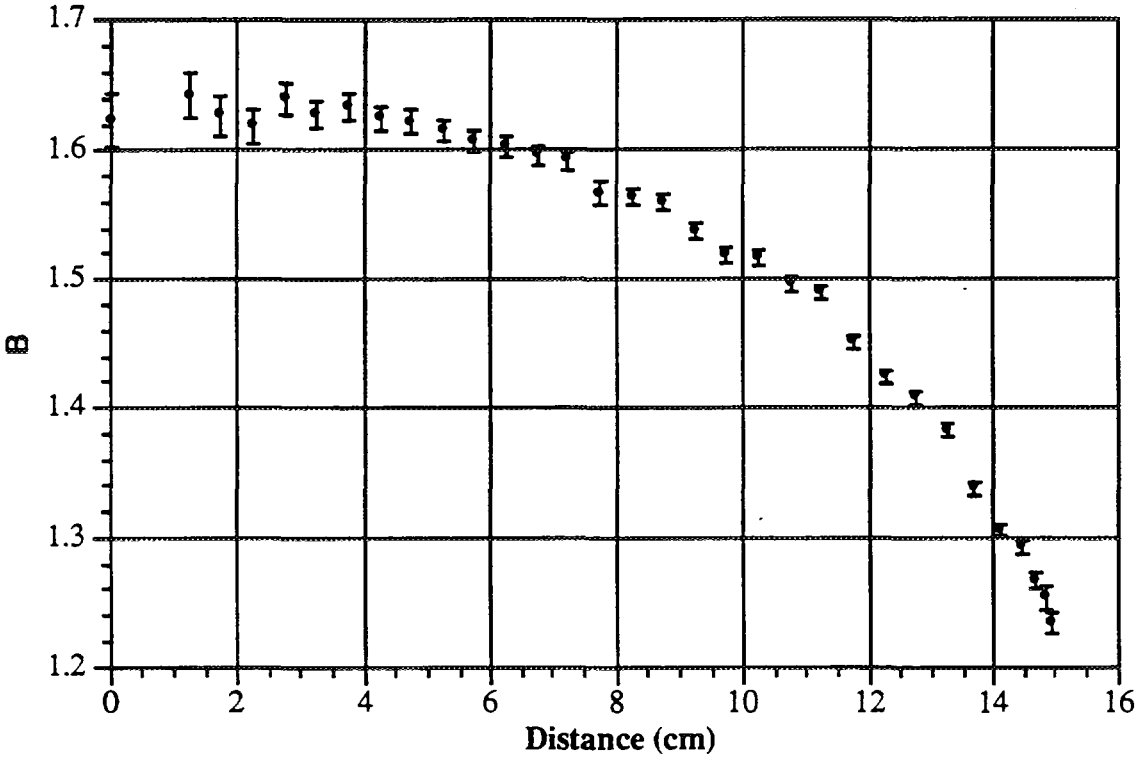

Narrow Spectrum Series (S5 120 kV) - PMMA slab phantom

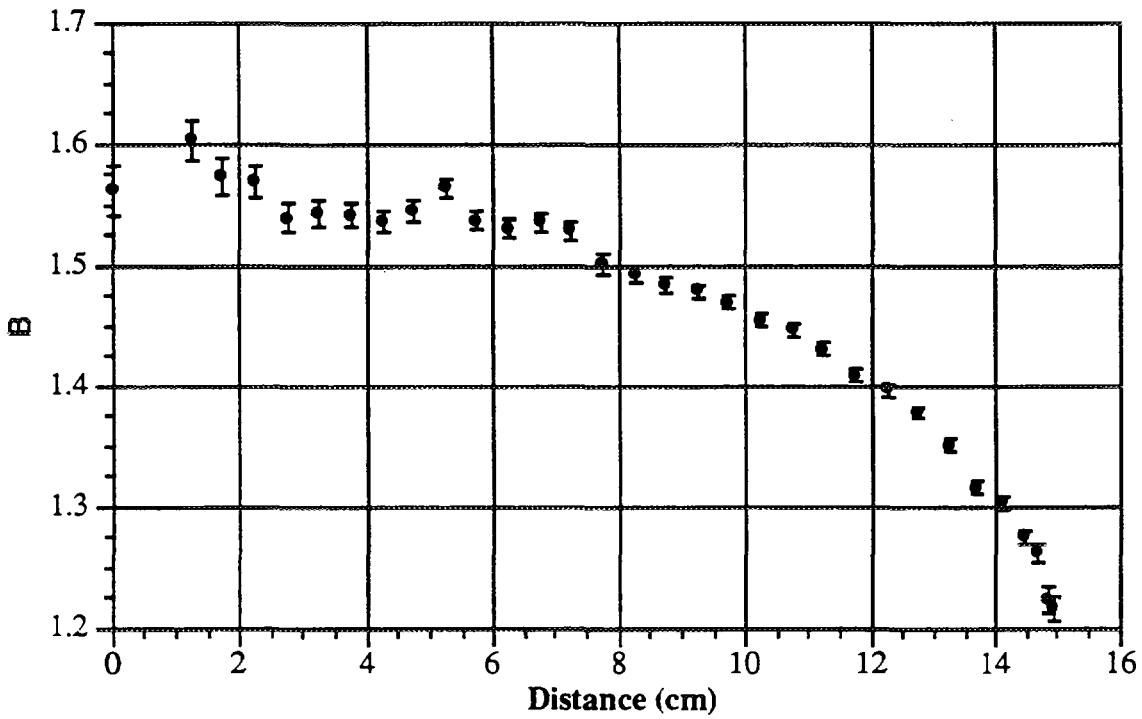

Narrow Spectrum Series (S6 150 kV) - PMMA slab phantom

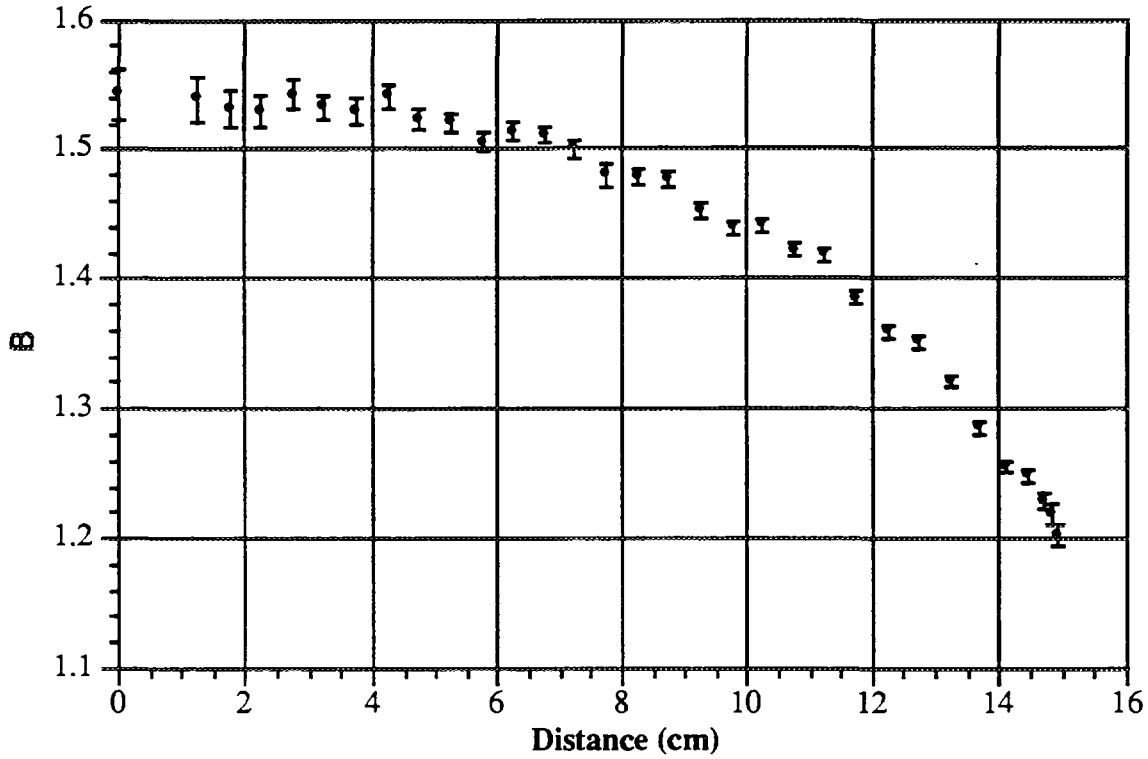

Narrow Spectrum Series (S6 150 kV) - Water PMMA slab phantom

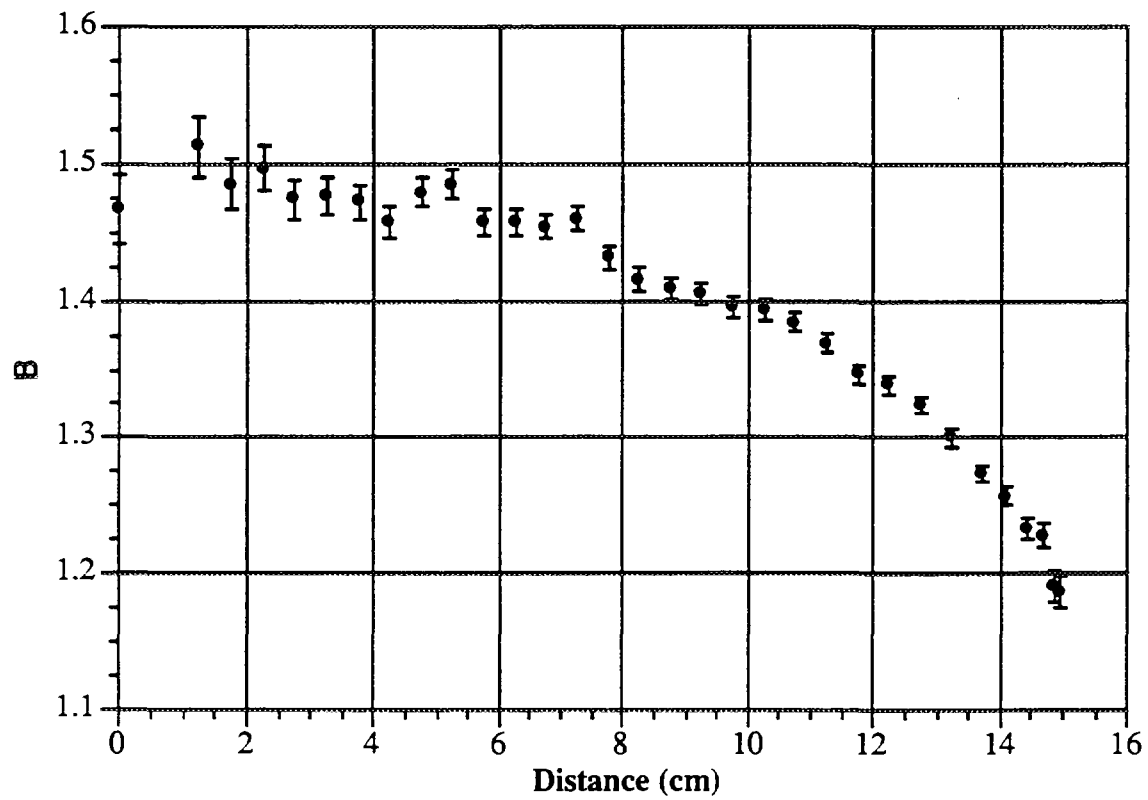

Narrow Spectrum Series (S7 200 kV) - PMMA slab phantom

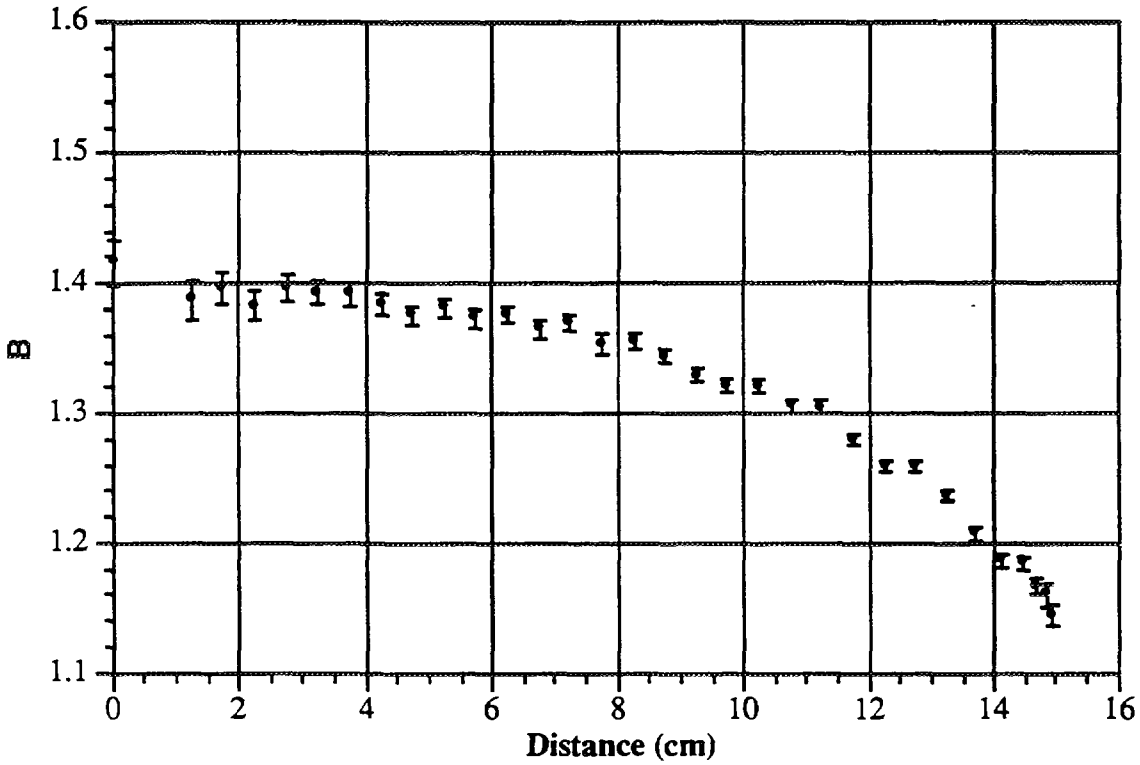

Narrow Spectrum Series (S7 200 kV) - Water in PMMA slab phantom

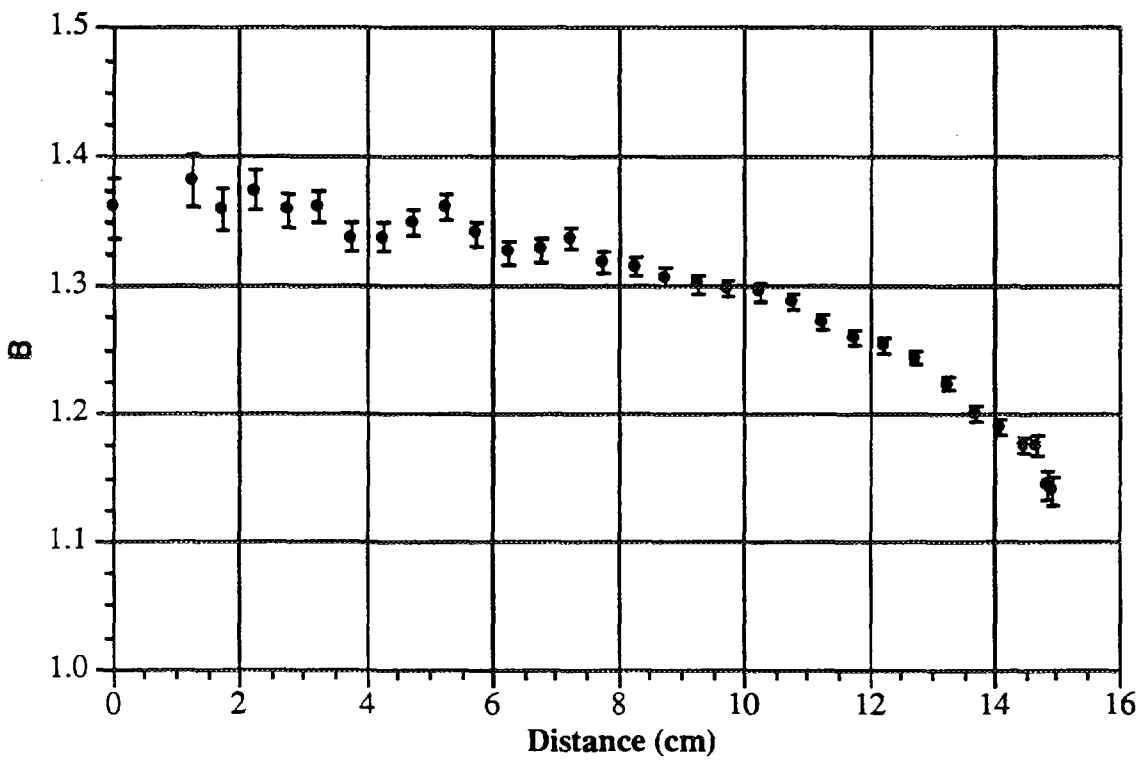

Narrow Spectrum Series (S8 250 kV) - PMMA slab phantom

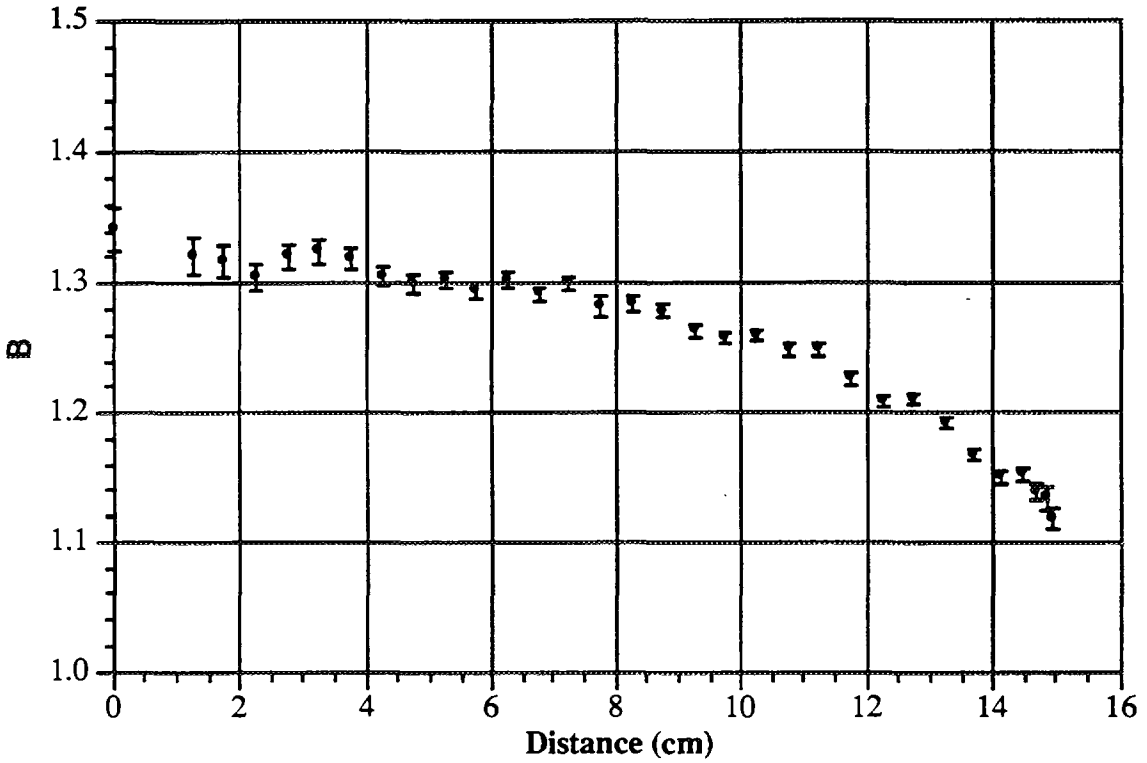

Narrow Spectrum Series (S8 250 kV) - Water in PMMA slab phantom

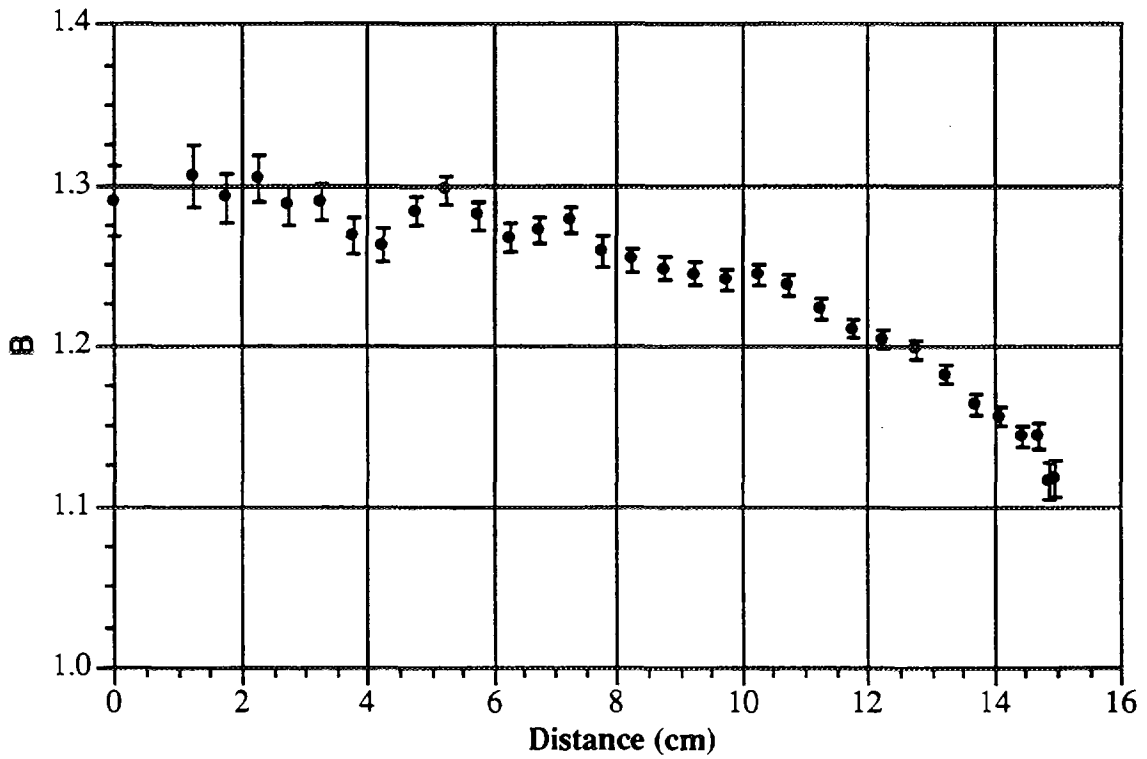

Narrow Spectrum Series (S9 300 kV) - PMMA slab phantom

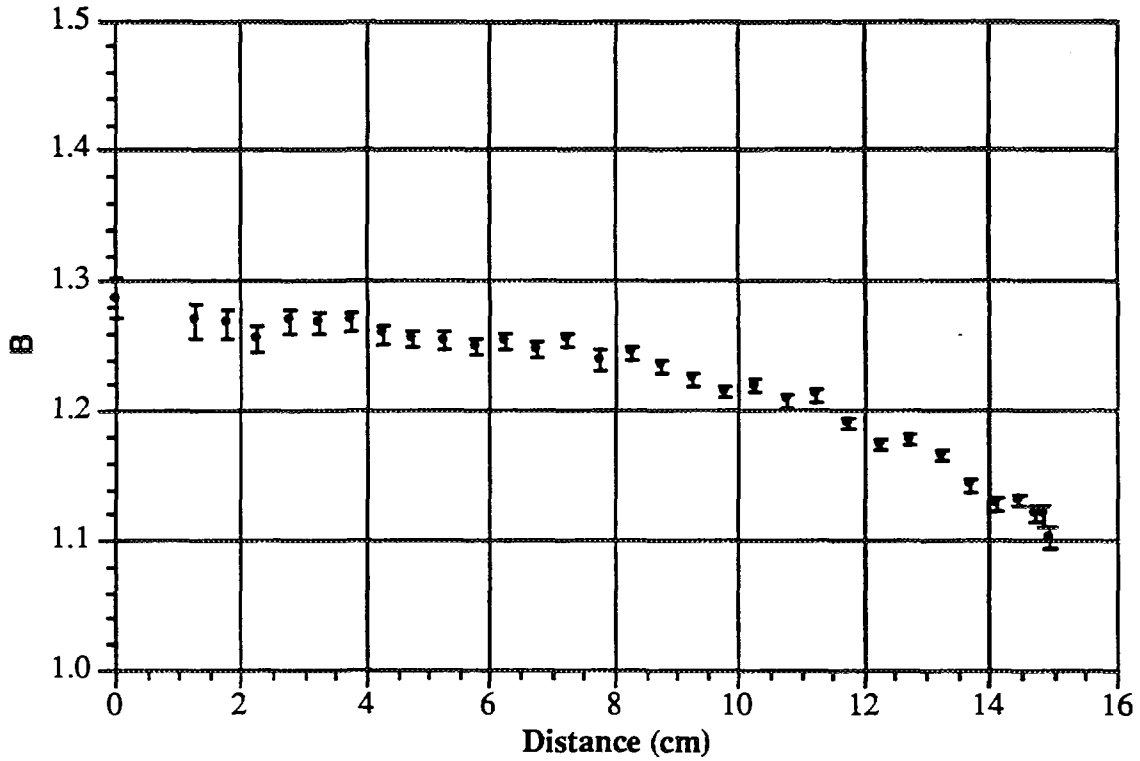

Narrow Spectrum Series (S9 300 kV) - Water in PMMA slab phantom

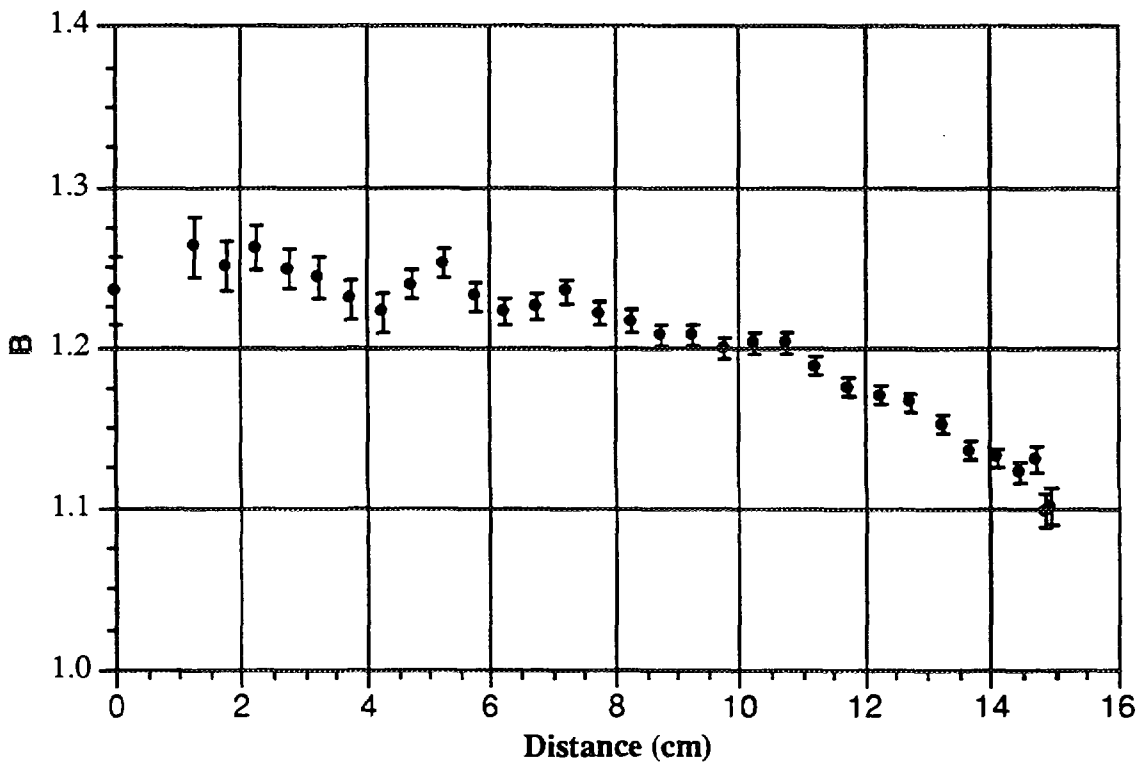

Wide Spectrum Series (L1 60 kV) - PMMA slab phantom

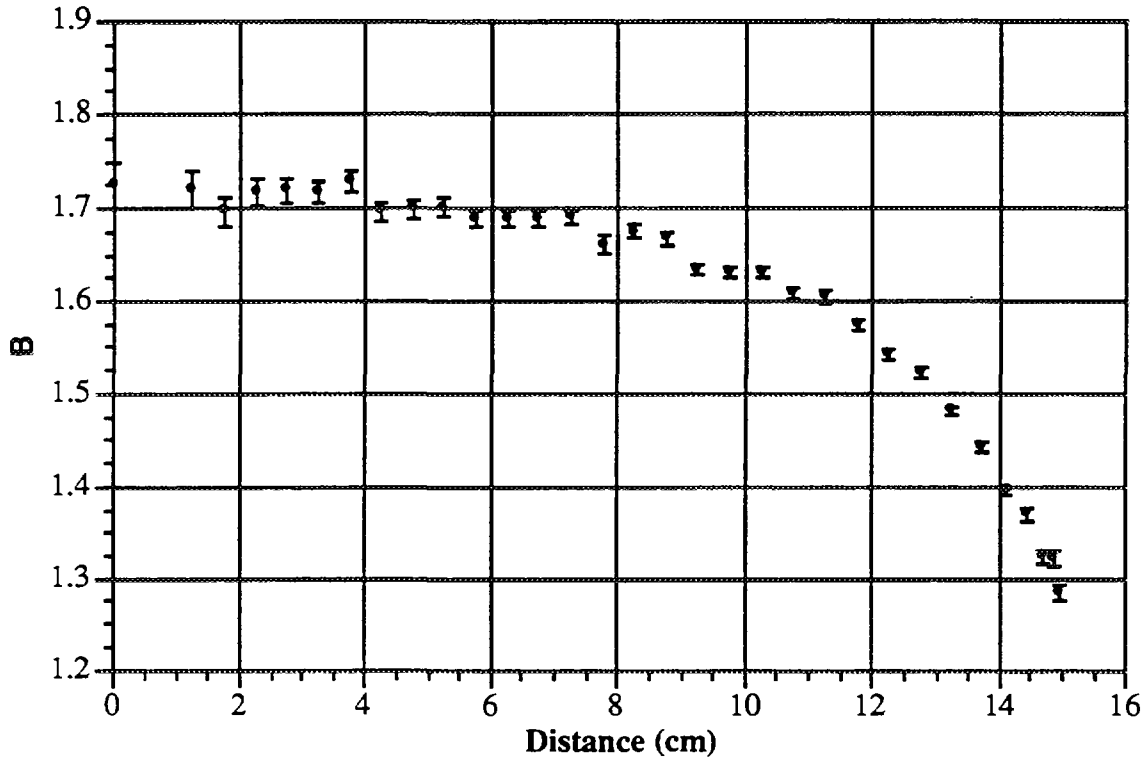

Wide Spectrum Series (L1 60 kV) - Water in PMMA slab phantom

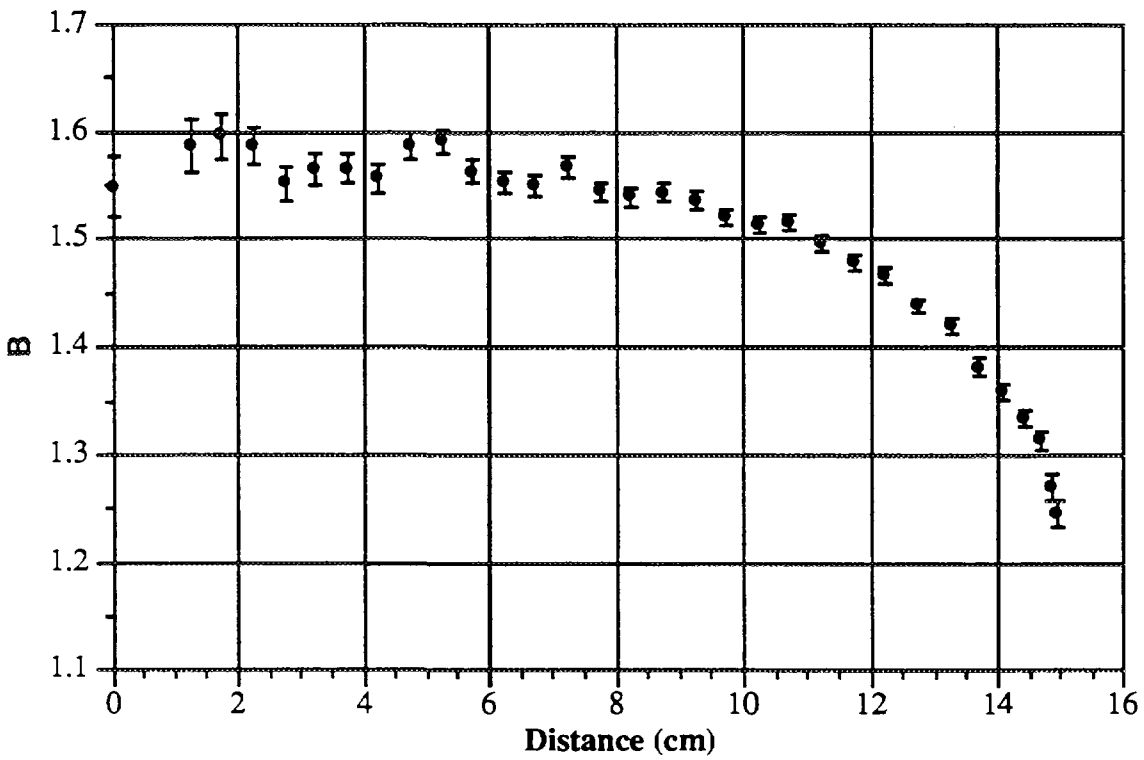

Wide Spectrum Series (L2 80 kV) - PMMA slab phantom

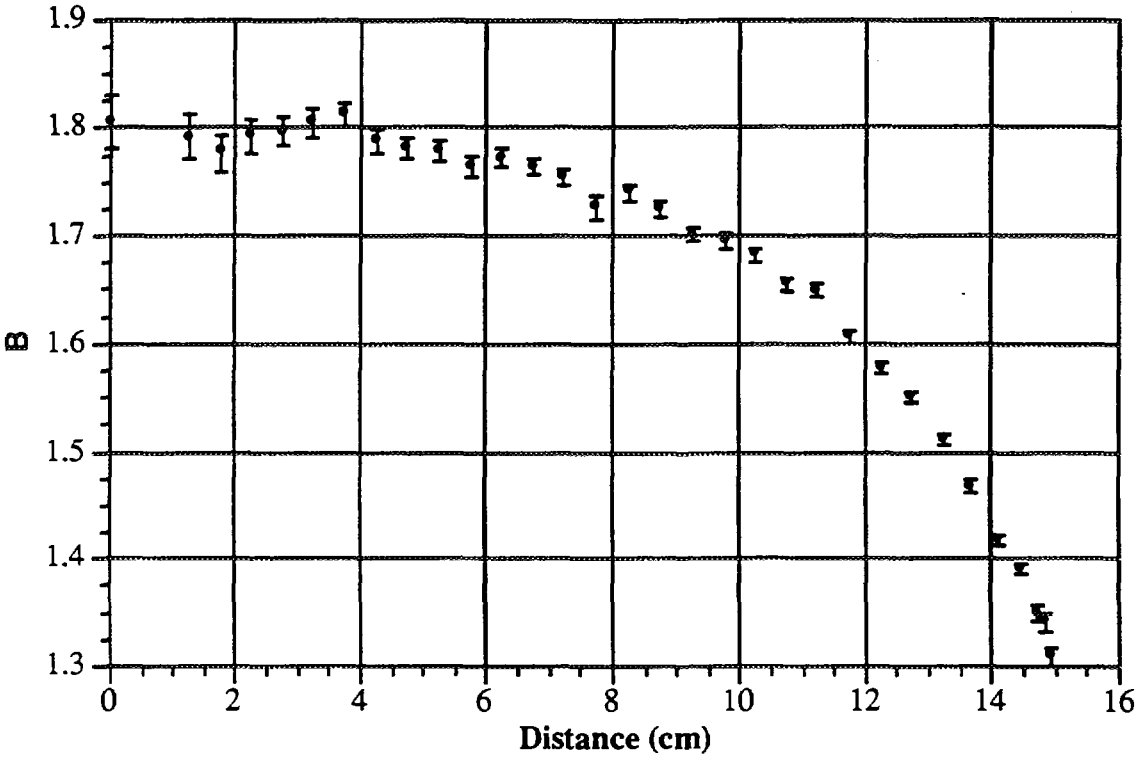

Wide Spectrum Series (L2 80 kV) - Water in PMMA slab phantom

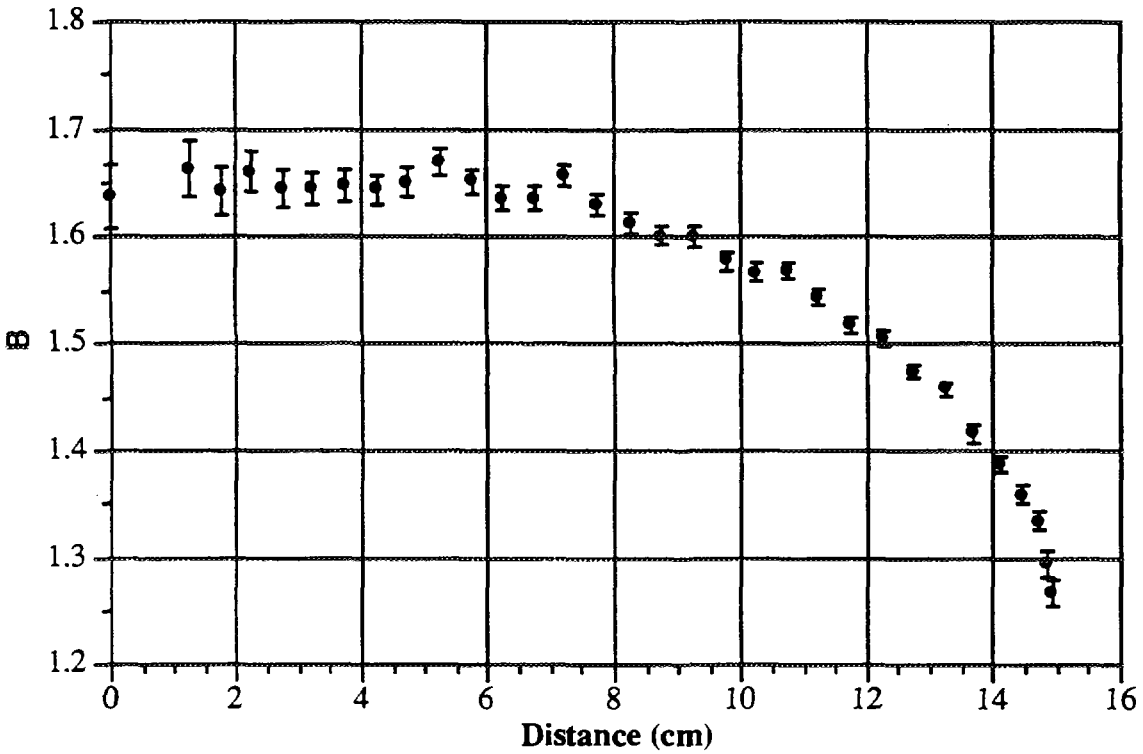

Wide Spectrum Series (L3 110 kV) - PMMA slab phantom

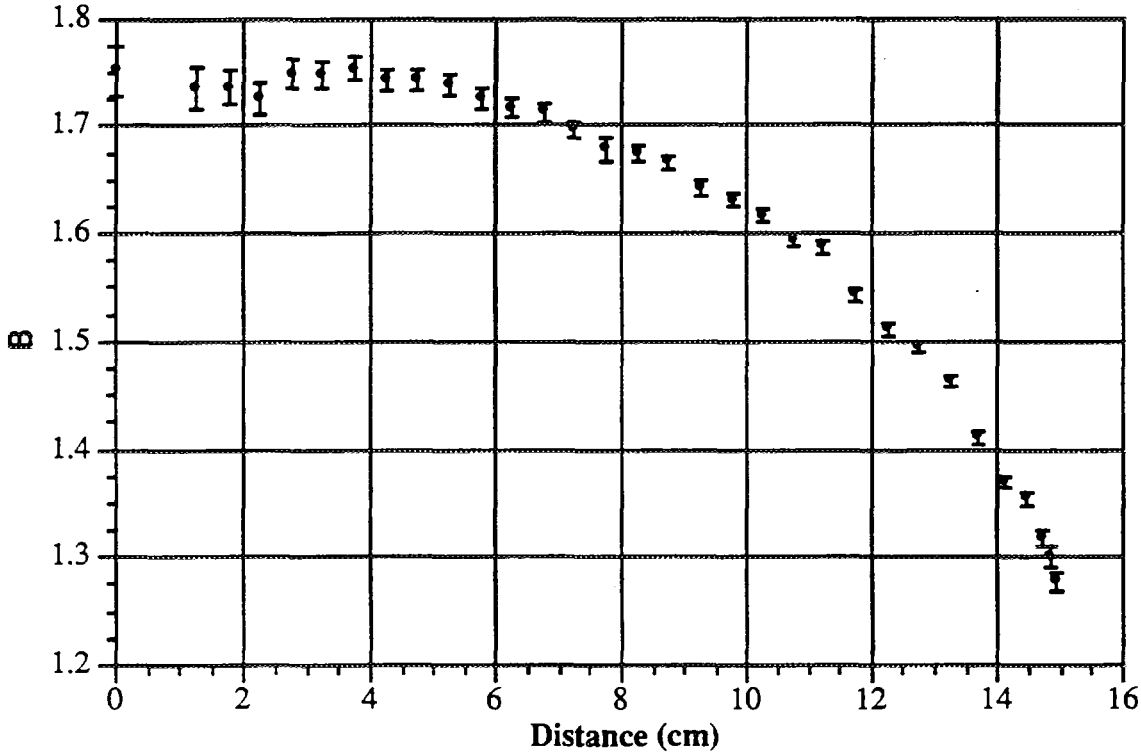

Wide Spectrum Series (L3 110 kV) - Water in PMMA slab phantom

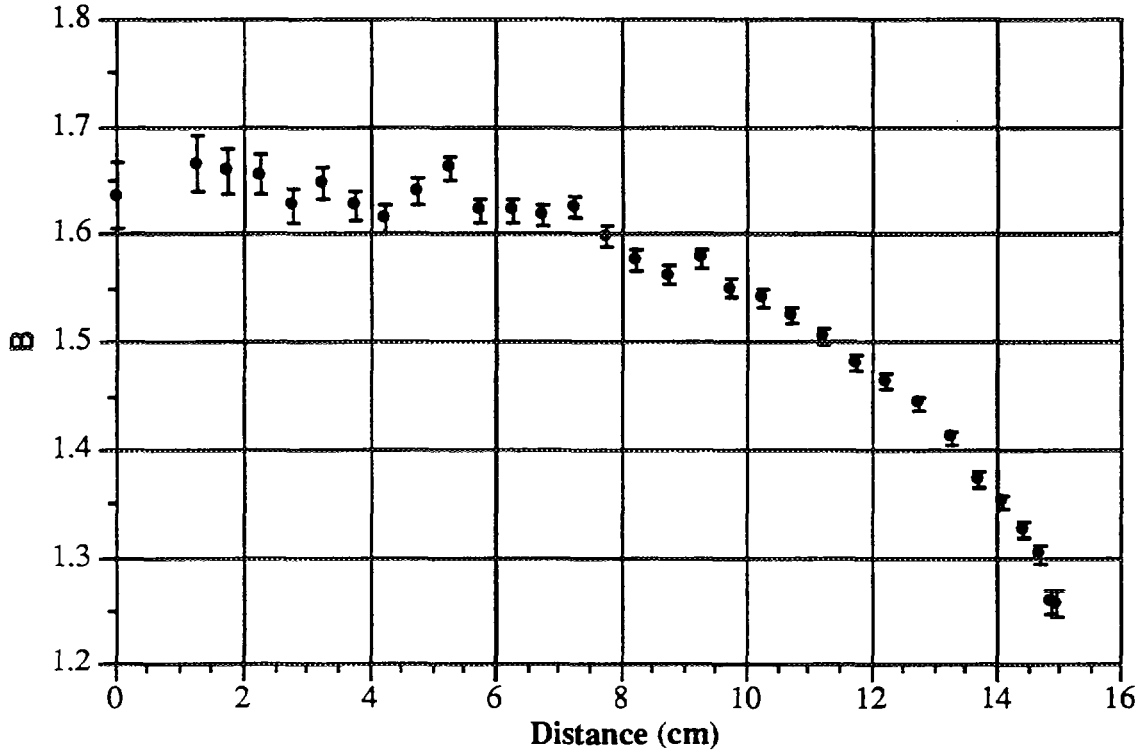

Wide Spectrum Series (L4 150 kV) - PMMA slab phantom

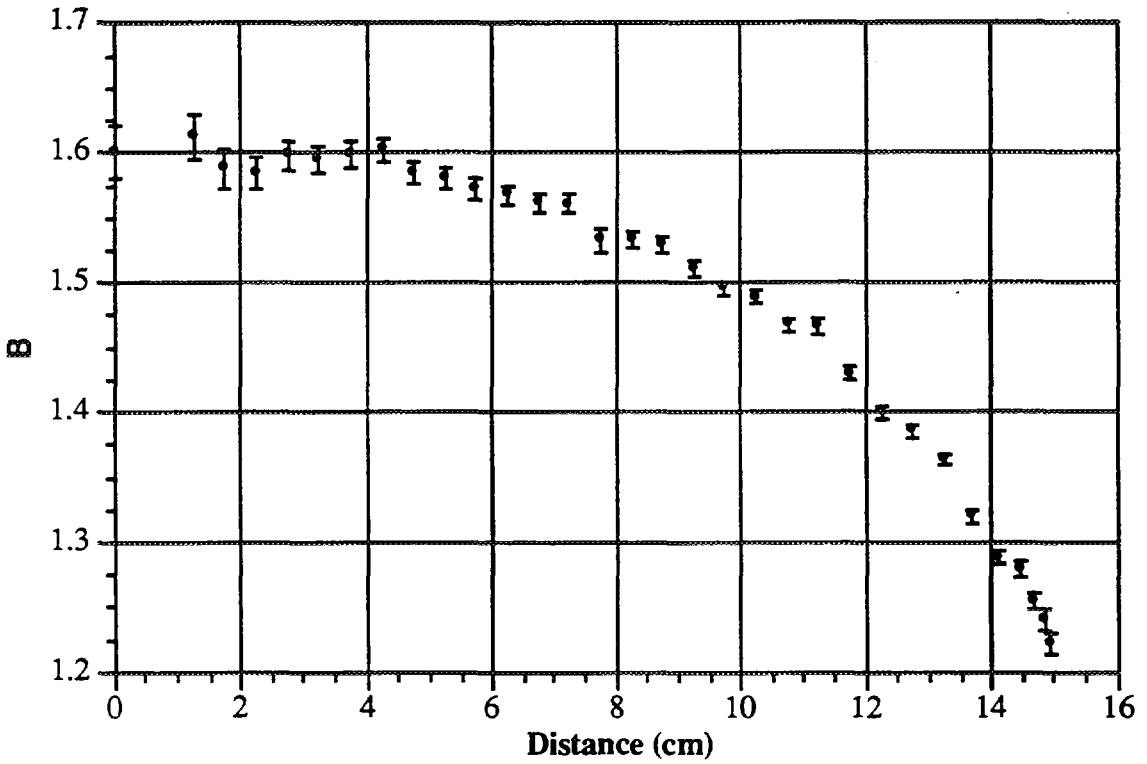

Wide Spectrum Series (L4 150 kV) - Water in PMMA slab phantom

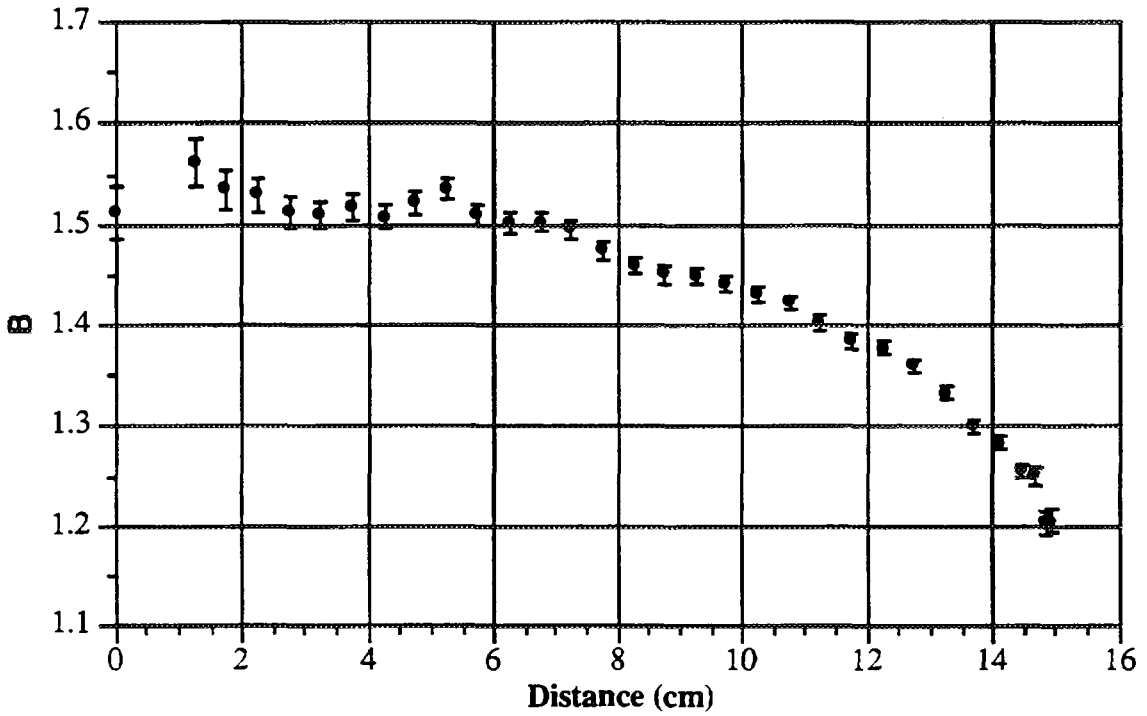

Wide Spectrum Series (L5 200 kV) - PMMA slab phantom

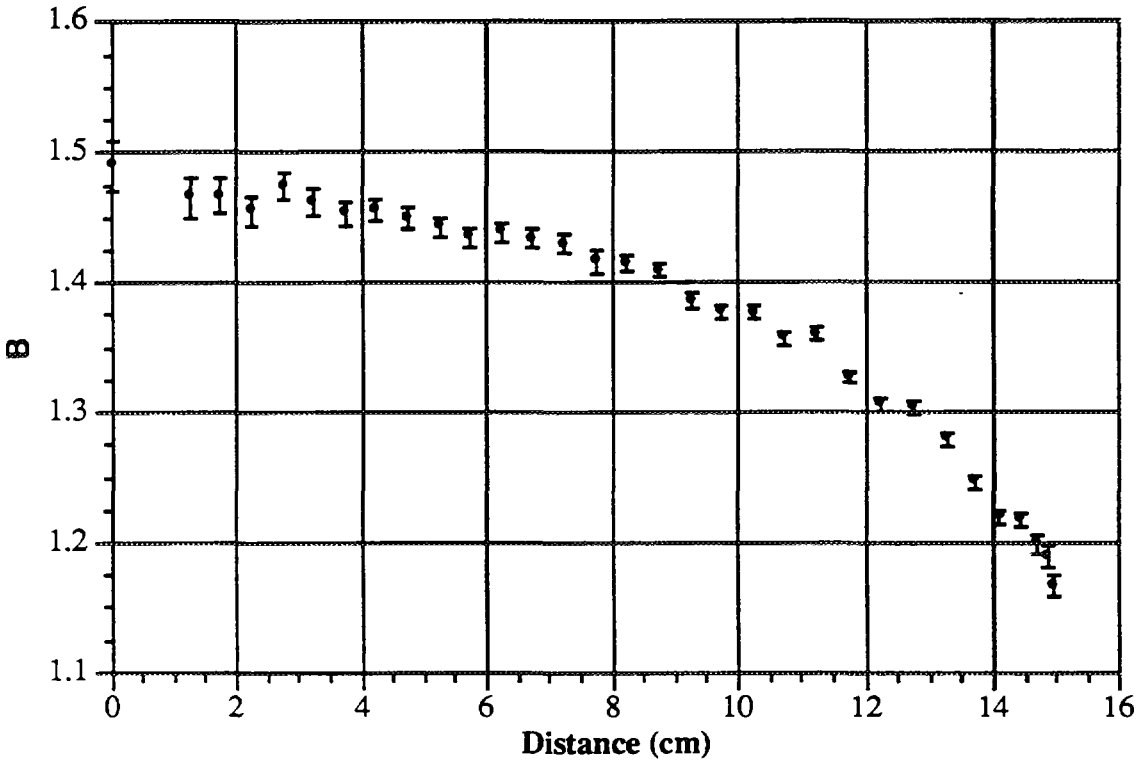

Wide Spectrum Series (L5 200 kV) - Water in PMMA slab phantom

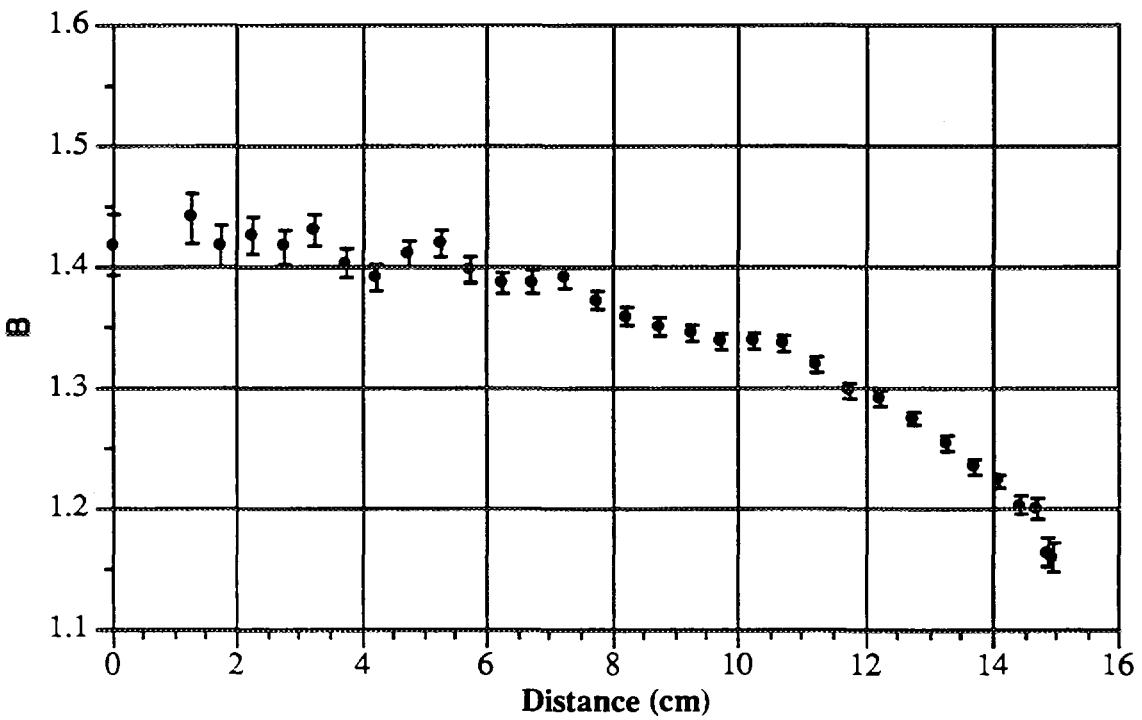

Wide Spectrum Series (L6 250 kV) - PMMA slab phantom

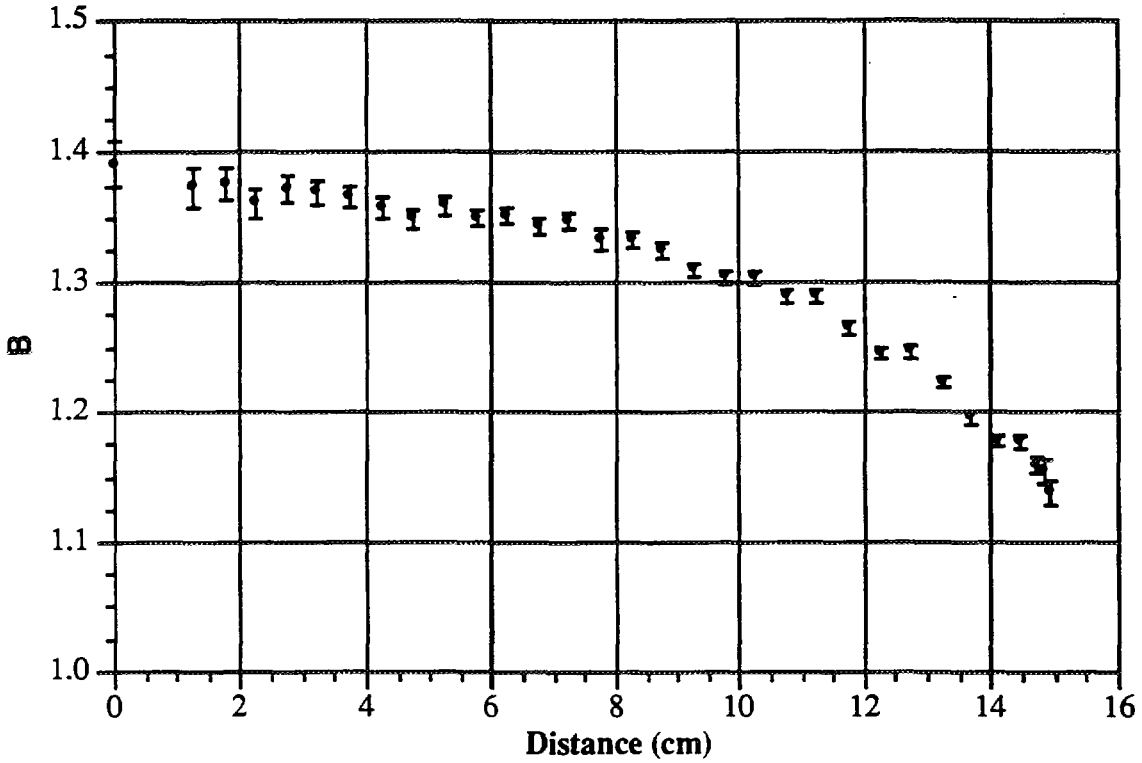

Wide Spectrum Series (L6 250 kV) - Water in PMMA slab phantom

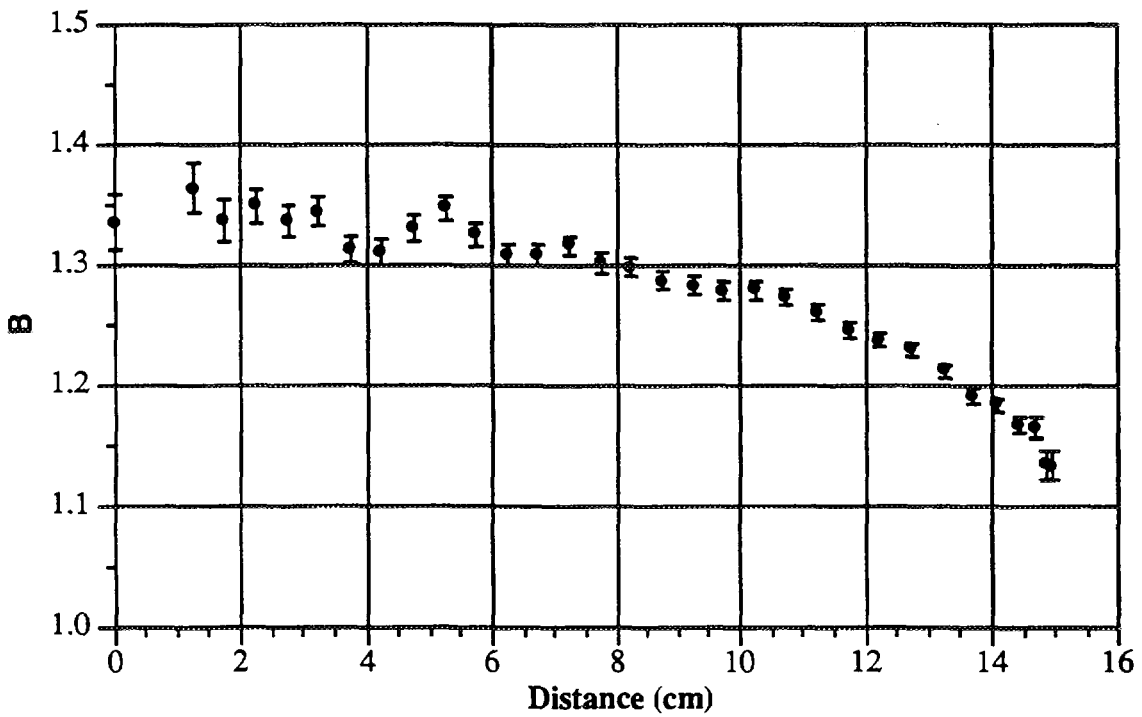

Wide Spectrum Series (L7 300 kV) - PMMA slab phantom

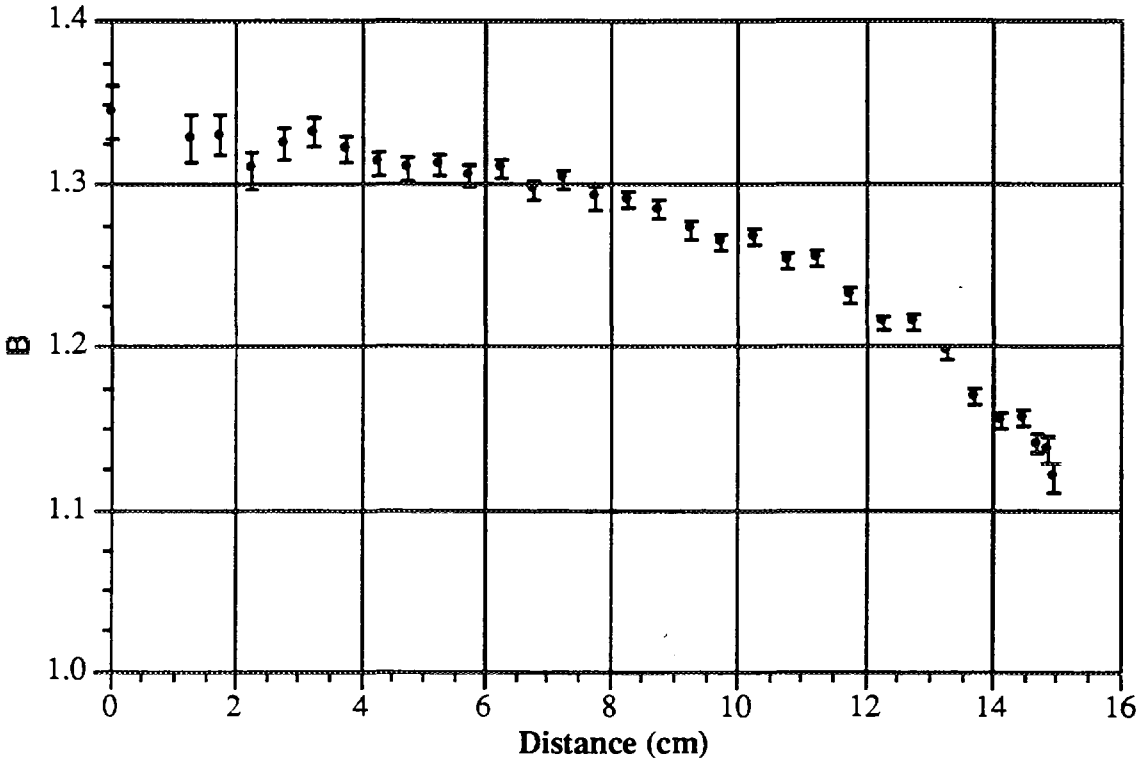

Wide Spectrum Series (L7 300 kV) - Water in PMMA slab phantom

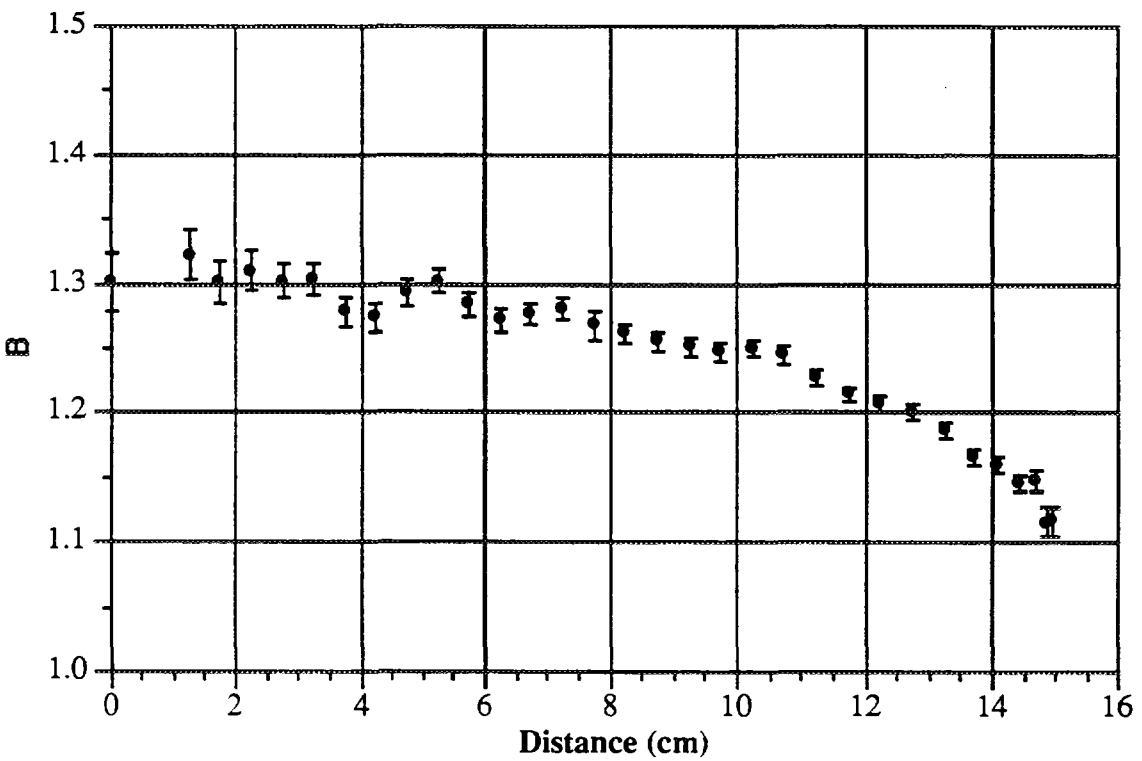

APPENDIX B

Air Kerma backscatter factor profiles on a PMMA phantom for 45°- 60° and 75° incident parallel radiation beams

NARROW AND WIDE SPECTRUM SERIES

45°

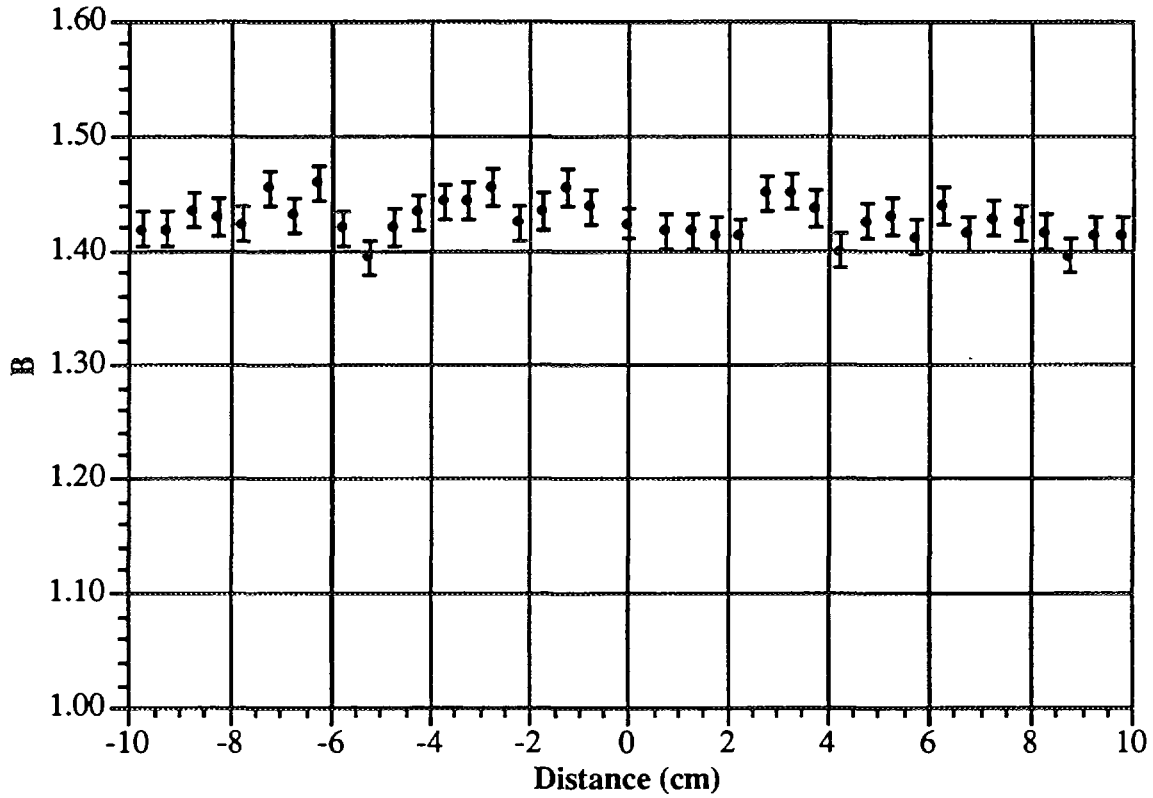

Narrow Spectrum Series - 40 kV (45°)

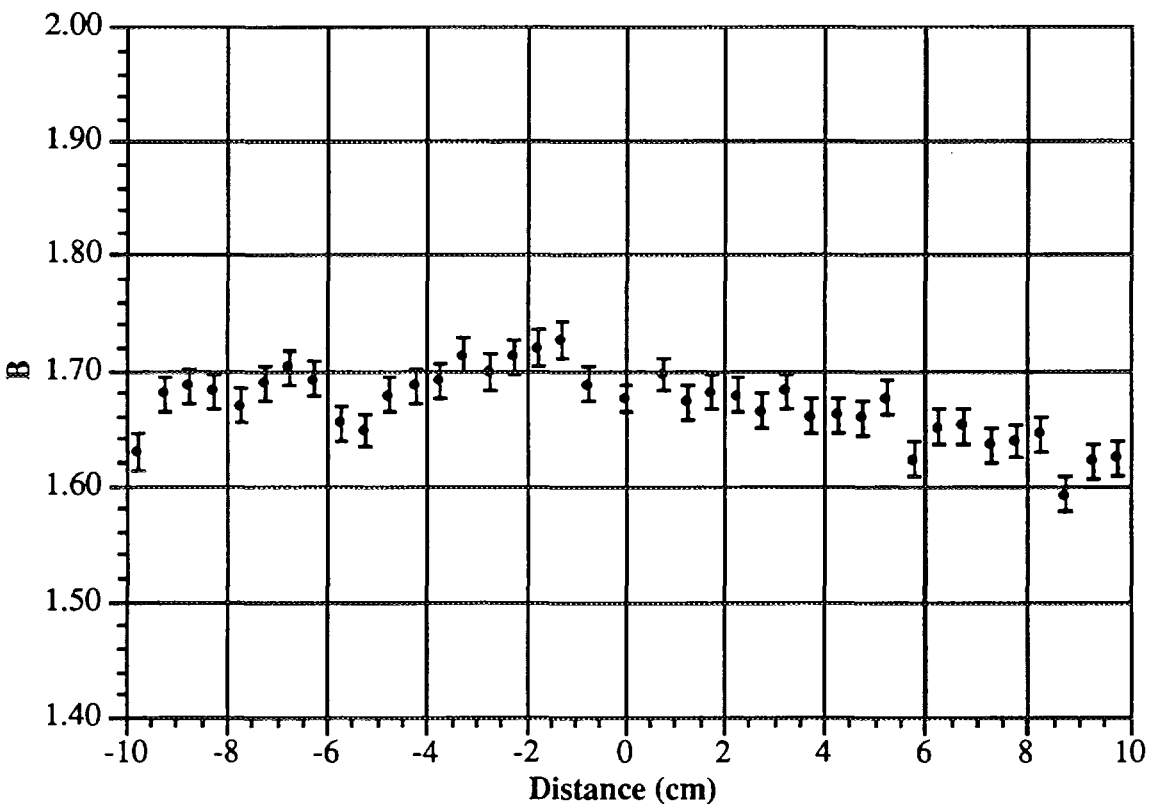

Narrow Spectrum Series - 60 kV (45°)

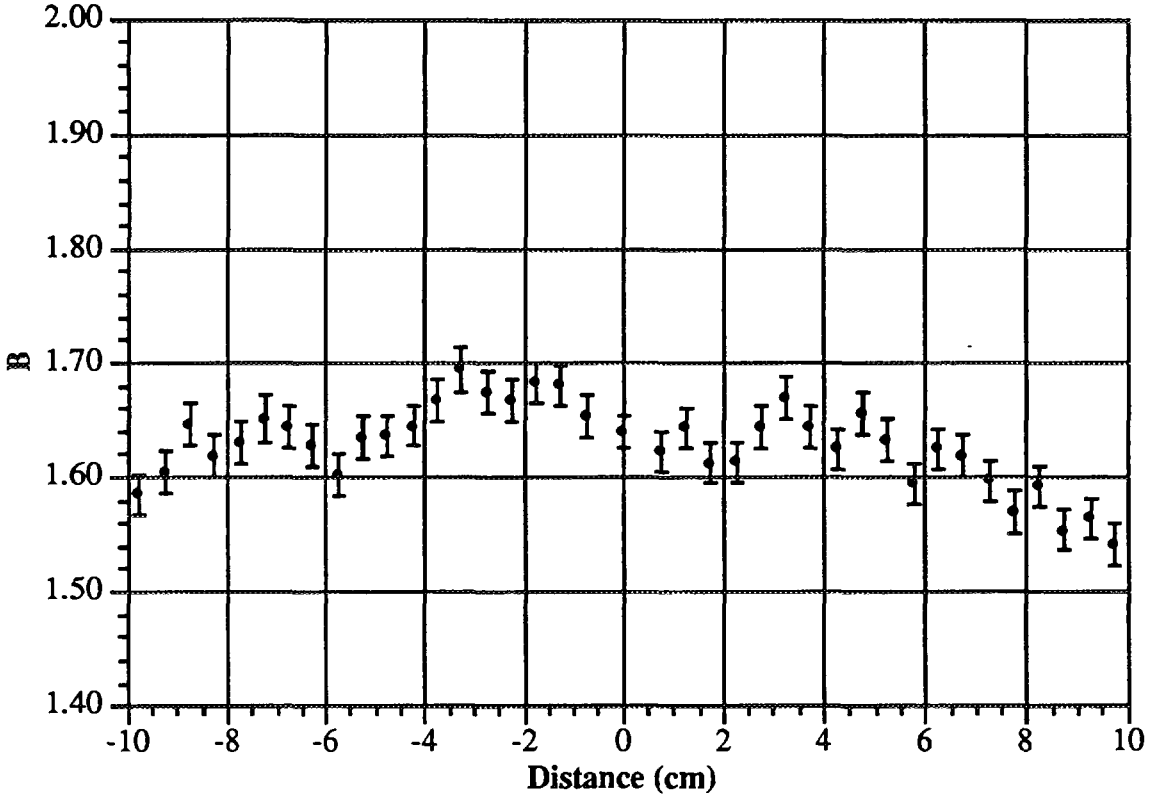

Narrow Spectrum Series - 80 kV (45°)

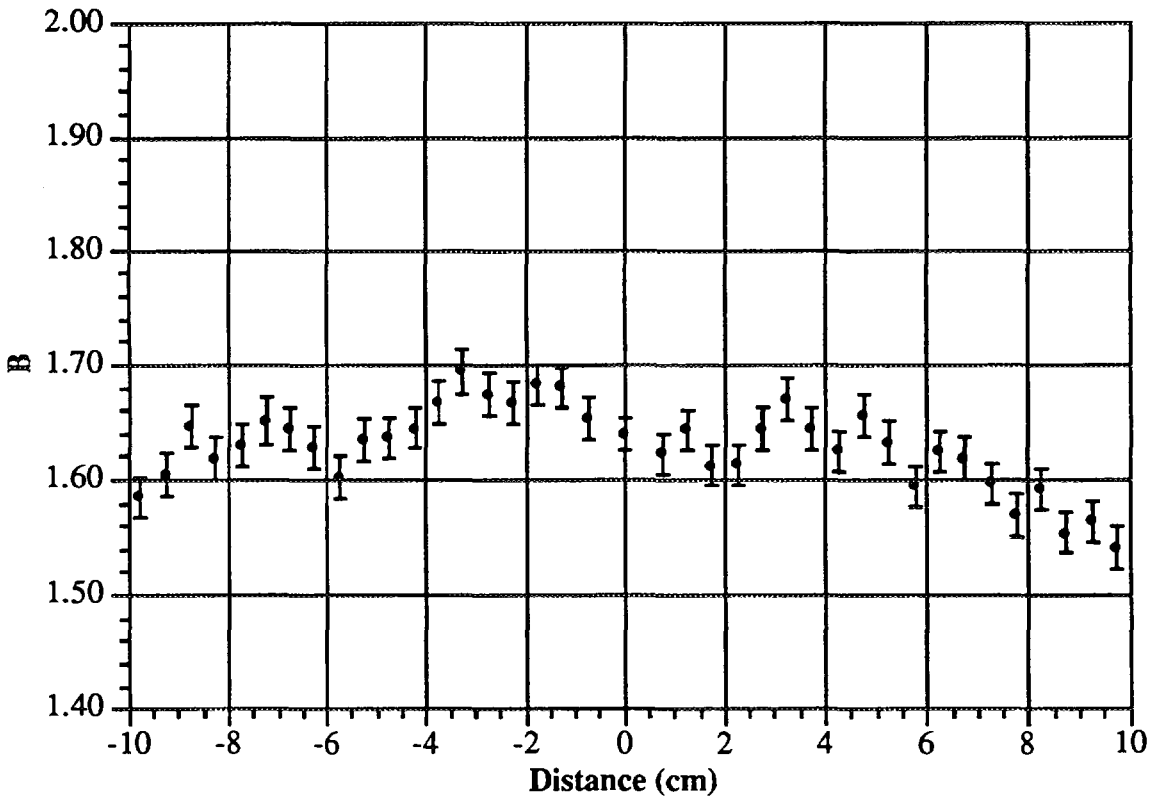

Narrow Spectrum Series - 100 kV (45°)

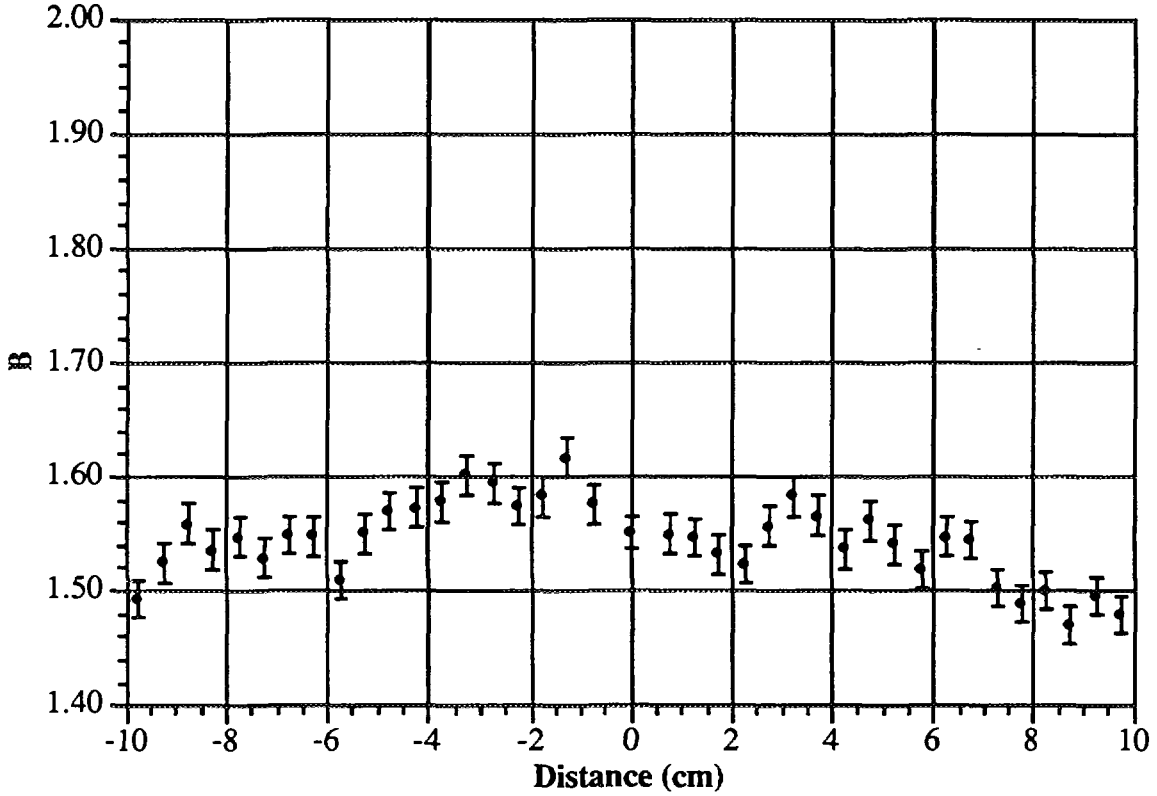

Narrow Spectrum Series - 120 kV (45°)

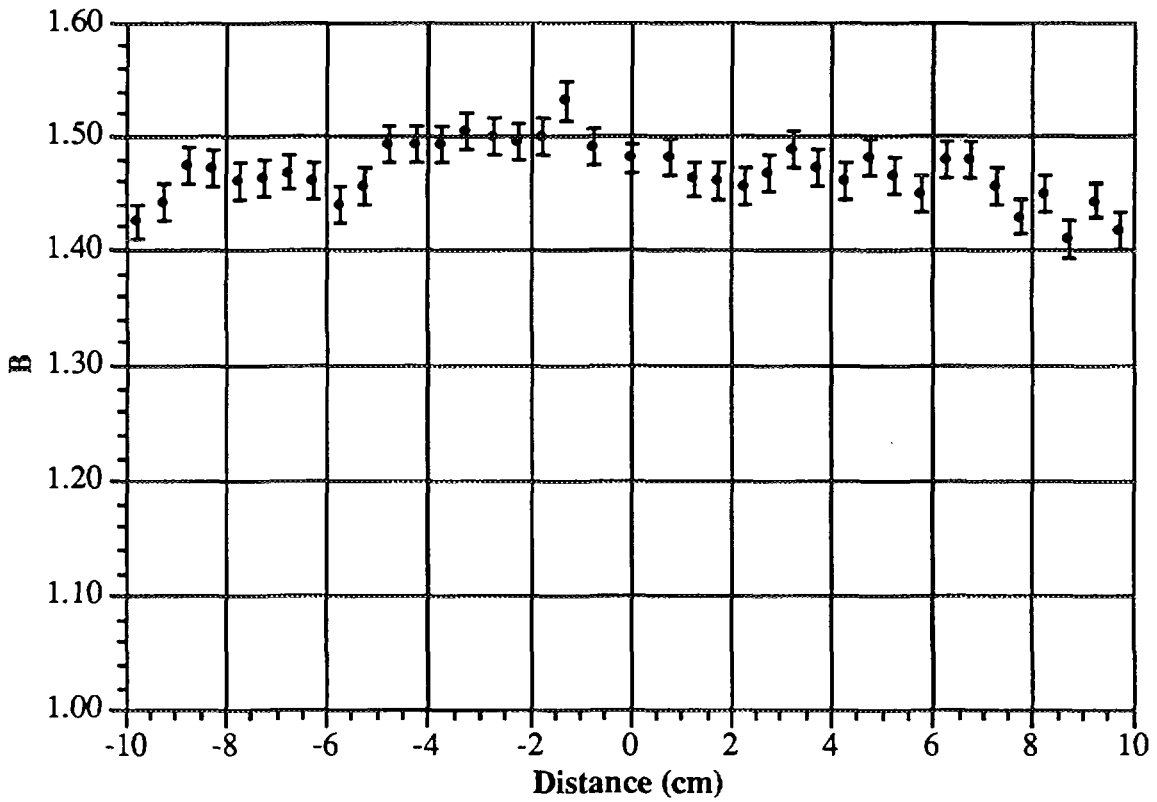

Narrow Spectrum Series - 150 kV (45°)

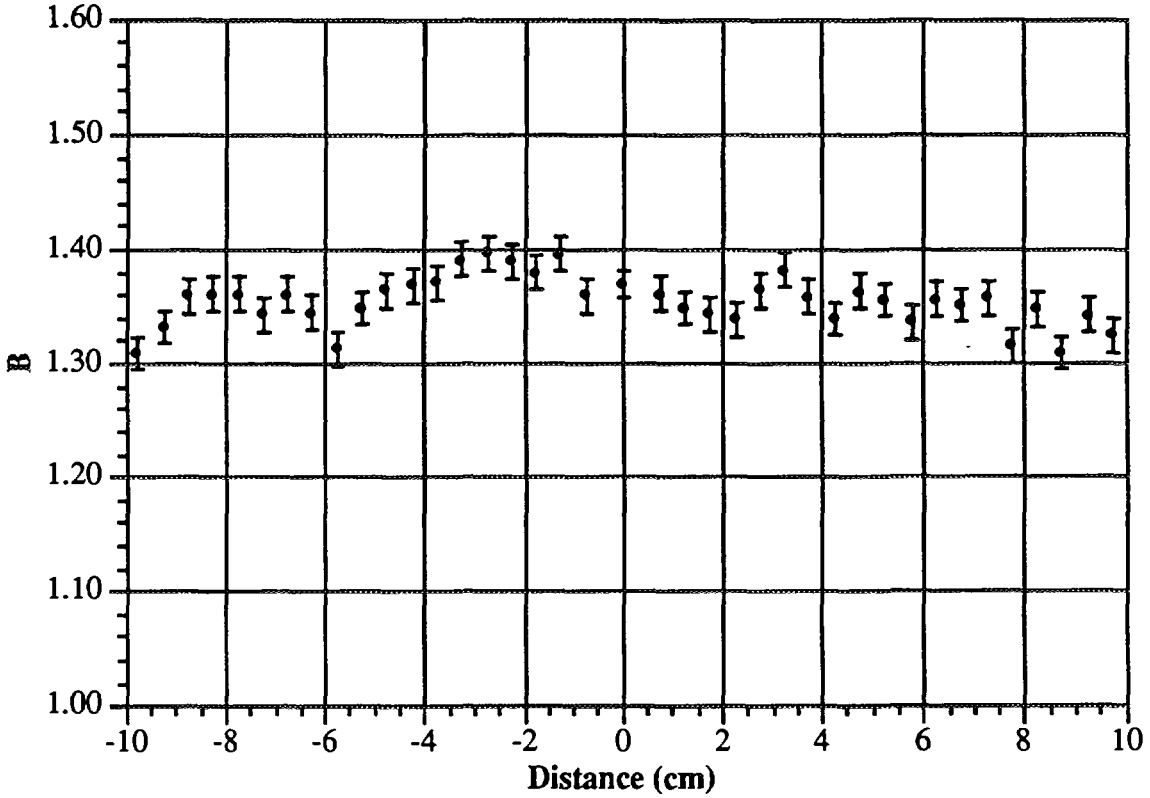

Narrow Spectrum Series - 200 kV (45°)

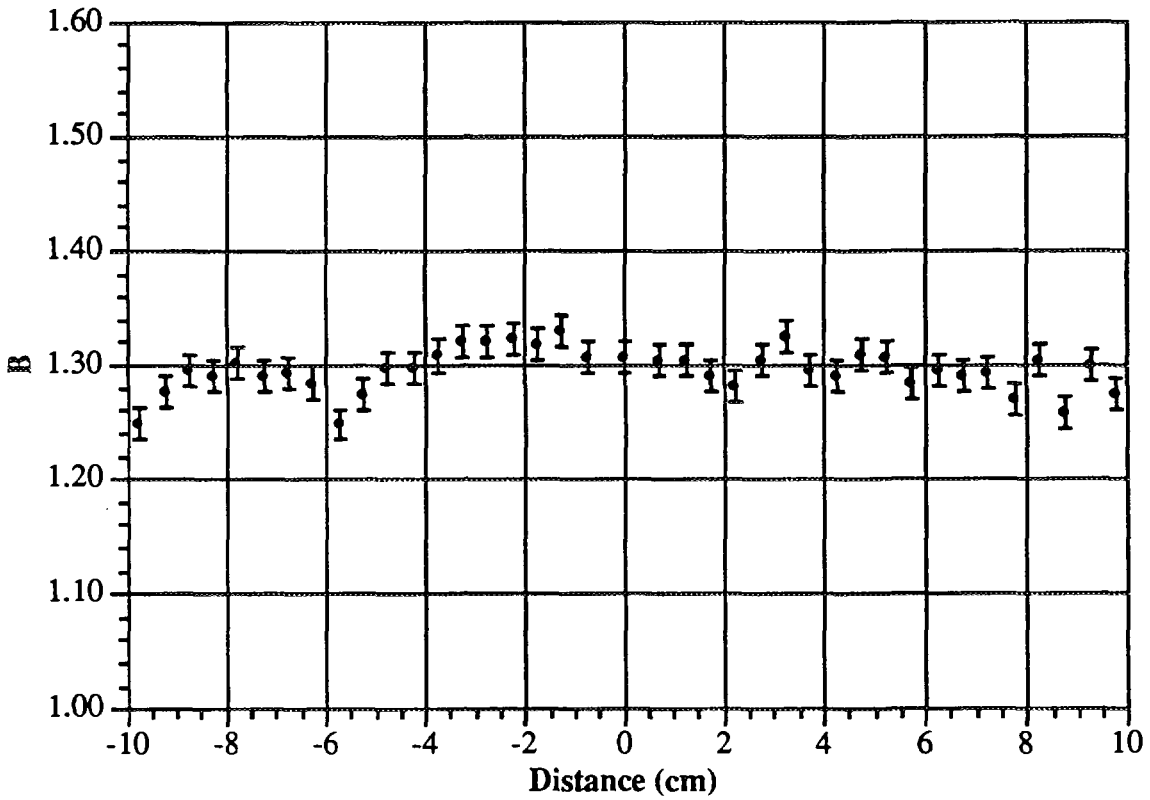

Narrow Spectrum Series - 250 kV (45°)

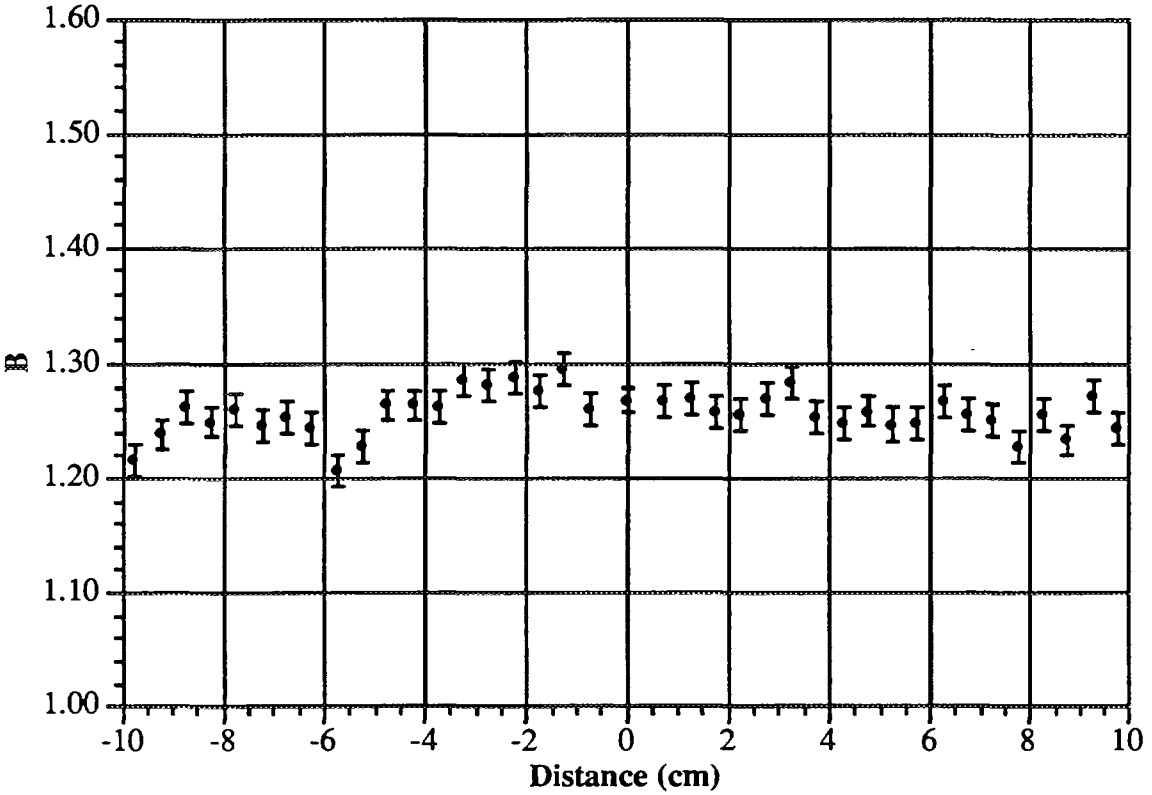

Narrow Spectrum Series - 300 kV (45°)

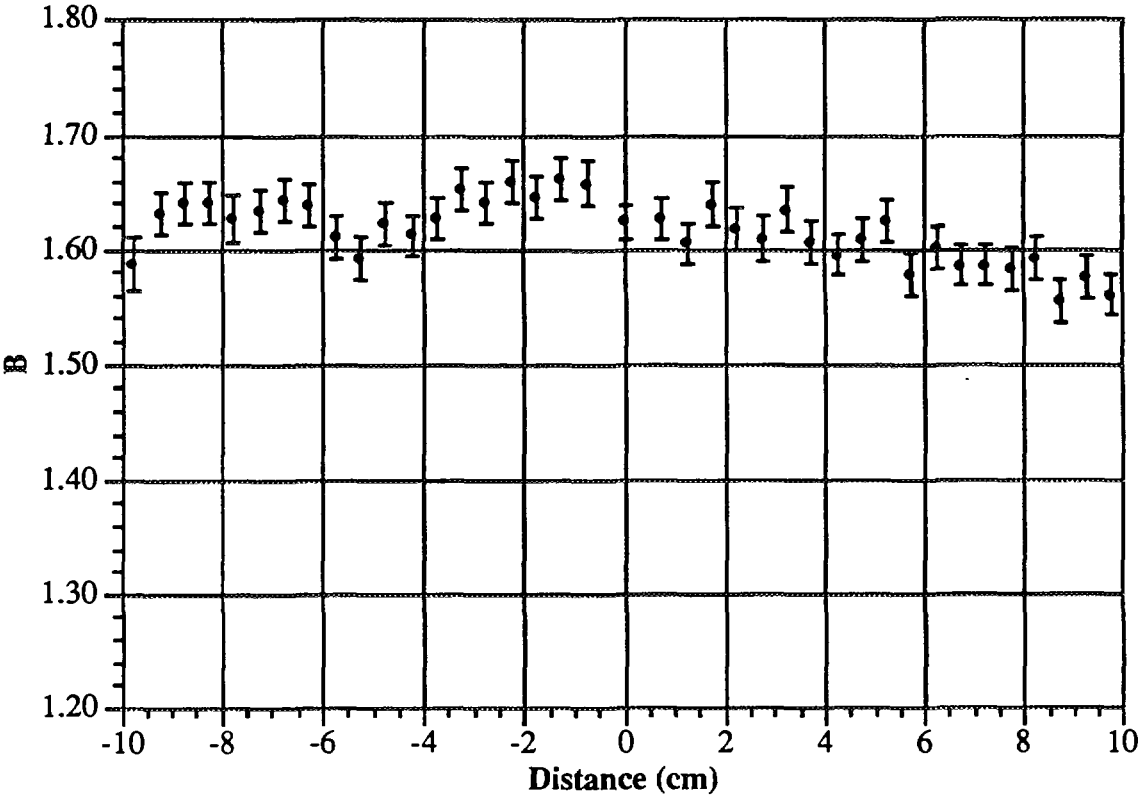

Wide Spectrum Series -60 kV (45°)

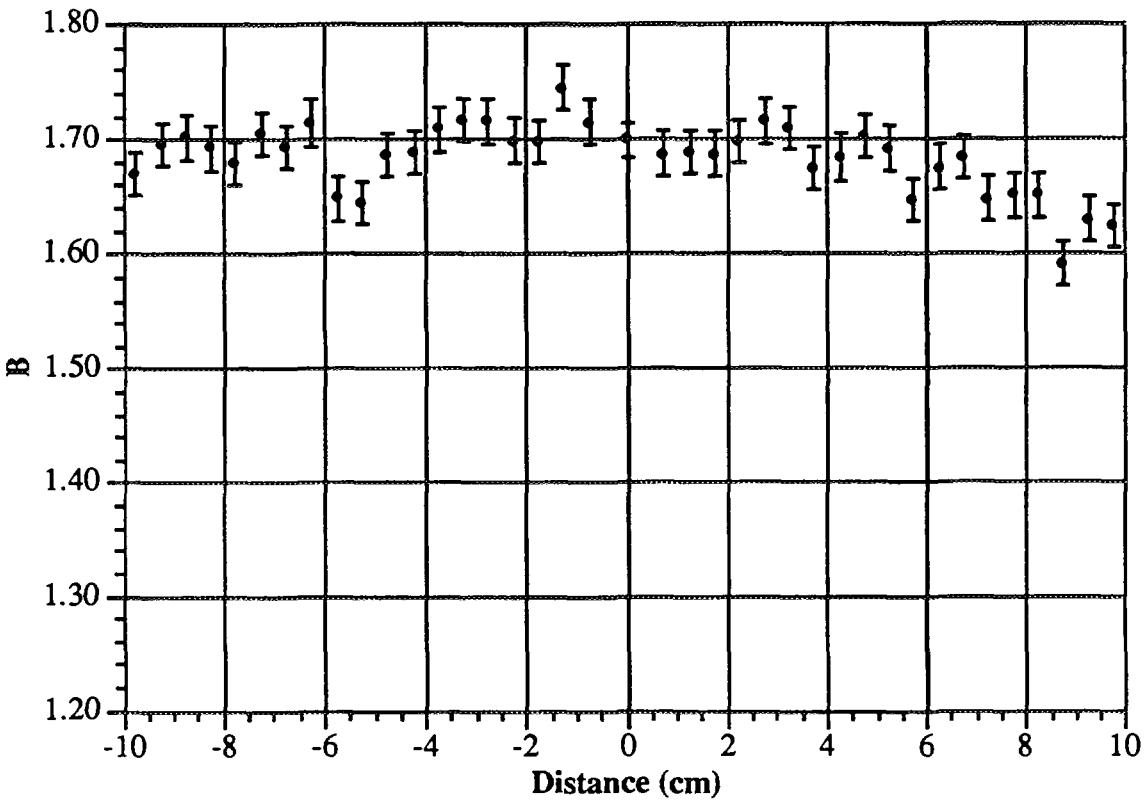

Wide Spectrum Series -80 kV (45°)

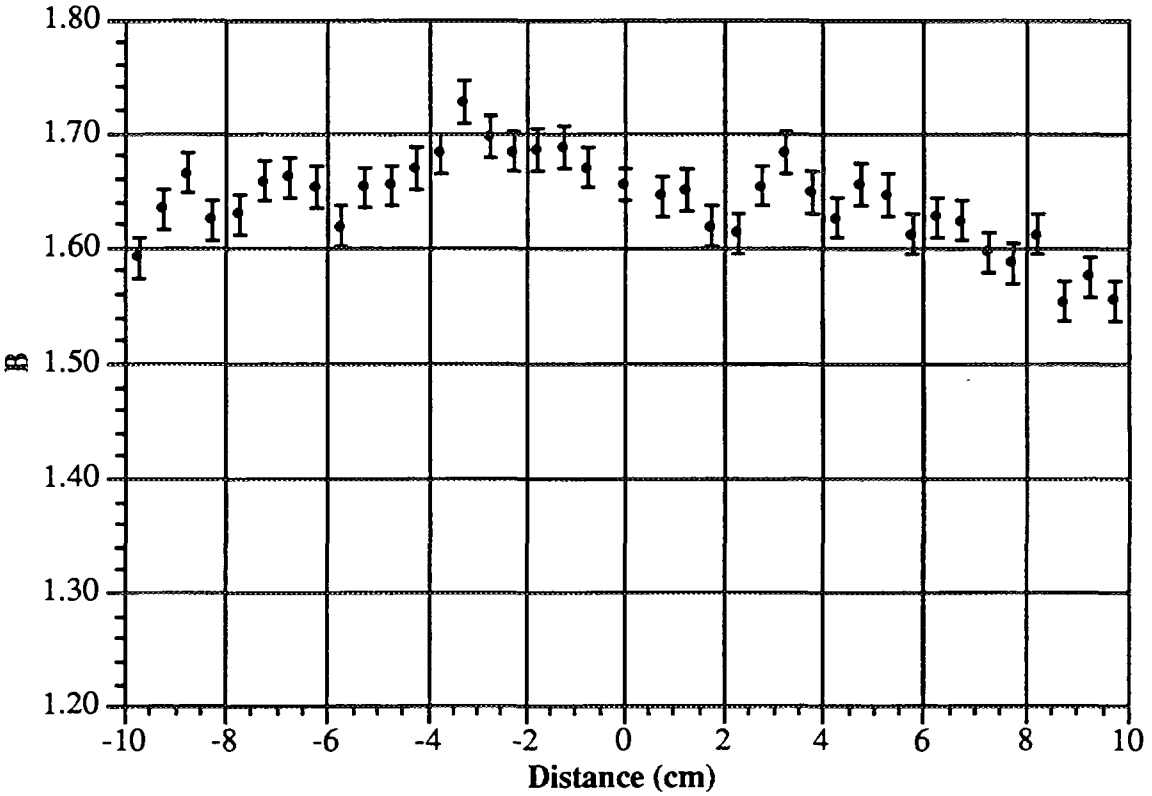

Wide Spectrum Series -110 kV (45°)

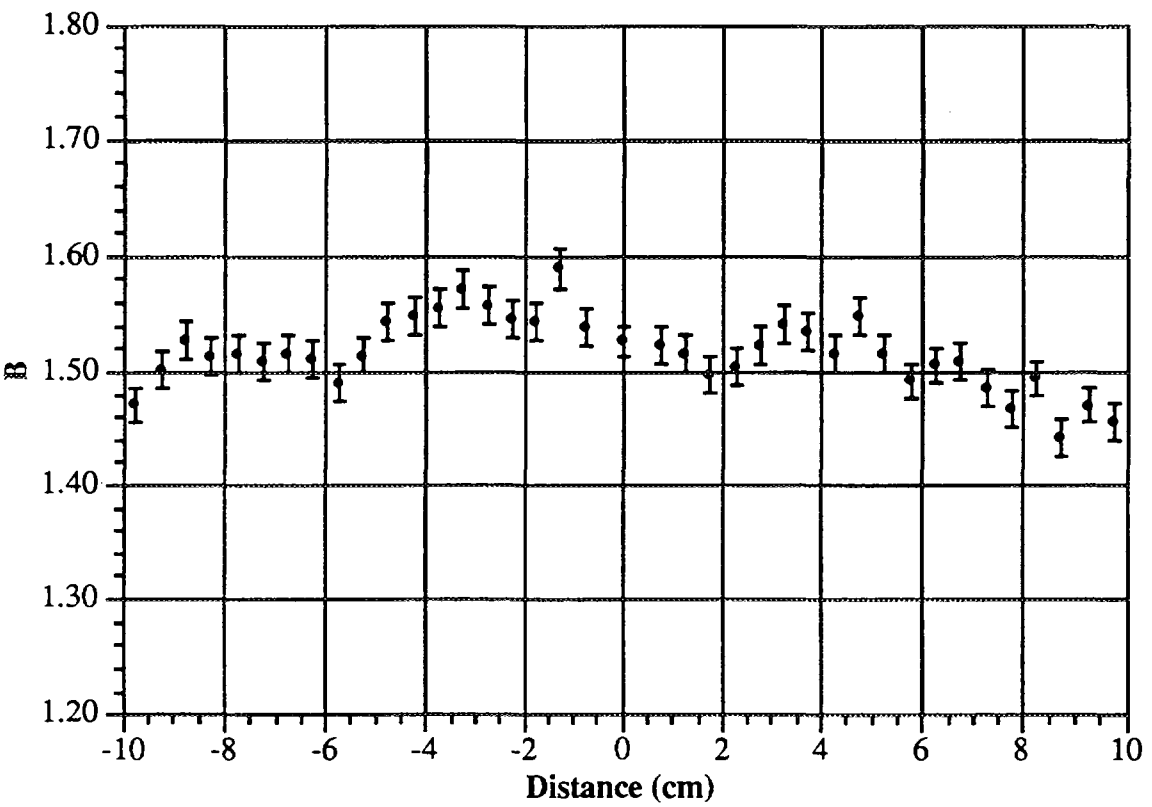

Wide Spectrum Series -150 kV (45°)

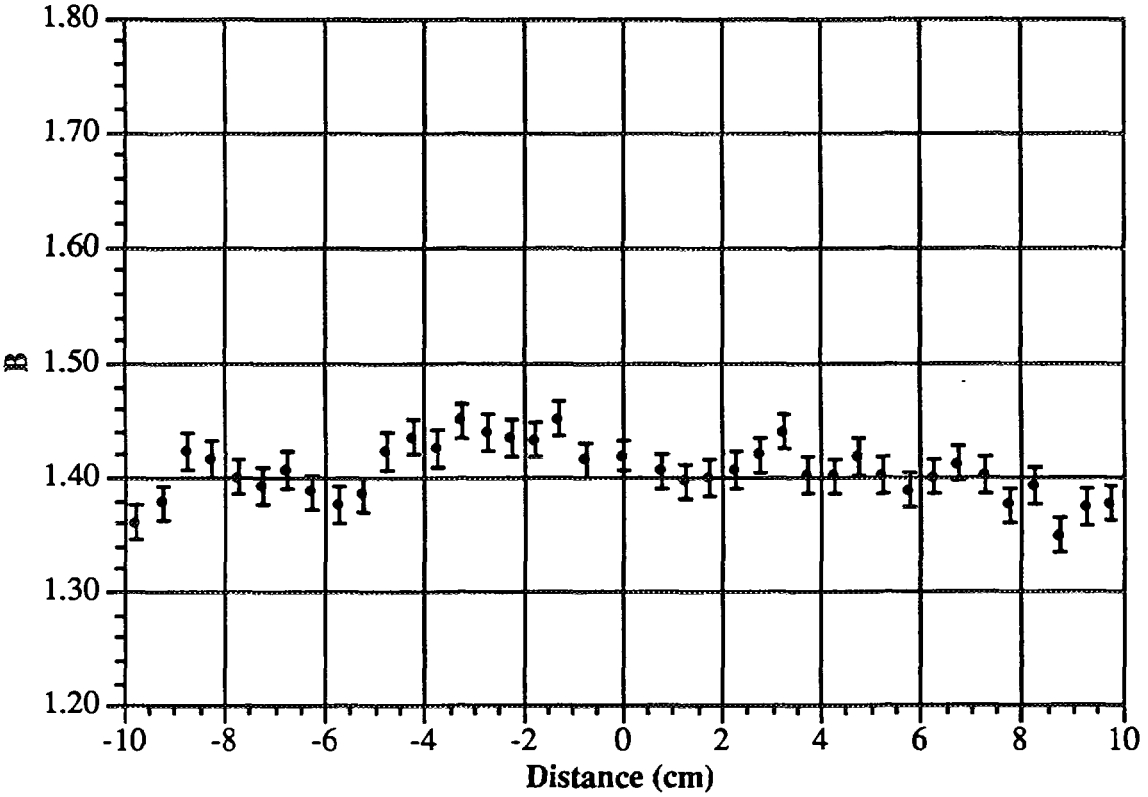

Wide Spectrum Series -200 kV (45°)

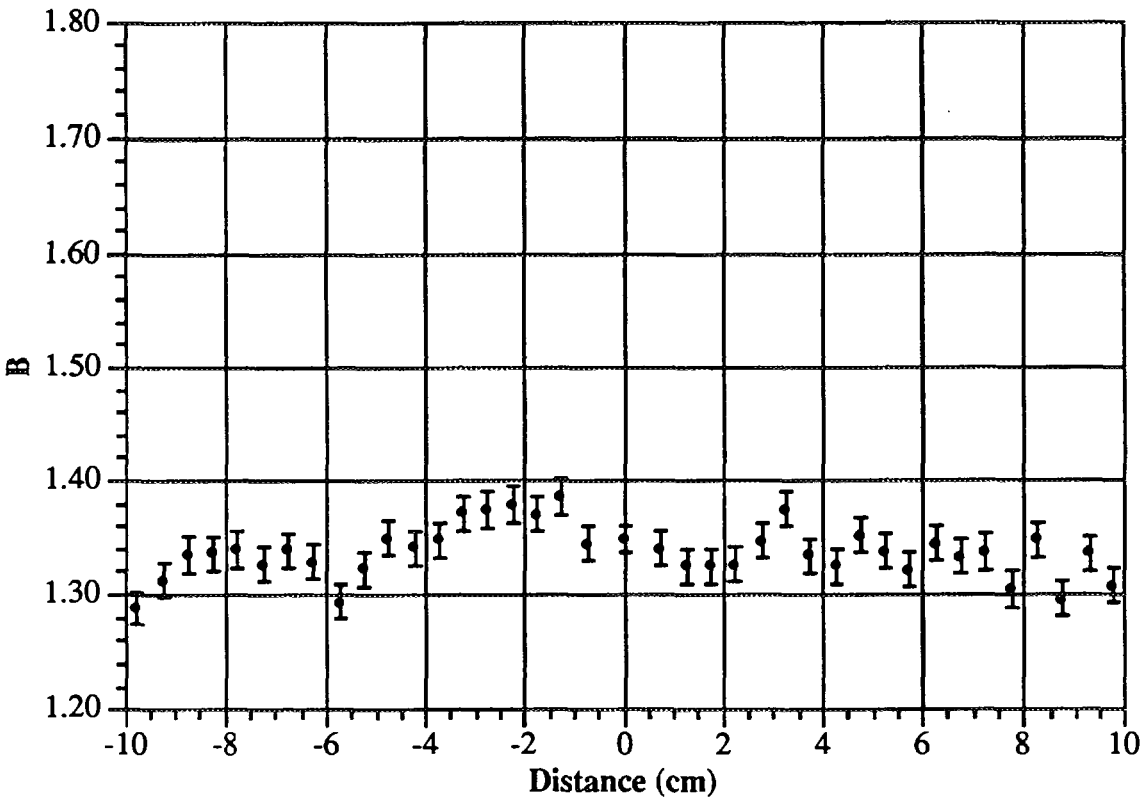

Wide Spectrum Series -250 kV (45°)

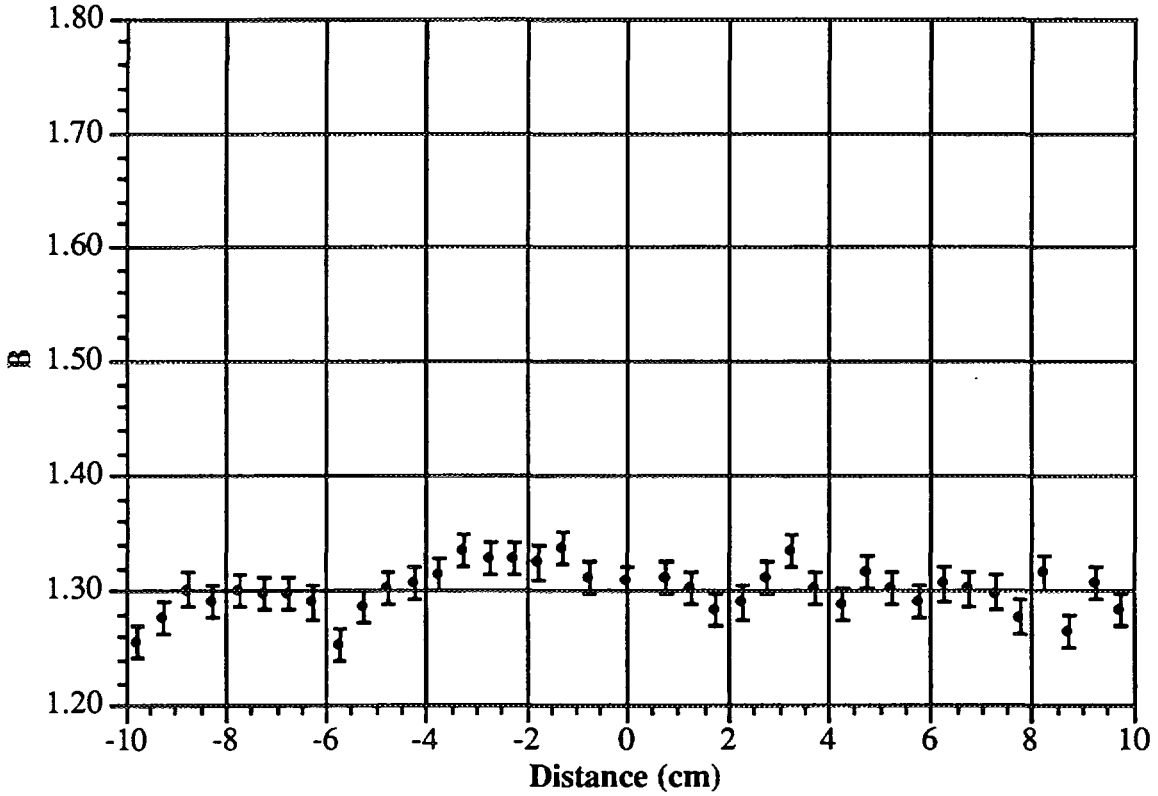

Wide Spectrum Series -300 kV (45°)

NARROW AND WIDE SPECTRUM SERIES

60°

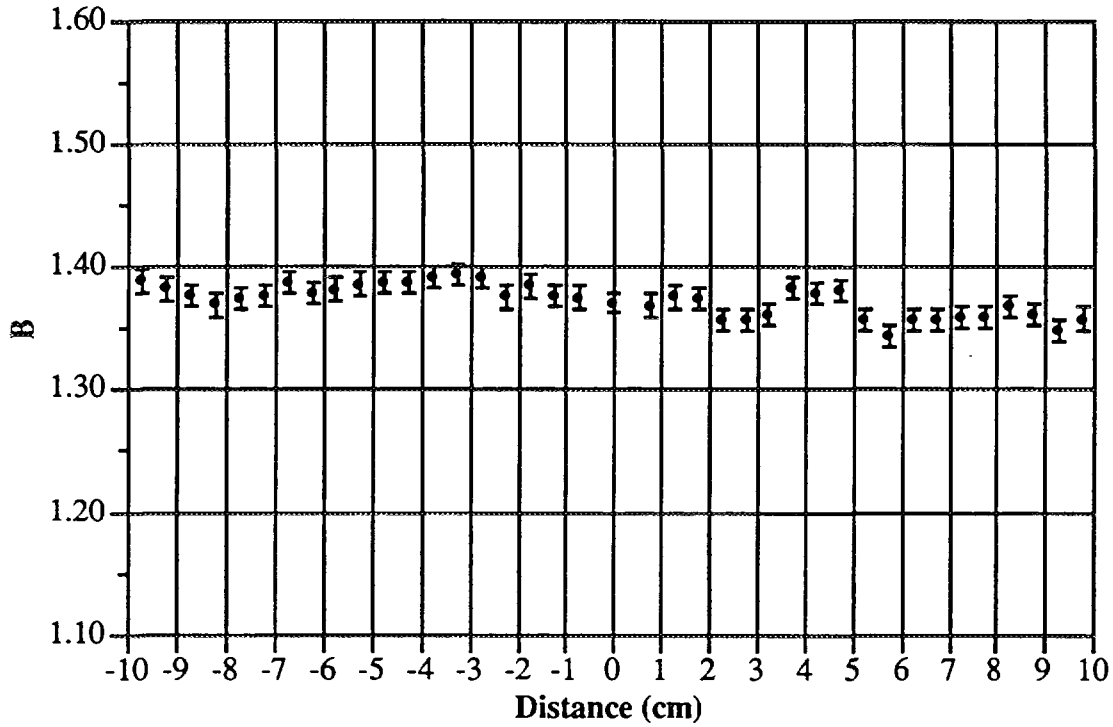

Narrow Spectrum Series - 40 kV (60°)

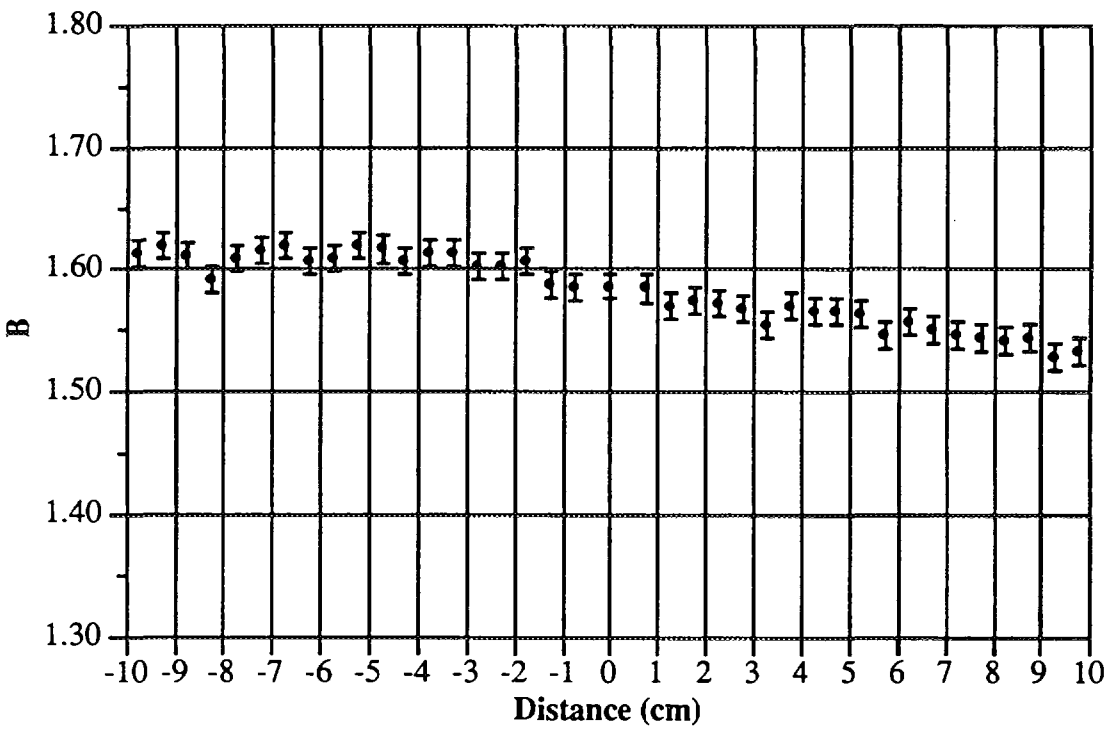

Narrow Spectrum Series - 60 kV (60°)

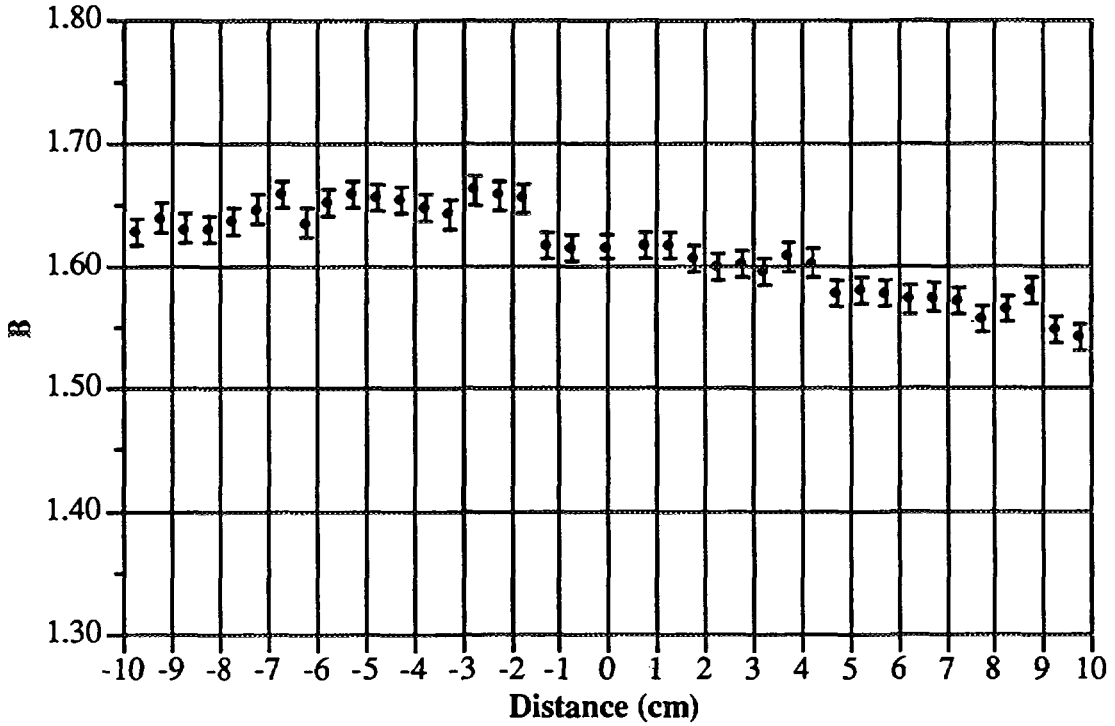

Narrow Spectrum Series - 80 kV(60°)

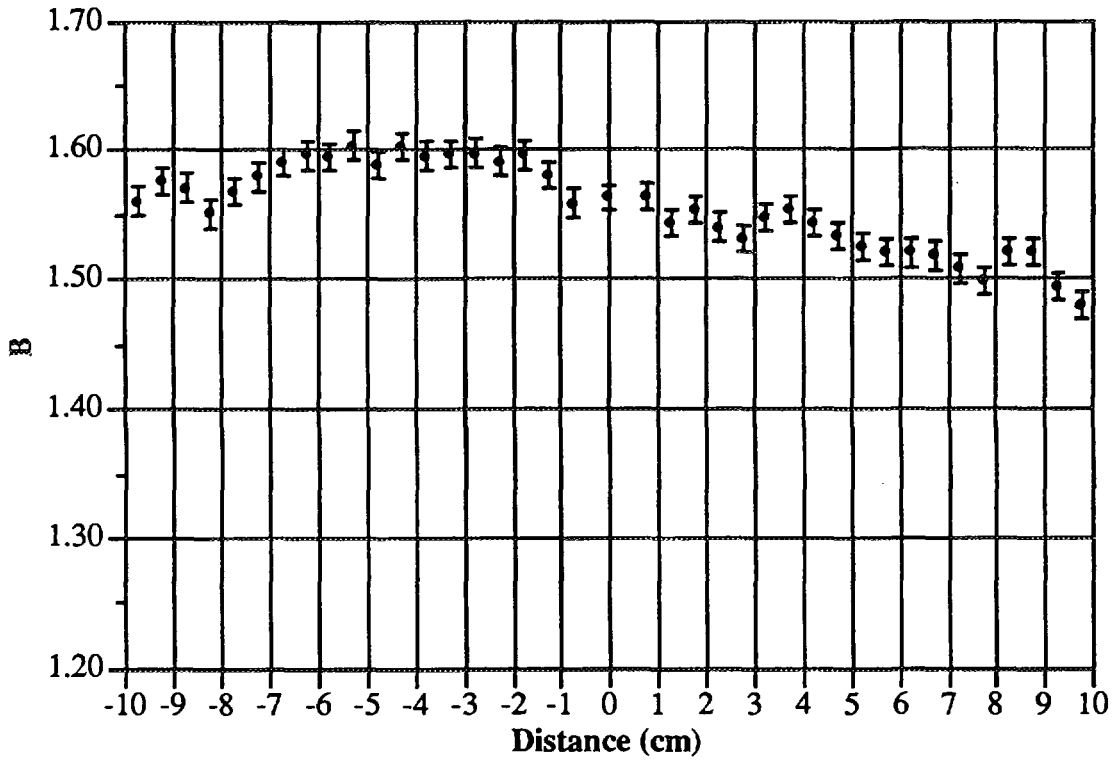

Narrow Spectrum Series - 100 kV(60°)

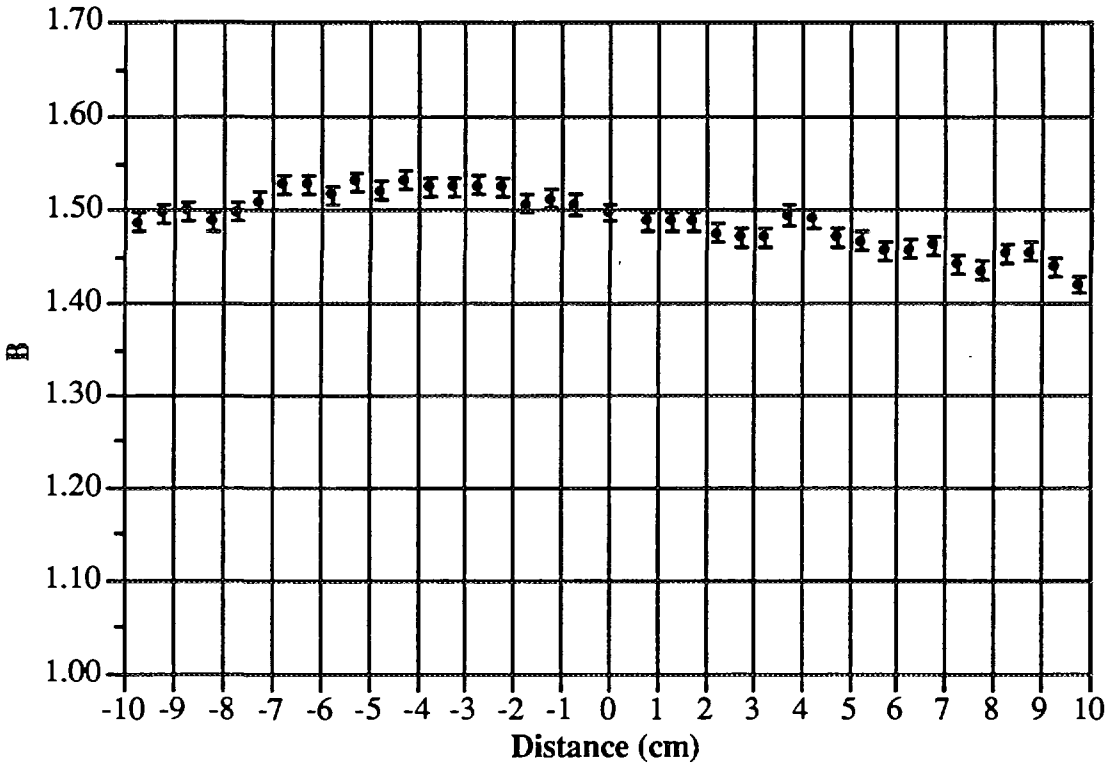

Narrow Spectrum Series - 120 kV(60°)

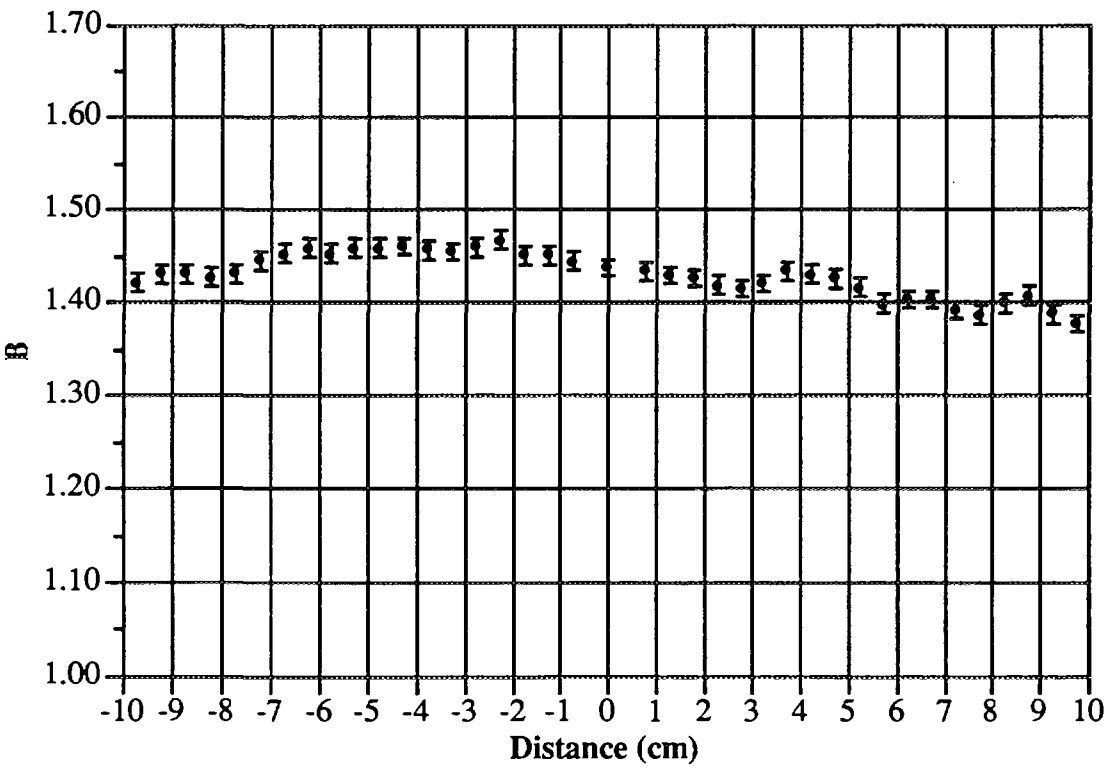

Narrow Spectrum Series - 150 kV (60°)

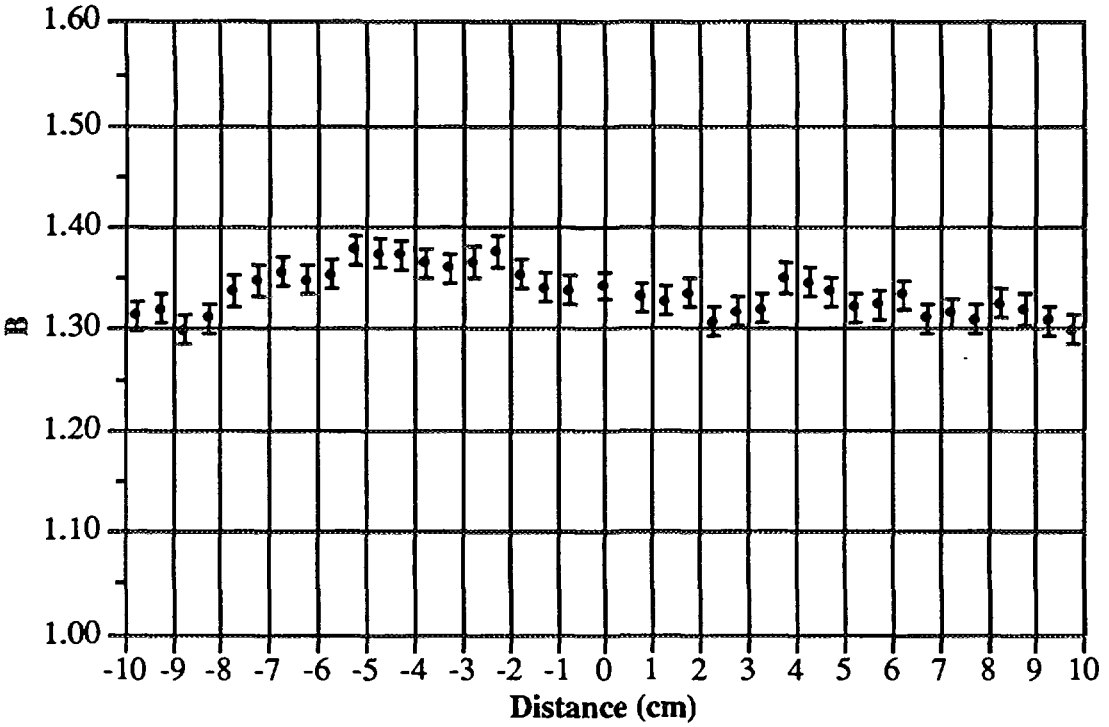

Narrow Spectrum Series - 200 kV (60°)

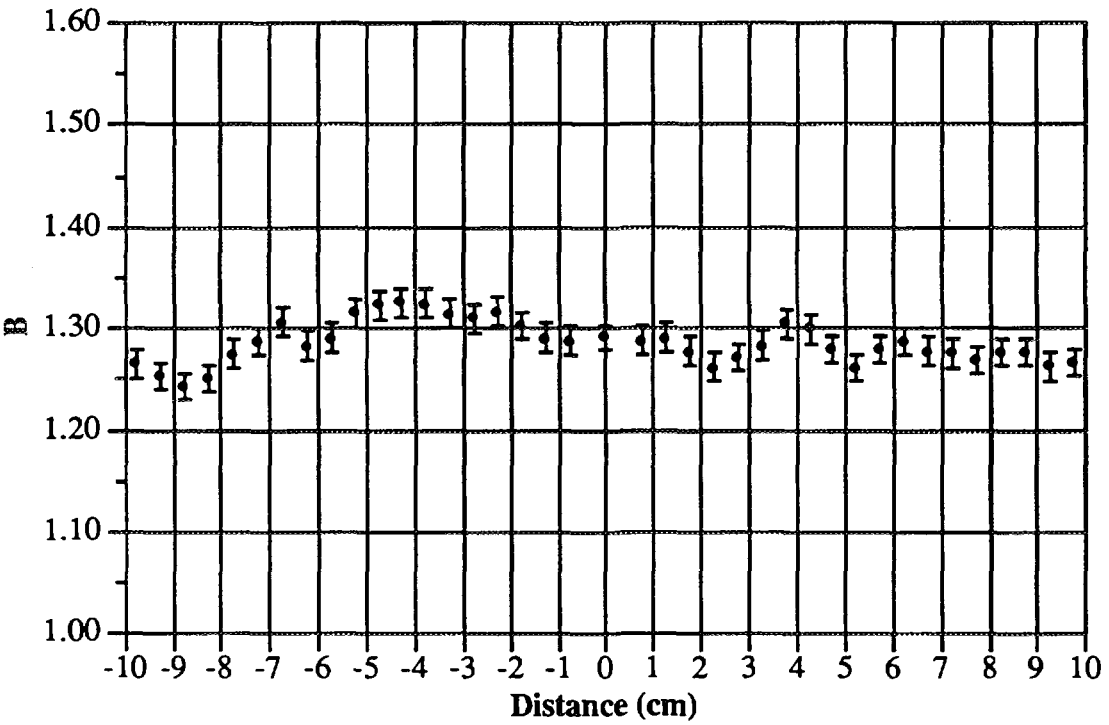

Narrow Spectrum Series - 250 kV (60°)

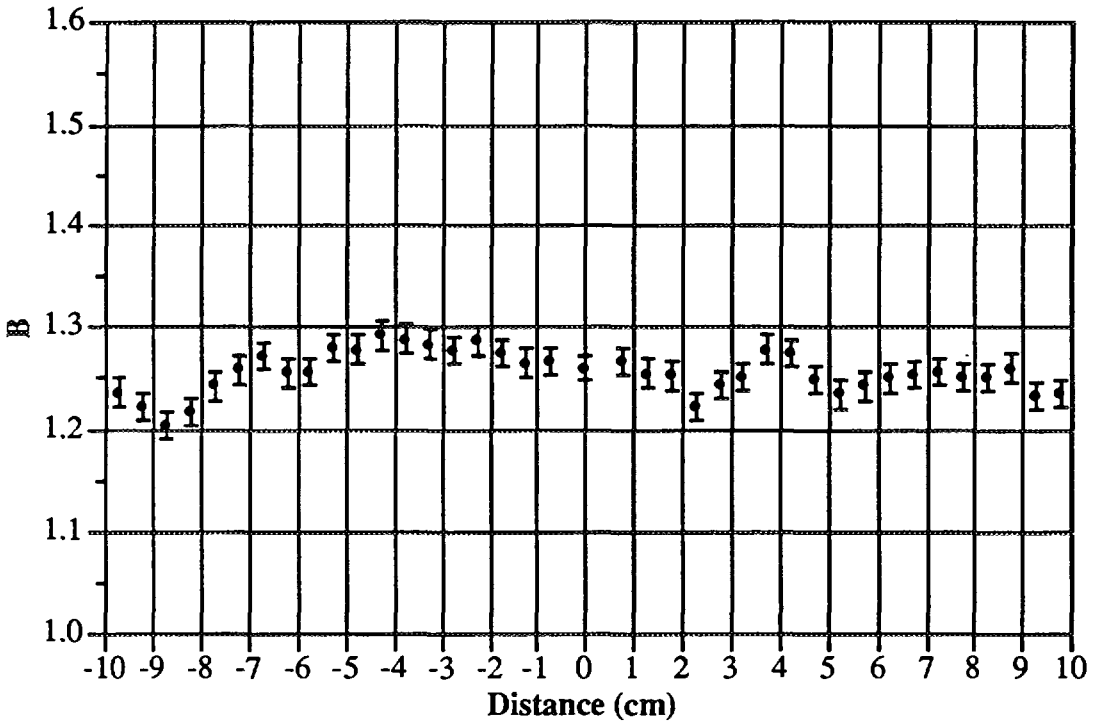

Narrow Spectrum Series - 300 kV (60°)

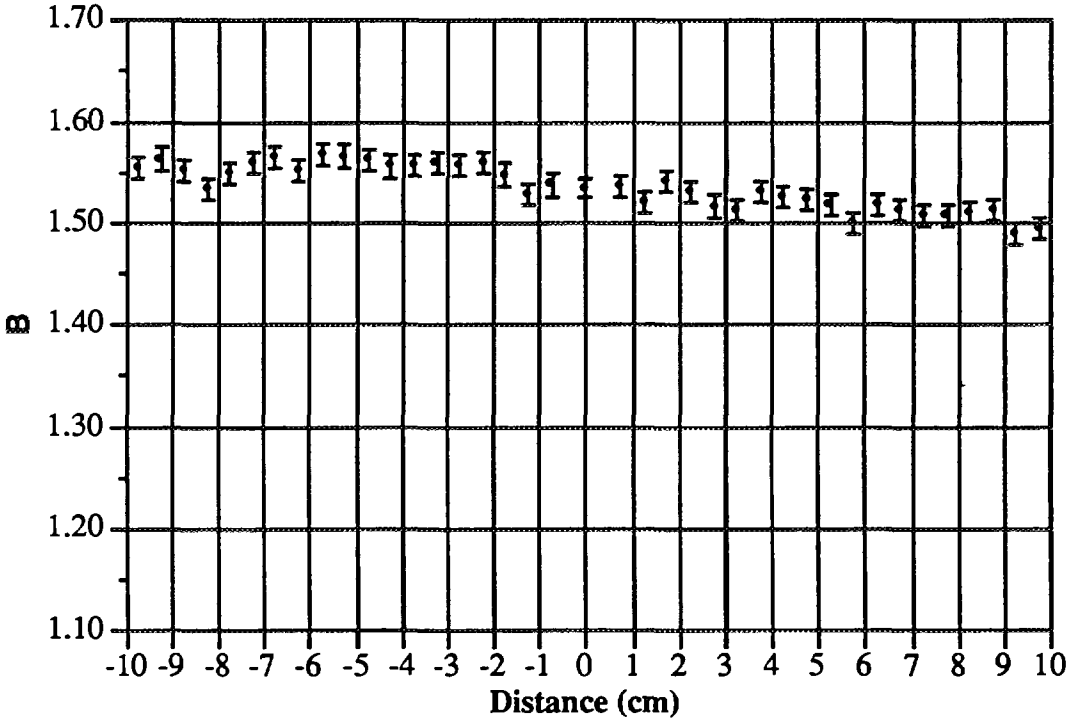

Wide Spectrum Series - 60 kV (60°)

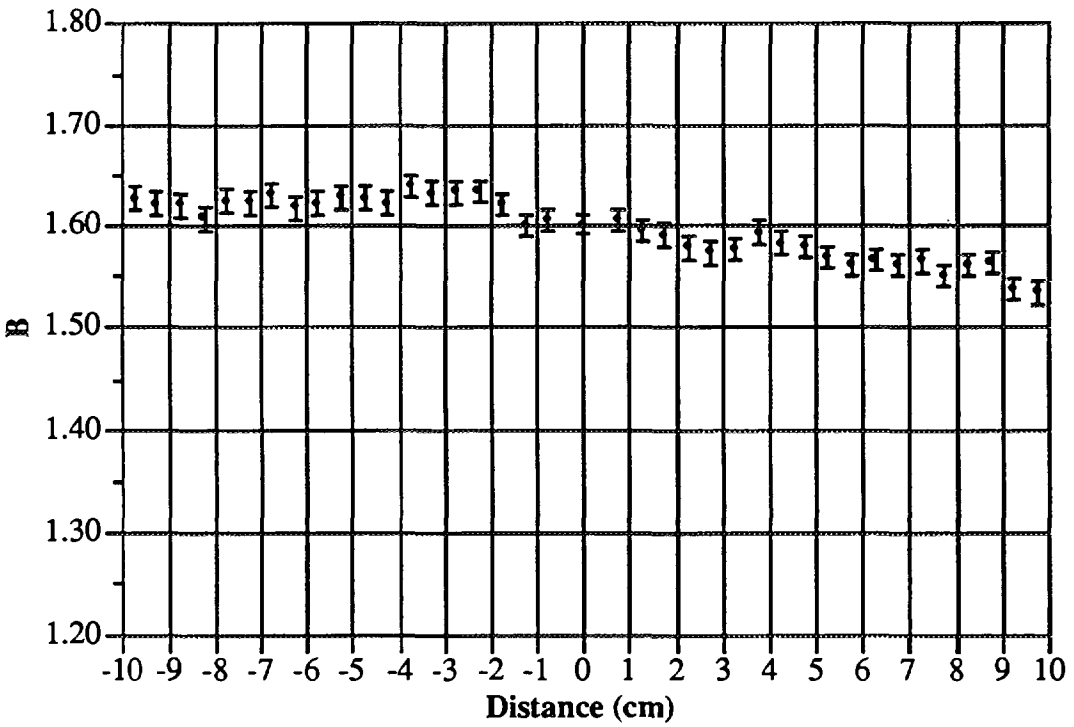

Wide Spectrum Series - 80 kV (60°)

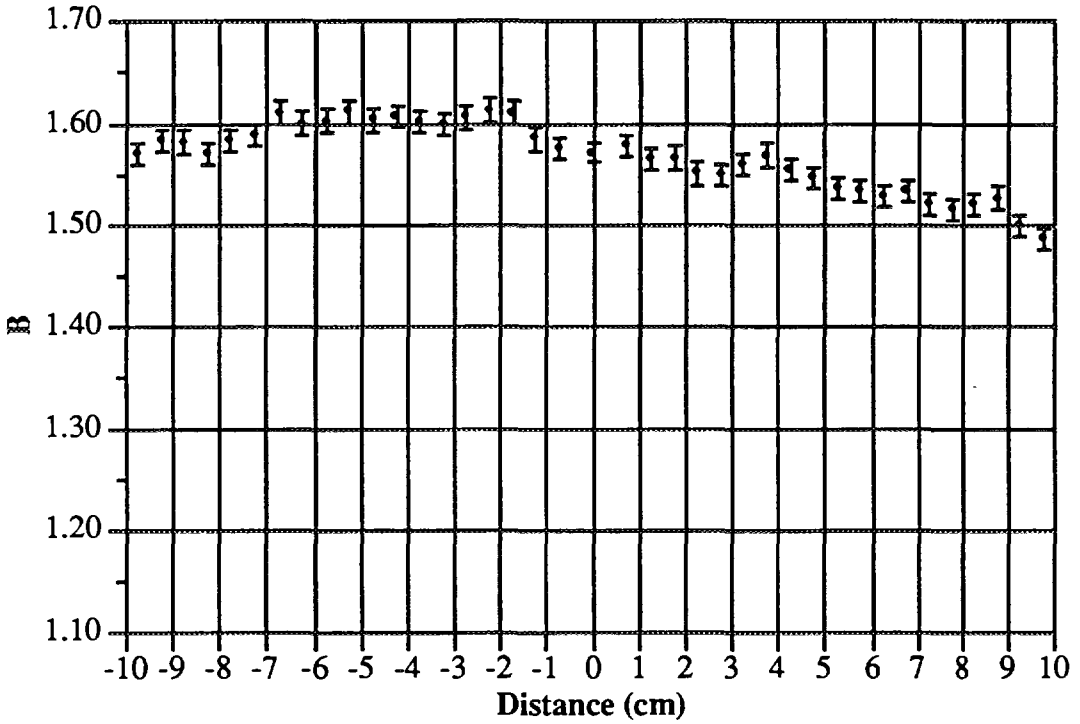

Wide Spectrum Series - 110 kV (60°)

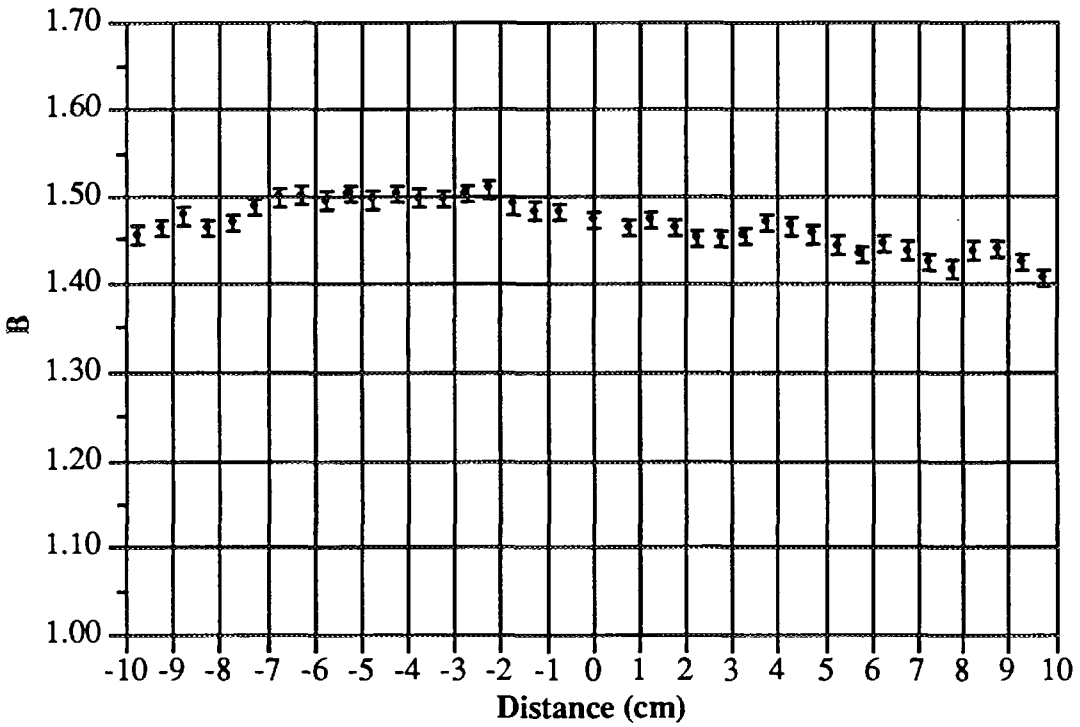

Wide Spectrum Series - 150 kV (60°)

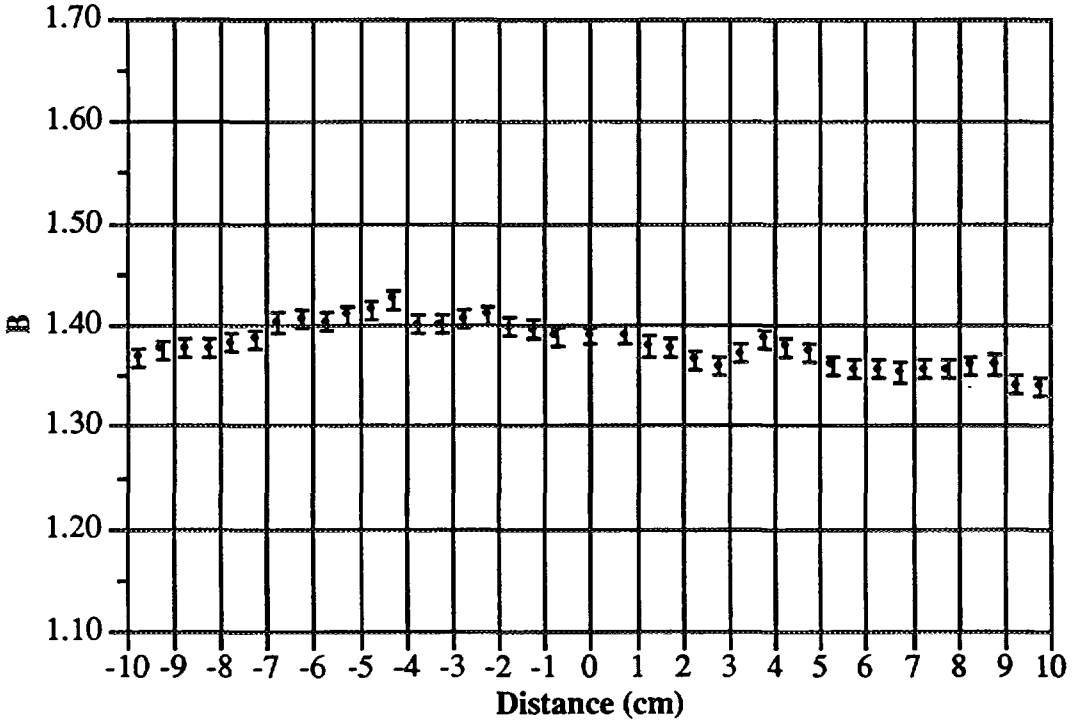

Wide Spectrum Series - 200 kV (60°)

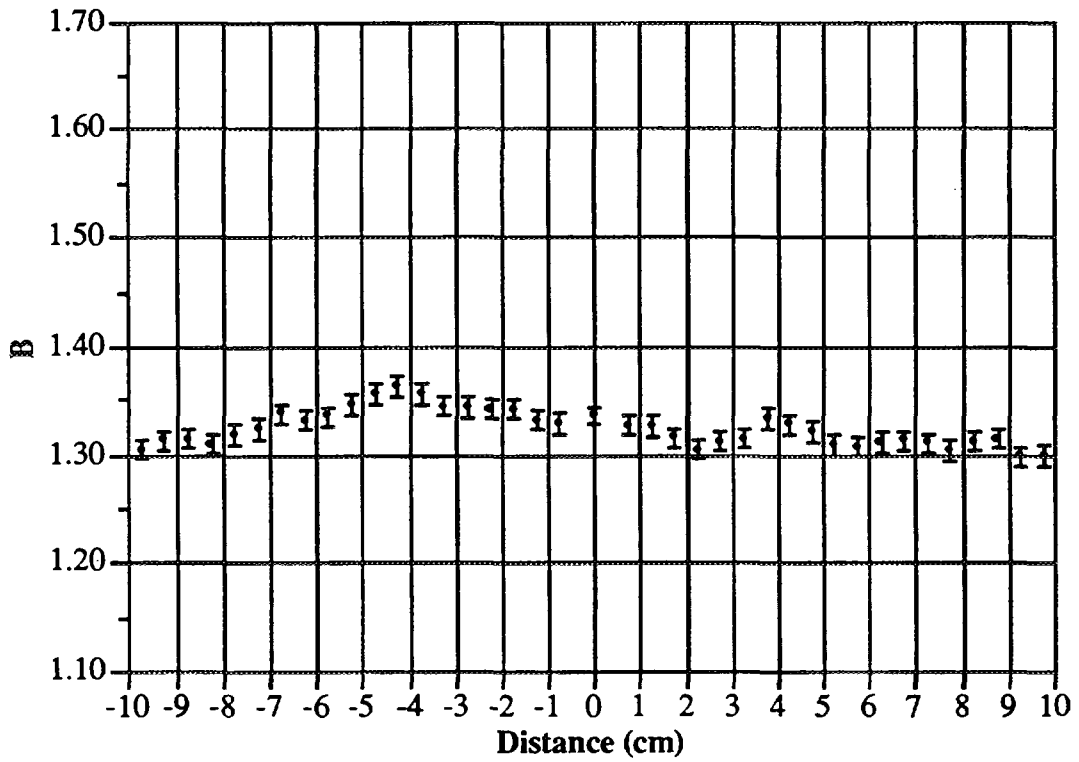

Wide Spectrum Series - 250 kV (60°)

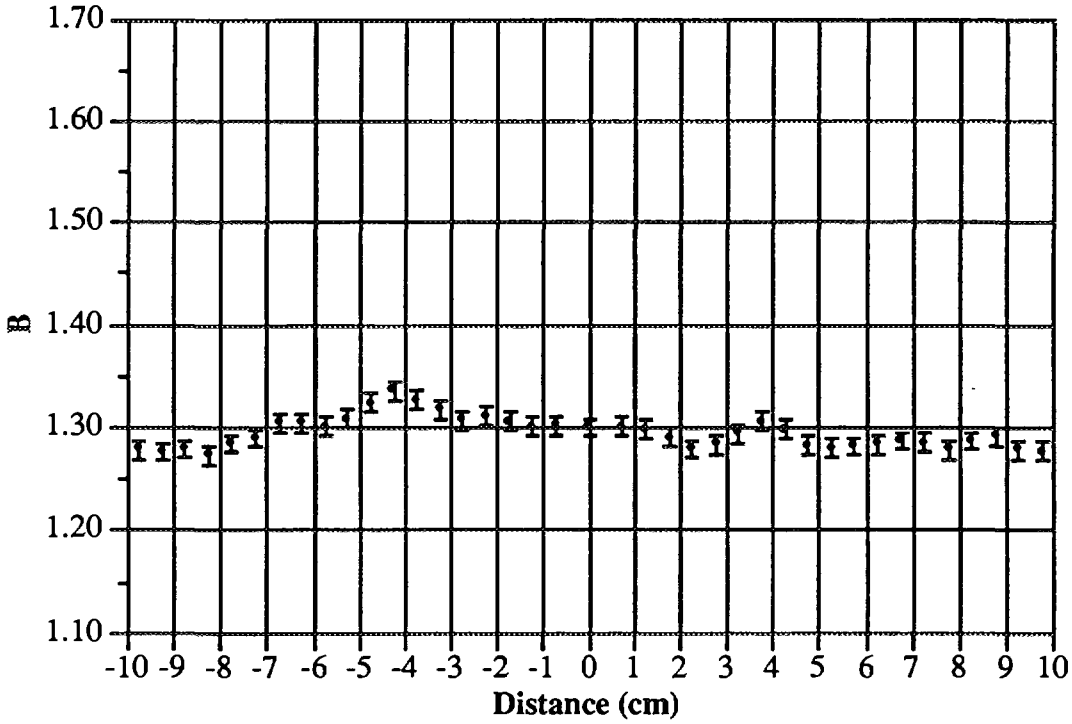

Wide Spectrum Series - 300 kV (60°)

NARROW AND WIDE SPECTRUM SERIES

75°

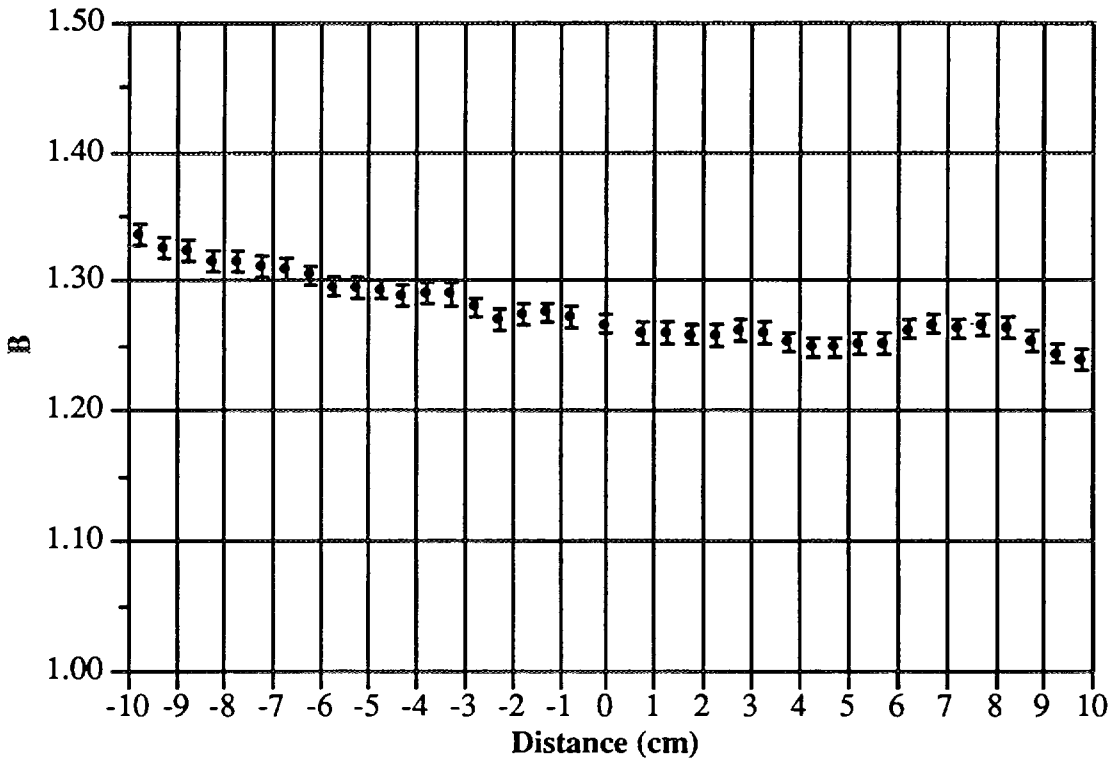

Narrow Spectrum Series - 40 kV (75°)

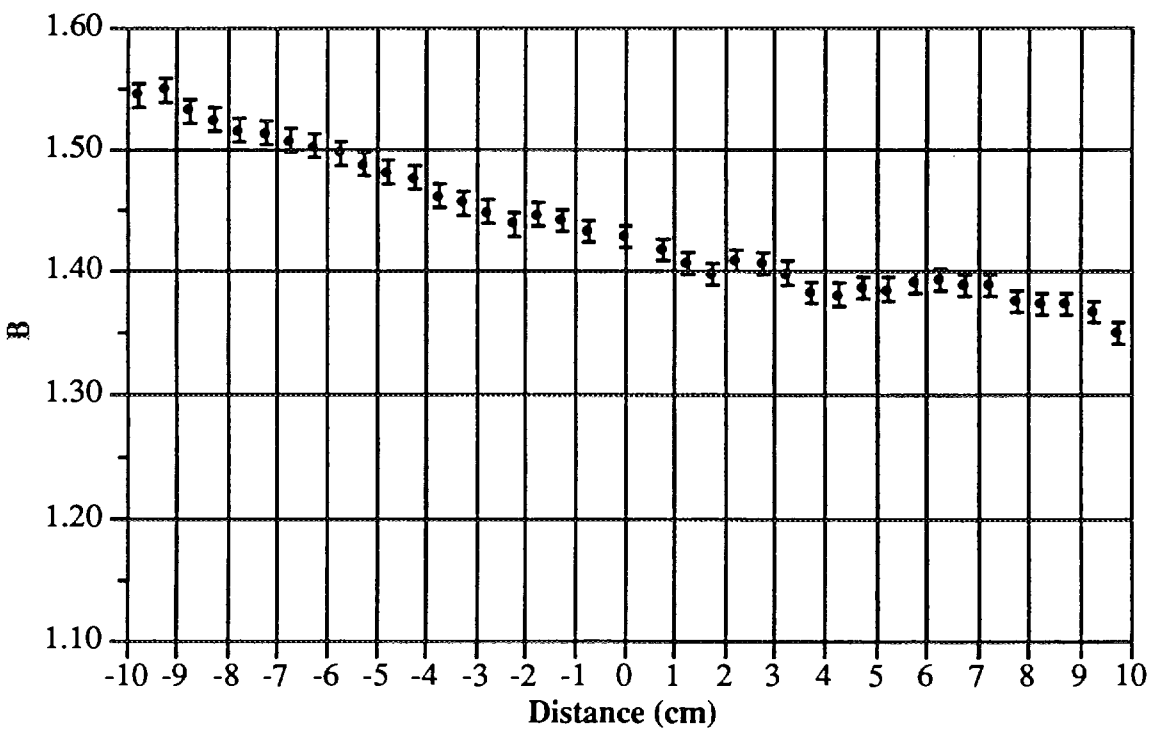

Narrow Spectrum Series - 60 kV (75°)

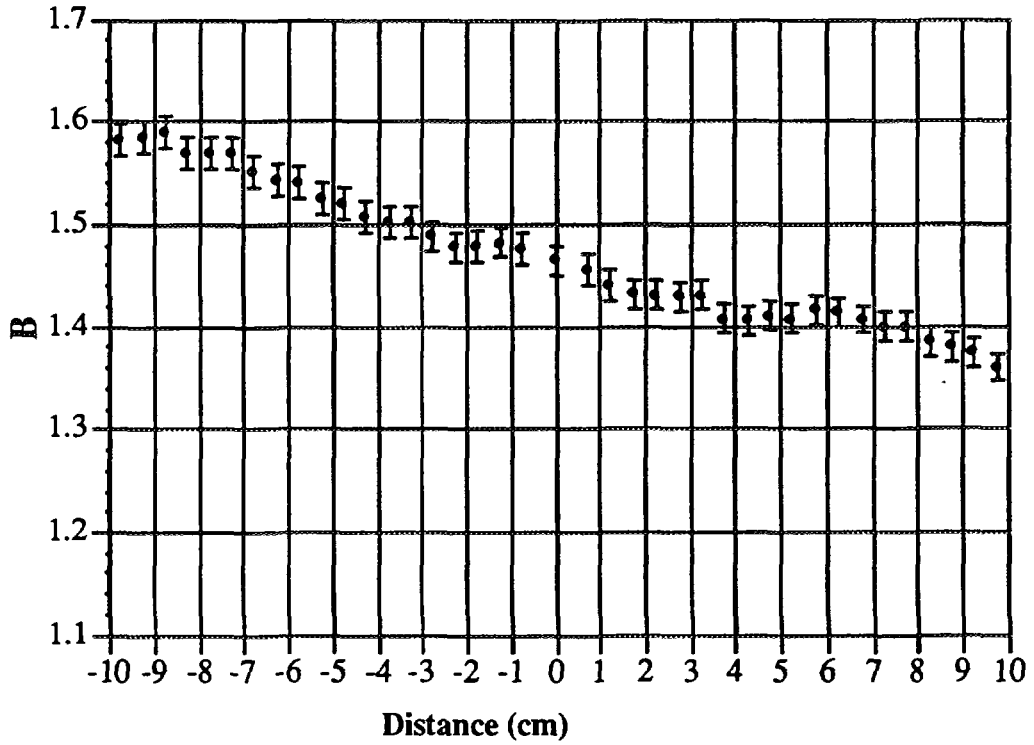

Narrow Spectrum Series - 80 kV (75°)

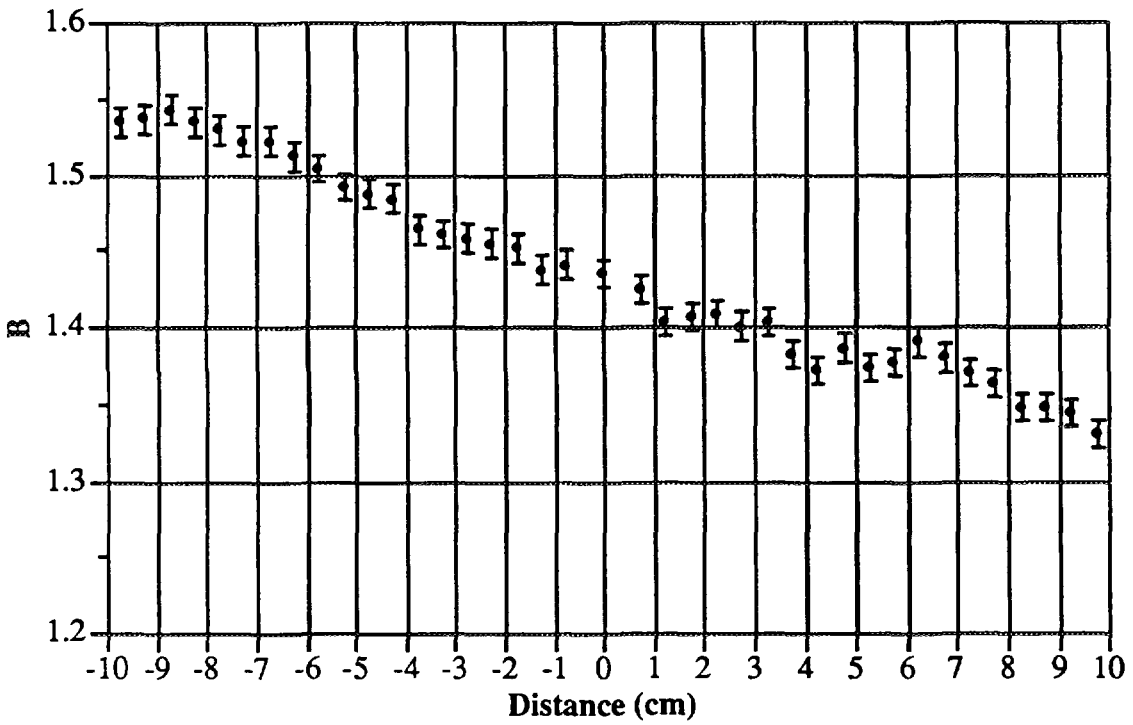

Narrow Spectrum Series - 100 kV (75°)

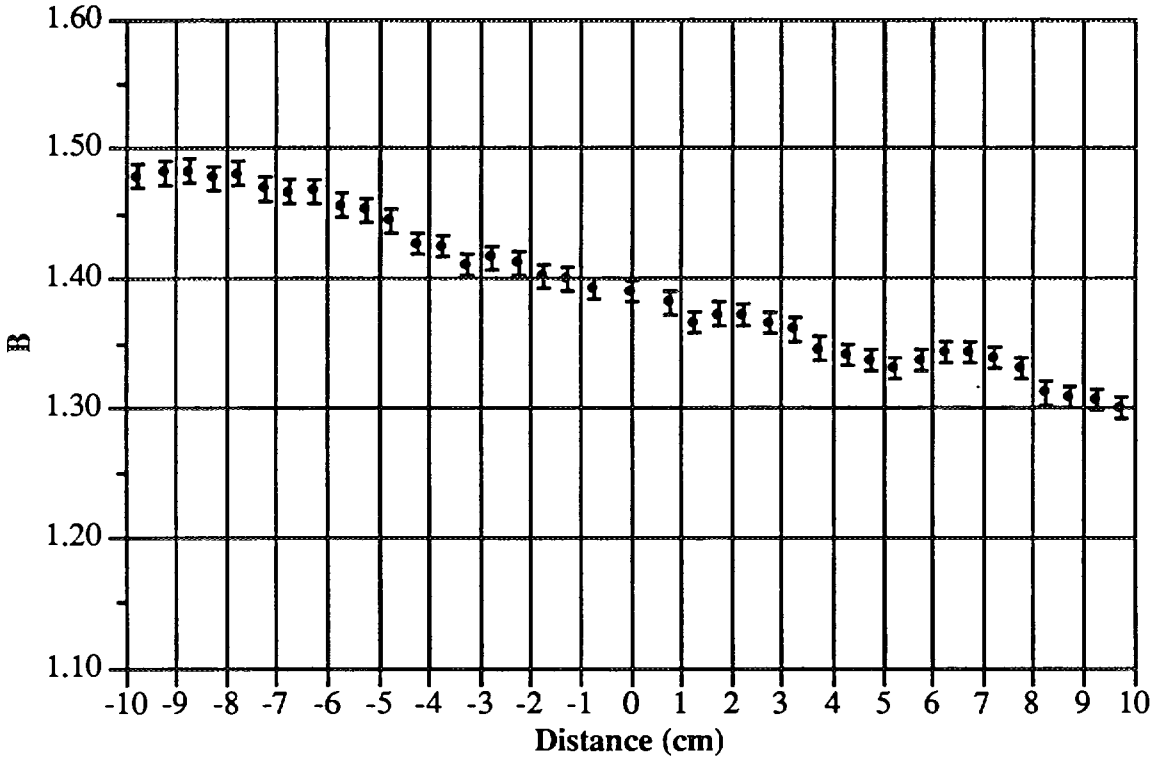

Narrow Spectrum Series - 120 kV (75°)

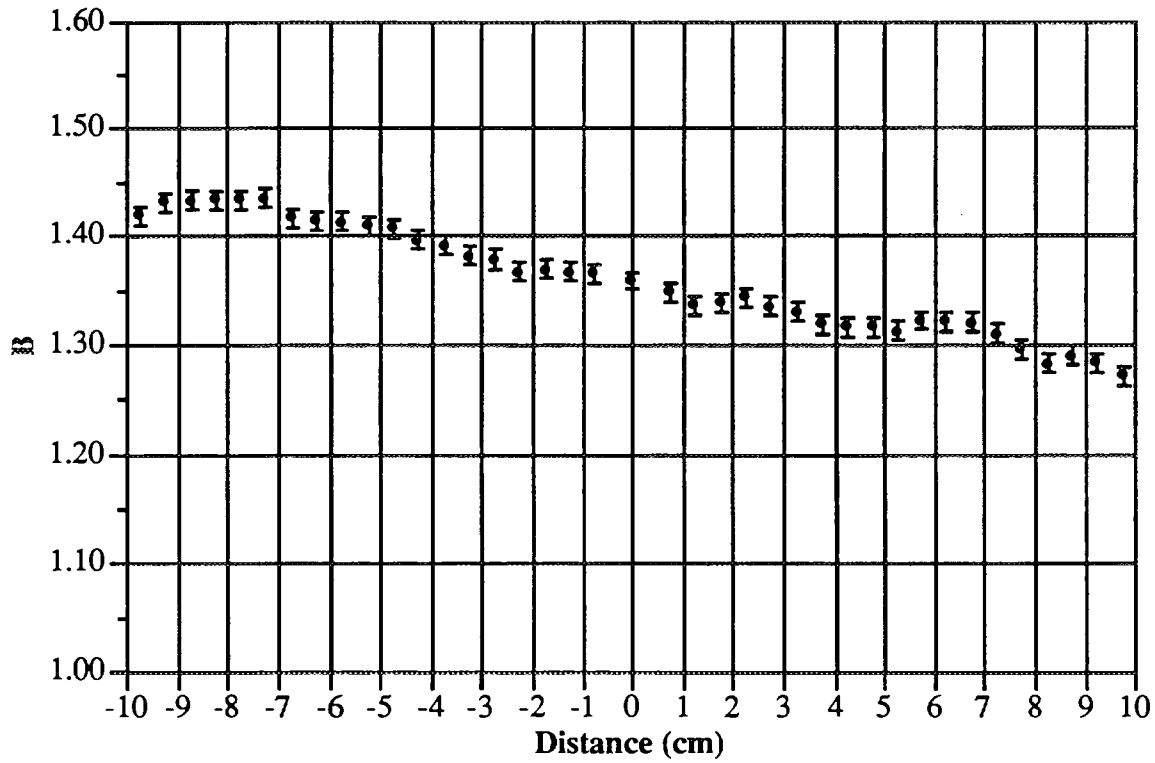

Narrow Spectrum Series - 150 kV (75°)

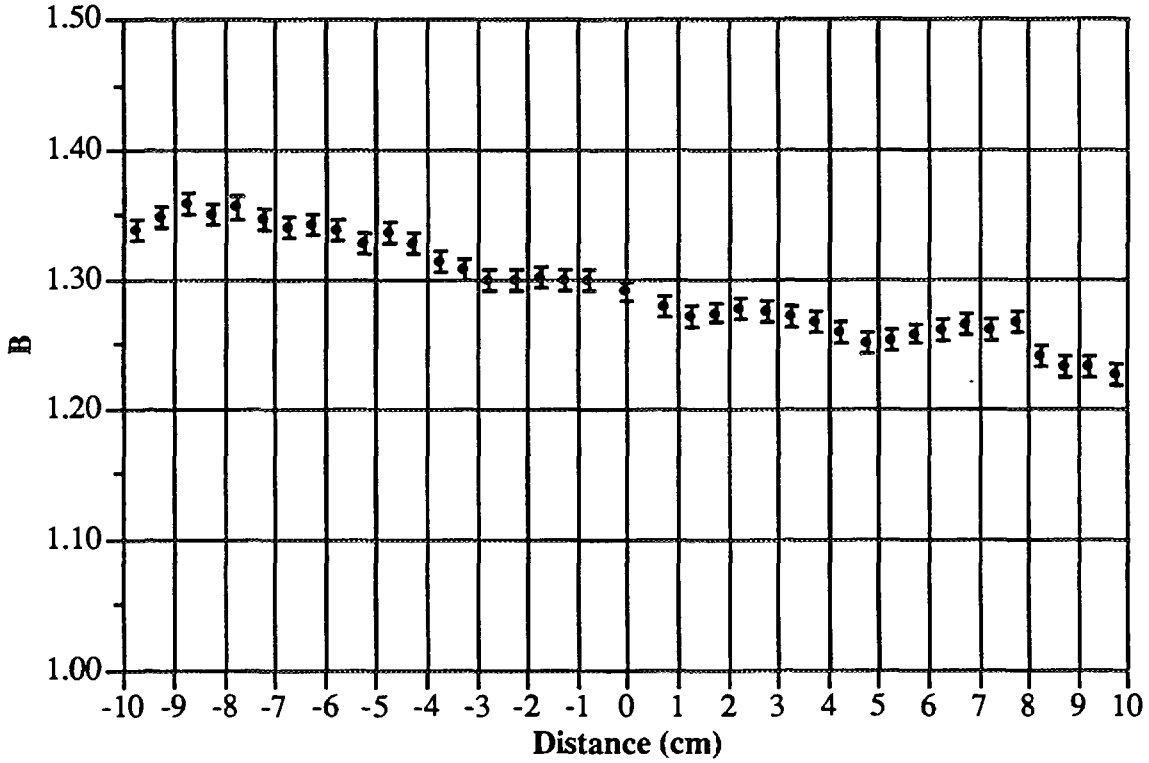

Narrow Spectrum Series - 200 kV (75°)

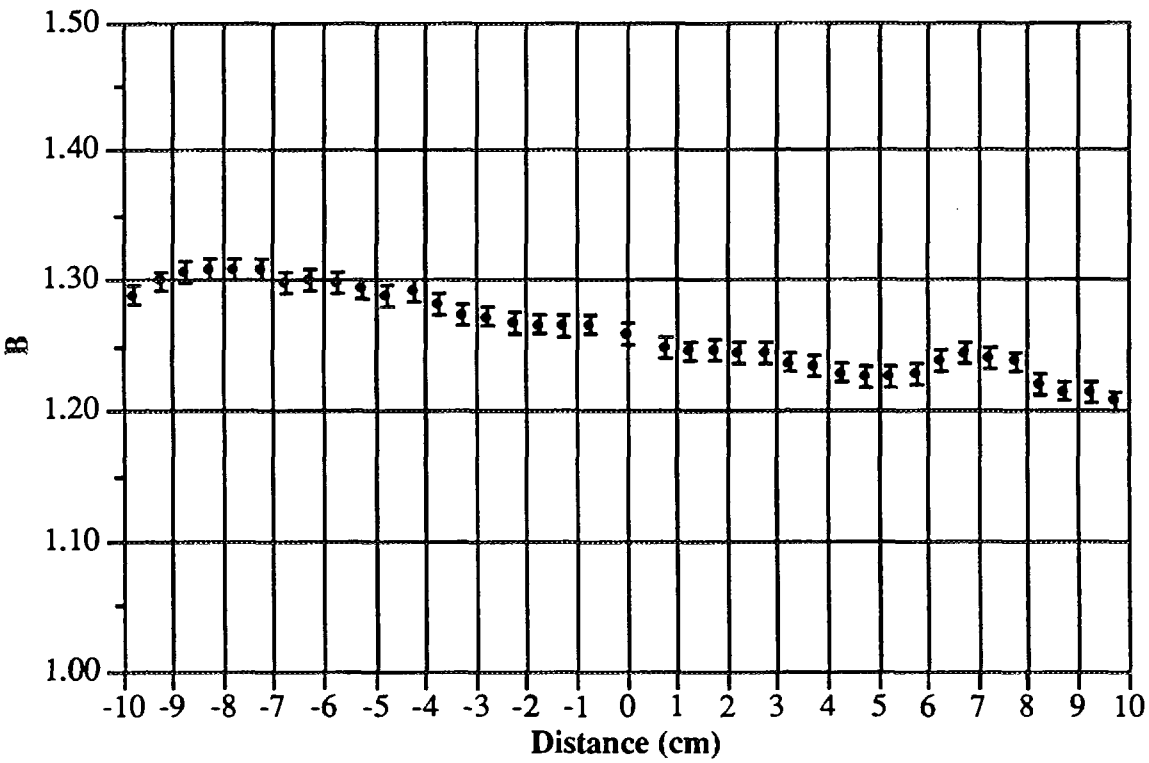

Narrow Spectrum Series - 250 kV (75°)

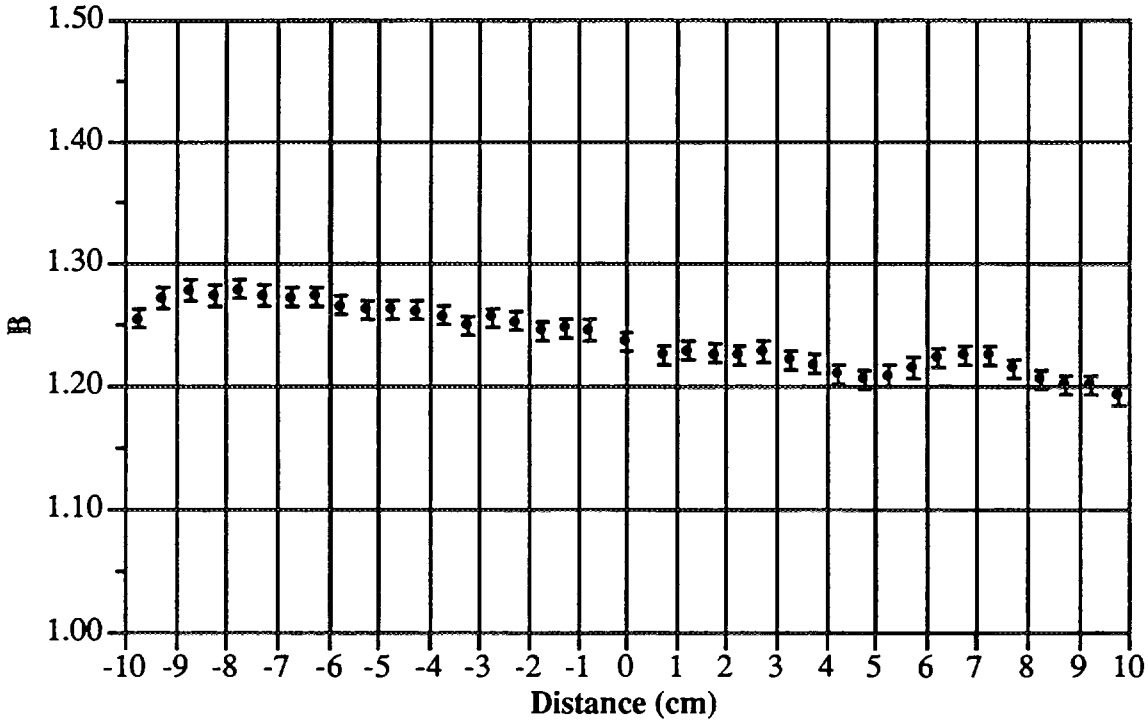

Narrow Spectrum Series - 300 kV (75°)

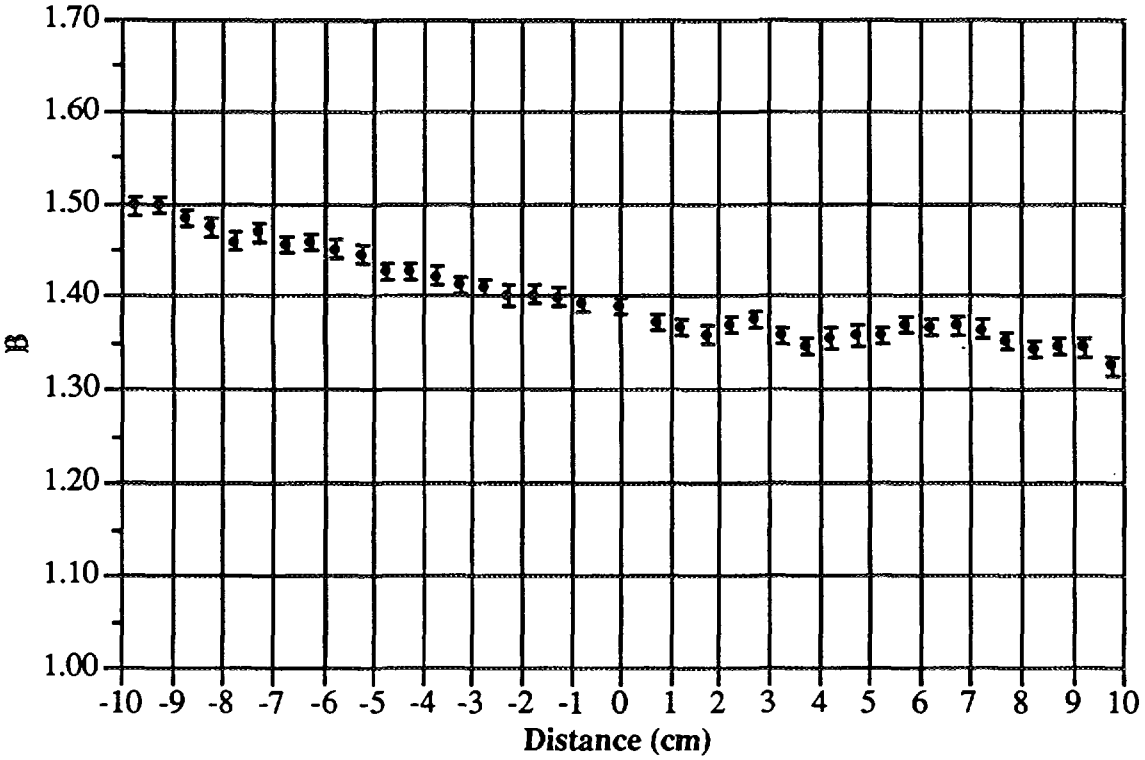

Wide Spectrum Series - 60 kV (75°)

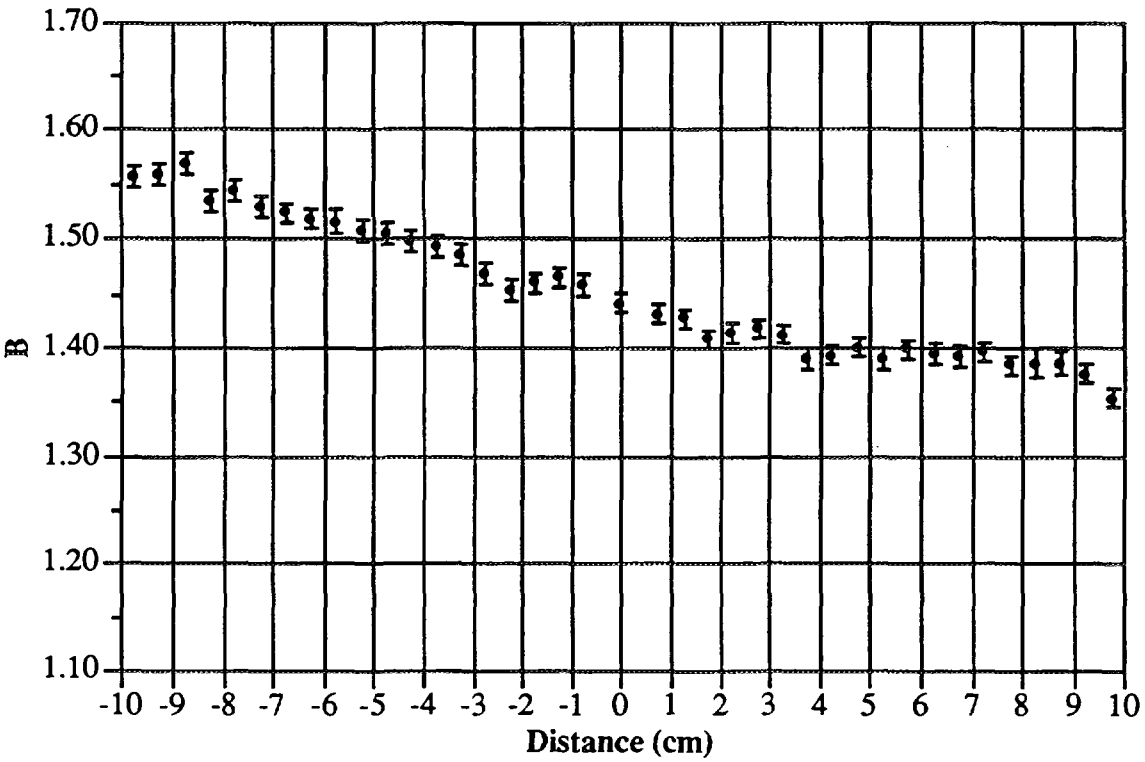

Wide Spectrum Series - 80 kV (75°)

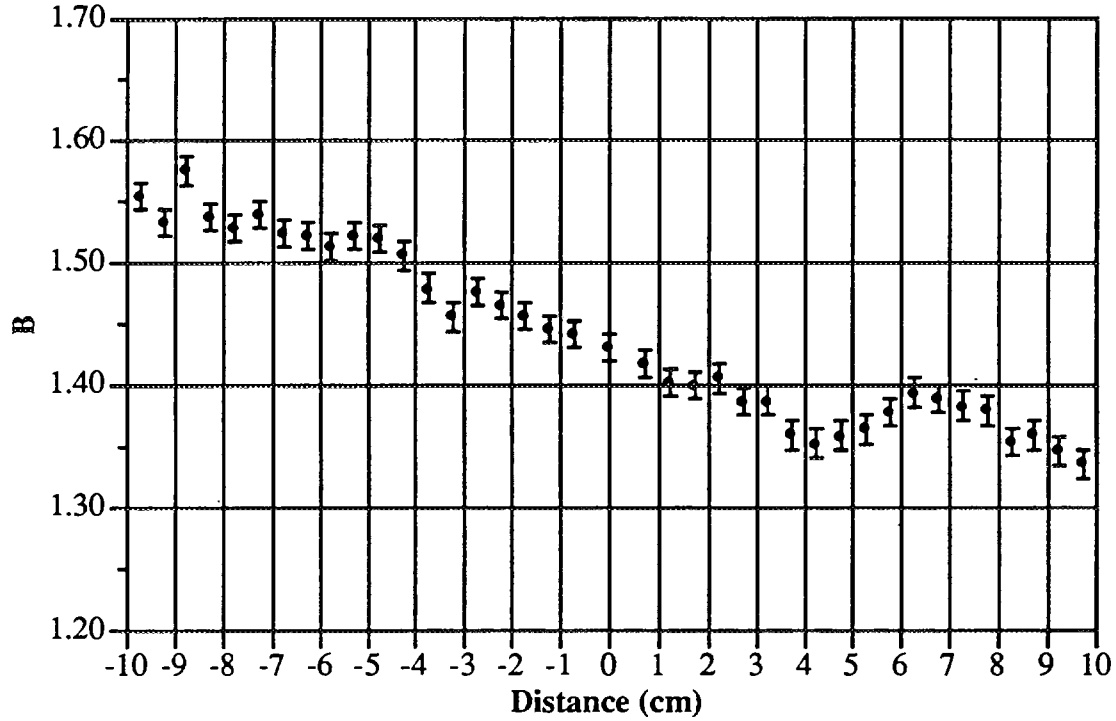

Wide Spectrum Series - 110 kV (75°)

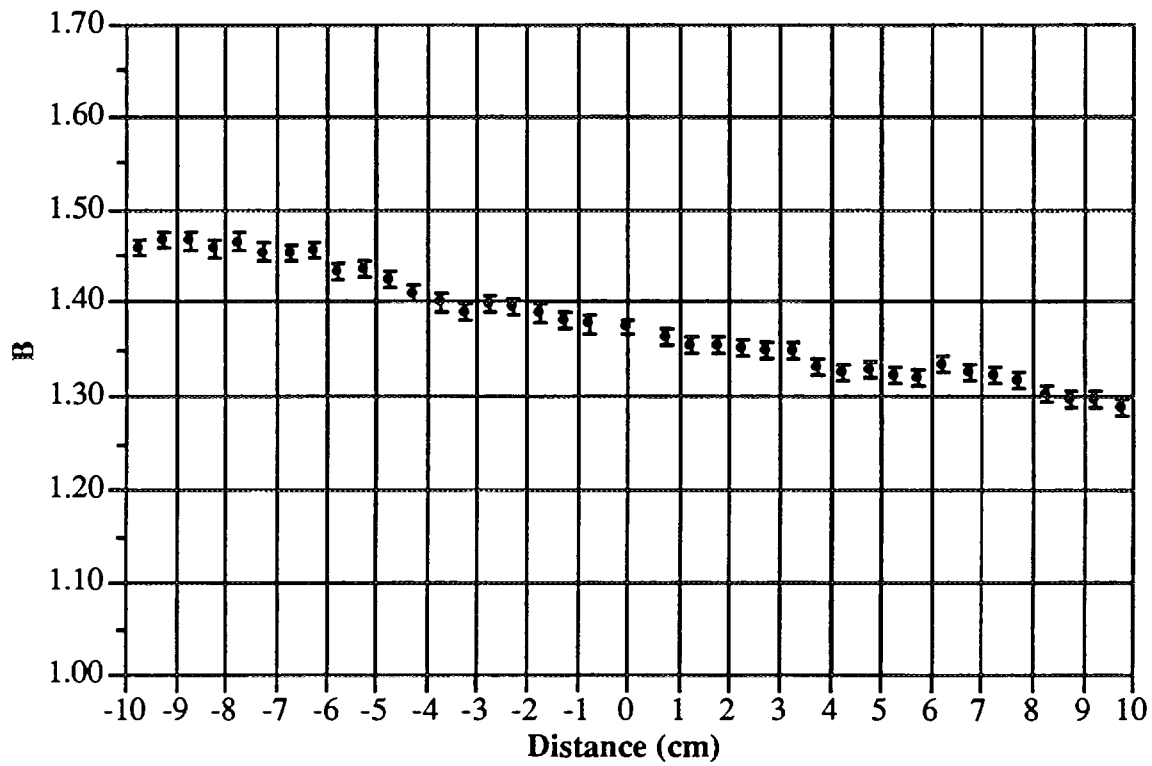

Wide Spectrum Series - 150 kV (75°)

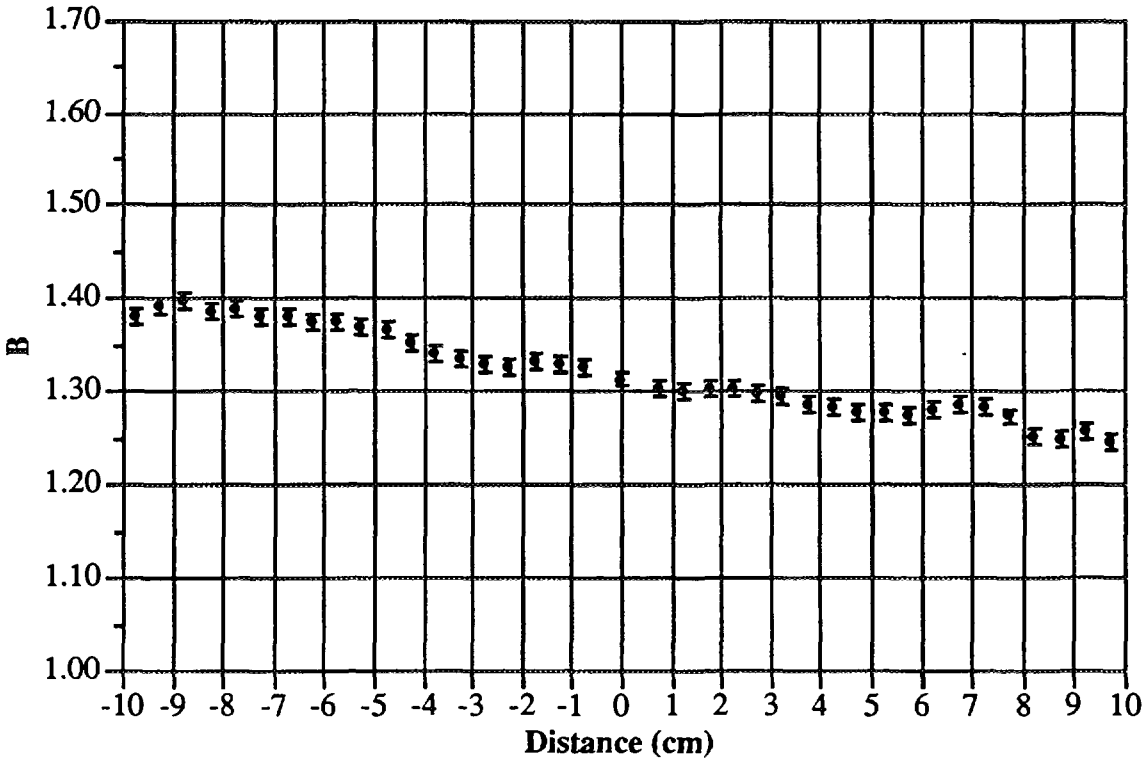

Wide Spectrum Series - 200 kV (75°)

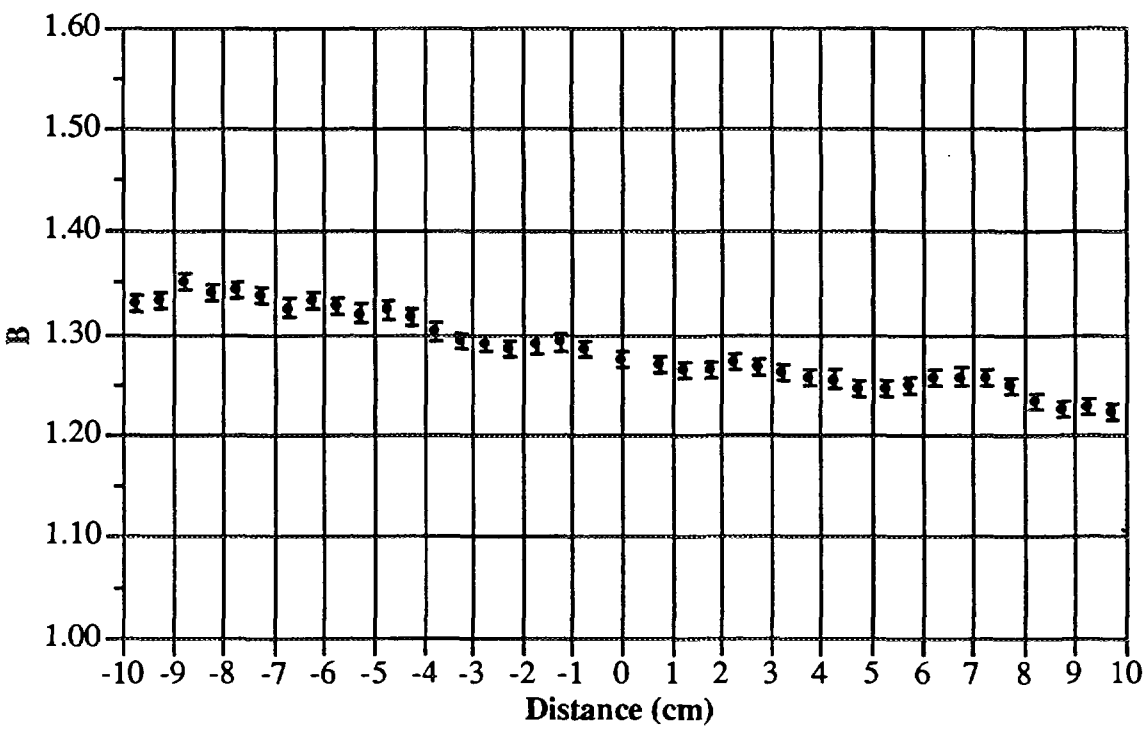

Wide Spectrum Series - 250 kV (75°)

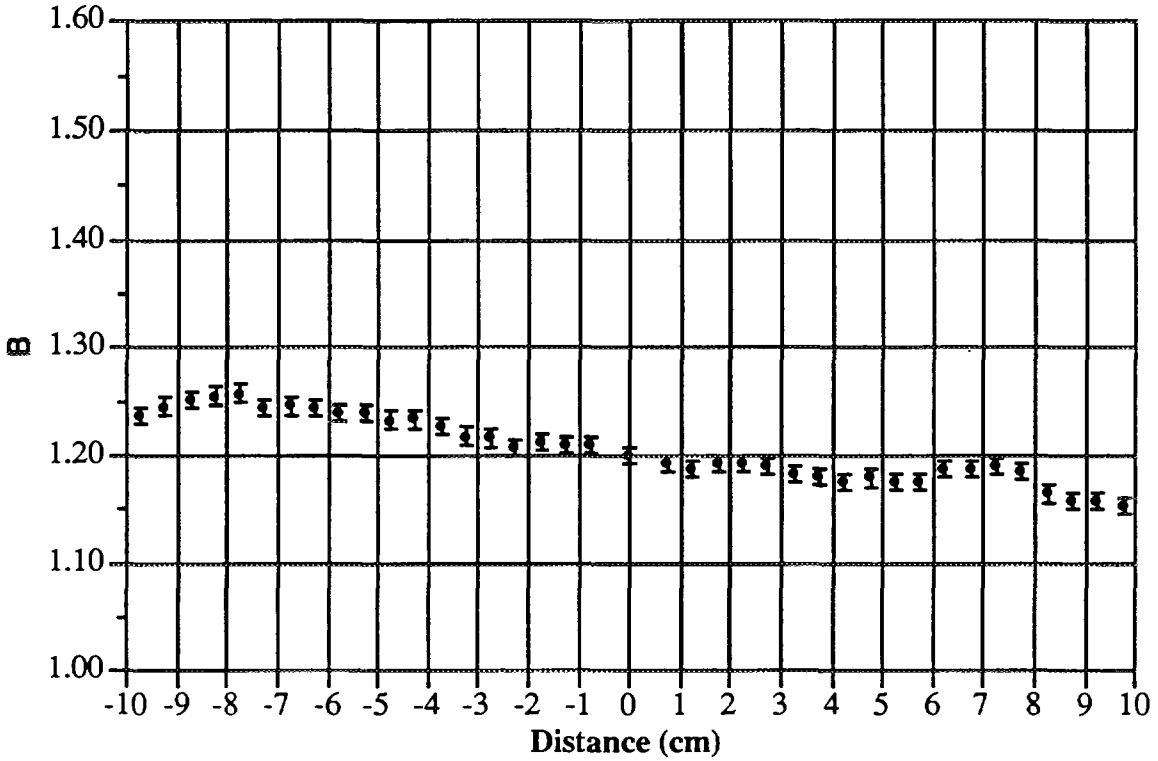

Wide Spectrum Series - 300 kV (75°)

APPENDIX C

Plots of Air Kerma free in air measurements as performed at PTB for Narrow and Wide Spectrum Series

NARROW SERIES (80 kV)

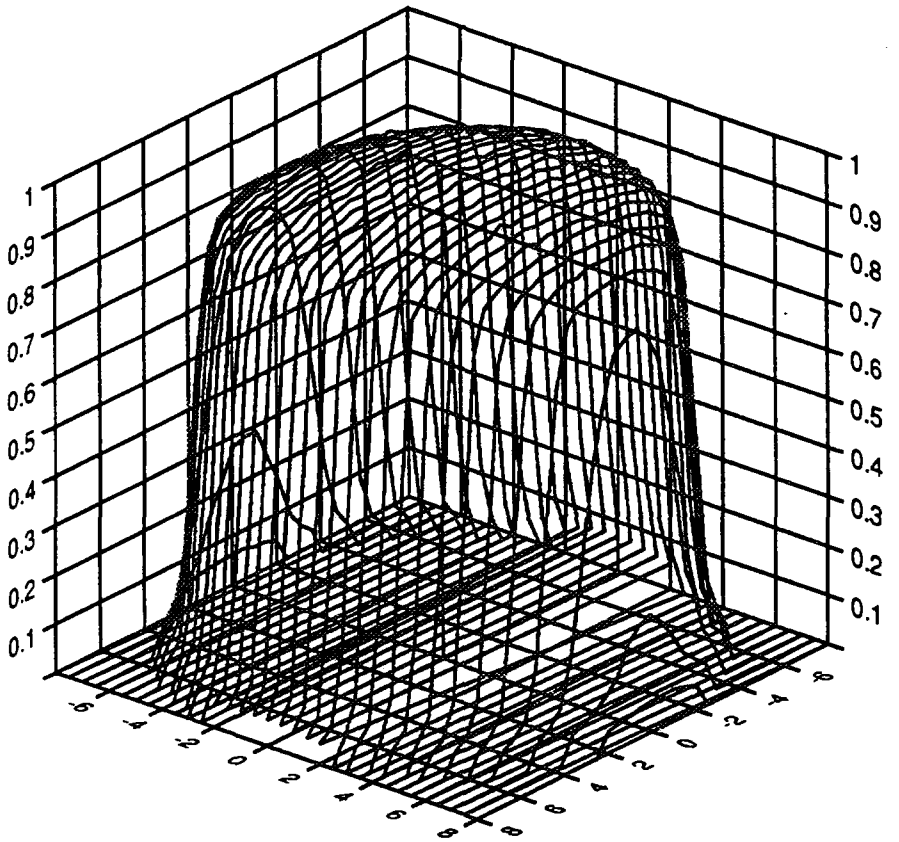

<Z>=0 ; -8 cm <Y< 8 cm

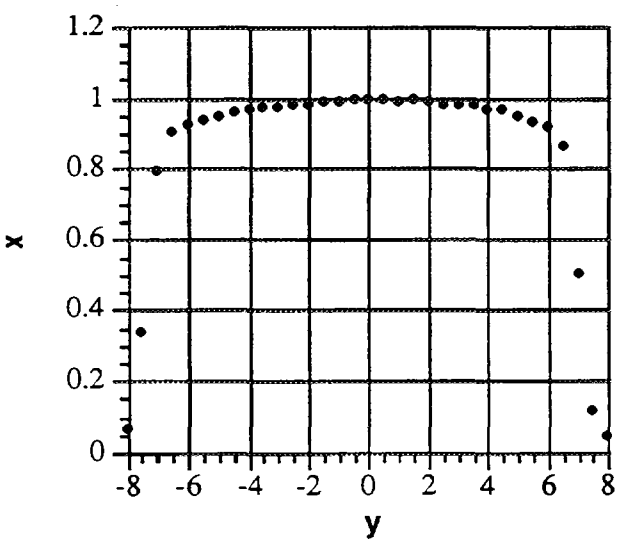

<Y>=0 ; -8 cm <Z< 8 cm

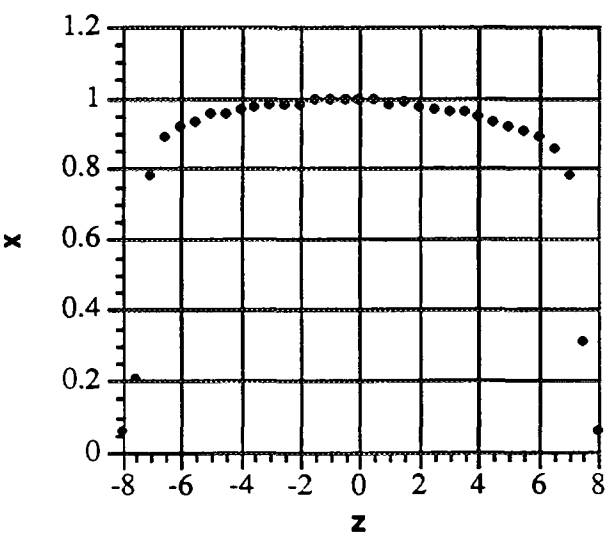

NARROW SERIES (150 kV)

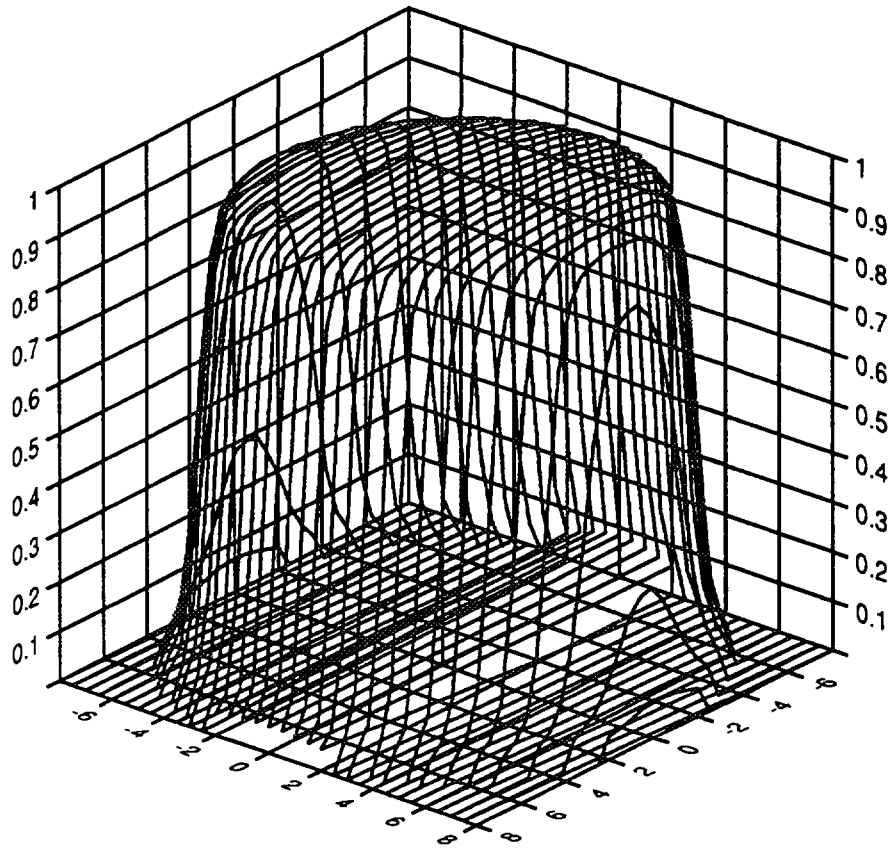

<Z>=0 ; -8 cm<Y< 8 cm

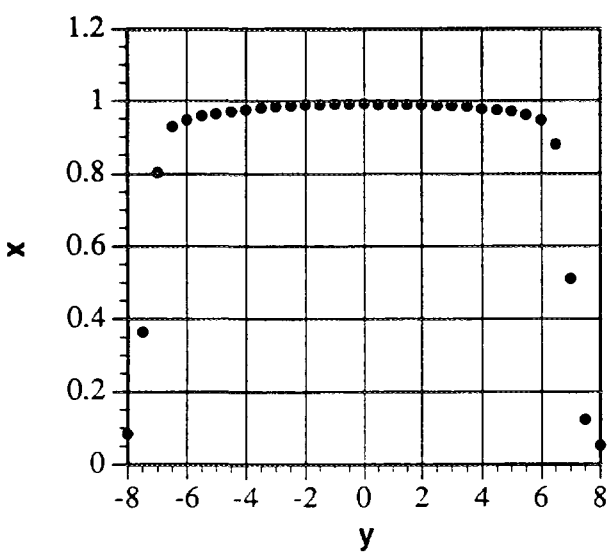

<Y>=0 ; -8 cm<Z< 8 cm

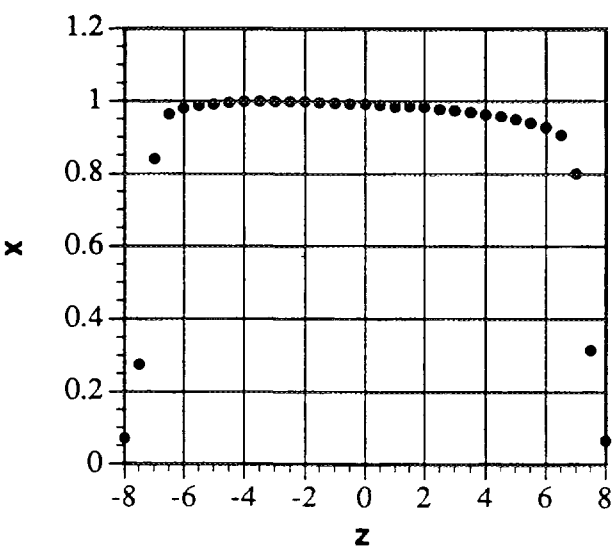

NARROW SERIES (300 kV)

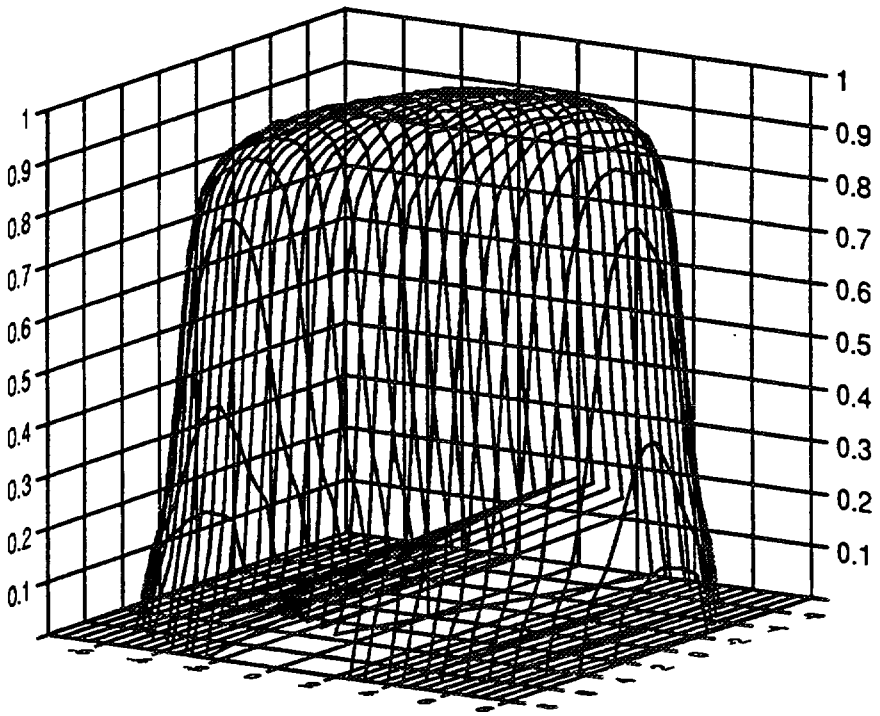

<Z>=0 ; -8 cm <Y< 8 cm

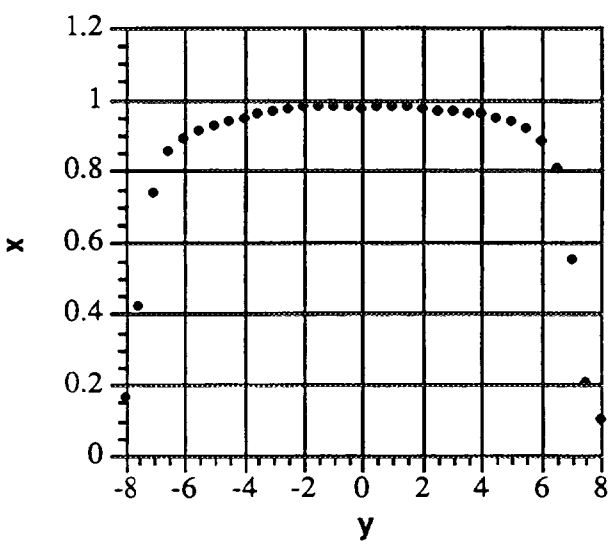

<Y>=0 ; -8 cm <Z< 8 cm

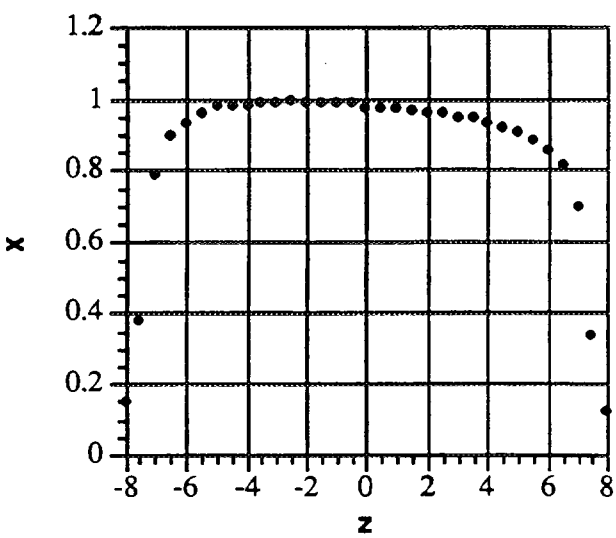

WIDE SERIES (80 kV)

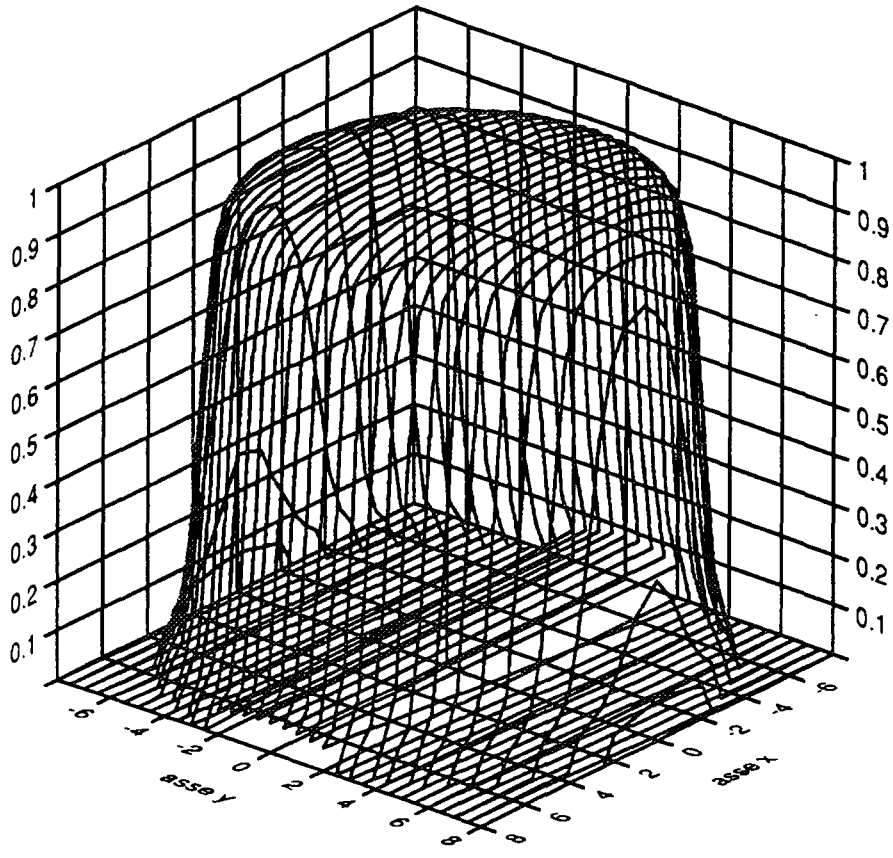

<Z>=0 ; -8 cm <Y< 8 cm

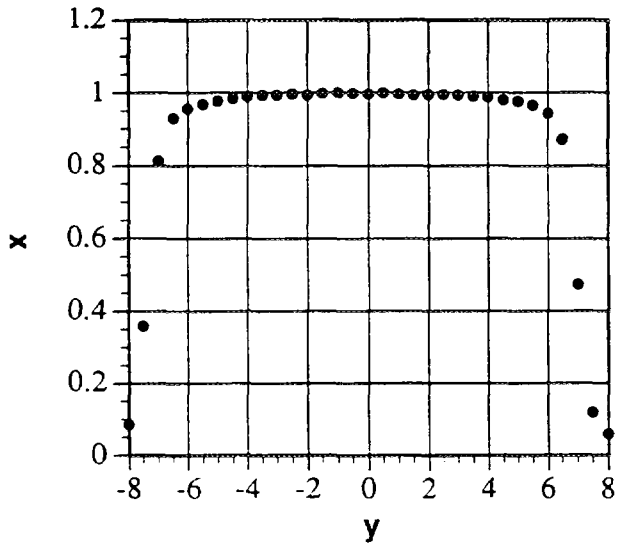

<Y>=0 ; -8 cm <Z< 8 cm

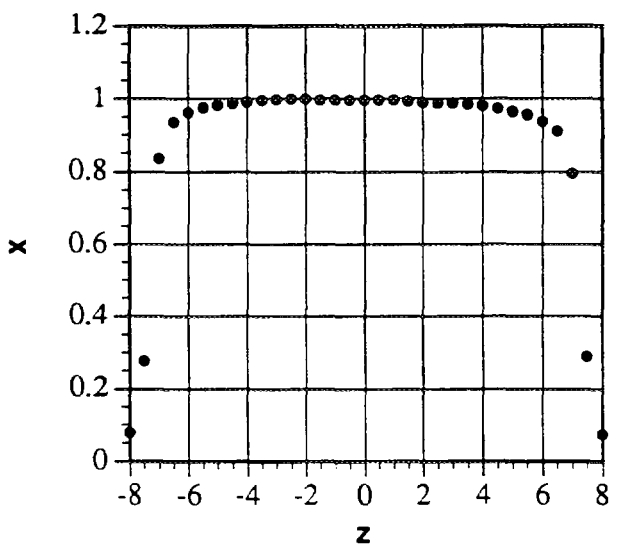

WIDE SERIES (150 kV)

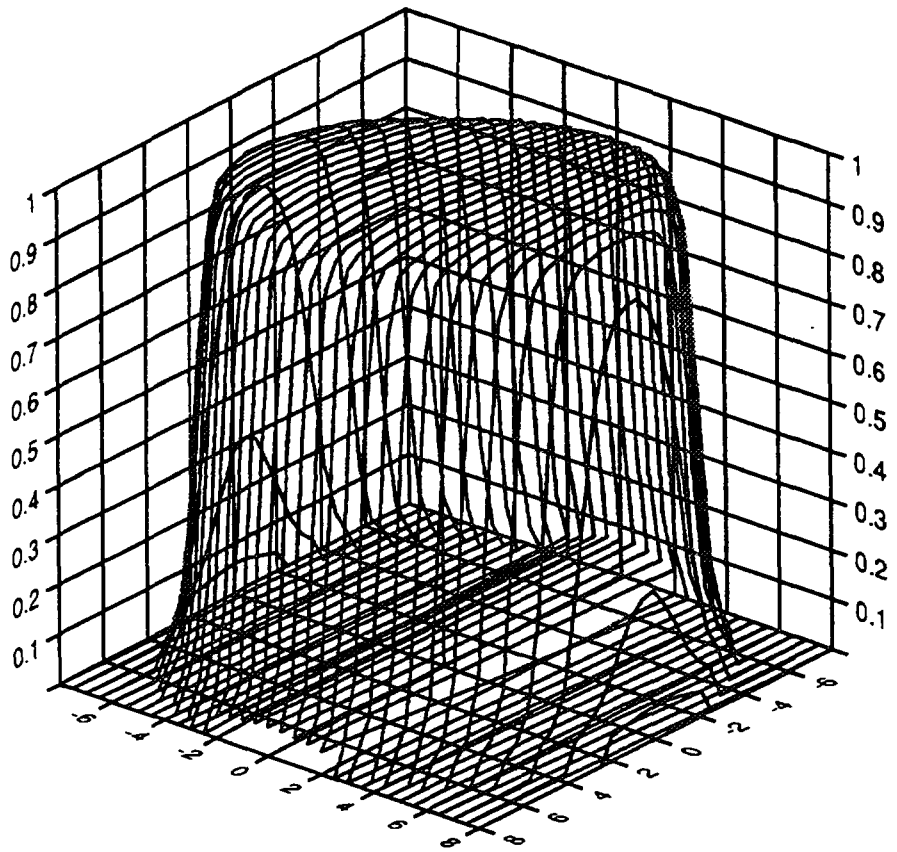

<Z>=0 ; -8 cm<Y<8 cm

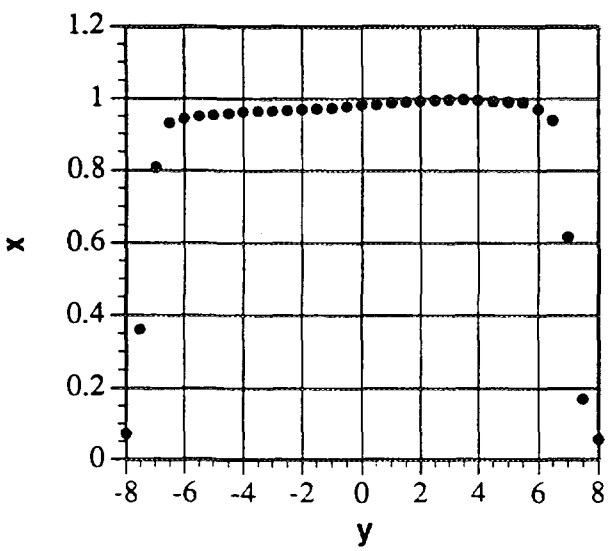

<Y>=0 ; -8 cm<Z<8 cm

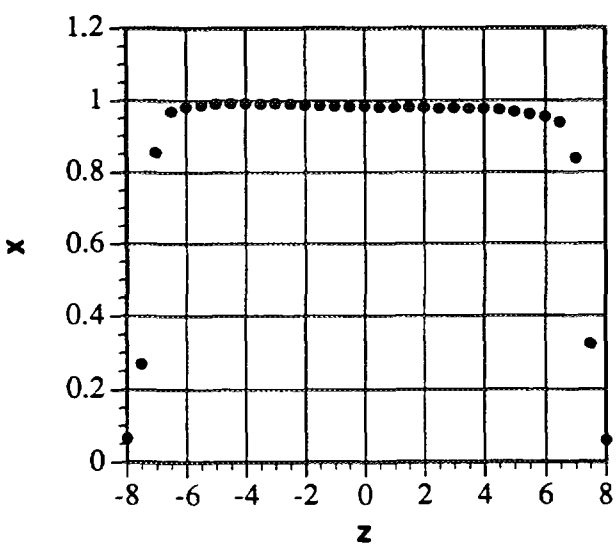

WIDE SERIES (200 kV)

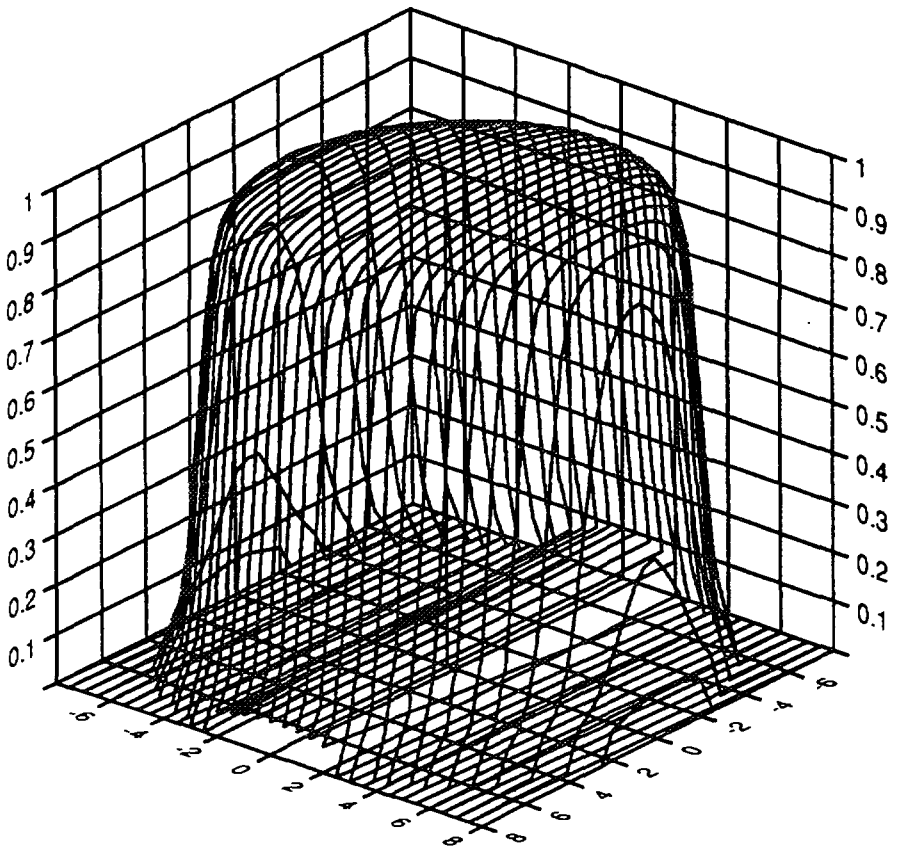

<Z>=0 ; -8 cm<Y< 8 cm

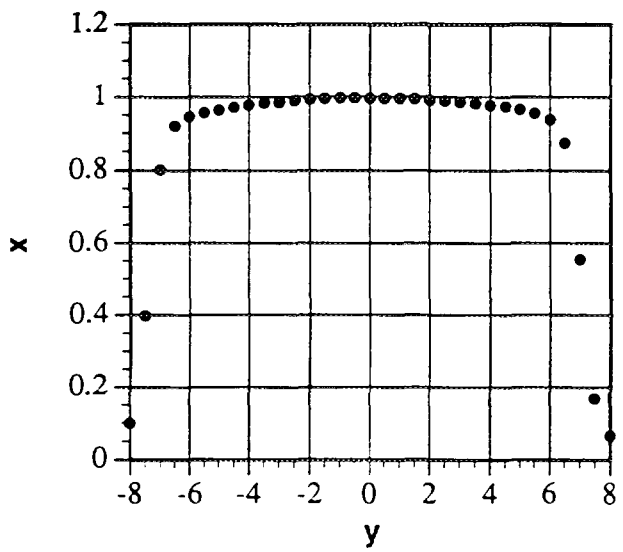

<Z>=0 ; -8 cm<Y< 8 cm

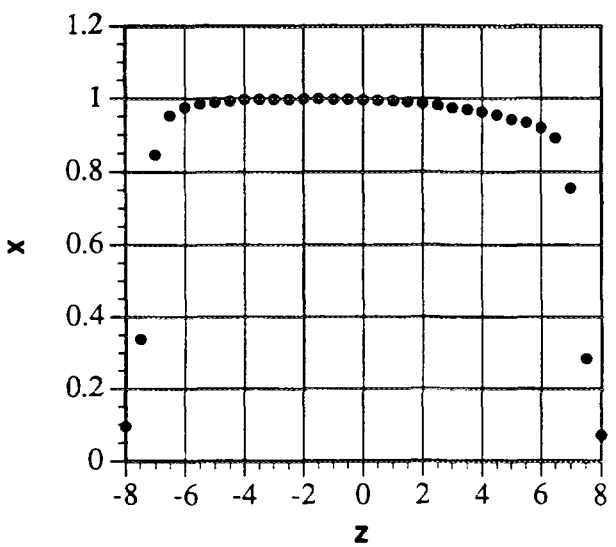

WIDE SERIES (300 kV)

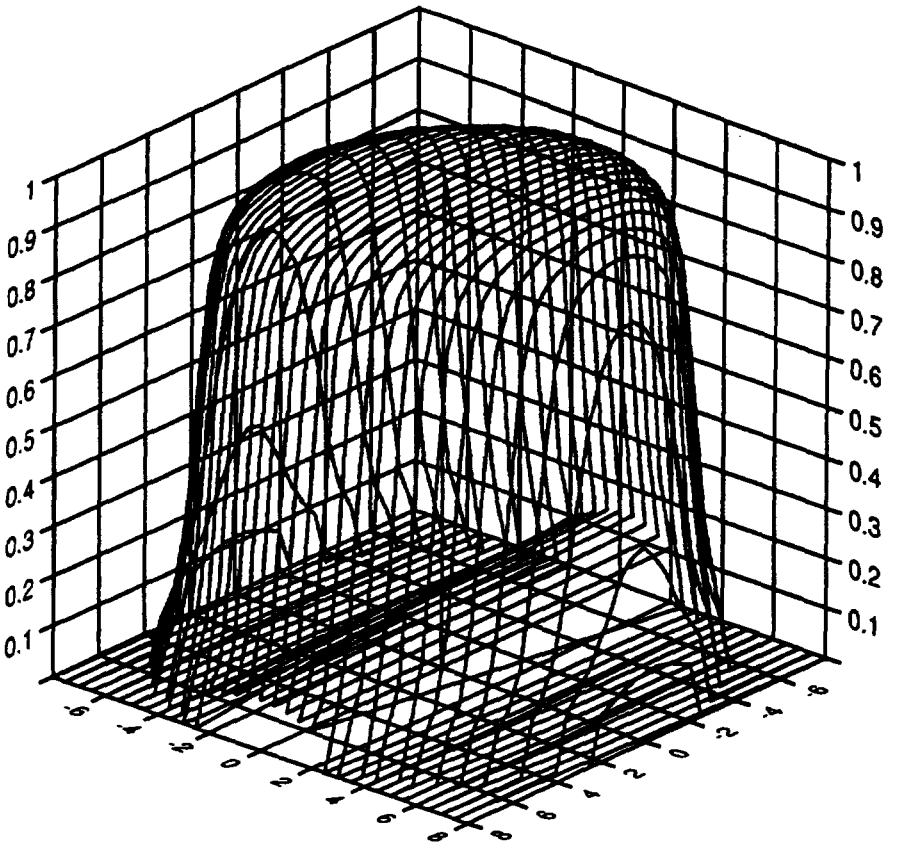

<Z>=0 ; -8 cm<Y<8 cm

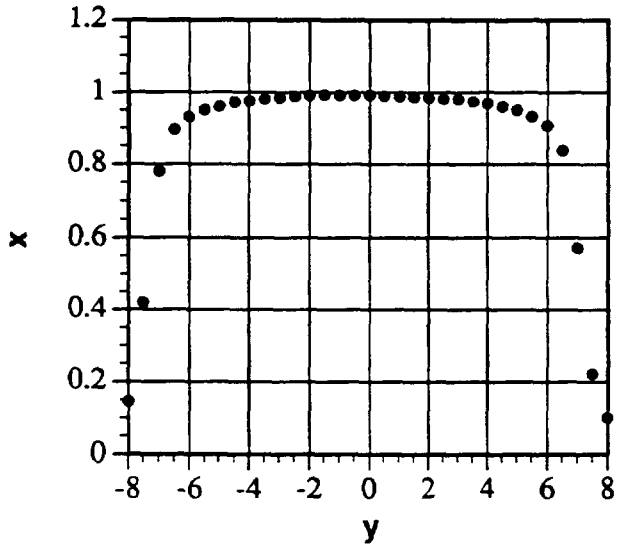

<Y>=0 ; -8 cm<Z<8 cm

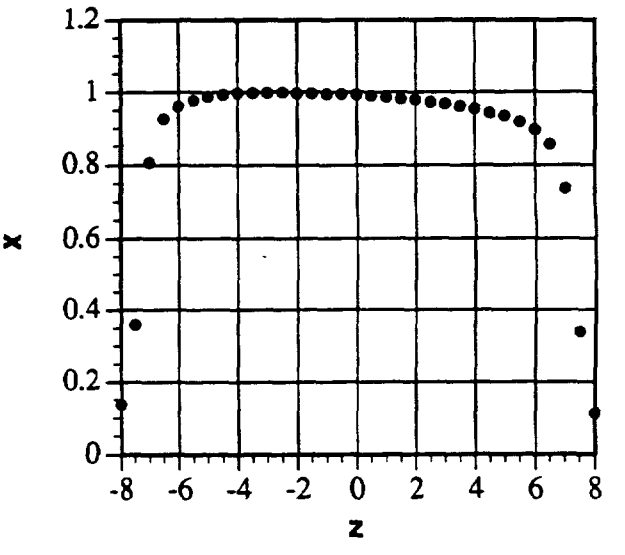

APPENDIX D

Air Kerma backscatter factor mapping for a PMMA slab phantom with realistic source shapes

NARROW SPECTRUM SERIES
(80 kV)

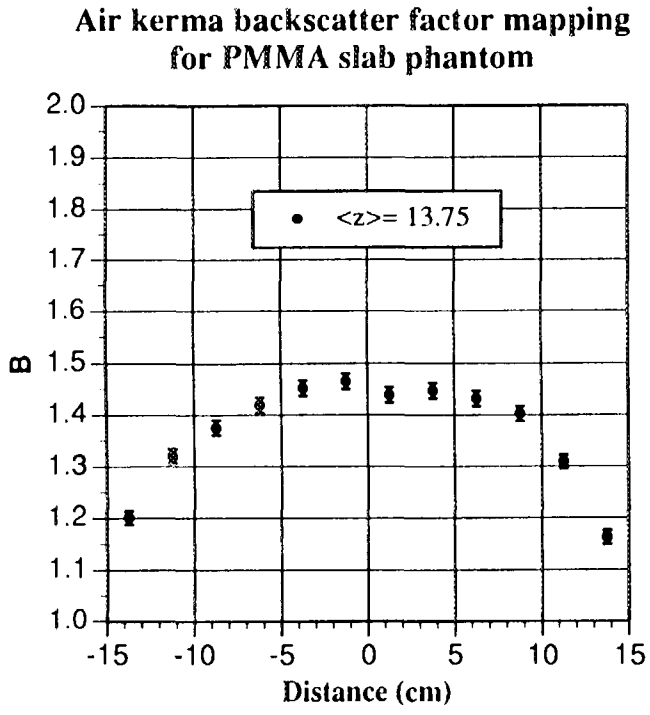
Air kerma backscatter factor mapping
for PMMA slab phantom
B
Distance (cm)
<z>= 13.75

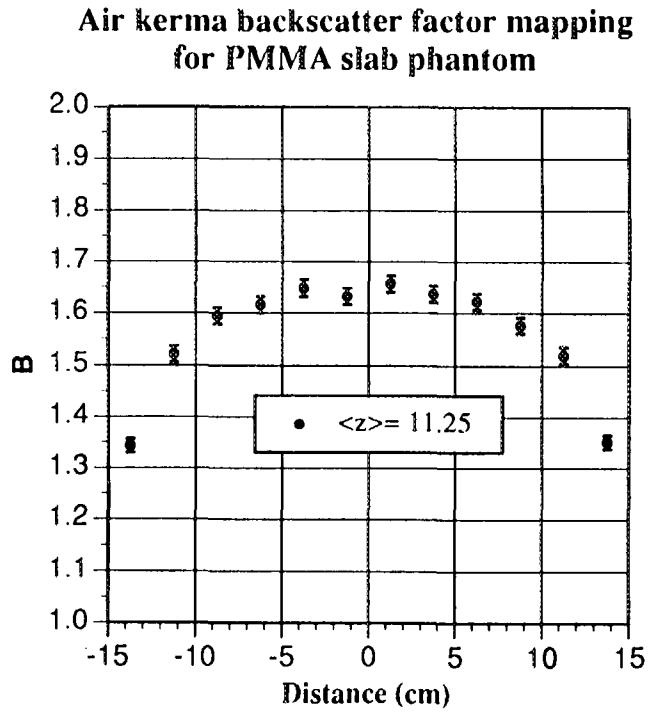
Air kerma backscatter factor mapping
for PMMA slab phantom
B
Distance (cm)
<z>= 11.25

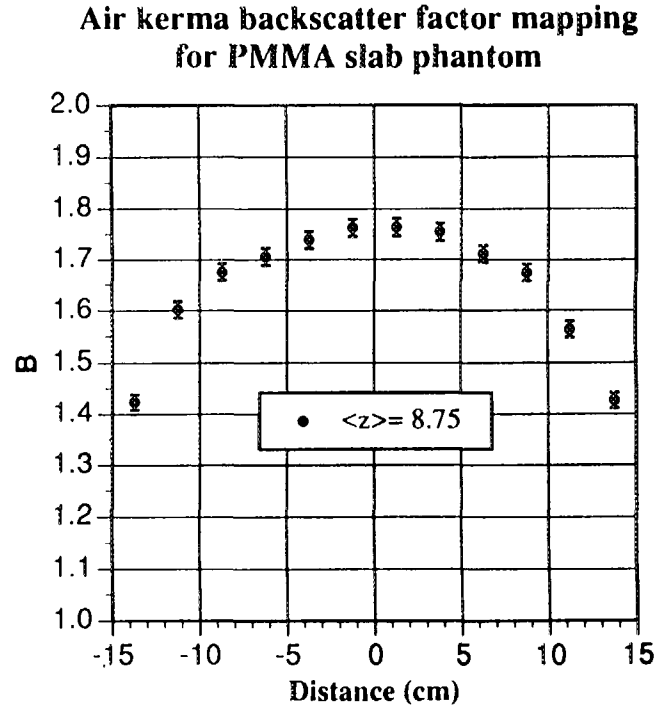
Air kerma backscatter factor mapping
for PMMA slab phantom
B
Distance (cm)
<z>= 8.75

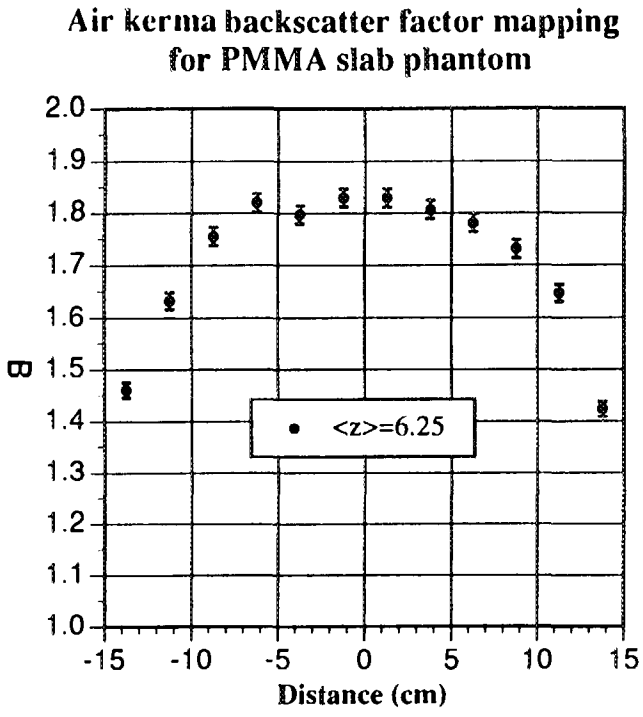
Air kerma backscatter factor mapping
for PMMA slab phantom
B
2.0
1.9
1.8
1.7
1.6
1.5
1.4
1.3
1.2
1.1
1.0
-15
-10
-5
0
5
10
15
Distance (cm)
<z>=6.25

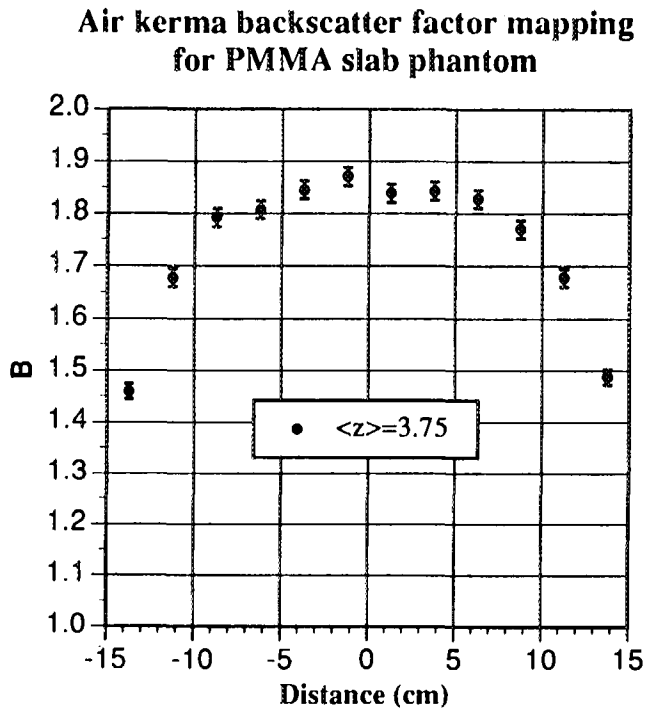
Air kerma backscatter factor mapping
for PMMA slab phantom
B
2.0
1.9
1.8
1.7
1.6
1.5
1.4
1.3
1.2
1.1
1.0
-15
-10
-5
0
5
10
15
Distance (cm)
<z>=3.75

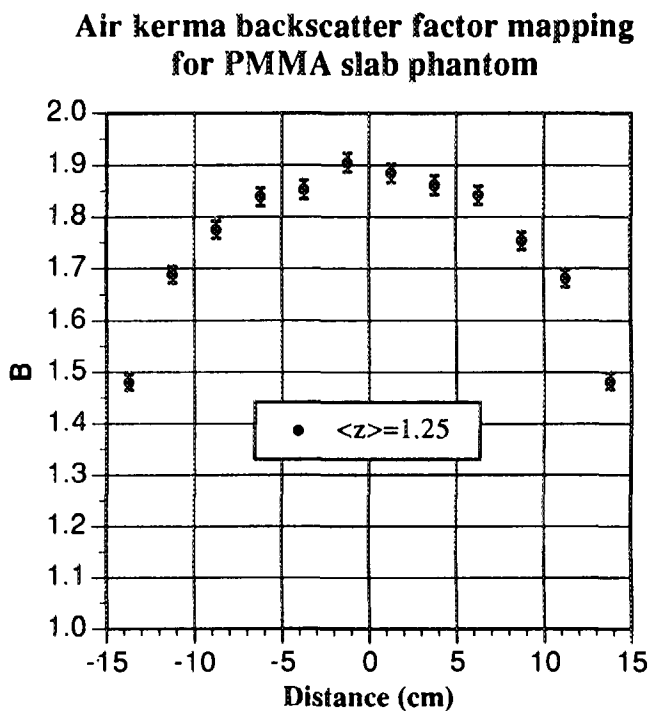
Air kerma backscatter factor mapping
for PMMA slab phantom
B
2.0
1.9
1.8
1.7
1.6
1.5
1.4
1.3
1.2
1.1
1.0
-15
-10
-5
0
5
10
15
Distance (cm)
<z>=1.25

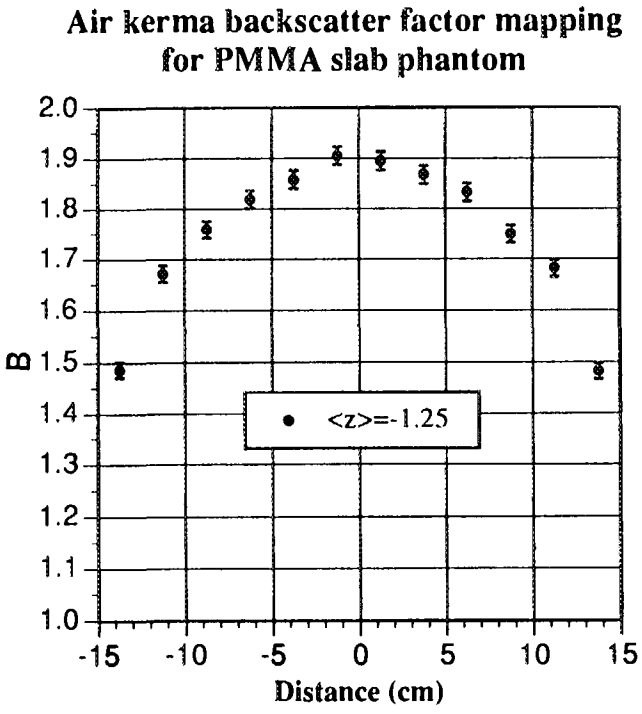
Air kerma backscatter factor mapping for PMMA slab phantom
B
2.0
1.9
1.8
1.7
1.6
1.5
1.4
1.3
1.2
1.1
1.0
-15
-10
-5
0
5
10
15
Distance (cm)
<z>=-1.25

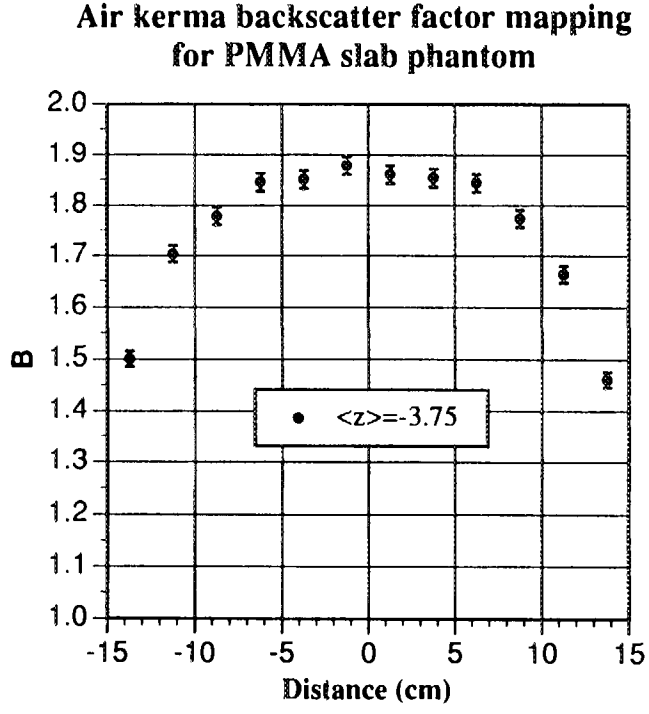
Air kerma backscatter factor mapping for PMMA slab phantom
B
2.0
1.9
1.8
1.7
1.6
1.5
1.4
1.3
1.2
1.1
1.0
-15
-10
-5
0
5
10
15
Distance (cm)
<z>=-3.75

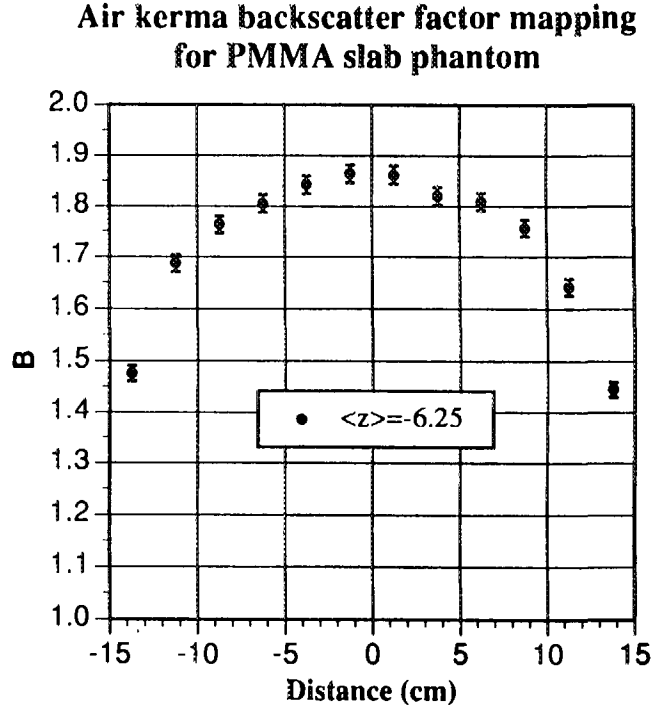
Air kerma backscatter factor mapping for PMMA slab phantom
B
2.0
1.9
1.8
1.7
1.6
1.5
1.4
1.3
1.2
1.1
1.0
-15
-10
-5
0
5
10
15
Distance (cm)
<z>=-6.25

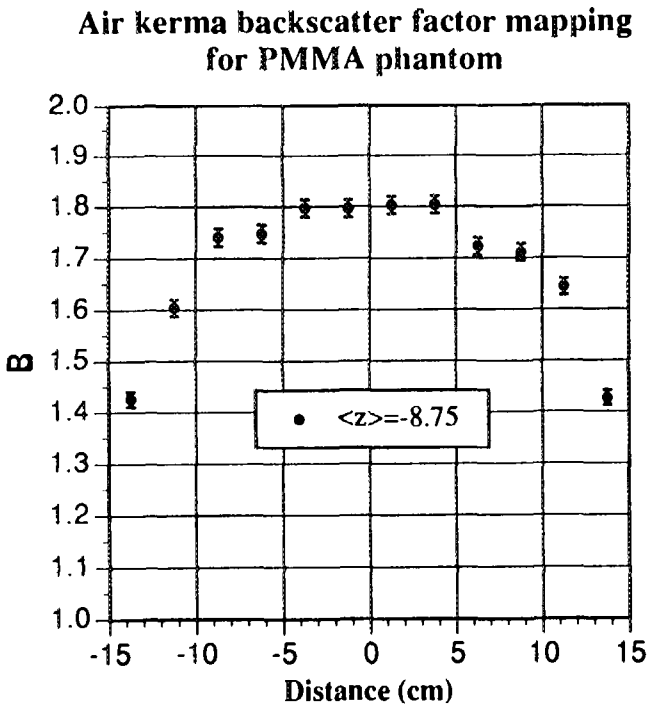
Air kerma backscatter factor mapping
for PMMA phantom
B
2.0
1.9
1.8
1.7
1.6
1.5
1.4
1.3
1.2
1.1
1.0
-15
-10
-5
0
5
10
15
Distance (cm)
<z>=-8.75

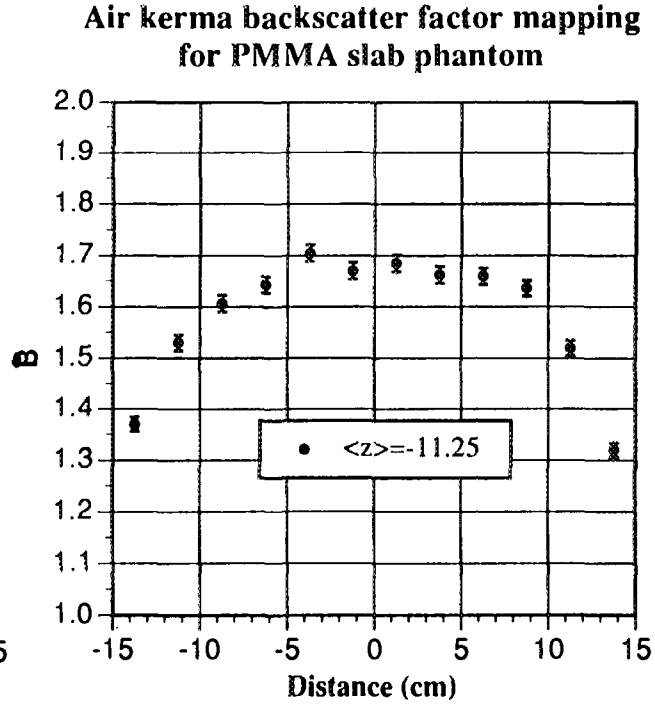
Air kerma backscatter factor mapping
for PMMA slab phantom
B
2.0
1.9
1.8
1.7
1.6
1.5
1.4
1.3
1.2
1.1
1.0
-15
-10
-5
0
5
10
15
Distance (cm)
<z>=-11.25

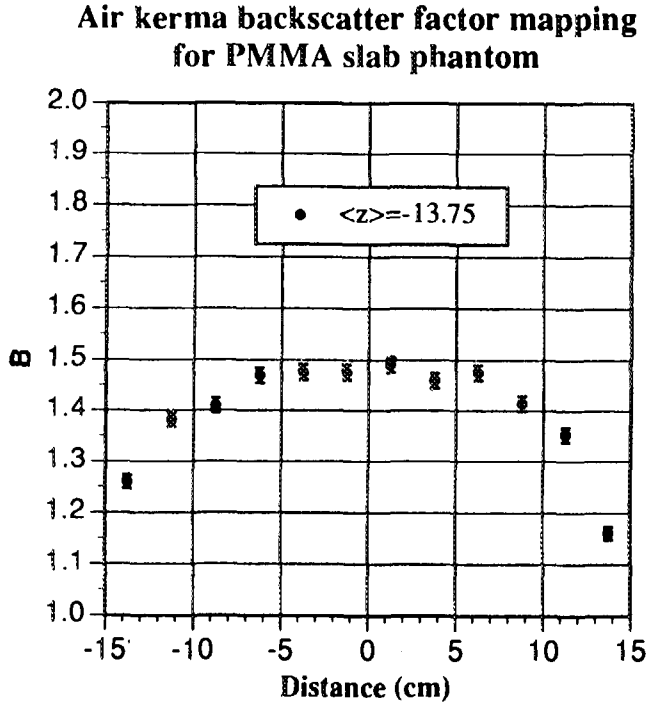
Air kerma backscatter factor mapping
for PMMA slab phantom
B
2.0
1.9
1.8
1.7
1.6
1.5
1.4
1.3
1.2
1.1
1.0
-15
-10
-5
0
5
10
15
Distance (cm)
<z>=-13.75

NARROW SPECTRUM SERIES
(150 kV)

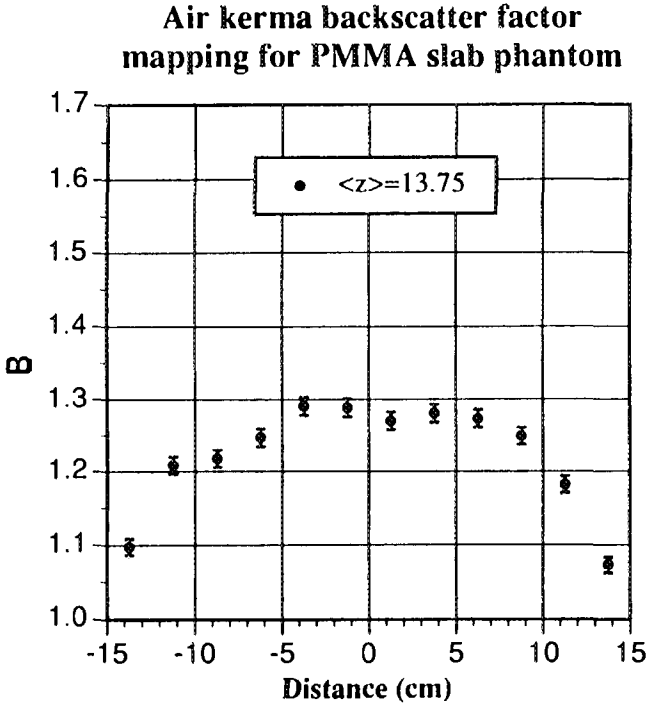
Air kerma backscatter factor mapping for PMMA slab phantom
<z>=13.75
B
Distance (cm)
1.7
1.6
1.5
1.4
1.3
1.2
1.1
1.0
-15
-10
-5
0
5
10
15

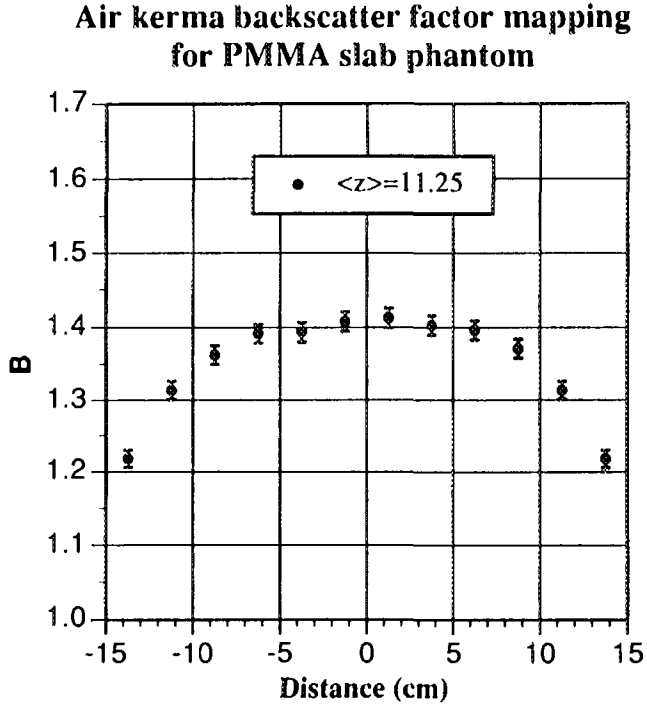
Air kerma backscatter factor mapping for PMMA slab phantom
<z>=11.25
B
Distance (cm)
1.7
1.6
1.5
1.4
1.3
1.2
1.1
1.0
-15
-10
-5
0
5
10
15

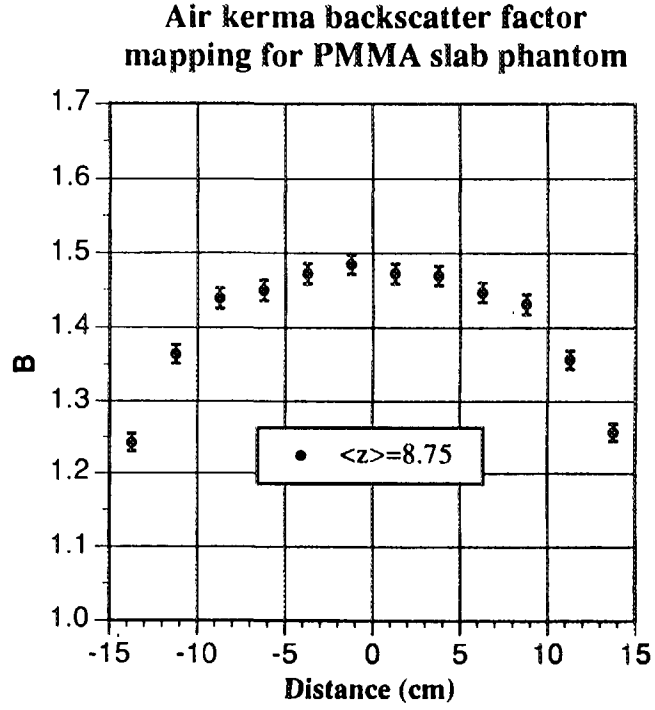
Air kerma backscatter factor mapping for PMMA slab phantom
<z>=8.75
B
Distance (cm)
1.7
1.6
1.5
1.4
1.3
1.2
1.1
1.0
-15
-10
-5
0
5
10
15

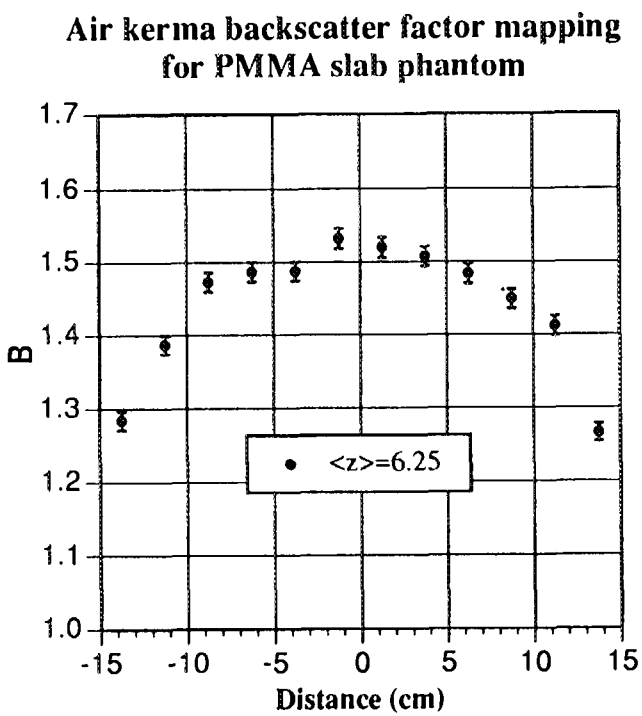
Air kerma backscatter factor mapping for PMMA slab phantom
B
Distance (cm)
<z>=6.25

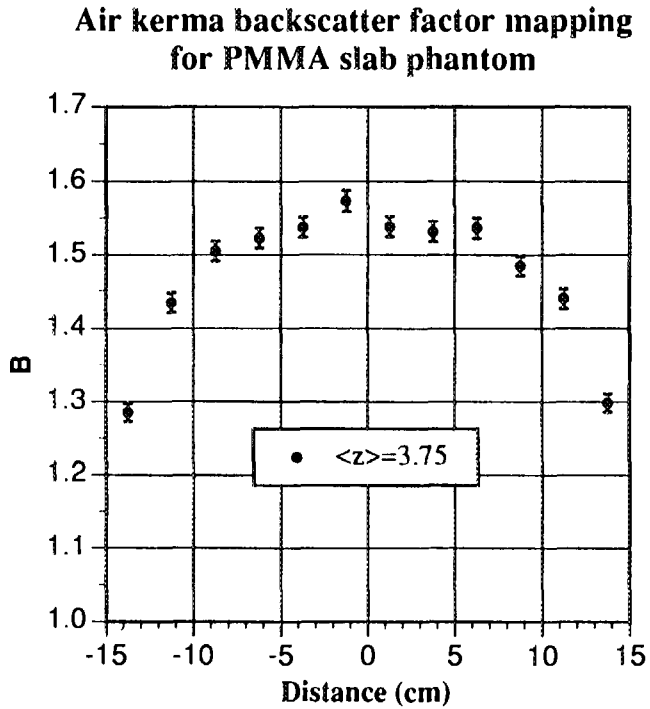
Air kerma backscatter factor mapping for PMMA slab phantom
B
Distance (cm)
<z>=3.75

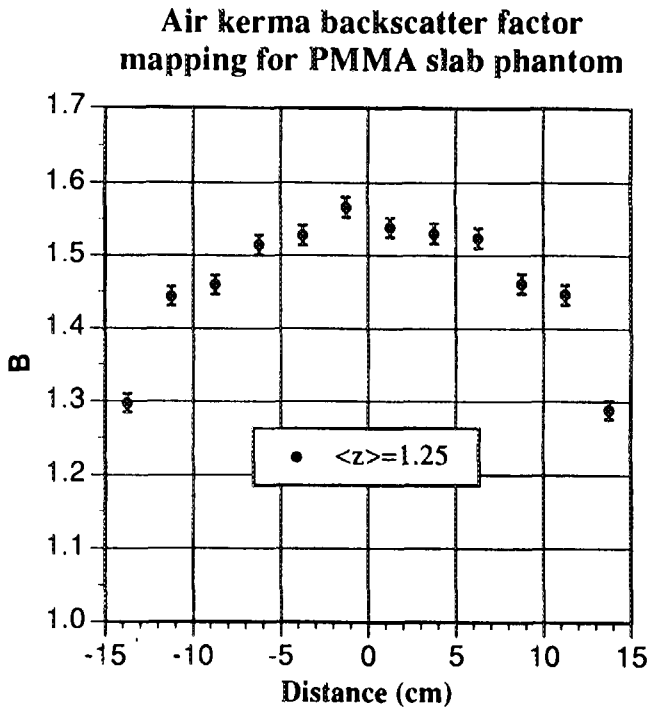
Air kerma backscatter factor mapping for PMMA slab phantom
B
Distance (cm)
<z>=1.25

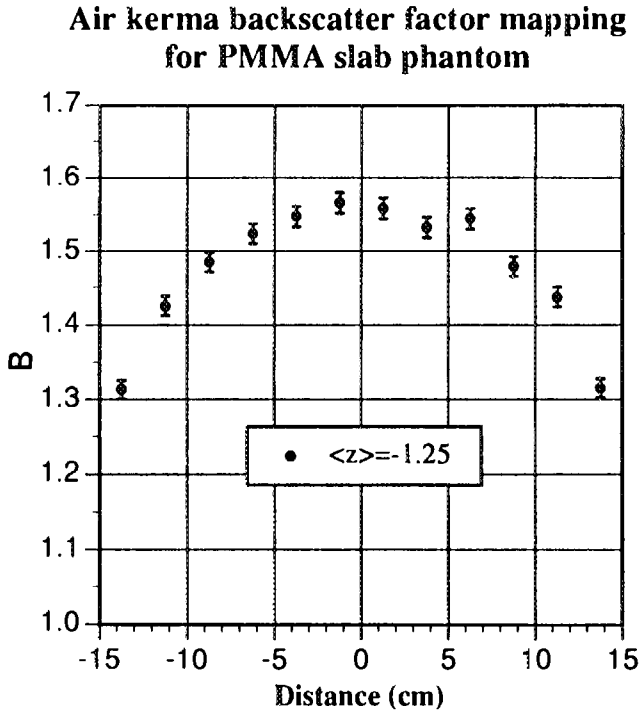
Air kerma backscatter factor mapping for PMMA slab phantom
B
Distance (cm)
<z>=-1.25

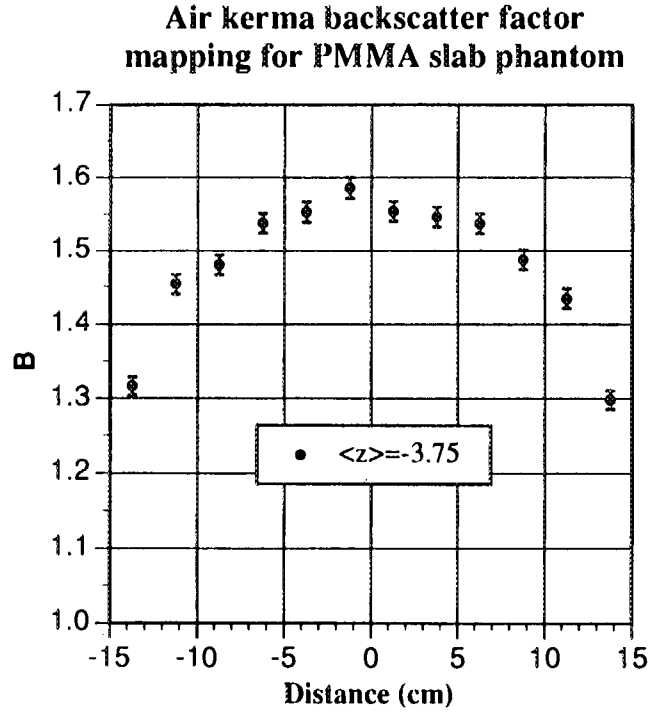
Air kerma backscatter factor mapping for PMMA slab phantom
B
Distance (cm)
<z>=-3.75

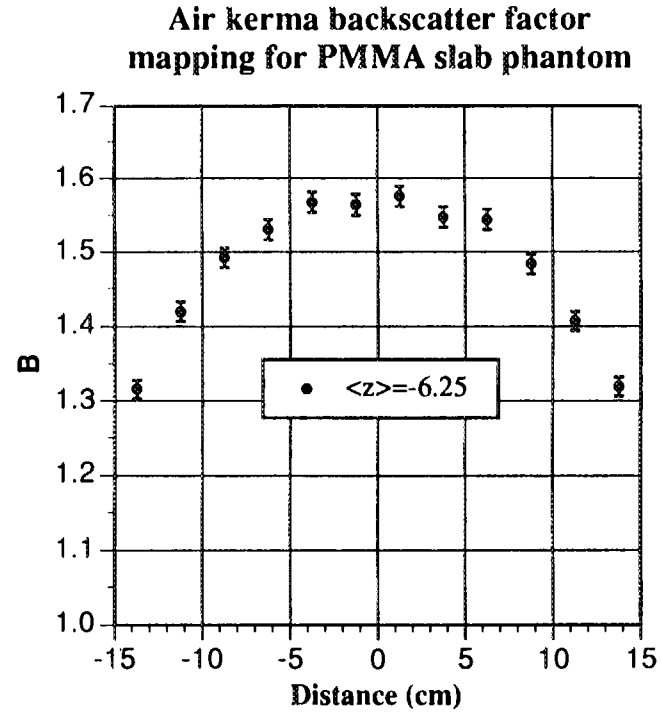
Air kerma backscatter factor mapping for PMMA slab phantom
B
Distance (cm)
<z>=-6.25

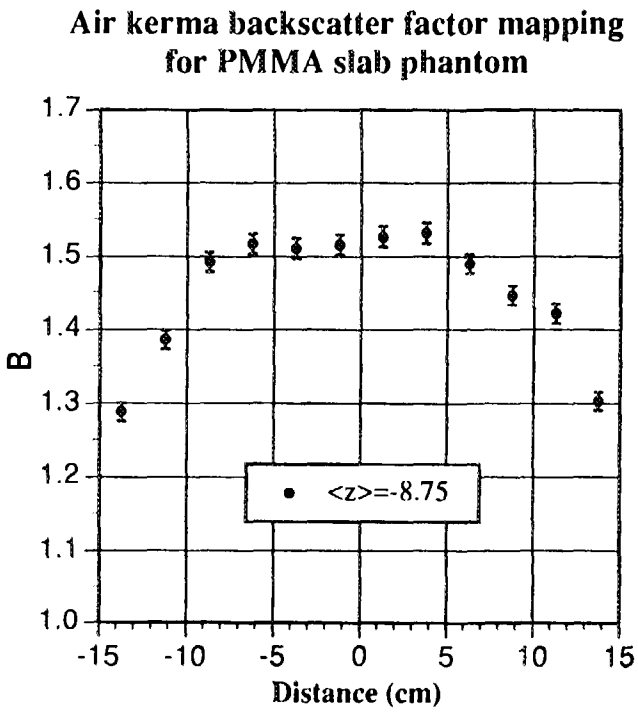
Air kerma backscatter factor mapping for PMMA slab phantom
B
Distance (cm)
<z>=-8.75

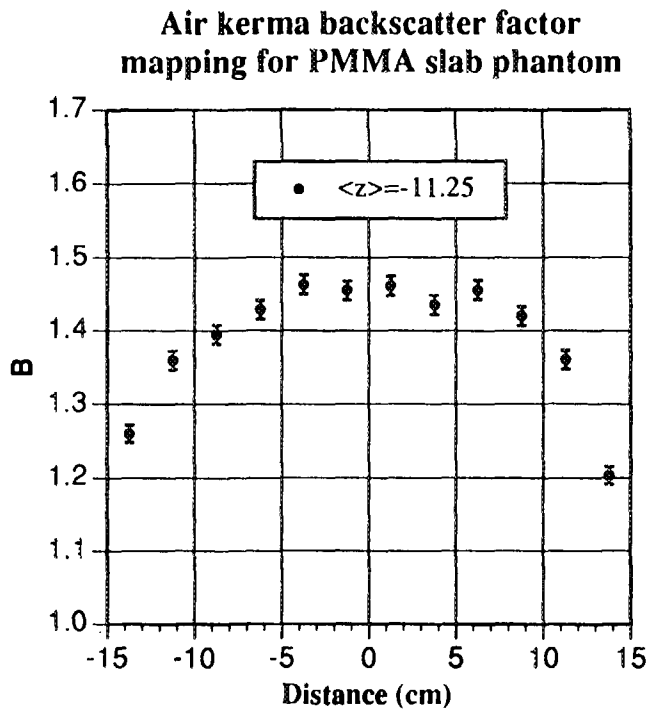
Air kerma backscatter factor mapping for PMMA slab phantom
B
Distance (cm)
<z>=-11.25

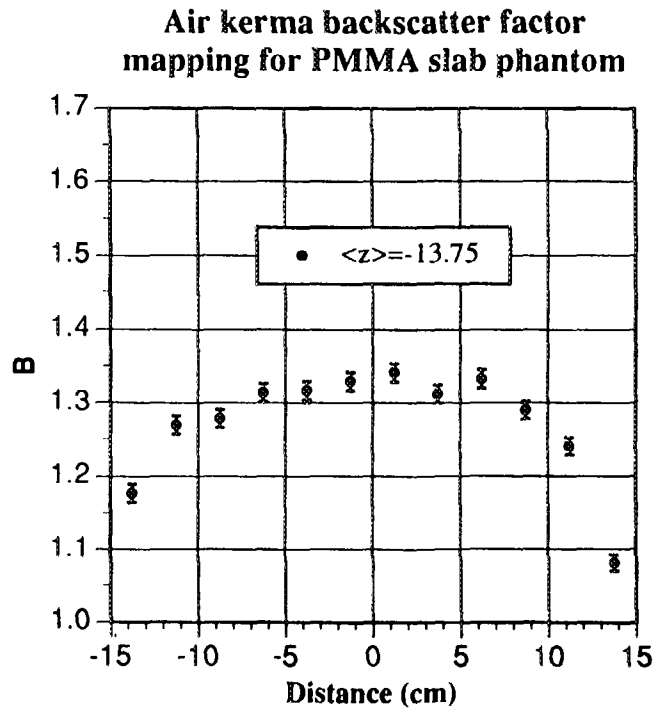
Air kerma backscatter factor mapping for PMMA slab phantom
B
Distance (cm)
<z>=-13.75

NARROW SPECTRUM SERIES
(300 kV)

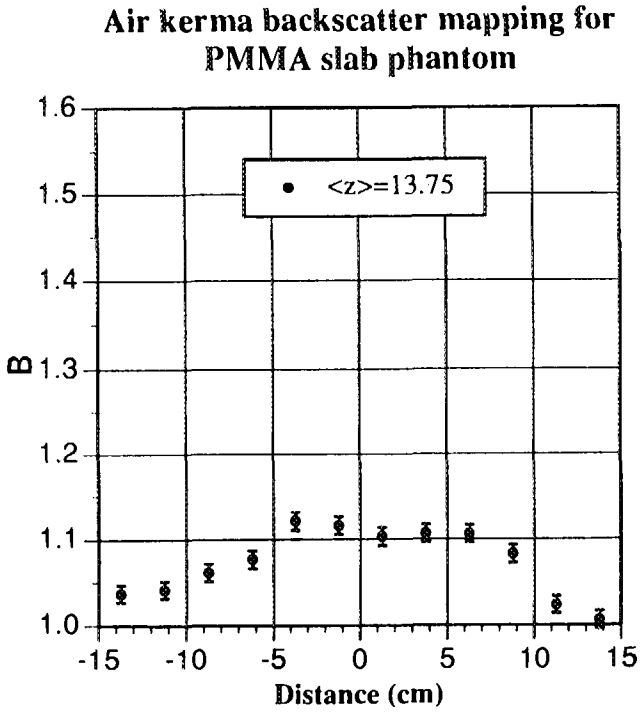
Air kerma backscatter mapping for PMMA slab phantom
<z>=13.75
B
Distance (cm)
1.6
1.5
1.4
1.3
1.2
1.1
1.0
-15
-10
-5
0
5
10
15

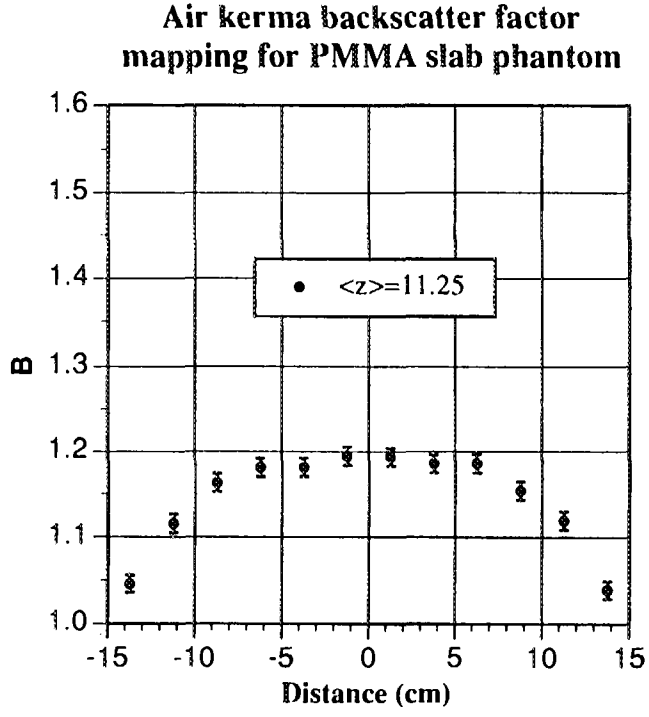
Air kerma backscatter factor mapping for PMMA slab phantom
<z>=11.25
B
Distance (cm)
1.6
1.5
1.4
1.3
1.2
1.1
1.0
-15
-10
-5
0
5
10
15

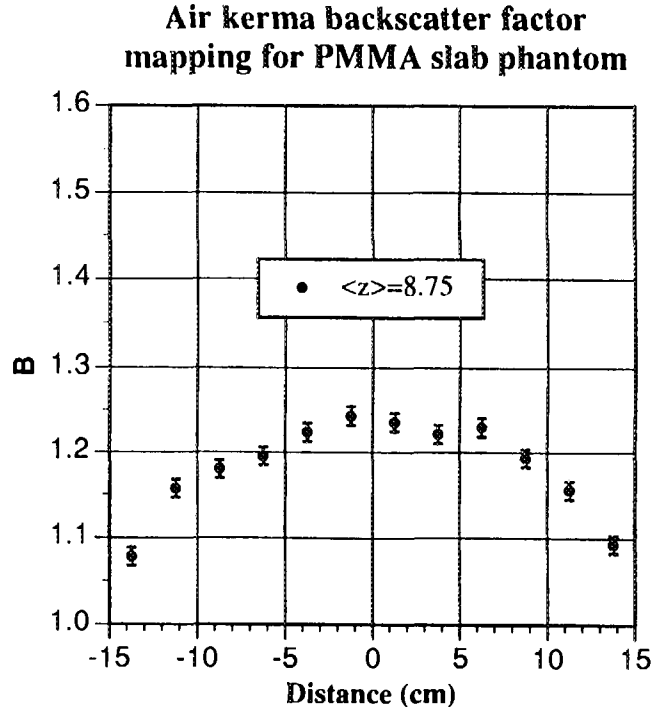
Air kerma backscatter factor mapping for PMMA slab phantom
<z>=8.75
B
Distance (cm)
1.6
1.5
1.4
1.3
1.2
1.1
1.0
-15
-10
-5
0
5
10
15

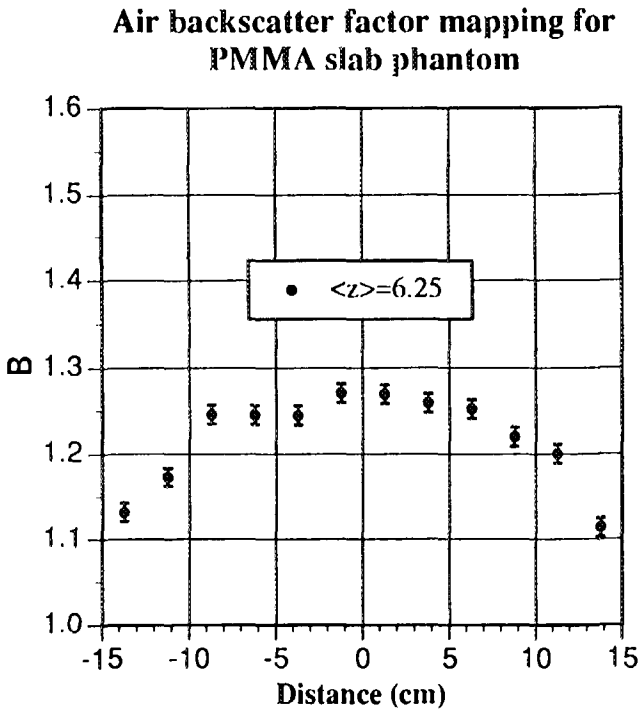
Air backscatter factor mapping for PMMA slab phantom
<z>=6.25
B
Distance (cm)
1.6
1.5
1.4
1.3
1.2
1.1
1.0
-15
-10
-5
0
5
10
15

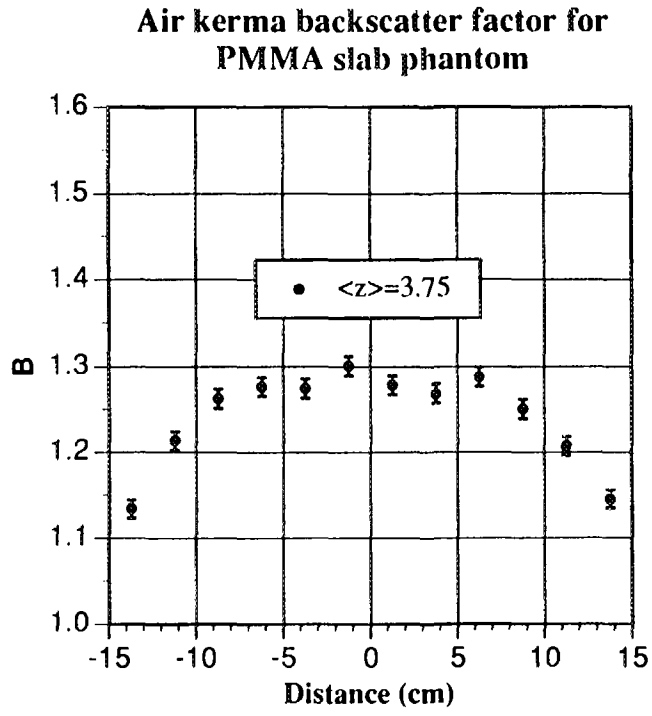
Air kerma backscatter factor for PMMA slab phantom
<z>=3.75
B
Distance (cm)
1.6
1.5
1.4
1.3
1.2
1.1
1.0
-15
-10
-5
0
5
10
15

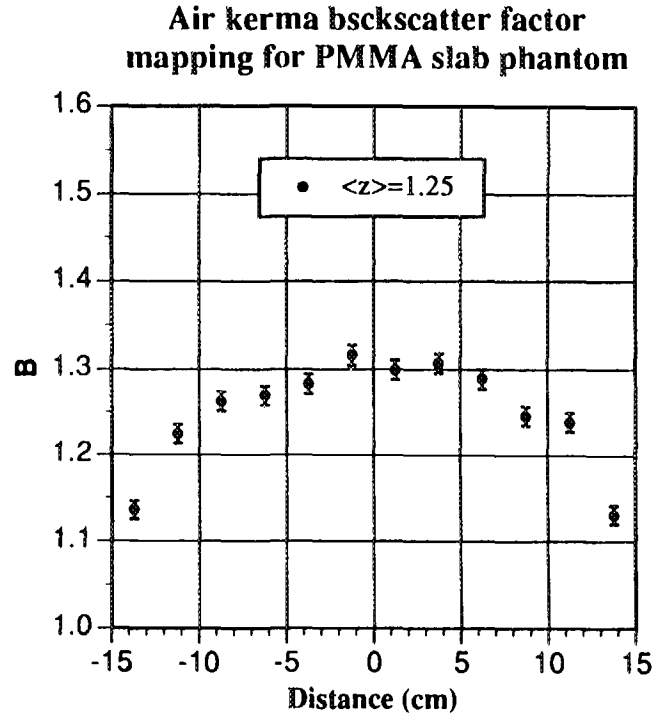
Air kerma bsckscatter factor mapping for PMMA slab phantom
<z>=1.25
B
Distance (cm)
1.6
1.5
1.4
1.3
1.2
1.1
1.0
-15
-10
-5
0
5
10
15

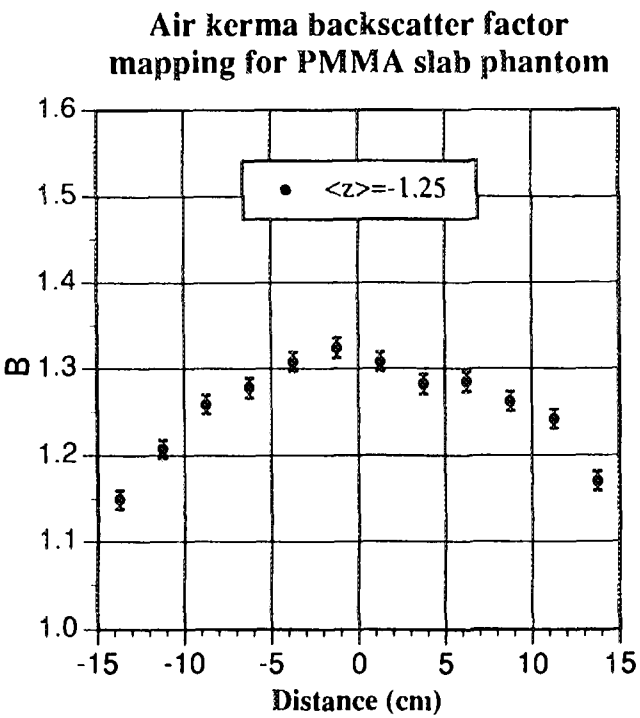
Air kerma backscatter factor mapping for PMMA slab phantom
<z>=-1.25
B
Distance (cm)
1.6
1.5
1.4
1.3
1.2
1.1
1.0
-15
-10
-5
0
5
10
15

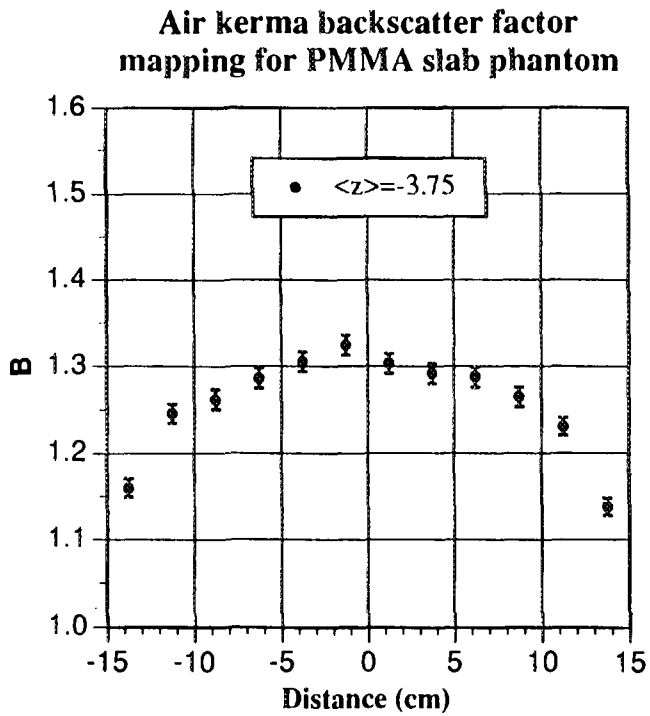
Air kerma backscatter factor mapping for PMMA slab phantom
<z>=-3.75
B
Distance (cm)
1.6
1.5
1.4
1.3
1.2
1.1
1.0
-15
-10
-5
0
5
10
15

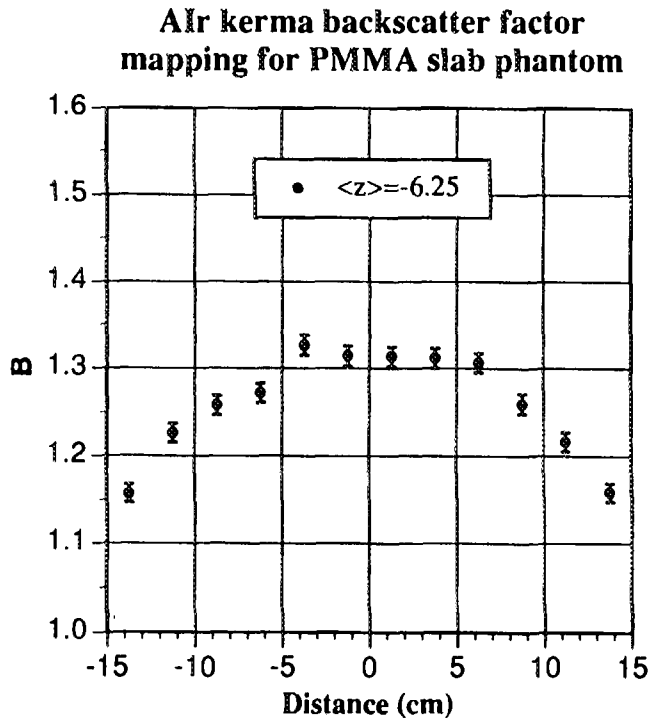
Air kerma backscatter factor mapping for PMMA slab phantom
<z>=-6.25
B
Distance (cm)
1.6
1.5
1.4
1.3
1.2
1.1
1.0
-15
-10
-5
0
5
10
15

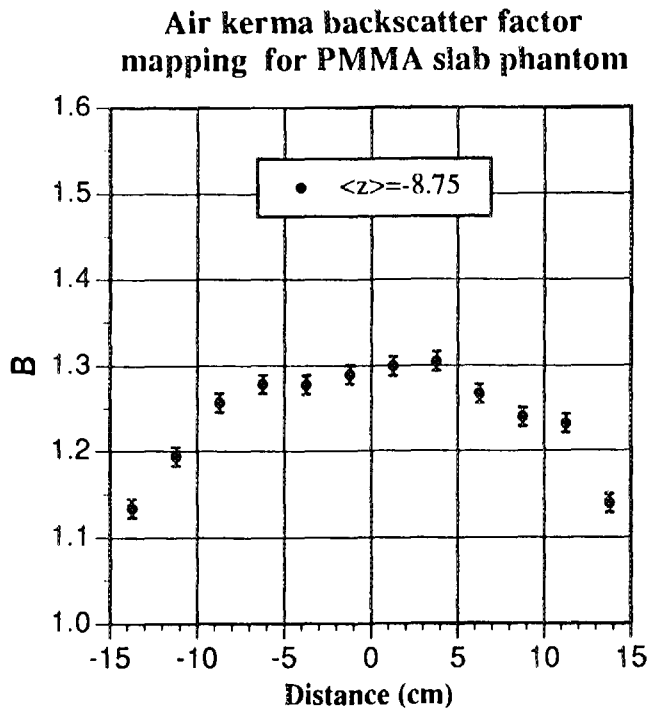
Air kerma backscatter factor mapping for PMMA slab phantom
<z>=-8.75
B
Distance (cm)
1.6
1.5
1.4
1.3
1.2
1.1
1.0
-15
-10
-5
0
5
10
15

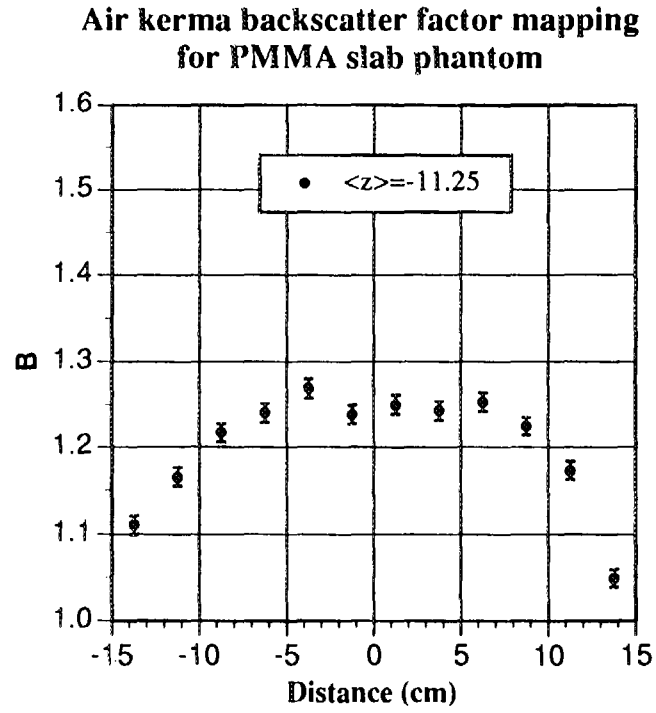
Air kerma backscatter factor mapping for PMMA slab phantom
<z>=-11.25
B
Distance (cm)
1.6
1.5
1.4
1.3
1.2
1.1
1.0
-15
-10
-5
0
5
10
15

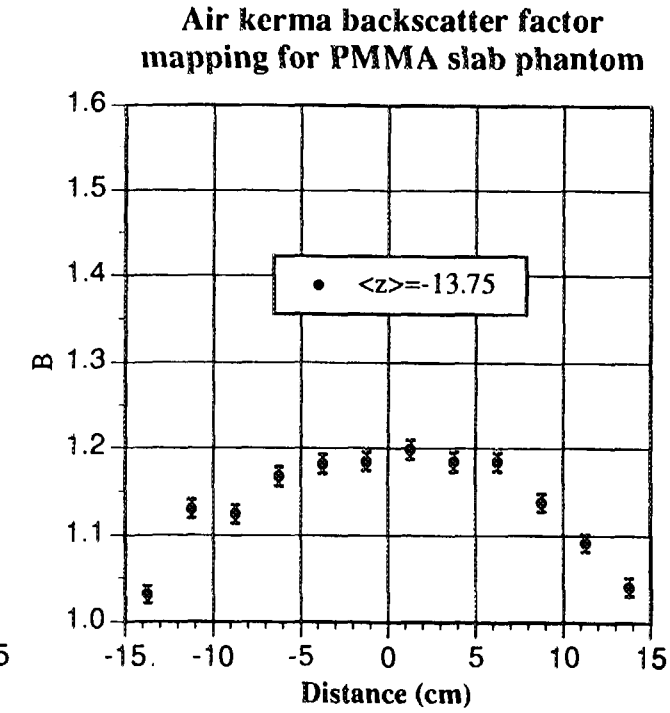
Air kerma backscatter factor mapping for PMMA slab phantom
<z>=-13.75
B
Distance (cm)
1.6
1.5
1.4
1.3
1.2
1.1
1.0
-15
-10
-5
0
5
10
15

WIDE SPECTRUM SERIES
(80 kV)

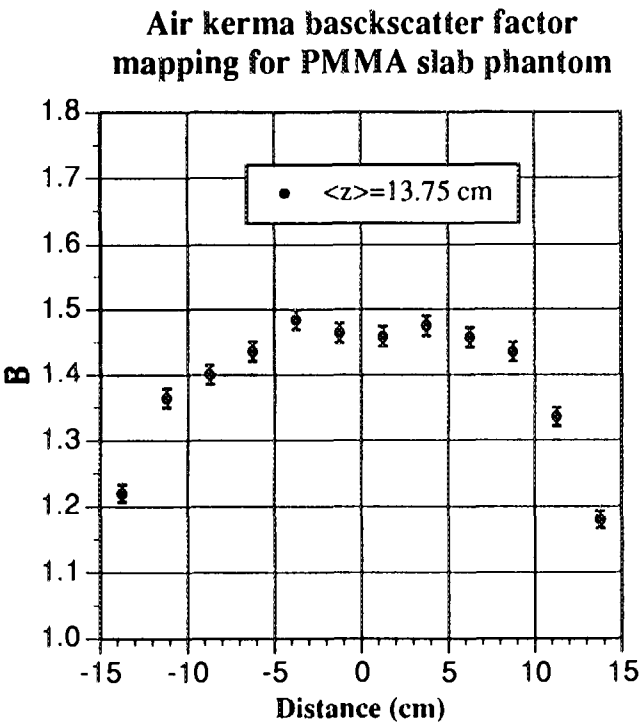
Air kerma basckscatter factor
mapping for PMMA slab phantom
<z>=13.75 cm
B
Distance (cm)
1.8
1.7
1.6
1.5
1.4
1.3
1.2
1.1
1.0
-15
-10
-5
0
5
10
15

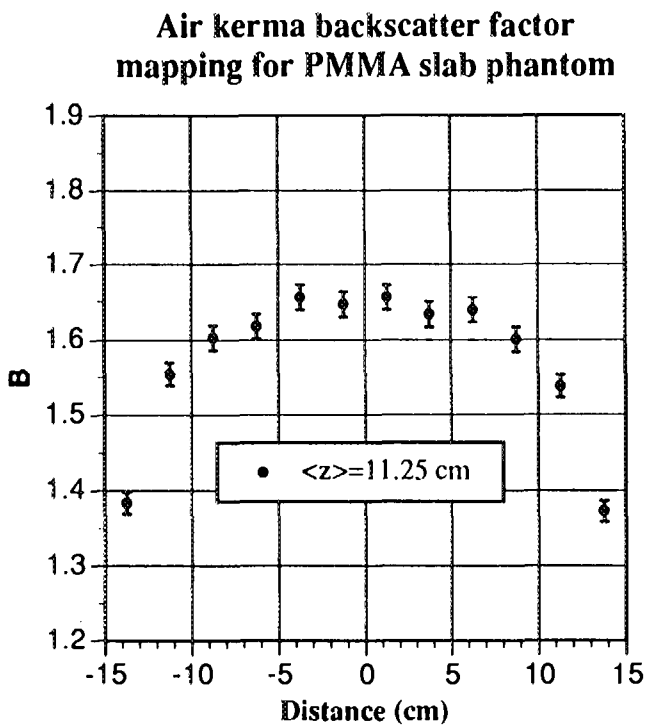
Air kerma backscatter factor
mapping for PMMA slab phantom
<z>=11.25 cm
B
Distance (cm)
1.9
1.8
1.7
1.6
1.5
1.4
1.3
1.2
-15
-10
-5
0
5
10
15

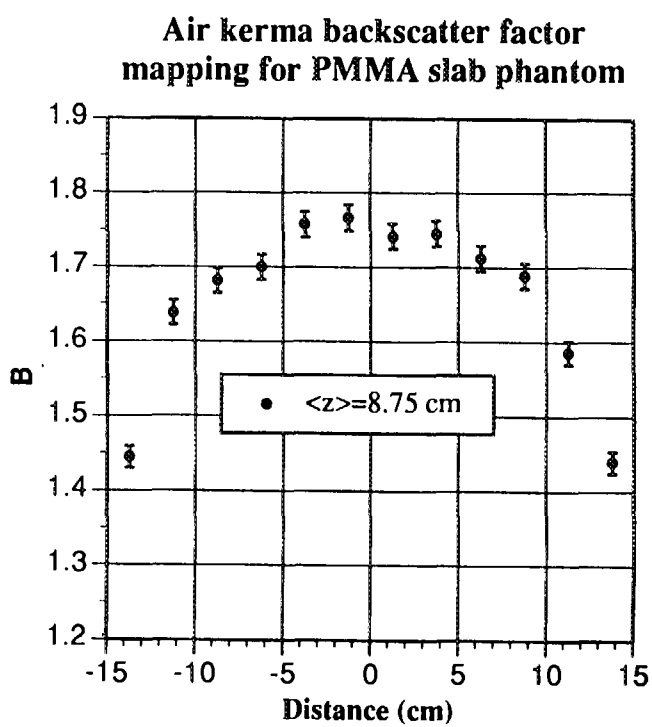
Air kerma backscatter factor
mapping for PMMA slab phantom
<z>=8.75 cm
B
Distance (cm)
1.9
1.8
1.7
1.6
1.5
1.4
1.3
1.2
-15
-10
-5
0
5
10
15

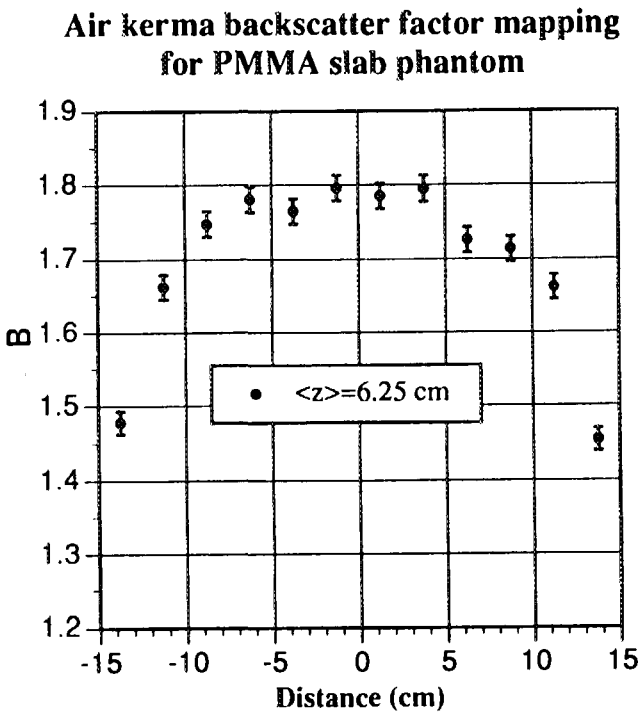
Air kerma backscatter factor mapping
for PMMA slab phantom
B
Distance (cm)
<z>=6.25 cm
1.9
1.8
1.7
1.6
1.5
1.4
1.3
1.2
-15
-10
-5
0
5
10
15

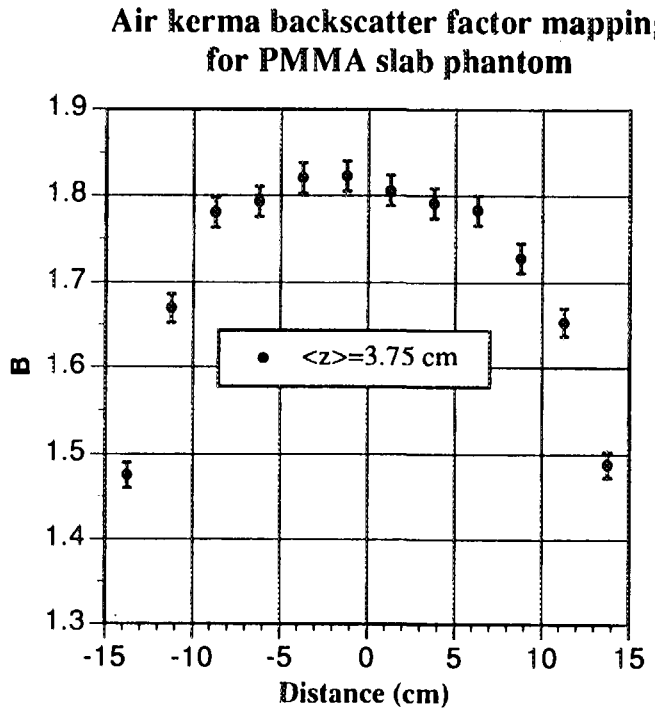
Air kerma backscatter factor mapping
for PMMA slab phantom
B
Distance (cm)
<z>=3.75 cm
1.9
1.8
1.7
1.6
1.5
1.4
1.3
-15
-10
-5
0
5
10
15

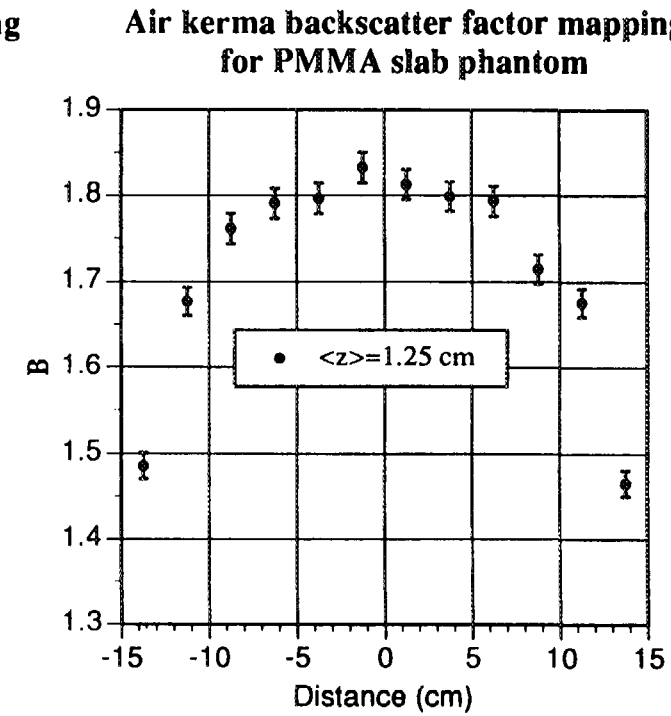
Air kerma backscatter factor mapping
for PMMA slab phantom
B
Distance (cm)
<z>=1.25 cm
1.9
1.8
1.7
1.6
1.5
1.4
1.3
-15
-10
-5
0
5
10
15

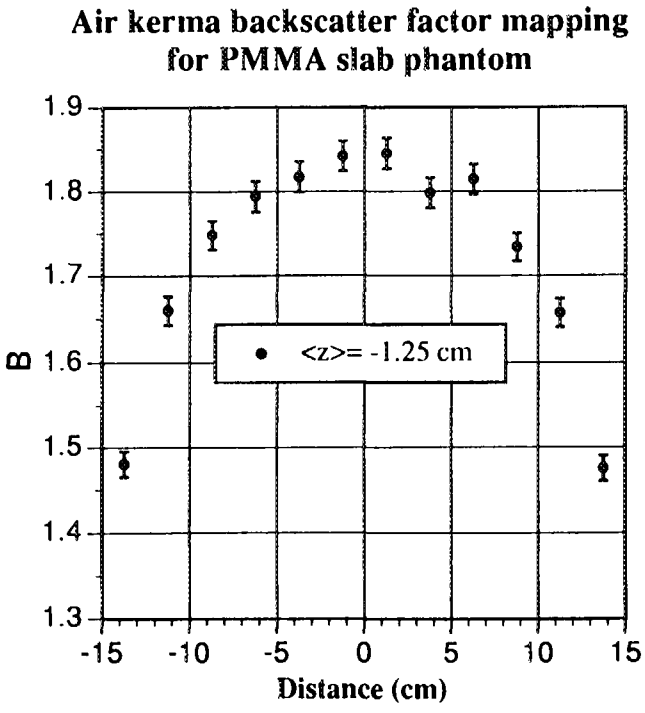
Air kerma backscatter factor mapping for PMMA slab phantom
B
Distance (cm)
<z>= -1.25 cm

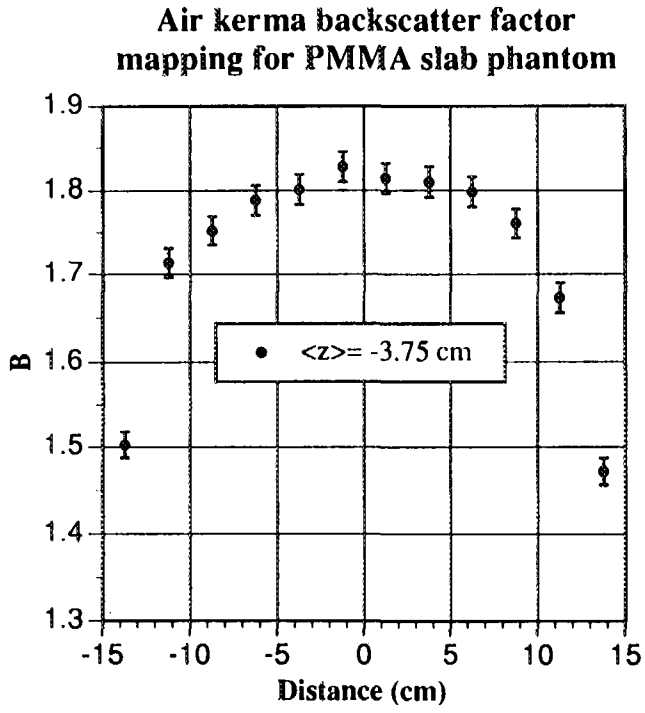
Air kerma backscatter factor mapping for PMMA slab phantom
B
Distance (cm)
<z>= -3.75 cm

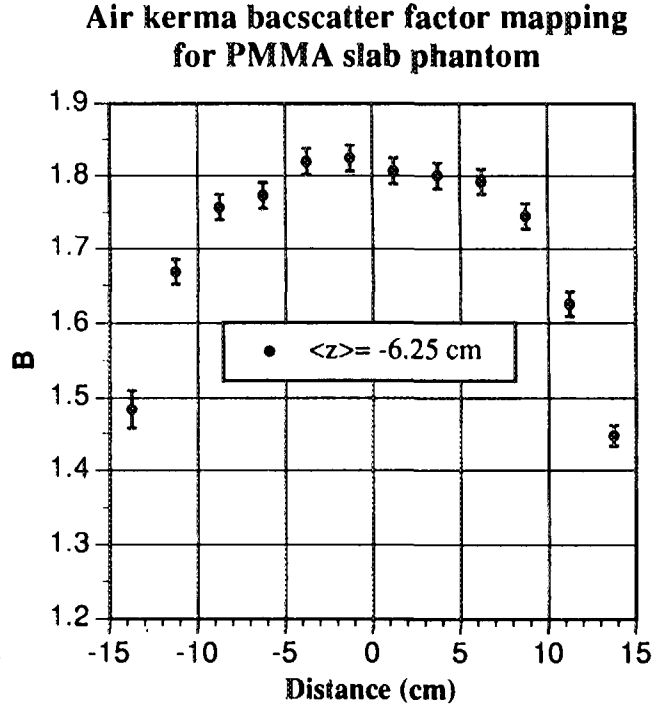
Air kerma bacscatter factor mapping for PMMA slab phantom
B
Distance (cm)
<z>= -6.25 cm

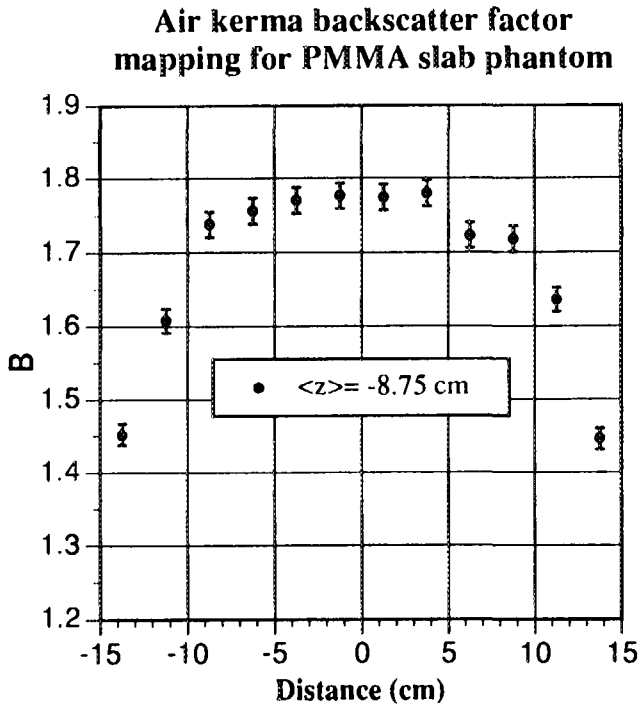
Air kerma backscatter factor mapping for PMMA slab phantom
B
Distance (cm)
<z>= -8.75 cm

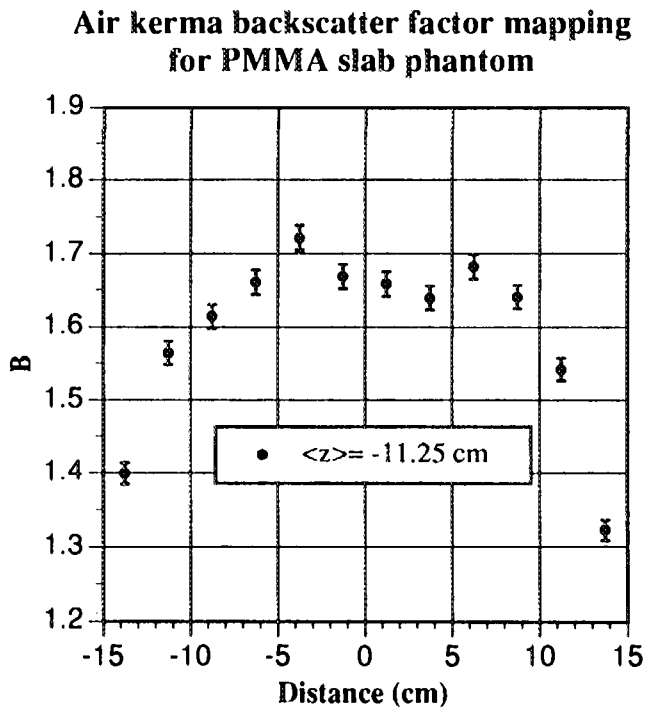
Air kerma backscatter factor mapping for PMMA slab phantom
B
Distance (cm)
<z>= -11.25 cm

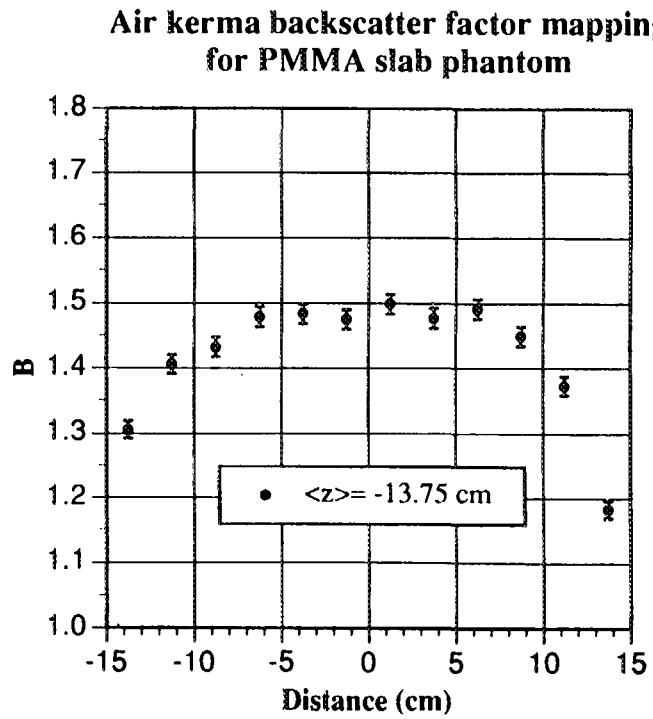
Air kerma backscatter factor mapping for PMMA slab phantom
B
Distance (cm)
<z>= -13.75 cm

WIDE SPECTRUM SERIES
(150 kV)

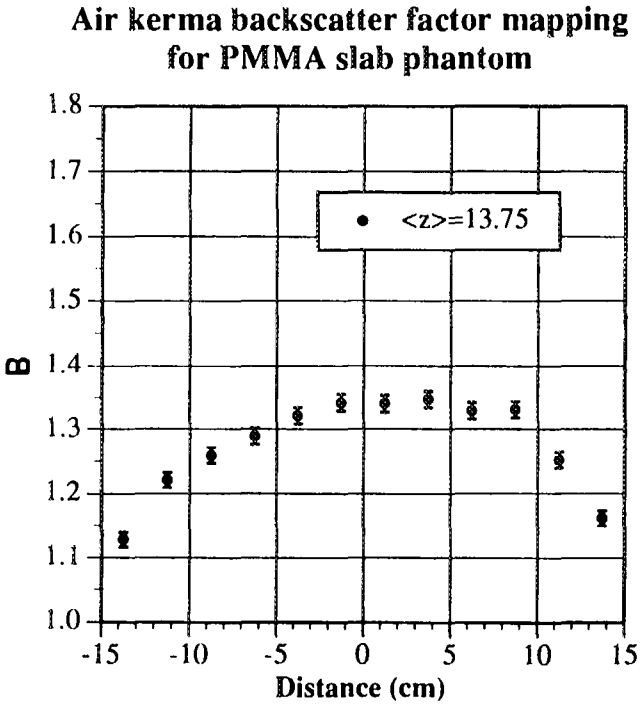
Air kerma backscatter factor mapping
for PMMA slab phantom
B
Distance (cm)
<z>=13.75
1.8
1.7
1.6
1.5
1.4
1.3
1.2
1.1
1.0
-15
-10
-5
0
5
10
15

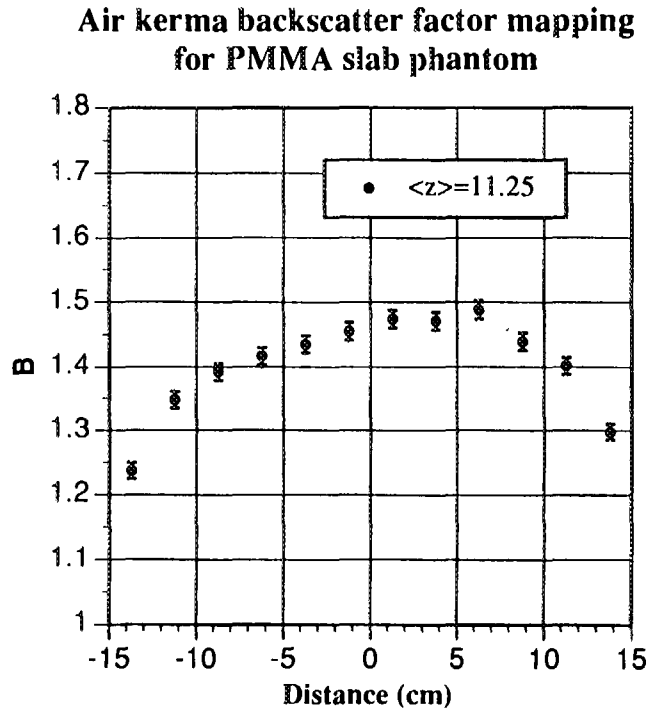
Air kerma backscatter factor mapping
for PMMA slab phantom
B
Distance (cm)
<z>=11.25
1.8
1.7
1.6
1.5
1.4
1.3
1.2
1.1
1
-15
-10
-5
0
5
10
15

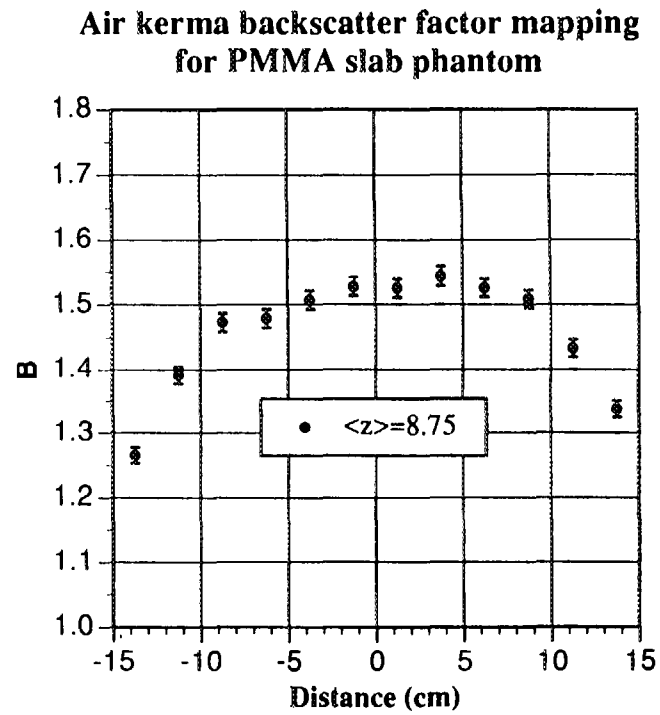
Air kerma backscatter factor mapping
for PMMA slab phantom
B
Distance (cm)
<z>=8.75
1.8
1.7
1.6
1.5
1.4
1.3
1.2
1.1
1.0
-15
-10
-5
0
5
10
15

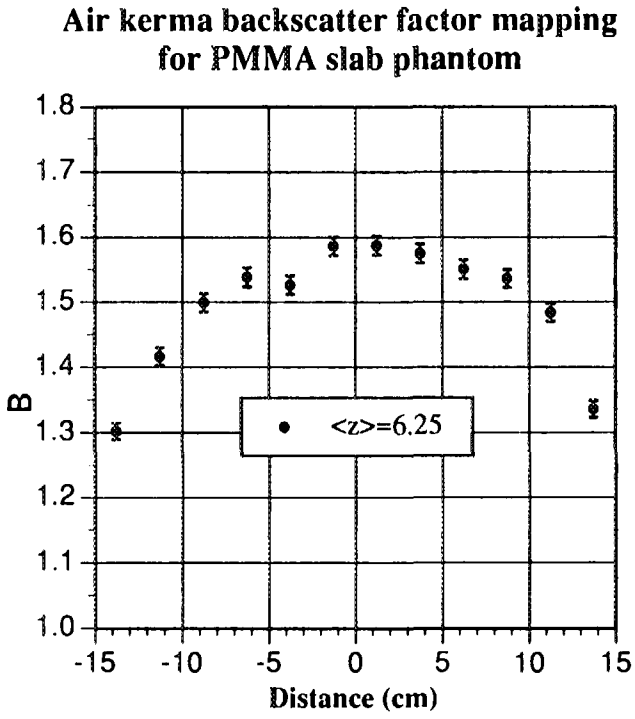
Air kerma backscatter factor mapping
for PMMA slab phantom
B
Distance (cm)
<z>=6.25
1.8
1.7
1.6
1.5
1.4
1.3
1.2
1.1
1.0
-15
-10
-5
0
5
10
15

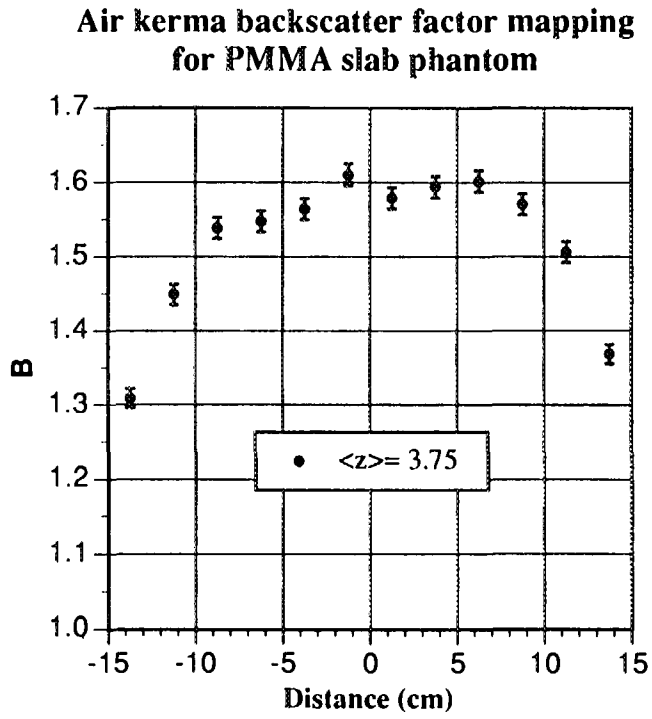
Air kerma backscatter factor mapping
for PMMA slab phantom
B
Distance (cm)
<z>= 3.75
1.7
1.6
1.5
1.4
1.3
1.2
1.1
1.0
-15
-10
-5
0
5
10
15

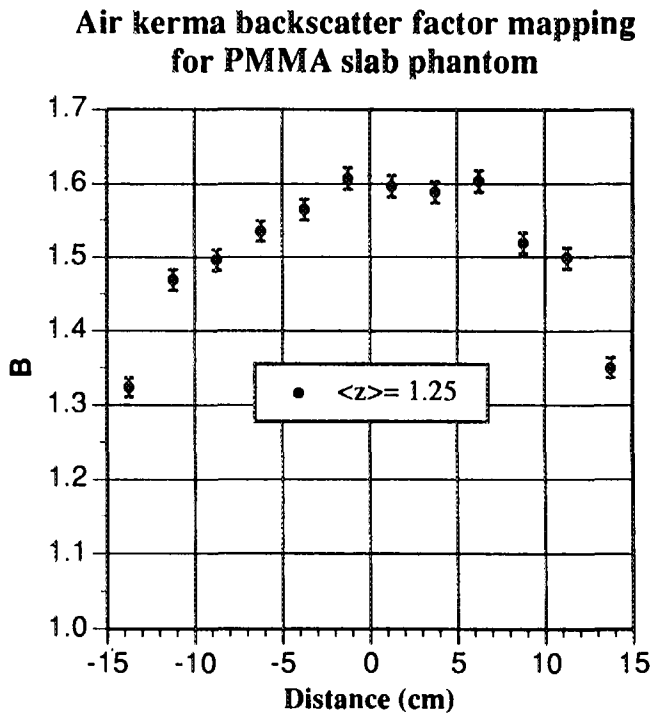
Air kerma backscatter factor mapping
for PMMA slab phantom
B
Distance (cm)
<z>= 1.25
1.7
1.6
1.5
1.4
1.3
1.2
1.1
1.0
-15
-10
-5
0
5
10
15

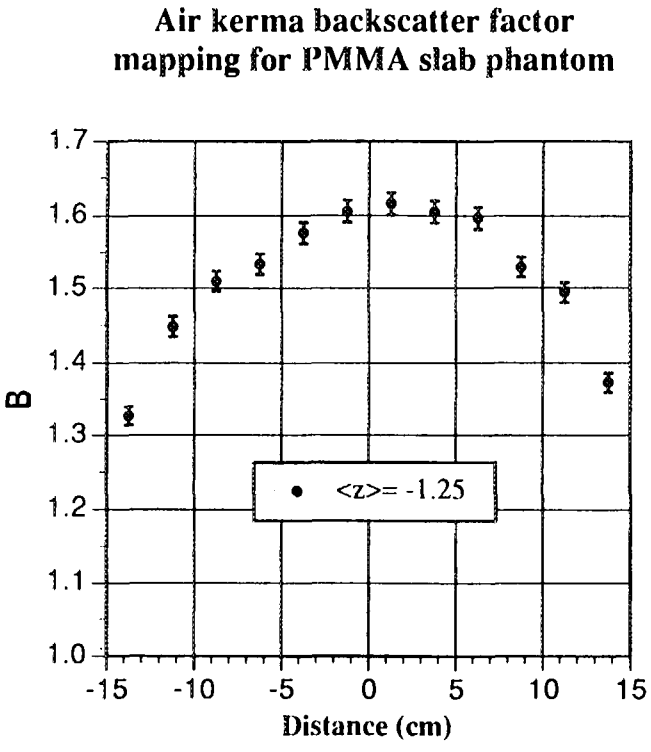
Air kerma backscatter factor mapping for PMMA slab phantom
B
1.7
1.6
1.5
1.4
1.3
1.2
1.1
1.0
-15
-10
-5
0
5
10
15
Distance (cm)
<z>= -1.25

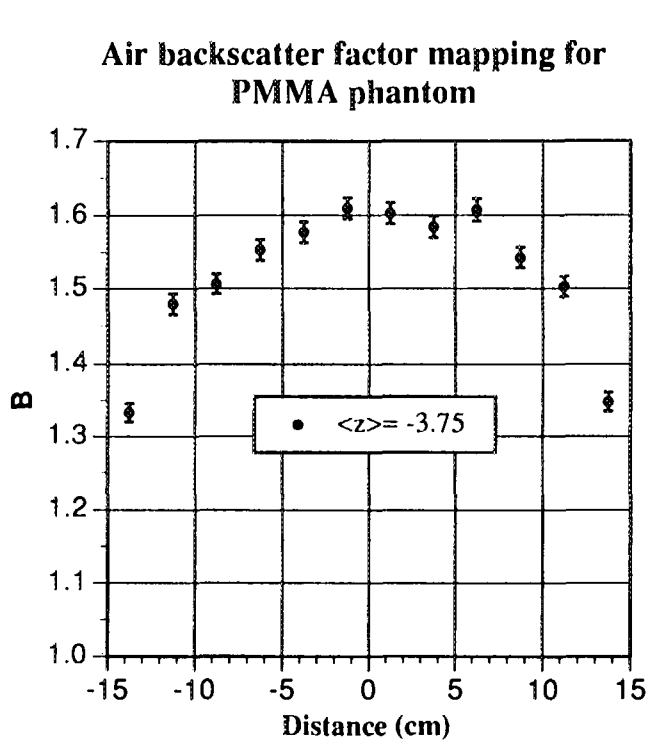
Air backscatter factor mapping for PMMA phantom
B
1.7
1.6
1.5
1.4
1.3
1.2
1.1
1.0
-15
-10
-5
0
5
10
15
Distance (cm)
<z>= -3.75

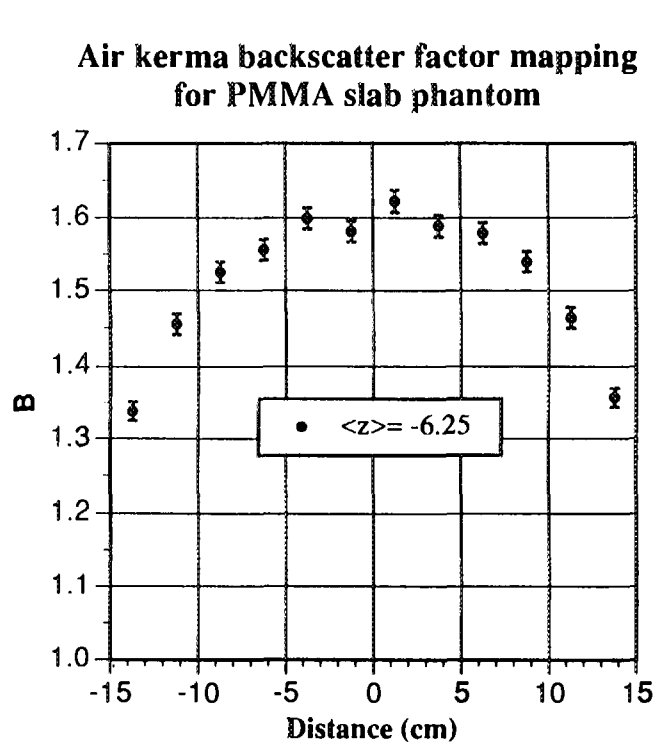
Air kerma backscatter factor mapping for PMMA slab phantom
B
1.7
1.6
1.5
1.4
1.3
1.2
1.1
1.0
-15
-10
-5
0
5
10
15
Distance (cm)
<z>= -6.25

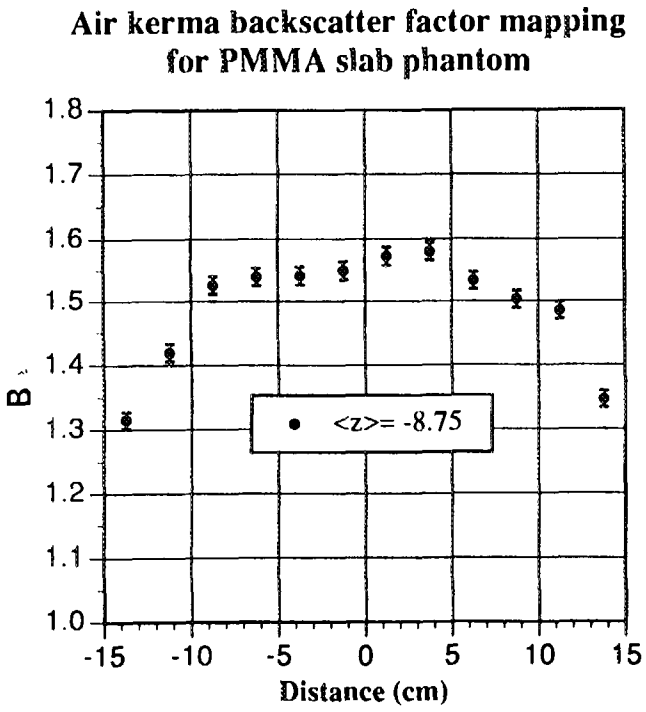
Air kerma backscatter factor mapping
for PMMA slab phantom
B
1.8
1.7
1.6
1.5
1.4
1.3
1.2
1.1
1.0
-15
-10
-5
0
5
10
15
Distance (cm)
<z>= -8.75

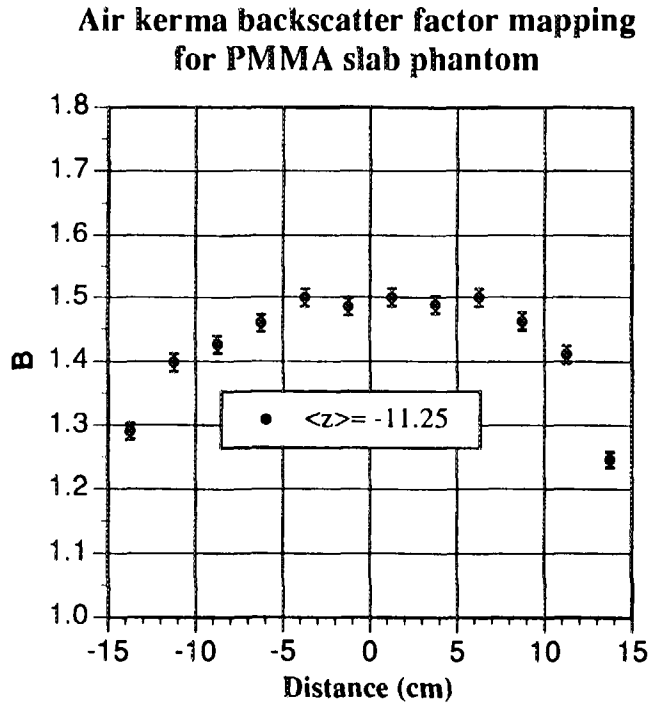
Air kerma backscatter factor mapping
for PMMA slab phantom
B
1.8
1.7
1.6
1.5
1.4
1.3
1.2
1.1
1.0
-15
-10
-5
0
5
10
15
Distance (cm)
<z>= -11.25

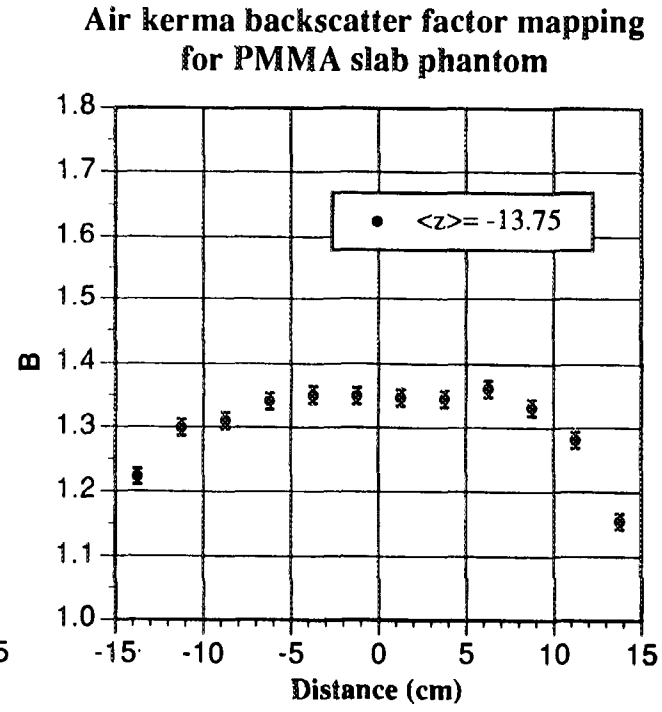
Air kerma backscatter factor mapping
for PMMA slab phantom
B
1.8
1.7
1.6
1.5
1.4
1.3
1.2
1.1
1.0
-15
-10
-5
0
5
10
15
Distance (cm)
<z>= -13.75

WIDE SPECTRUM SERIES
(200 kV)

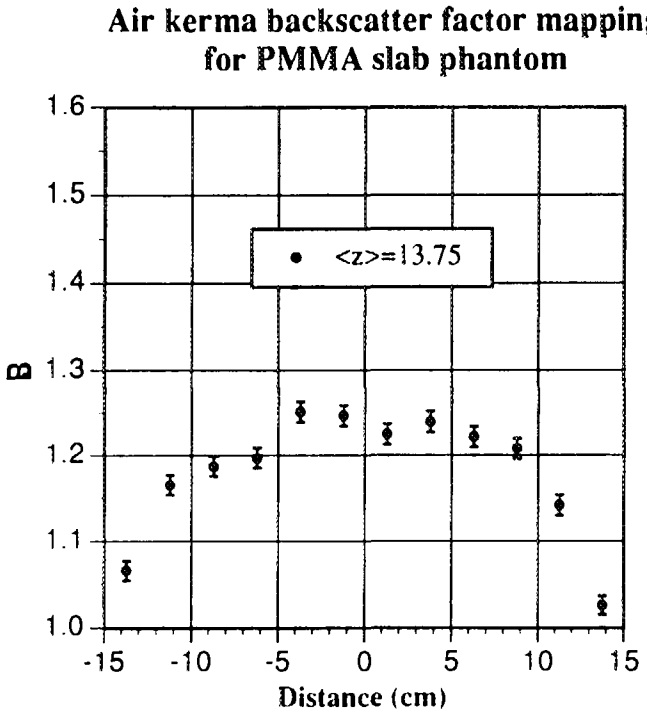
Air kerma backscatter factor mapping for PMMA slab phantom
B
1.6
1.5
1.4
1.3
1.2
1.1
1.0
<z>=13.75
-15
-10
-5
0
5
10
15
Distance (cm)

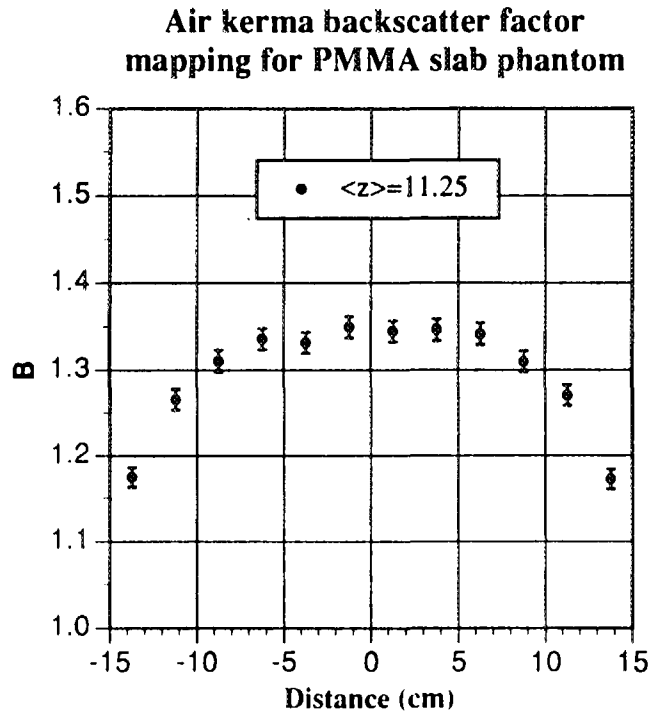
Air kerma backscatter factor mapping for PMMA slab phantom
B
1.6
1.5
1.4
1.3
1.2
1.1
1.0
<z>=11.25
-15
-10
-5
0
5
10
15
Distance (cm)

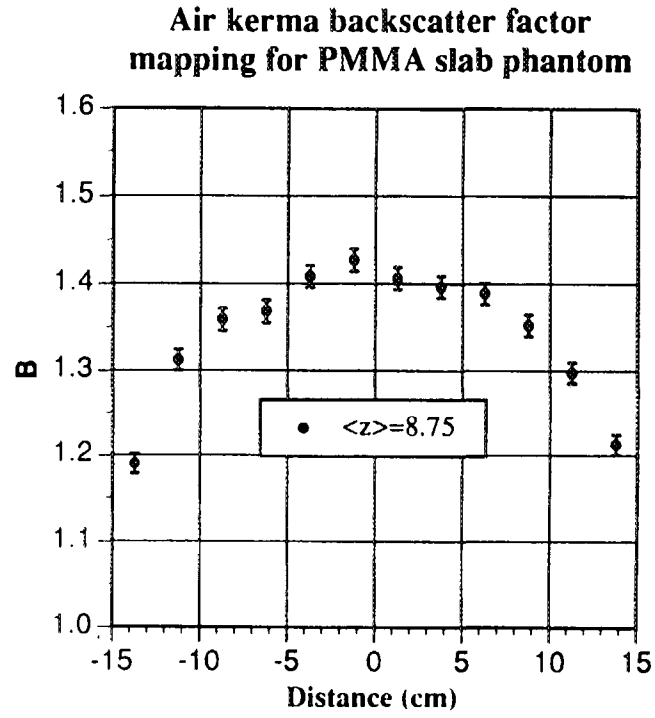
Air kerma backscatter factor mapping for PMMA slab phantom
B
1.6
1.5
1.4
1.3
1.2
1.1
1.0
<z>=8.75
-15
-10
-5
0
5
10
15
Distance (cm)

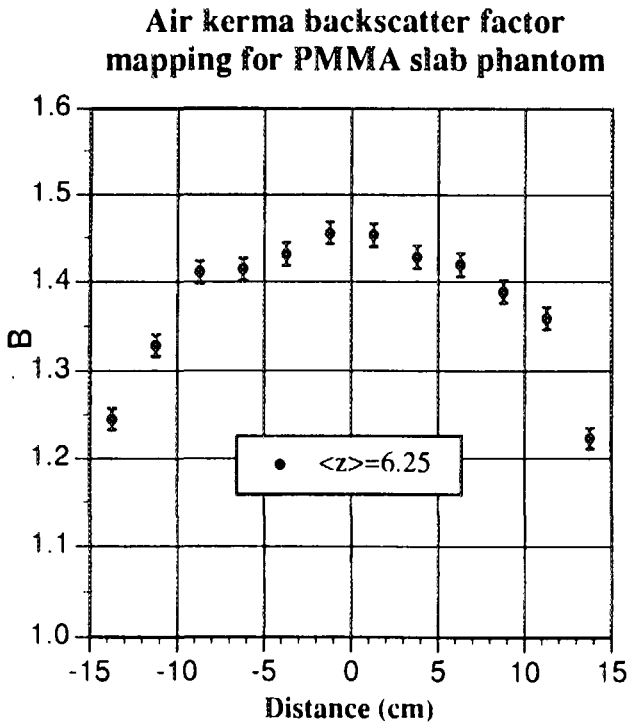
Air kerma backscatter factor mapping for PMMA slab phantom
B
1.6
1.5
1.4
1.3
1.2
1.1
1.0
-15
-10
-5
0
5
10
15
Distance (cm)
<z>=6.25

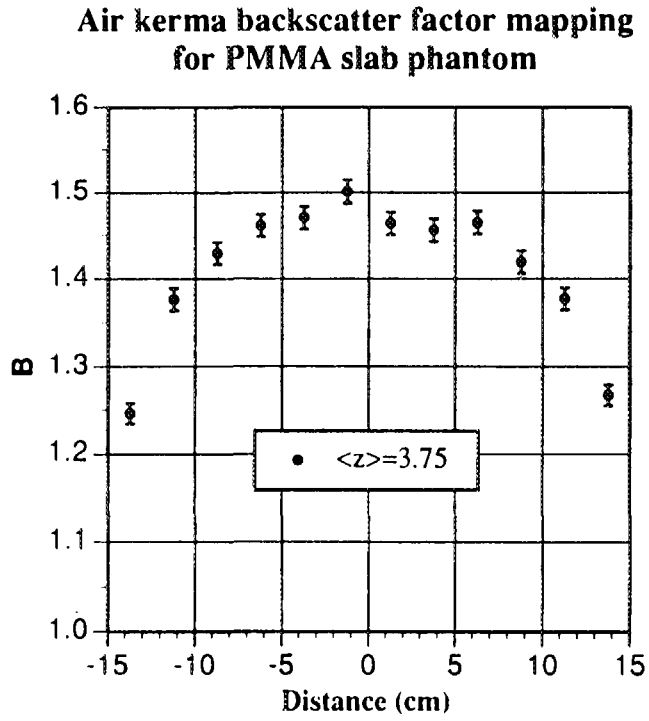
Air kerma backscatter factor mapping for PMMA slab phantom
B
1.6
1.5
1.4
1.3
1.2
1.1
1.0
-15
-10
-5
0
5
10
15
Distance (cm)
<z>=3.75

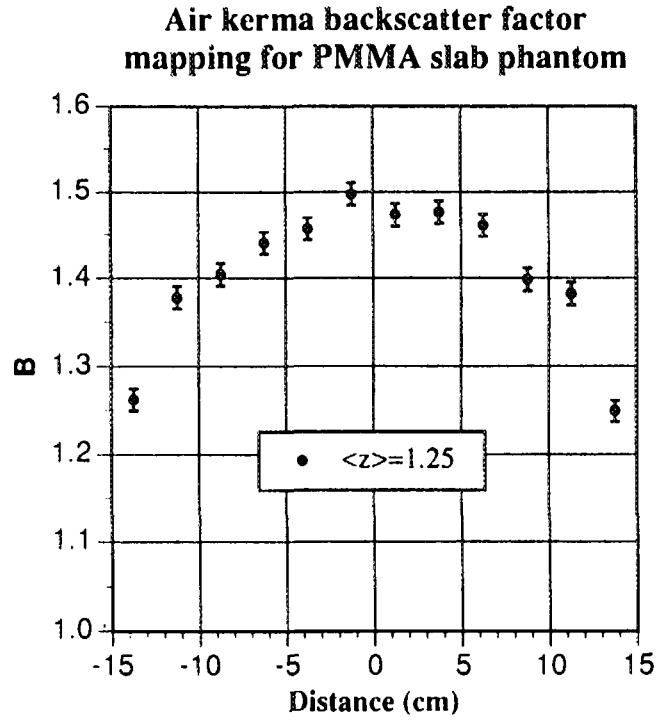
Air kerma backscatter factor mapping for PMMA slab phantom
B
1.6
1.5
1.4
1.3
1.2
1.1
1.0
-15
-10
-5
0
5
10
15
Distance (cm)
<z>=1.25

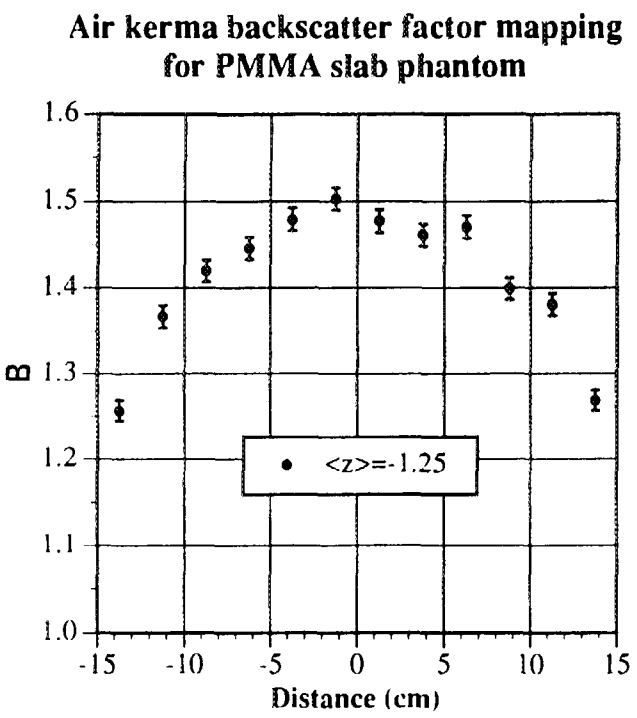
Air kerma backscatter factor mapping
for PMMA slab phantom
B
1.6
1.5
1.4
1.3
1.2
1.1
1.0
-15
-10
-5
0
5
10
15
Distance (cm)
<z>=-1.25

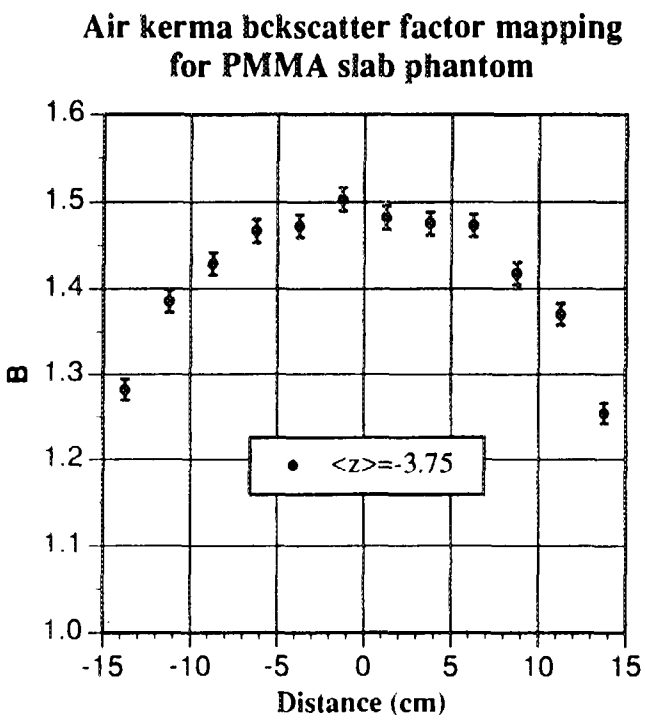
Air kerma bckscatter factor mapping
for PMMA slab phantom
B
1.6
1.5
1.4
1.3
1.2
1.1
1.0
-15
-10
-5
0
5
10
15
Distance (cm)
<z>=-3.75

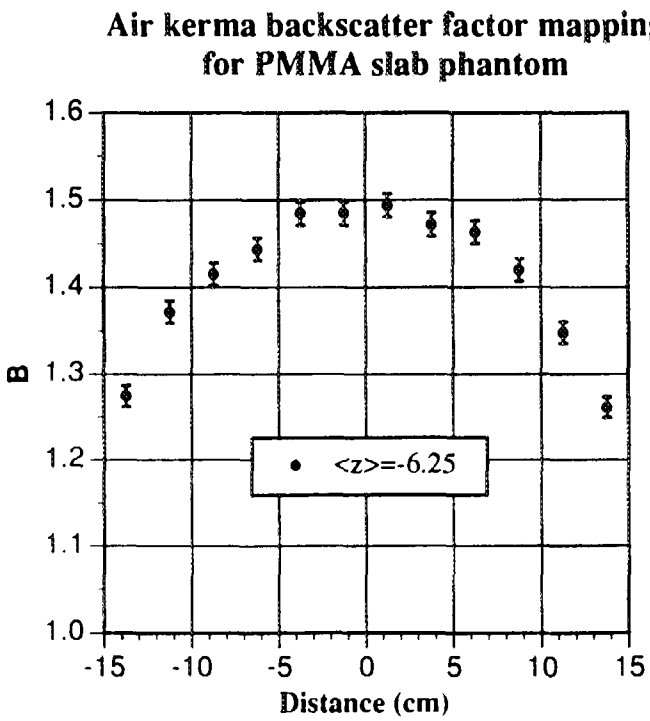
Air kerma backscatter factor mapping
for PMMA slab phantom
B
1.6
1.5
1.4
1.3
1.2
1.1
1.0
-15
-10
-5
0
5
10
15
Distance (cm)
<z>=-6.25

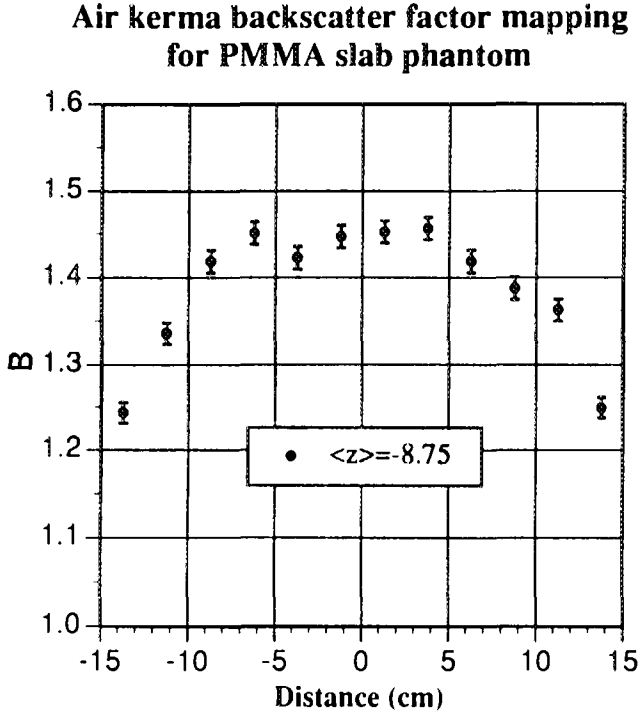
Air kerma backscatter factor mapping
for PMMA slab phantom
B
1.6
1.5
1.4
1.3
1.2
1.1
1.0
-15
-10
-5
0
5
10
15
Distance (cm)
<z>=-8.75

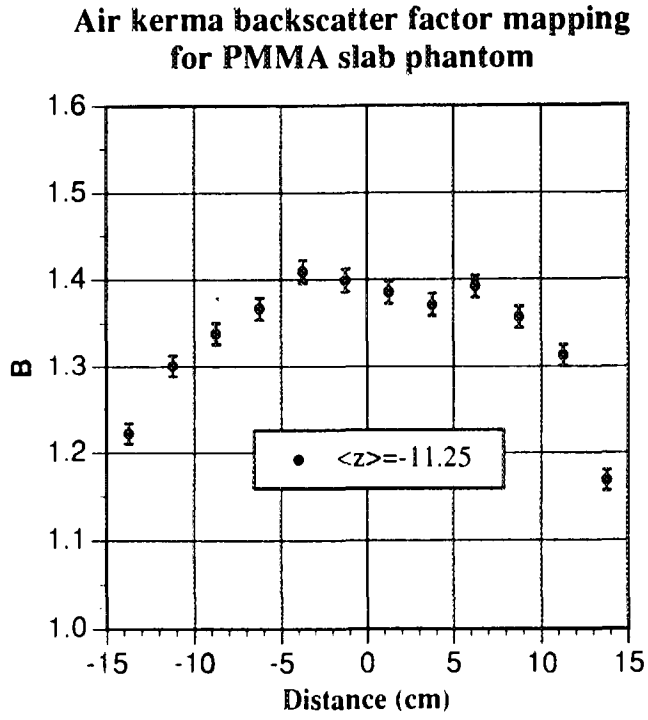
Air kerma backscatter factor mapping
for PMMA slab phantom
B
1.6
1.5
1.4
1.3
1.2
1.1
1.0
-15
-10
-5
0
5
10
15
Distance (cm)
<z>=-11.25

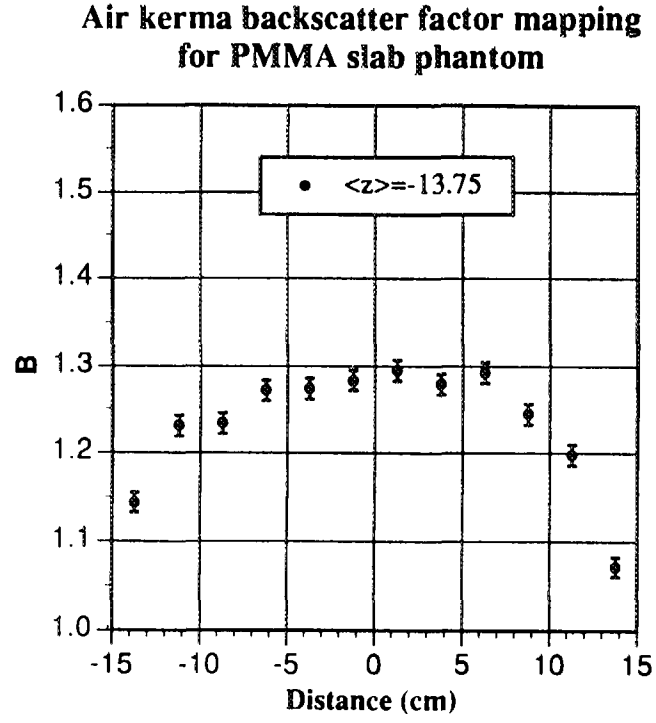
Air kerma backscatter factor mapping
for PMMA slab phantom
B
1.6
1.5
1.4
1.3
1.2
1.1
1.0
-15
-10
-5
0
5
10
15
Distance (cm)
<z>=-13.75

WIDE SPECTRUM SERIES
(300 kV)

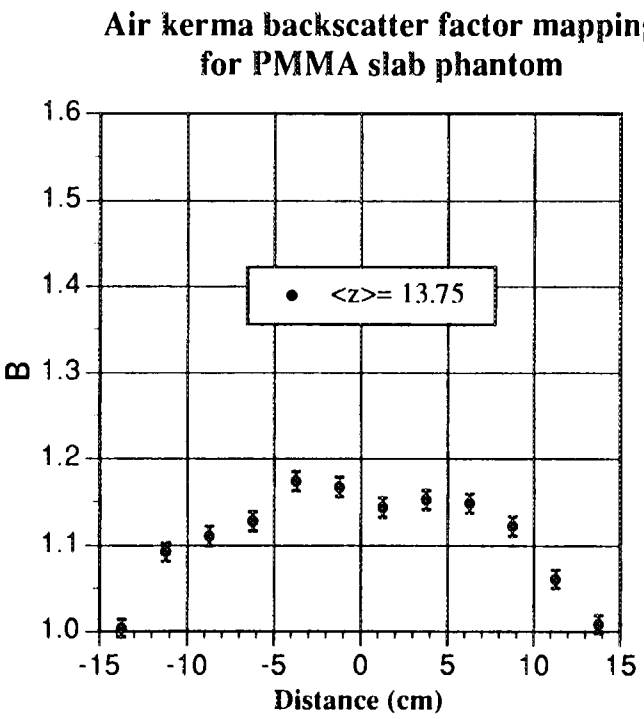
Air kerma backscatter factor mapping
for PMMA slab phantom
<z>= 13.75
B
Distance (cm)
1.6
1.5
1.4
1.3
1.2
1.1
1.0
-15
-10
-5
0
5
10
15

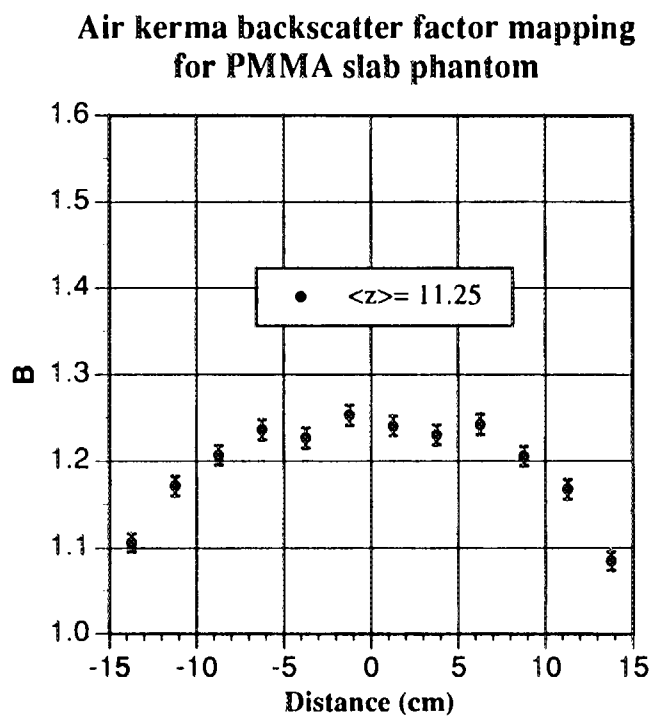
Air kerma backscatter factor mapping
for PMMA slab phantom
<z>= 11.25
B
Distance (cm)
1.6
1.5
1.4
1.3
1.2
1.1
1.0
-15
-10
-5
0
5
10
15

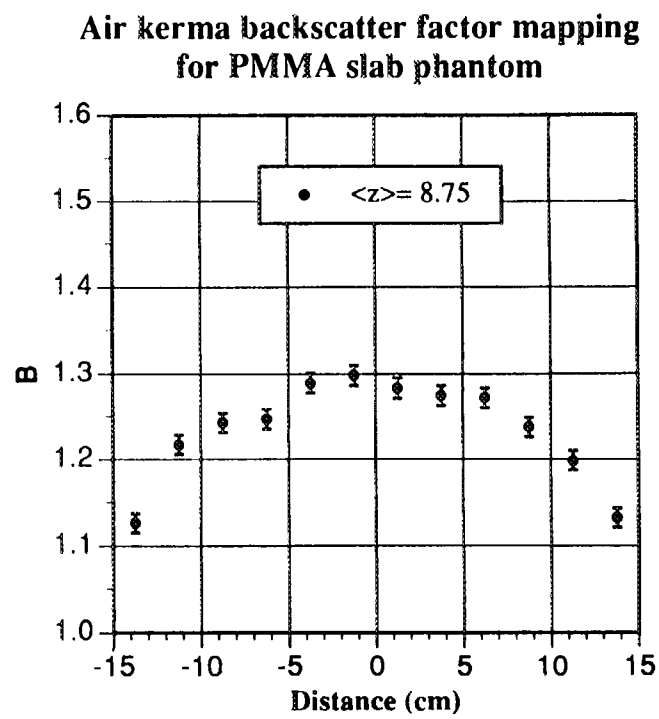
Air kerma backscatter factor mapping
for PMMA slab phantom
<z>= 8.75
B
Distance (cm)
1.6
1.5
1.4
1.3
1.2
1.1
1.0
-15
-10
-5
0
5
10
15

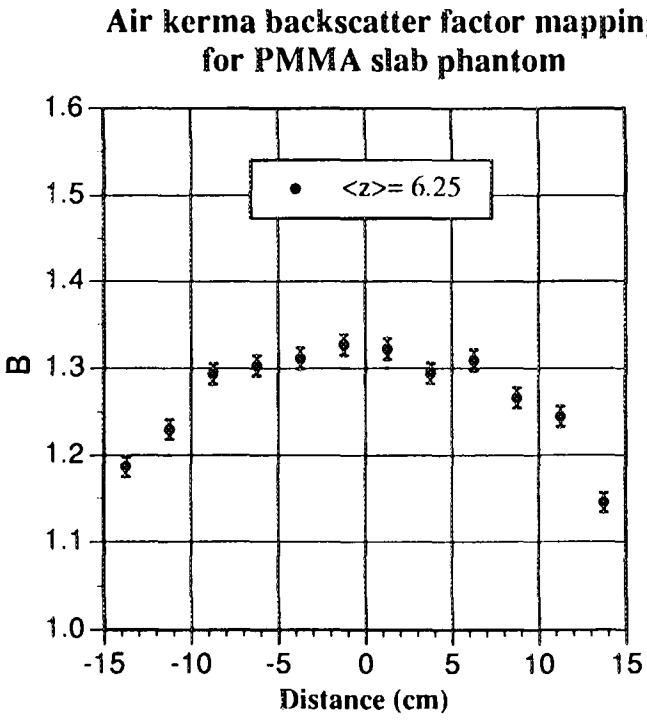
Air kerma backscatter factor mapping for PMMA slab phantom
<z>= 6.25
B
Distance (cm)
1.6
1.5
1.4
1.3
1.2
1.1
1.0
-15
-10
-5
0
5
10
15

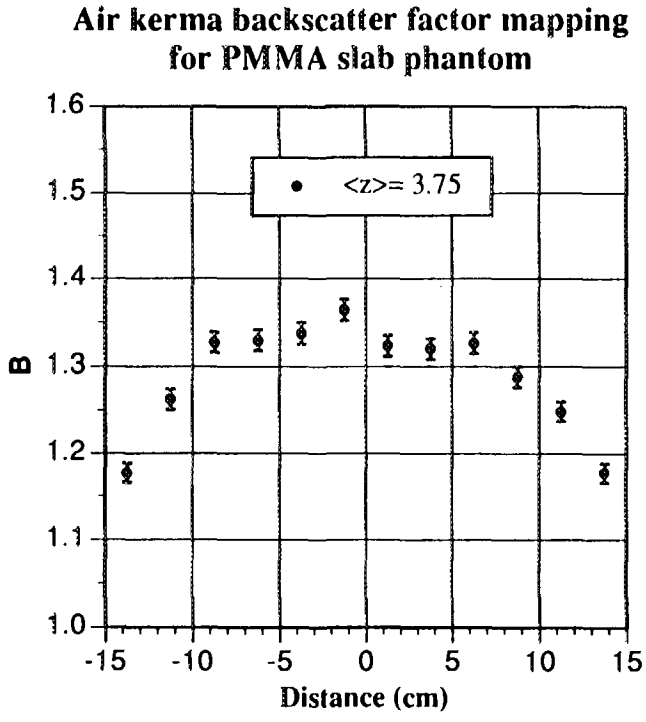
Air kerma backscatter factor mapping for PMMA slab phantom
<z>= 3.75
B
Distance (cm)
1.6
1.5
1.4
1.3
1.2
1.1
1.0
-15
-10
-5
0
5
10
15

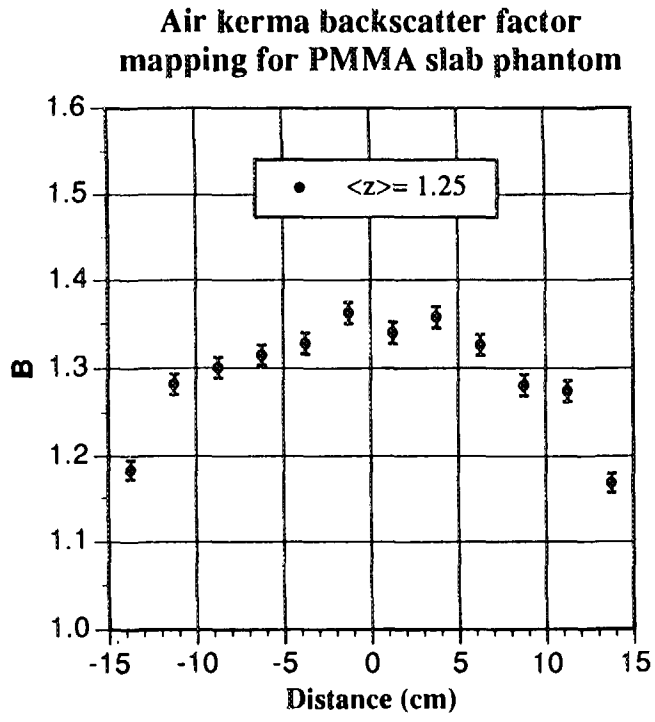
Air kerma backscatter factor mapping for PMMA slab phantom
<z>= 1.25
B
Distance (cm)
1.6
1.5
1.4
1.3
1.2
1.1
1.0
-15
-10
-5
0
5
10
15

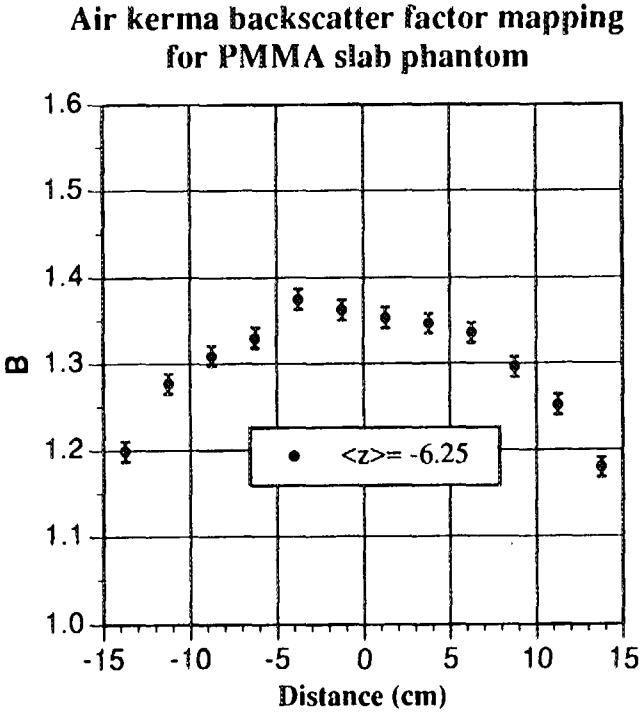
Air kerma backscatter factor mapping for PMMA slab phantom
B
1.6
1.5
1.4
1.3
1.2
1.1
1.0
-15
-10
-5
0
5
10
15
Distance (cm)
<z>= -6.25

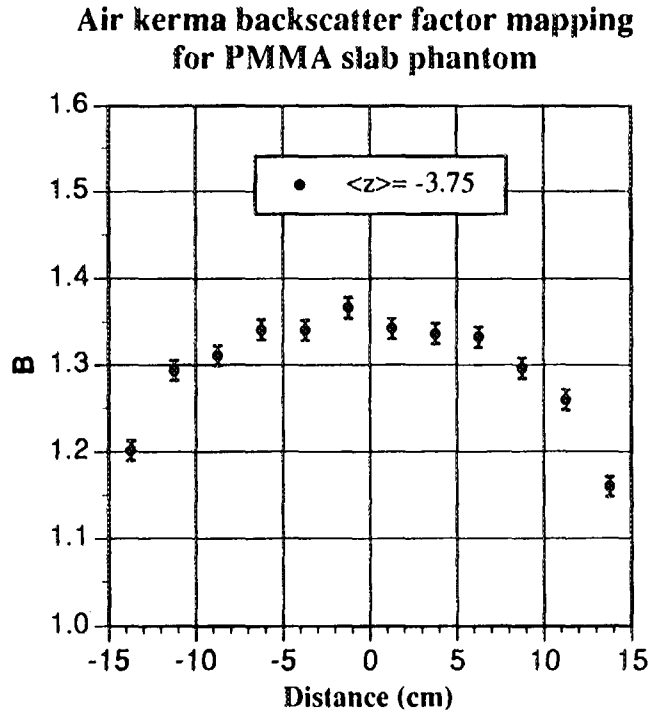
Air kerma backscatter factor mapping for PMMA slab phantom
B
1.6
1.5
1.4
1.3
1.2
1.1
1.0
-15
-10
-5
0
5
10
15
Distance (cm)
<z>= -3.75

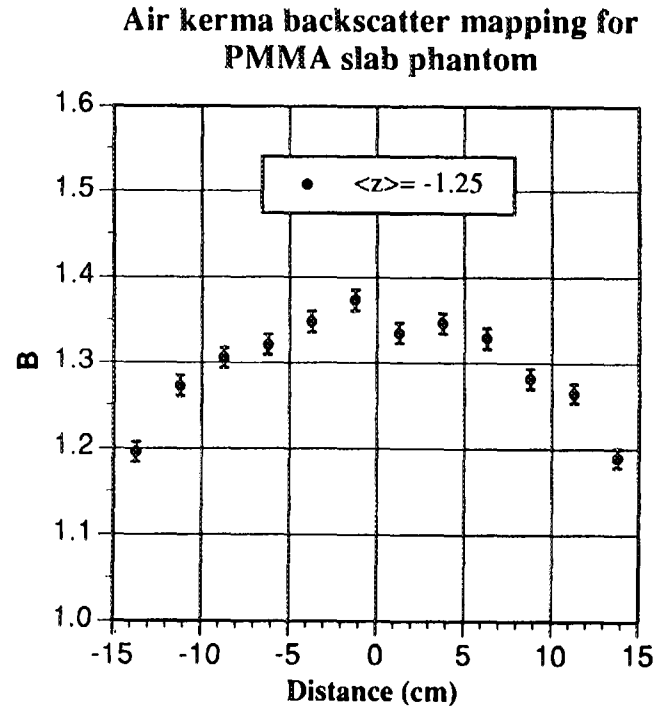
Air kerma backscatter mapping for PMMA slab phantom
B
1.6
1.5
1.4
1.3
1.2
1.1
1.0
-15
-10
-5
0
5
10
15
Distance (cm)
<z>= -1.25

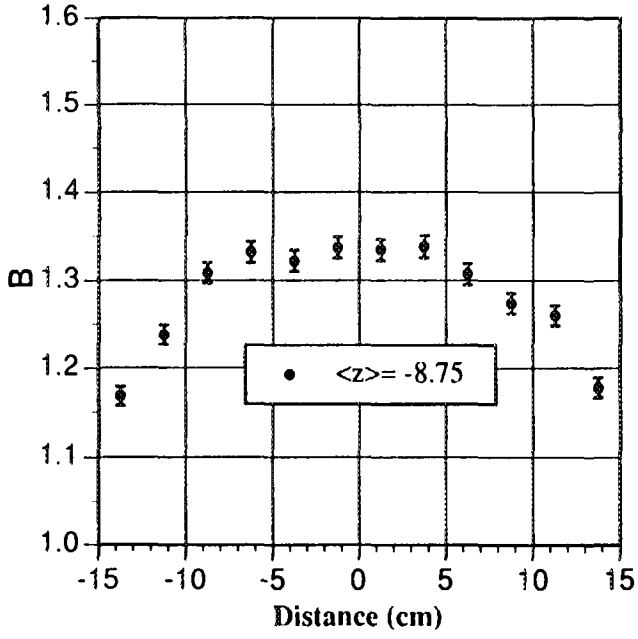
Air kerma backscatter factor mapping
for PMMA slab phantom
B
1.6
1.5
1.4
1.3
1.2
1.1
1.0
<z>= -8.75
-15
-10
-5
0
5
10
15
Distance (cm)

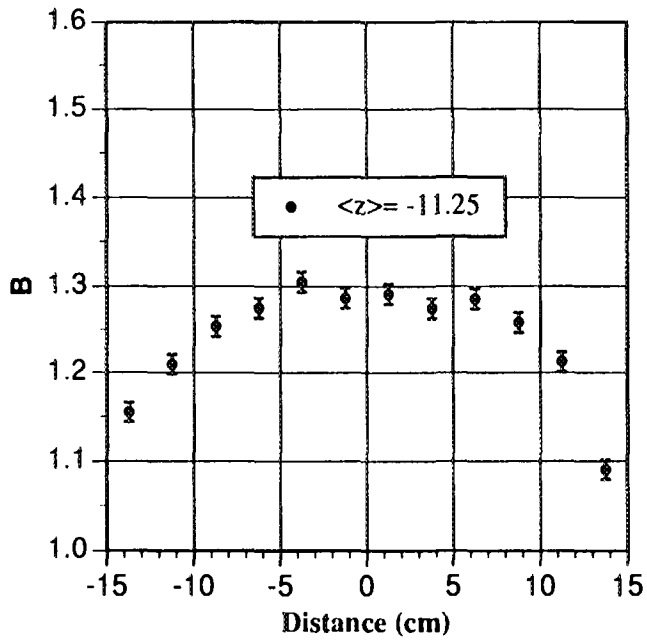
Air kerma backscatter factor mapping
for PMMA slab phantom
B
1.6
1.5
1.4
1.3
1.2
1.1
1.0
<z>= -11.25
-15
-10
-5
0
5
10
15
Distance (cm)

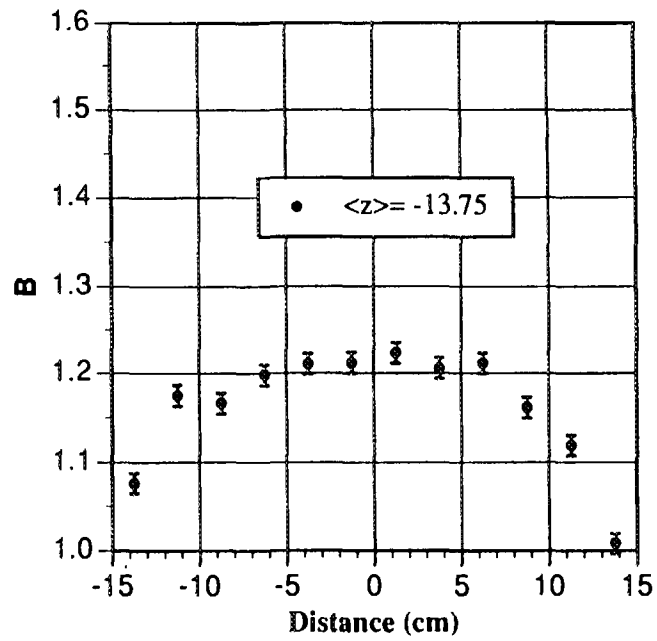
Air kerma backscatter factor mapping
for PMMA slab phantom
B
1.6
1.5
1.4
1.3
1.2
1.1
1.0
<z>= -13.75
-15
-10
-5
0
5
10
15
Distance (cm)

Edito dall' ENEA
Unità Comunicazione e Informazione
Lungotevere Grande Ammiraglio Thaon di Revel, 76 - 00196 Roma

Stampa: COM - Centro Stampa Tecnografico - C. R. Frascati

Finito di stampare nel mese di febbraio 1997